Variability and Processes of the Denmark Strait Overflow

Dissertation
zur Erlangung des Doktorgrades
der Christian-Albrechts-Universität
zu Kiel

vorgelegt von
Andreas Macrander

Kiel
2004

IFM-GEOMAR
Leibniz-Institut für Meereswissenschaften
an der Universität Kiel

Leibniz-Institut für Meereswissenschaften IFM-GEOMAR an der Universität Kiel
Düsternbrooker Weg 20, D-24105 Kiel, Germany
E-Mail: amacrander@ifm-geomar.de

I. Abstract

The formation of North Atlantic Deep Water (NADW) is an important part of the global Thermohaline Circulation (THC). Warm and saline surface waters are carried by the North Atlantic Current into the Nordic Seas. Here, cold dense water is produced by surface cooling and vertical mixing, that enters the deep North Atlantic as dense overflows across the sills of the Greenland-Scotland Ridge. The densest contribution to the NADW is the Denmark Strait Overflow Water.

The meridional heat transport of the THC contributes significantly to the global climate system, and it particularly influences the North Atlantic and Northern Europe region. There is growing evidence, that the THC reacts sensitive to climate change, and most climate models predict a substantial weakening of the THC in global warming scenarios.

Hence, the Denmark Strait between Iceland and Greenland may be considered as a key region to assess the deep branch of the THC with respect to climate change.

In this study, time series of the Denmark Strait Overflow, obtained in the framework of the SFB 460 project at the University of Kiel, are investigated.

It is found, that the chosen bottom mounted Acoustic Doppler Current Profilers and bottom Pressure sensors / Inverted Echo Sounders deployed at the sill of Denmark Strait are capable to monitor the dense overflow.

During the observation period from 1999 to 2003, the Denmark Strait overflow, previously regarded as stable on interannual timescales, exhibited significant changes: In 1999, the measured transport of $3.7\,\mathrm{Sv}$ [1] was about $30\,\%$ larger than previous observations. Until 2003, the volume transport of dense overflow water decreased from 3.7 to $3.1\,\mathrm{Sv}$, while the temperature increased temporarily by $0.5\,^{\circ}\mathrm{C}$.

The investigation of the dynamic relations that control the overflow reveals, that the overflow may be considered as a combination of a density driven, hydraulically controlled flow and a barotropic, wind driven component. It is suggested, that an upstream reservoir height reduction and a decrease of the wind stress forcing contributed equally to the observed overflow transport decrease.

The transport reduction is consistent with a decrease of the North Atlantic Oscillation, though the time series are too short yet to prove this relation. Moreover, the observations confirm theoretical predictions of a negative correlation with the Faroe Bank Channel overflow, which is the second important dense water gateway across the Greenland-Scotland Ridge.

There is evidence, that the key region controlling both dense overflows from the Nordic Seas to the deep Atlantic ocean is located in the Iceland Sea. Hence, the data give new insight into the controlling mechanisms of the Denmark Strait Overflow, and open perspectives for long time monitoring of the THC with respect to climate change.

---

[1]Sv: Sverdrup. $1\,\mathrm{Sv} = 1 \cdot 10^{6}\,\mathrm{m}^{3}/\mathrm{s}$.

II. Zusammenfassung

Die Produktion von Nordatlantischem Tiefenwasser (NADW) ist ein wichtiger Teil der globalen Thermohalinen Zirkulation (THC). Warmes und salzreiches Oberflächenwasser wird durch den Nordatlantischen Strom in die Nordische See[1] transportiert, wo es durch Abkühlung und vertikale Vermischung zu Wassermassen großer Dichte transformiert wird. Diese strömen als kalte, dichte „Overflows" über die Schwellen des Grönland-Schottland-Rückens in den tiefen Nordatlantik. Die dichteste Komponente des NADW wird durch das Dänemarkstraßen-Overflowwasser gebildet.

Der meridionale Wärmetransport der THC trägt wesentlich zum globalen Klimasystem bei, und beeinflußt insbesondere die Nordatlantik- und Nordeuropa-Region. Es gibt Anzeichen dafür, daß die THC empfindlich auf Klimaänderungen reagiert, und die meisten numerischen Modelle sagen eine erhebliche Abschwächung der THC in Treibhausszenarien voraus. Daher kann die Dänemarkstraße zwischen Island und Grönland als eine Schlüsselregion betrachtet werden, um Klimaveränderungen zu beobachten.

In dieser Arbeit werden Zeitserien des Dänemarkstraßen-Overflows im Rahmen des SFB 460 an der Universität Kiel untersucht. Es wird gezeigt, daß der dichte Overflow mit am Meeresboden ausgelegten profilierenden akustischen Strömungsmessern, Bodendrucksensoren und Echoloten beobachtet werden kann.

Während des Beobachtungszeitraumes von 1999 – 2003 zeigte der Dänemarkstraßen-Overflow, der bislang auf saisonalen und interannualen Zeitskalen für stabil gehalten wurde, deutliche Änderungen: 1999 war der gemessene Transport mit 3.7 Sv [2] ca. 30 % höher als bei früheren Beobachtungen. Bis 2003 nahm der Transport um 0.6 auf 3.1 Sv ab. Die Temperatur stieg vorübergehend um 0.5 °C an.

Die Untersuchung der dynamischen Relationen, die den Overflow kontrollieren, zeigt, daß der Overflow einen dichtegetriebenen, hydraulisch kontrollierten Anteil und eine barotrope, windgetriebene Komponente umfaßt. Die Beobachtungen lassen den Schluß zu, daß eine Abnahme der stromaufwärtigen Reservoirhöhe und der Windschubspannung zu gleichen Teilen zu der beobachteten Transportabnahme beitrugen.

Die Transportabnahme ist konsistent mit einer Abnahme der Nordatlantischen Oszillation, obgleich die Zeitserien bislang nicht lang genug sind, um eine kausale Relation zu verifizieren. Ferner bestätigten die Beobachtungen theoretische Vorhersagen einer gegensätzlichen Korrelation mit dem Faröer-Bank-Kanal-Overflow, der den zweiten wichtigen Exportweg für dichtes Tiefenwasser über den Grönland-Schottland-Rücken darstellt.

Es gibt Anzeichen dafür, daß die Islandsee eine Schlüsselregion für die Kontrolle beider dichter Overflows von der Nordischen See in den tiefen Atlantik ist. Die Beobachtungen vertiefen das Verständnis von den Prozessen, die den Dänemarkstraßen-Overflow kontrollieren, und eröffnen Perspektiven für eine Langzeitbeobachtung der THC im Bezug auf Klimaänderungen.

---

[1] Nordische See: Grönland-, Island- und Norwegische See.
[2] Sv: Sverdrup. $1\,\text{Sv} = 1 \cdot 10^6\,\text{m}^3/\text{s}$.

Contents

List of Figures

List of Tables

1. Introduction

1.1. The Denmark Strait as a gateway for the Thermohaline Circulation

The Thermohaline Circulation (THC) is an important part of the global heat budget (IPCC, 2001), carrying warm surface waters to high latitudes, where these are transformed to cold, dense deep waters. The North Atlantic as a particular convective ocean has a key role for the deep branch of the THC (IPCC, 2001).

Estimates of the total Atlantic Meridional Overturning Circulation (AMOC)[1] range between 11 and 18 Sv [2] (SCHMITZ, 1995; GANACHAUD AND WUNSCH, 2000; BRYDEN AND IMAWAKI, 2001). The AMOC effects a northward heat transport of 1.3 PW (at 24°N, LAVÍN ET AL., 1998) over the entire Atlantic ocean. Numerical experiments of VELLINGA AND WOOD (2002) showed, that a total shut-down of the AMOC has a global impact on climate. The largest changes are observed over the northern hemisphere, and in particular over the North Atlantic, a breakdown of the AMOC might lead to a temperature decrease of $3 - 6\,°C$.

There is evidence, that the formation processes of North Atlantic Deep Water (NADW), i.e. gradual cooling and subduction in the Nordic Seas[3] (MAURITZEN, 1996a) and convection (e.g. in the Labrador Sea, MARSHALL AND SCHOTT, 1999) are sensitive to forcing changes, since they depend on a weak density stratification to allow vertical mixing. Evidence from paleorecords and numerical models suggest, that large freshwater fluxes, that frequently occurred during the last interglacial cycle, significantly reduced the NADW formation and hence the AMOC strength (SARNTHEIM ET AL., 2001). Large freshwater fluxes are also expected due to Arctic ice melt and enhanced atmospheric moisture transport related to global warming (IPCC, 2001), and might weaken the dense water formation (RAHMSTORF, 1996), whereas advection of more saline surface water may have a stabilizing effect on the AMOC (LATIF ET AL., 2000). Hence, the reaction of the AMOC to global warming is presently uncertain, although most numerical climate models predict, that the THC decreases substantially for greenhouse scenarios (for a review, see IPCC, 2001).

---

[1] The THC is characterized as the buoyancy driven circulation of the ocean. Different definitions of the THC exist in the literature (WUNSCH, 2002). The actual meridional overturning comprises both a buoyancy and and wind driven component (RAHMSTORF, 2003). However, the AMOC is commonly used as a representative for the THC.

[2] Sv: Sverdrup. $1\,\mathrm{Sv} = 1 \cdot 10^6\,\mathrm{m}^3/\mathrm{s}$.

[3] Nordic Seas: Greenland, Iceland and Norwegian Seas.

At present, approximately 6 Sv of the NADW are produced in the Nordic Seas. These enter the deep ocean as dense overflows across the Greenland-Scotland Ridge (GSR). The topographic constrictions of the GSR control the density driven exchange between North Atlantic and Nordic Seas and focus the deep flow through a few gateways. A volume flux of approximately 3 Sv leaves the Nordic Seas via the Denmark Strait between Iceland and Greenland to form the deepest part of the NADW (HANSEN AND ØSTERHUS, 2000).

Ocean circulation models suggest, that the density of the Denmark Strait Overflow Water (DSOW) has a major impact on the total AMOC strength further south (SCHWECKENDIEK AND WILLEBRAND, 2004). Moreover, it has been shown, that the Denmark Strait Overflow is at least critical for the northernmost extension of the THC into the Nordic Seas, and the presence of the dense overflow is considered as essential for the present stability of the global THC (LOHMANN AND GERDES, 1998).

The Denmark Strait Overflow may therefore be considered as a critical location to assess global warming induced changes of the deep branch of the THC.

In contrast to predictions of numerical models (NILSEN ET AL., 2003; BIASTOCH ET AL., 2003), previous observations characterized the Denmark Strait Overflow as rather stable on interannual to decadal timescales (DICKSON AND BROWN, 1994).

The aim of the observations carried out in the framework of the Sonderforschungsbereich 460 "Dynamik thermohaliner Zirkulationsschwankungen" at the University of Kiel is to detect possible changes of the Denmark Strait Overflow, and to identify the mechanisms that govern the dense water transport.

The multi-year time series may thus improve the understanding of the role of the Denmark Strait Overflow with respect to climate change.

1.2.   Past observations

The Denmark Strait Overflow and the descent of dense water downstream of the sill has been known from observations since KNUDSEN (1899). The hydrographic conditions of the Nordic Seas and the North Atlantic suggested, that the overflow contributes to the North Atlantic Deep Water (NADW; HELLAND-HANSEN AND NANSEN, 1909). However, research specifically focused on the Denmark Strait Overflow did not start before COOPER (1955) proposed, that the Denmark Strait Overflow Water (DSOW) is an important source for the NADW. Since then, the nature and variability of the overflow has been investigated by various research cruises and deployed instruments.

1.2.1.   Hydrographic surveys of the Denmark Strait Overflow

The first quantitative estimates of the Denmark Strait Overflow have been obtained from hydrographic sections taken in 1958 and 1962 and yielded a transport of 2.8 Sv (for $T < 1.8\,°C$; WORTHINGTON, 1969).

HARVEY AND SHOR (1961) observed sporadic overflow of cold, dense Norwegian Sea Deep Water in current meter records at the Denmark Strait sill.

Direct current measurements during a cruise in 1967 revealed 2.7 Sv (for $T < 4\,^\circ\text{C}$; WORTHINGTON, 1969); from current meter deployments, only one instrument delivered useful data. The time series showed near-bottom currents up to 1.4 m/s and large temporal variability on timescales of a few days (WORTHINGTON, 1969). Repeated hydrographic surveys exhibited high spatial variability of water mass distribution in Denmark Strait on timescales less than 10 days (MANN, 1969; STEIN, 1972).

The first successful mooring array that covered the overflow across the sill (see Fig. 2.1, page 27) was deployed for a time of five weeks as part of the OVERFLOW'73 project in 1973 (ROSS, 1984). These observations again confirmed the high variability on timescales of a few days, and did not show any "long-term" (i.e. multi-weekly) variability. Two current meter moorings 160 km downstream of the sill (MONA-array, Fig. 2.1, page 27) obtained the first one-year long records of the overflow. The time series exhibited no significant seasonal or interannual variability (AAGARD AND MALMBERG, 1978).

Between 1986 and 1994, three long-term current meter arrays were deployed in the "Lowestoft" arrays (Fig. 2.1, page 27) to observe the downstream evolution and entrainment into the Denmark Strait Overflow (DICKSON AND BROWN, 1994). The observations supported the apparent long term stability of the overflow. These measurements have been continued at several locations until present (later referred to as "Angmagssalik" array; Fig. 2.1, page 27). In contrast to the findings of DICKSON AND BROWN (1994), preliminary results of the multi-year "Angmagssalik" array time series revealed at least some interannual transport and temperature variability (unpublished, DYE ET AL., 2004).

JÓNSSON (1999) investigated the upstream regions, based on Icelandic observations from a current meter array 200 km northeast of the sill (close to "KG5", Fig. 2.1, page 27), and a single ADCP[4] that was deployed at the sill from 1996 to 1999. In combination with hydrographic observations, the results changed the view of the sources of the DSOW. JÓNSSON AND VALDIMARSSON (2004a) found, that a significant fraction of the overflow approaches the sill from the Iceland Sea instead of the deeper part of the East Greenland Current, as was concluded from water mass analysis by RUDELS ET AL. (2002).

As part of the SFB 460 project, the overflow dynamics have been studied on three cruises of R/V Poseidon (P222, P230, P244). These cruises gave new insight into dynamical processes of the descending plume. The observed downstream eddy generation was investigated by KRAUSS AND KÄSE (1998). Further extensive analysis of eddy activity and energy budget of the plume was carried out by GIRTON (2001) and GIRTON ET AL. (2001), and was compared to a high resolution model of the overflow (GIRTON AND SANFORD, 2003; KÄSE ET AL., 2003).

At the sill, DSOW transport estimates were always in the range of 2.9 Sv (ROSS, 1984; GIRTON ET AL., 2001) to 2.5 Sv (SAUNDERS, 2001) with high variability on timescales of 2 to 10 days (SAUNDERS, 2001), but with no significant seasonal or interannual transport or temperature signals (DICKSON AND BROWN, 1994).

The apparent long-term constancy lead to the assumption, that the overflow is

---

[4]Acoustic Doppler Current Profiler, see page 39.

limited by hydraulic control (see WHITEHEAD, 1998, for a review), which agrees with model results (KÄSE AND OSCHLIES, 2000).

1.2.2.   Interannual variability and external forcing

The dominant mode of atmospheric variability over the North Atlantic is the North Atlantic Oscillation (NAO; HURRELL, 1995), which closely interacts with the ocean (BJERKNES, 1964). The ocean exhibits both a local and fast response to forcing changes, and a delayed response on interannual and longer timescales, in particular for the large scale and overturning circulation (VISBECK ET AL., 2003).

In recent time, there have been speculations which link the observed NADW variability to the North Atlantic Oscillation (NAO) or changes in deep water formation in the Nordic Seas. DICKSON ET AL. (1996) analyzed convection and dense water formation in the Greenland and Labrador Seas and their correlation with the large-scale atmospheric circulation pattern reflected by the NAO. In hydrographic data near Southern Greenland, that include both dense overflows from the Nordic Seas into the Atlantic Ocean, BACON (1998) found large interdecadal variability, which the author attributes to polar air temperature. MCCARTNEY ET AL. (1998) discussed a negative lagged response of the DSOW transport to the NAO, with low NAO enhancing the buoyancy forcing of the overflow. DICKSON ET AL. (1999) speculated, that an anomalous warming of the plume, observed in 1996/1997 by the "Angmagssalik" array, had been advected from Fram Strait three years earlier, which in turn reflected a positive NAO phase.

Model experiments show an almost instantaneous response of the barotropic circulation around Iceland to wind stress curl changes over the North Atlantic (BIASTOCH ET AL., 2003), with positive NAO wind stress curl pattern enhancing the net southward flow through Denmark Strait. Since the overflow at the sill is predominantly barotropic (GIRTON, 2001), this implies a positive correlation between NAO and overflow (KÖSTERS, 2004b). The positive correlation of the outflow through Denmark Strait is also supported by numerical studies of NILSEN ET AL. (2003).

While a recent study of the Faroe Bank Channel overflow revealed a possible correlation with the NAO (HANSEN ET AL., 2001), observational evidence for the Denmark Strait Overflow has been little so far. Data from hydrographic cruises are always likely to be biased by the large short-term variability. Coherent long-term observations only exist further downstream (DICKSON AND BROWN, 1994), where the DSOW is already modified by entrainment processes and merged with Iceland Scotland Overflow Water (ISOW), which originates from the overflows through the Faroe Bank Channel and the Iceland-Faroe Ridge (HANSEN AND ØSTERHUS, 2000).

These time series did not show any signs of interannual variability (DICKSON AND BROWN, 1994). However, recent results of the Angmagssalik array (unpublished, DYE ET AL., 2004) and this study might modify this view.

1.2.3. Overflow response to climate change

A major concern in global warming scenarios is a possible weakening or total shut-down of the Thermohaline Circulation (THC; IPCC, 2001). The THC sensitivity to increased CO_2 forcing varies between different climate models, ranging from a stable THC (LATIF ET AL., 2000) to a moderate to strong reduction in most other climate models (for a review, see IPCC, 2001). A substantial reduction of the THC would have a global impact on ocean circulation and climate (IPCC, 2001), in particular for the temperatures over the North Atlantic region (VELLINGA AND WOOD, 2002). Numerical studies suggest, that a total shut-down of the THC leads to a cooling by 5 °C over the North Atlantic, which regionally counteracts the global warming (RAHMSTORF, 2002). The individual influence of the Denmark Strait Overflow on surface air temperature has been estimated to 1.5 − 0.5 °C over the northern North Atlantic (KÖSTERS, 2004b).

The current state of the THC with cooling and dense water formation in high latitudes depends critically on high surface densities in the northern North Atlantic, and since the conceptual box model of STOMMEL (1961), it is known, that other stable states of the THC are possible. Since then, multiple equilibria of the THC have been investigated in several studies (e.g. BROECKER ET AL., 1985).

RAHMSTORF (1995) found, that the production rates and convection sites of North Atlantic Deep Water (NADW) are highly sensitive to surface freshwater fluxes. The freshwater budget is influenced by net precipitation, continental runoff, and sea ice. The effects of sea ice include brine release during freezing, thermal insulation of the ocean in ice-covered regions and freshwater input from ice melt. Further, the NADW formation is affected by wind stress and surface heat fluxes, and the properties of the water masses advected from the Atlantic ocean and the Arctic Mediterranean (for a comprehensive review, see MARSHALL AND SCHOTT, 1999).

While some of the coupling mechanisms have a stabilizing effect on the AMOC, enhanced freshwater input in high latitudes is regarded as the key process that leads to a weaker overturning in global warming scenarios (e.g. RAHMSTORF, 1996; OTTERÅ ET AL., 2003), and it may be expected that the dense overflows over the GSR, that feed the NADW as the deep branch of the AMOC, are sensitive to climate variability.

Changes of the Denmark Strait Overflow Water (DSOW) production rates and properties are likely to influence the total strength of the Meridional Overturning Circulation (GERDES AND KÖBERLE, 1995; DÖSCHER AND REDLER, 1997) and hence the oceanic heat transport to the North Atlantic (BÖNING ET AL., 1996).

Paleoclimatic records give evidence, that during the past 120,000 years, the THC experienced abrupt changes, being greatly reduced at times of maximal glaciation (RAHMSTORF, 2002). Model studies of KÖSTERS ET AL. (2004) showed, that the Denmark Strait Overflow has been reduced by a factor of 5 during the Last Glacial Maximum, compared to present-day conditions, being a measure for the strength of the Meridional Overturning Circulation.

Focusing on present-day measurements, large interannual fluctuations have been observed in the Labrador Sea, where the least dense part of the NADW is formed. The

variability in convection depth and Labrador Sea Water production rates are linked to changes of freshwater fluxes (SCHMIDT, 2003) and wind stress forcing (DICKSON ET AL., 1996).

The dense overflows across the GSR mainly originate from intermediate water masses in the Nordic Seas, that are formed by shallow convection (SWIFT ET AL., 1980) and through gradual cooling of the inflowing Atlantic Water (MAURITZEN, 1996a). During the past decade, significant changes of water mass properties have been observed in the Greenland Sea, that in turn may influence the overflows. A density decrease of the entire water column, associated with a warming and freshening in the upper and intermediate layers, and a warming and salinification in the deep layers might lead to a reduced density and higher temperature of the Denmark Strait Overflow Water (KARSTENSEN ET AL., 2004).

The study of DICKSON ET AL. (2002) has put emphasis on interdecadal trends in salinity, questioning, whether the observed freshening in the northern North Atlantic, including the Denmark Strait Overflow, may be attributed to climate change. These observations are consistent with CURRY ET AL. (2003), who observed a salinification in the subtropics, and a freshening in the high latitudes of the Atlantic ocean, which they attribute to changes of the global freshwater fluxes.

This issue has been further addressed by HANSEN ET AL. (2004b), including the observational evidence for a 20 % decrease in the Faroe Bank Channel Overflow from 1950 to 2000 (HANSEN ET AL., 2001).

For the Denmark Strait Overflow, however, no continuous time series exist, which allow for consistent estimates of variability on interannual and interdecadal timescales. In contrast to the known variability of the dense water formation processes, it is widely believed, that the Denmark Strait Overflow is stable on timescales longer than a few weeks (DICKSON AND BROWN, 1994). However, conclusions regarding the lack of interannual variability of the Denmark Strait Overflow have been based on either short-term studies, hydrographic sections or result from mooring time series further downstream, where entrainment has already changed the initial properties of the overflow.

1.3. Present study

To evaluate the sensitivity of the present-day Denmark Strait Overflow to climate variability, and to overcome the lack of consistent observation time series, the SFB 460 TP A1 project at the University of Kiel was focused on observations of the Denmark Strait Overflow right at the sill. Here, the geographical constrictions of the strait focus the flow in a narrow zone, making this point predestinated for direct observations. Also, the overflow water mass properties are less affected by mixing and entrainment processes as further downstream. Thus, observations at the sill are better suited to detect the influence of changes in production rates and water mass properties in the Nordic Seas.

The long term goal of the ongoing SFB study carried out in cooperation with Hafrannsóknastofnunin (Marine Research Institute, MRI) Reykjavík, is to

– quantify the overflow during a longer period and with higher cross-strait resolution than before by means of moored Acoustic Doppler Current Profilers (ADCP),

– detect overflow plume thickness and sea surface height (SSH) acoustically for geostrophic estimates of both baroclinic and barotropic transports,

– verify the governing dynamic relations, particularly of hydraulic control mechanisms, geostrophy and upstream pathways, and NAO-related barotropic wind stress forcing,

– establish reliable relationships for overflow transport estimates to optimize long term monitoring with respect to climate change.

In the following paragraphs, a brief outline of this thesis is given:

- **Chapter 2** gives an introduction to the dominant hydrographic features and water masses of the Denmark Strait.

- In **Chapter 3**, the observation and data processing methods applied to the field experiment are described in detail. By comparison of time series, the performance of three independent methods to acoustically observe the overflow plume thickness is validated.

- **Chapter 4** introduces a high resolution process model that has proven to realistically reproduce the structure, strength and short-term variability of the overflow. In the numerical simulation, the deployment positions for the acoustic observation array have been optimized by a multilinear regression, and the ability of the array to capture the DSOW transport variability has been determined.

- **Chapter 5** deals with the SFB observations in the Denmark Strait from 1999 to 2003. After a summary over all research cruises and deployment activities (section 5.1), the following sections 5.2 and 5.3 give a descriptive overview of the observed time series with emphasis on both short and long term timescales.

  The observations are then analyzed to evaluate the governing mechanisms that control the Denmark Strait Overflow.

- **Chapter 6** investigates the hydraulically controlled component of the overflow, that is driven by the density gradient between the Nordic Seas and the North Atlantic ocean.

- The relation of the barotropic flow through Denmark Strait to wind stress forcing is discussed in **Chapter 7**.

- **Chapter 8** evaluates the upstream pathways to the Denmark Strait sill and investigates large scale coupling mechanisms with the Faroe Bank Channel overflow.

- In **Chapter 9**, a synthesis of density and wind stress forcing is proposed and will be merged with the observational evidence of large scale coupling mechanisms that may explain the observed variability and interannual decrease of the Denmark Strait overflow.

- **Chapter 10** gives an outlook to future observation plans and further investigations to establish long-term monitoring of the dense overflows, including the perspectives for remote sensing and in-situ measurements.

- Conclusions and a summary of the main results of this study are found in **Chapter 11**.

- The **Appendix** contains a complete glossary of all abbreviations and acronyms used in this thesis. All geographical locations are shown in Fig. 2.1 on page 27.

2. Denmark Strait Hydrography

2.1.   General circulation pattern

Across the Greenland-Scotland Ridge (GSR), warm surface waters of the North Atlantic Current enter the Nordic Seas in several branches. One of these is the Irminger Current (IC) / North Iceland Irminger Current (NIIC, Fig. 2.1 [1]), which flows through Denmark Strait between Iceland and Greenland (for a review, see HANSEN AND ØSTERHUS, 2000).

From the Nordic Seas, cold, low-saline surface waters of the East Greenland Current (EGC, Fig. 2.1) flow southward along the east Greenland coast through Denmark Strait into the Atlantic. Additionally, sea ice is exported by the EGC from the Arctic Ocean. Its gradual melting contributes to the low salinity characteristics of the EGC.

Dense waters, that are formed in the Nordic Seas due to air/sea interaction, enter the Atlantic across the sills between Greenland, Iceland, the Faroe Islands and Scotland. For these deeper layer currents, topographical restrictions play a major role.

The Denmark Strait Overflow (DSO, Fig. 2.1) flows across the roughly 600 m deep Denmark Strait sill. Downstream of the sill, it descends rapidly along the East Greenland shelf edge, and forms the deepest part of the North Atlantic Deep Water (NADW; SAUNDERS, 2001).

The width of the part deeper than 300 m that can be occupied by the dense overflow water is larger than 100 km. Since the internal Rossby radius $R = \sqrt{g \frac{\Delta \varrho}{\varrho} H_2} / f$ is around 10 km (GIRTON, 2001) to 14 km (WHITEHEAD, 1998), the overflow dynamics are heavily influenced by Earth's rotation. The Denmark Strait may thus be considered as "wide strait" (WHITEHEAD, 1998).

A number of theoretical studies have been performed to describe the governing relations that limit the flow through sea straits (a.o. GILL, 1977; KILLWORTH AND MCDONALD, 1993; BORENÄS AND LUNDBERG, 1986; NIKOLOPOULOS ET AL., 2003, further details: see section 6.1).

---

[1] Legend to Fig. 2.1: *Explanation of moorings indicated on the map: Red + mark the ADCP moorings A, B, C at the sill, a red ▽ the upstream TP mooring and ✗ the Icelandic IS7 current meter mooring. Two PIES, that have been deployed halfway between ADCPs A and B, and B and C, respectively, have been omitted for clarity. Black symbols denote current meter moorings of previous studies:* △: *OVERFLOW'73 (*ROSS, *1984),* ⋆: *MONA (*AAGARD AND MALMBERG, *1978),* □: *"Lowestoft" arrays (*DICKSON AND BROWN, *1994). Violet* ◇ *mark positions of the Angmagssalik array 1986 – 2004 (*DICKSON ET AL., *2002;* DYE ET AL., *2004), mooring codes F1, F2, UK1, G1, UK2, G2 from northwest to southeast.*
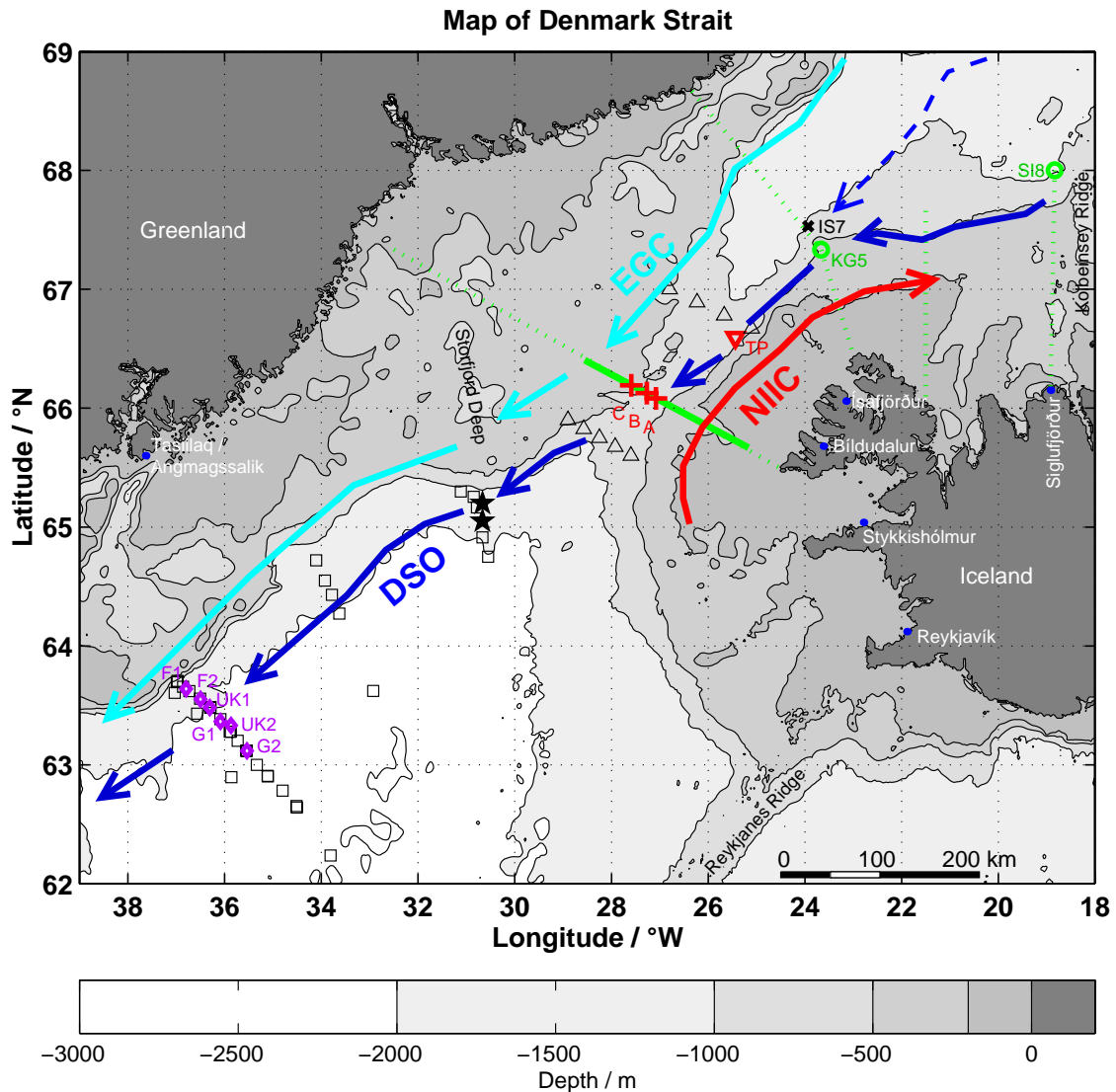
Figure 2.1.: *Map of Denmark Strait. Contours show* SMITH AND SANDWELL *(1997) topography. Current vectors indicate principal circulation pattern, following* HANSEN AND ØSTERHUS *(2000) and* JÓNSSON AND VALDIMARSSON *(2004a). EGC: East Greenland Current, NIIC: North Iceland Irminger Current, DSO: Denmark Strait Overflow. For orientation, this map shows all of the locations mentioned in this thesis. Dotted green lines denote hydrographic standard sections of Hafrannsóknastofnunin, named Látrabjarg, Kögur, Hornbanki and Siglunes from southwest to northeast. KG5, SI8 denote particular repeated stations. The bold green line across Denmark Strait sill on Látrabjarg section marks the central section regularly occupied by R/V Poseidon and Meteor on the SFB cruises. Explanations of mooring symbols, see footnote 1 on page 26.*
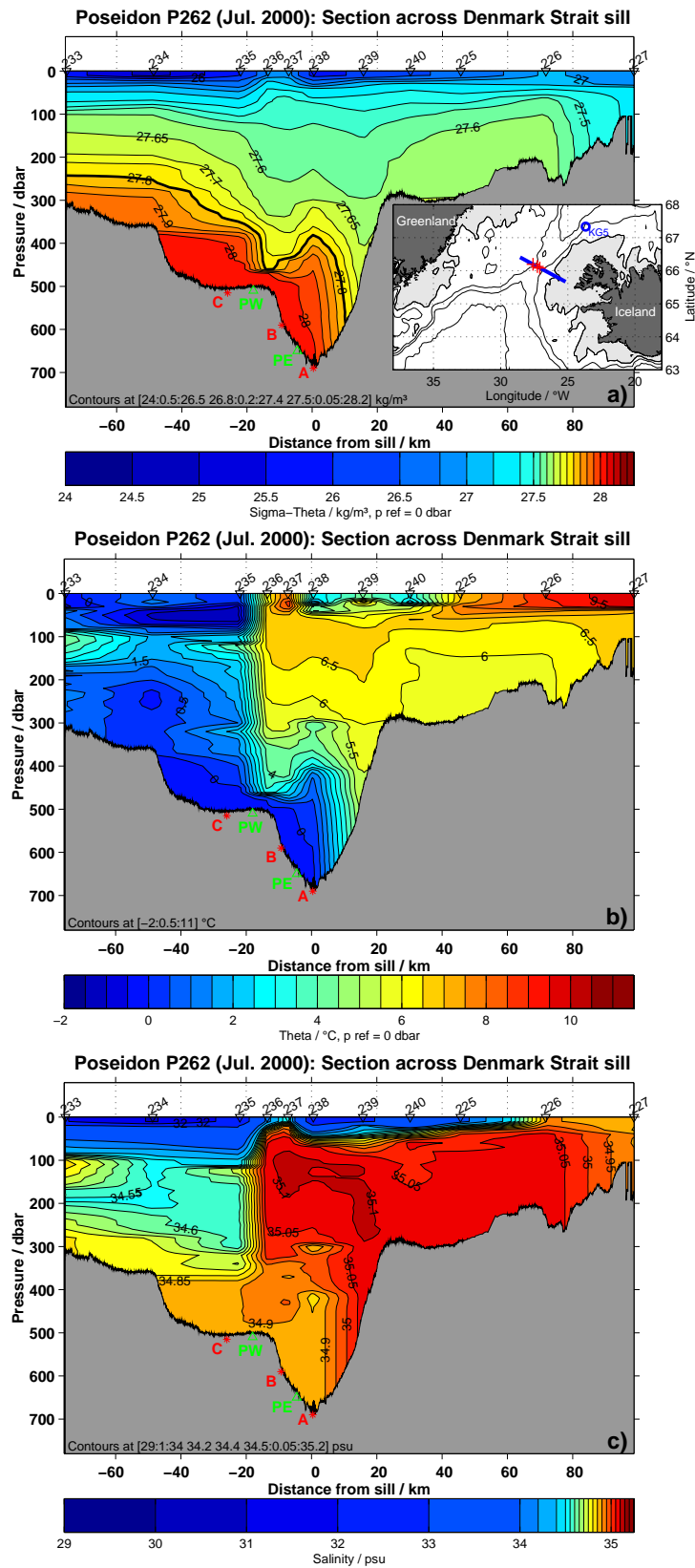
Figure 2.2.: *Hydrographic sections across Denmark Strait sill from R/V Poseidon cruise P262, 2000. Section location marked on inset map. Panel a: Potential density. Panel b: Potential temperature. Panel c: Salinity. Note the nonlinear colour scales in panels a and c to show the different water masses more clearly. Red ∗: ADCPs, green △: PIES.*

The typical features and water mass distribution for a section across the Denmark Strait sill is shown in Fig. 2.2. The hydrography is dominated by the three main water masses discussed above:

On the Iceland side of the Strait, warm, haline Atlantic Water (AW) of the NIIC (HANSEN AND ØSTERHUS, 2000) is flowing into the Nordic Seas. On the Greenland side, cold, fresh water masses of arctic origin are advected southward with the EGC (RUDELS ET AL., 2002). Below, dense water of low temperatures and intermediate salinity represents the Denmark Strait Overflow Water (DSOW), which downstream of the sill descends into the deep Atlantic (observations: e.g. GIRTON ET AL., 2001).

The dominant density contrast of 0.3 to 0.45 kg/m^3 (WHITEHEAD, 1998; GIRTON, 2001, respectively) between DSOW and the NIIC and EGC water masses is the major driving force for the exchange flow through the strait. Due to the effects of rotation, the dense overflow is banked to the Greenland side of the sill section (Fig. 2.2).

2.2. Water masses in the Denmark Strait

2.2.1. Sources of the Denmark Strait Overflow

In the literature, Denmark Strait Overflow Water (DSOW) has most often been characterized by potential density $\sigma_\Theta \geq 27.8$ kg/m^3 (DICKSON AND BROWN, 1994). This water occupies the deeper part of the Denmark Strait to the Greenland side, as visible in Fig. 2.2 a. It has an intermediate salinity ($S \approx 34.88$, as observed by R/V Poseidon in 2000) and low temperatures, which generally lie in the range of $-0.3\,°C$ to $+0.8\,°C$ (Fig. 2.2 b), but at times reach $1.5,°C$, as will be shown in the mooring time series (Fig. 5.4, page 68).

The origin and formation processes of the dense overflow water have been debated in water mass analyses by SWIFT ET AL. (1980), STRASS ET AL. (1993), MAURITZEN (1996a) and RUDELS ET AL. (2002).

Based on T/S and Tritium data, SWIFT ET AL. (1980) attributed most of the overflow to Polar Intermediate Water (PIW), formed in the Greenland Sea due to winter cooling, and Arctic Intermediate Water (AIW), which is produced by cooling in the Greenland and Iceland Seas.

From newer hydrographic data, STRASS ET AL. (1993) emphasized the formation of water with DSOW characteristics due to isopycnal mixing of Returned Atlantic Water (RAW) and Upper Arctic Intermediate Water (UAIW) in the Greenland Sea rather than the Iceland sea.

This view was questioned by MAURITZEN (1996a), since the production rates in the Greenland and Iceland Seas appeared to be too low to feed the overflows across the GSR. Based on a comprehensive review of hydrographic data sets and an inverse model (MAURITZEN, 1996b), a revised circulation scheme was suggested, where Atlantic Water (AW) is already gradually cooled on its northward way in the Norwegian Atlantic Current, and returns in Fram Strait as RAW (also referred to as Lower Arctic Intermediate Water, LAIW, $0\,°C < \Theta < 2\,°C$, $34.9 < S < 35.0$). A second branch passes through the Arctic Ocean, and joins the EGC as slightly

fresher Arctic Atlantic Water (AAW, also referred to as UAIW, $0\,°C < \Theta < 2\,°C$, $34.7 < S < 34.9$), being the primary source for the Denmark Strait Overflow.

In contrast to the long-distance advection of DSOW suggested by MAURITZEN (1996a), the role of local water mass modification and mixing processes in the Greenland and Iceland Seas and close to Denmark Strait was highlighted by RUDELS ET AL. (2002), who concluded, that the dense overflow is formed by diapycnal mixing of Polar Intermediate Water (PIW) and Iceland Sea Arctic Intermediate Water (IAIW) close to the sill. Referring to RUDELS ET AL. (2002), PIW represents the colder, less dense part of the thermocline of the EGC. IAIW in turn results from mainly isopycnal mixing of RAW and AAW in the Greenland Sea, and is further modified locally in the Iceland Sea.

Conspicuously, RUDELS ET AL. (2002) could not continuously track the RAW core in the EGC in the region just north of the Denmark Strait. From current meter and hydrographic observations, JÓNSSON AND VALDIMARSSON (2004a) found a direct pathway from the Iceland Sea to the Denmark Strait sill, which supports the importance of processes in the Iceland Seas. The assumption of a branch of the deep EGC, that is flowing through the Iceland Sea and along the north Icelandic shelf edge towards Denmark Strait sill would merge these findings. Recent model results agree with this theory (KÄSE, pers. comm.; KÖSTERS, 2004b). If this current is fed by a deep EGC branch flowing through the Iceland Sea, the findings of RUDELS ET AL. (2002) and JÓNSSON AND VALDIMARSSON (2004a) are not in opposition, though.

2.2.2. Irminger current and East Greenland Current

On the Iceland side of the section, warm ($T > 5\,°C$) and saline ($S > 35.0$) Atlantic Water (AW) is carried northward by the NIIC.

On the Greenland side, different water masses contribute to the southward flowing EGC. Much of the EGC part of the section is occupied by modified Polar Intermediate Water (PIW), following the definitions of RUDELS ET AL. (2002). This water mass, formed presumably by mixing of PIW and AW of the Irminger Current, is characterized by temperatures in the range $1\,°C < \Theta < 3\,°C$ and slightly higher salinities ($S > 34.5$).

Water masses of $S < 34.5$ and $\Theta < 0\,°C$ represent Polar Surface Water (PSW). This water mass, additionally fed by the freshwater flux due to ice melt, spreads far out to the Icelandic side in a thin layer at the surface. As is evident in Icelandic CTD[2] data at the Kögur 5 station (Fig. 6.12, page 105), this low-saline surface water exhibits a large seasonal cycle.

2.2.3. Θ/S properties observed on SFB cruises

Reasoning from any of the studies mentioned above, the Θ/S characteristics of the overflow do not only reflect property changes of the upstream source water masses,

---

[2]CTD: **C**onductivity-**T**emperature-**D**epth: Instrument lowered from a vessel to obtain vertical profiles of temperature, salinity and other properties.

but also depend on the actual mixing ratios of the different sources.

The SFB sections at Denmark Strait sill corroborate this conclusion. In Fig. 2.3, all CTD-profiles taken on the annual SFB cruises from 2000 to 2004 are shown in the Θ/S space.
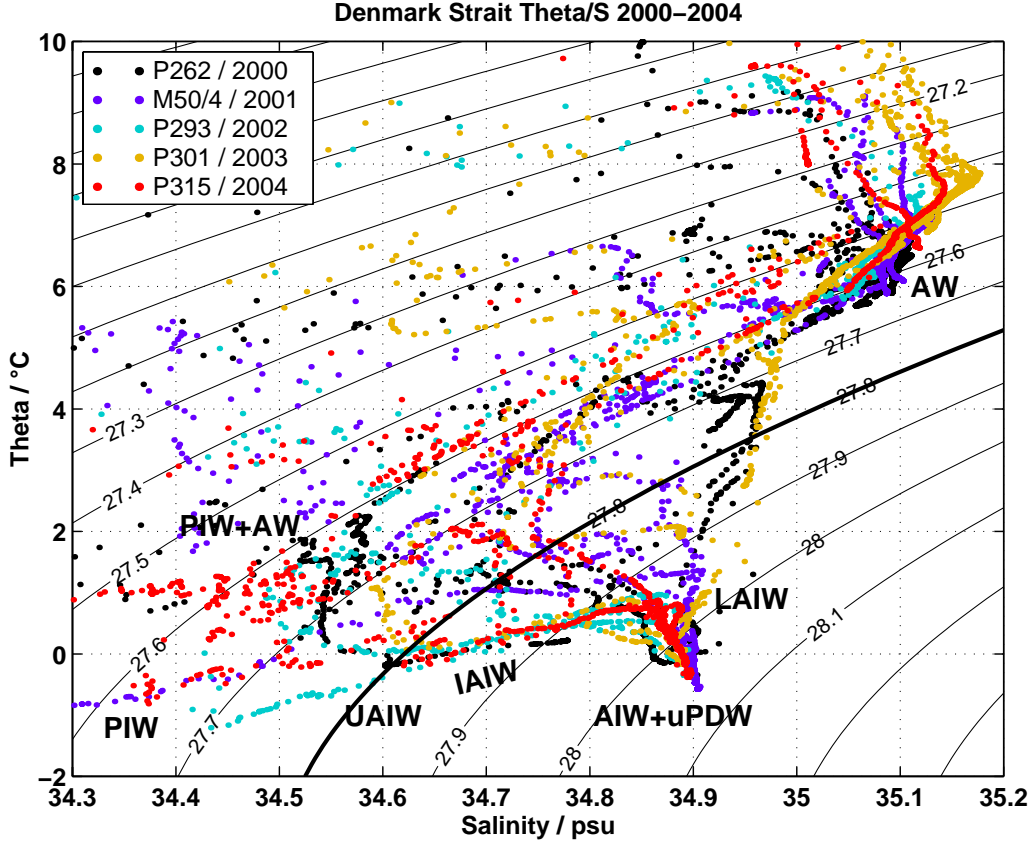
Figure 2.3.: Θ/S diagram for all sill sections. The $\sigma_\Theta = 27.8\,\mathrm{kg/m^3}$ isopycnal, typi-cally used as upper overflow boundary, is highlighted as bold line. Different colours denote the years 2000 - 2004. All stations on the central section contributing to the sections in Fig. 2.4 are shown on 2 dbar intervals. Water mass labels according to RUDELS ET AL. (2002). IAIW includes the range from UAIW to LAIW.

Above the dense overflow, in the density range $\sigma_\Theta < 27.7\,\mathrm{kg/m^3}$, PIW ($\Theta < 0\,°\mathrm{C}$), AW ($\Theta > 5\,°\mathrm{C}$ / $S > 35$) and a PIW/AW compound water mass ($1\,°\mathrm{C} < \Theta < 3\,°\mathrm{C}$ / $S > 34.5$; RUDELS ET AL., 2002) is present. Between the 27.7 and 27.6 isopycnals, a broad range of intermediate water masses indicates isopycnic mixing of PIW and AW (Fig. 2.3).

The densest part of the DSOW is fairly stable in Θ/S properties, compared with the larger variability above. According to RUDELS ET AL. (2002), it is a mixture of AIW and uPDW (upper Polar Deep Water, occupies the deeper parts of the Iceland Sea basin, $\sigma_\Theta > 27.97\,\mathrm{kg/m^3}$). From $\sigma_\Theta = 27.95\,\mathrm{kg/m^3}$ ($\Theta \approx +0.5\,°\mathrm{C}/S \approx 34.89$) to $\sigma_\Theta = 27.8\,\mathrm{kg/m^3}$ ($\Theta \approx -0.3\,°\mathrm{C}/S \approx 34.6$), the Θ/S characteristics match almost

exactly the RUDELS ET AL. (2002) definition of IAIW. The high temperature / salinity end of this range also represents the LAIW (RAW/AAW mixture) mentioned by MAURITZEN (1996a).

In the less dense part of the overflow ($27.8\,\mathrm{kg/m^3} < \sigma_\Theta < 27.95\,\mathrm{kg/m^3}$), the Θ/S characteristics are delimited by the IAIW on the cold/fresh side, and by mixing products between LAIW and AW on the warm/salty side. In between, all kinds of mixing products between LAIW/IAIW and the aforementioned waters of the PIW-AW range exist. There exists both high spatial variability (Fig. 2.3, consider the profiles of the same year, but taken at different positions on the section) and temporal variability (Fig. 2.3, consider profiles of different years).

Other, temperature-based definitions of the overflow ($\Theta < 2\,°\mathrm{C}$; ROSS (1984); or $\Theta < 3\,°\mathrm{C}$; SAUNDERS (2001)) include much of the less saline and hence less dense waters of the EGC (Fig. 2.2, page 28), which do not contribute to the descending plume.

2.3. Variability of circulation and water mass properties

Baroclinic instability mechanisms (first applied to the overflow by SMITH, 1976) lead to high spatial and temporal variability of the overflow. This is evident in five realizations of the central CTD section, as shown in Fig. 2.4. The location of the temperature and salinity fronts is highly variable due to the strong eddy activity in the Denmark Strait (for an extensive discussion, based on observations, see GIRTON, 2001). The horizontal extension of the warm, saline AW varies by around 50 km. In some of the sections (Fig. 2.4, M50/4, P301, P315), isolated intrusions of AW can be found in the EGC. This feature has already been observed by DEFANT (1931). RUDELS ET AL. (2002) assumes that most likely these AW lenses have been separated from the northward flowing NIIC in the strait.

The structure of the EGC is much less homogeneous than that of the NIIC, and reflects the different source water masses that are advected southward by the EGC. Water of lower salinity is regularly found over large parts of the upper boundary of the dense overflow. This low-salinity lid has also been observed downstream of the sill (RUDELS ET AL., 2002). Even in 2003, when the horizontal extent of AW was at its maximum, an isolated lens of low saline ($S \approx 34.65$) and cold ($\Theta \approx 0\,°\mathrm{C}$) water resembling IAIW properties was found on the upper boundary of the overflow.

Considering interannual changes, the large short-term variability in the Denmark Strait has to be taken into account, which aliases the sections taken once per year only. However, some consistent signals are evident in the hydrographic sections.

The AW has warmed by $\approx 1\,°\mathrm{C}$ from 2000 to 2003, coherent with a salinity increase by 0.05. This agrees with the seasonal Icelandic hydrographic surveys that showed stronger Atlantic inflow with higher temperatures and salinities during this time (VALDIMARSSON, pers. comm.). The larger AW extent and the increased temperature contrast between AW and the dense overflow might have consequences for
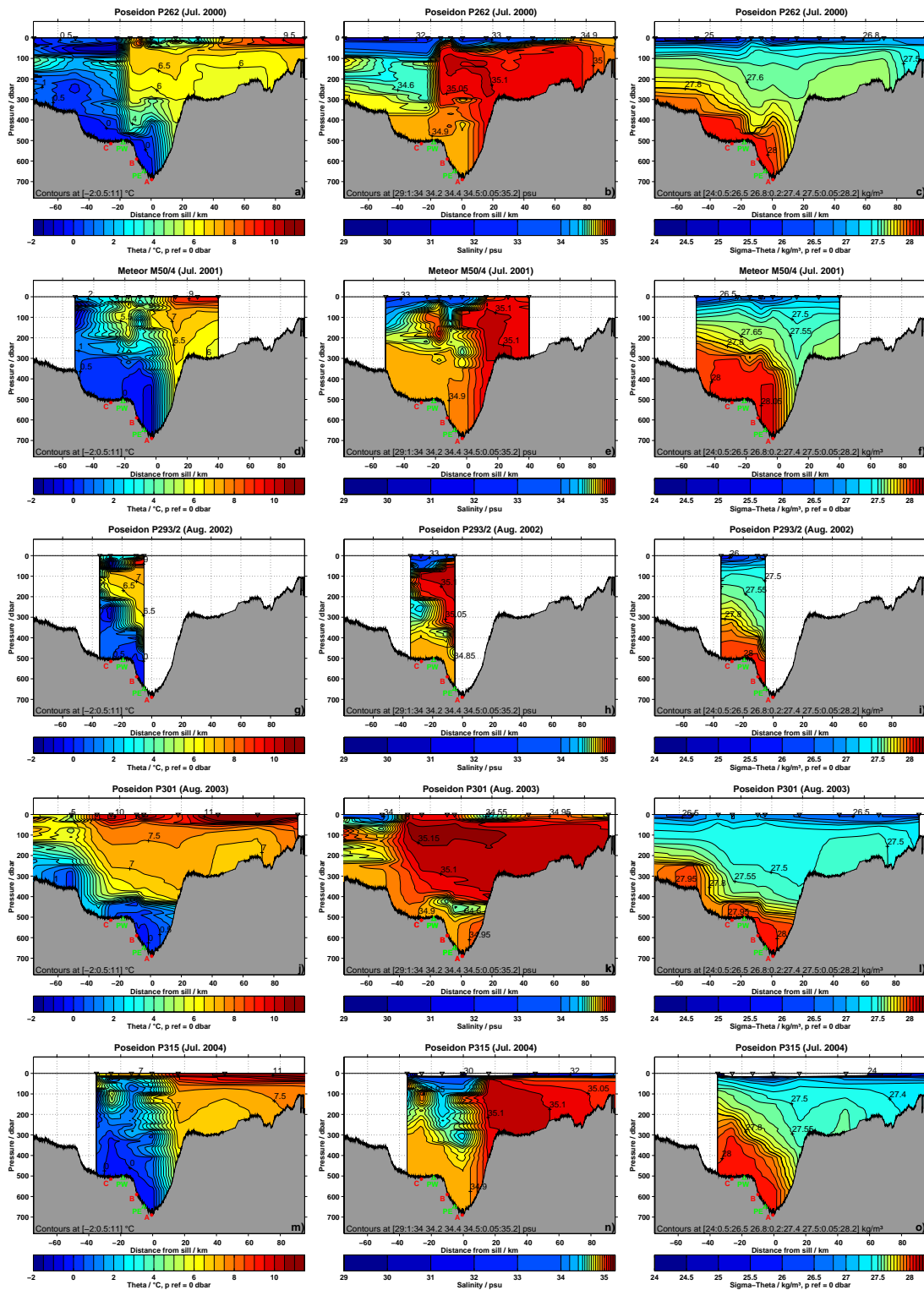
Figure 2.4.: *Central section across the Denmark Strait. All five SFB cruises since 1999, i.e. P262 (2000, panels a, b, c), M50/4 (2001, panels d, e, f), P293 (2002, panels g, h, i), P300/301 (2003, panels j, k, l) and P315 (2004, panels m, n, o). Left: Potential temperature. Centre: Salinity. Right: Potential density; $\sigma_\Theta = 27.8\,\mathrm{kg/m^3}$ marked as heavy line. Section location, colour scaling and mooring symbols similar to Fig. 2.2, page 28. For several cruises, the extension of the hydrographic sections is limited by sea ice, weather and cruise schedules.*

entrainment processes in the upstream approaches to the sill, as will be discussed in chapter 8.

The salinity of the dense overflow, typically in the range from 34.85 to 34.90, is spatially less homogeneous in 2003. Particularly in those regions, where AW is located directly above the overflow plume, dense water with higher salinity ($S > 34.90$) and higher temperature (in parts, Θ lies between 2 and 2.5 °C) exists. In the Θ/S diagram (Fig. 2.3, page 31), these direct mixing products of LAIW and AW are evident only in 2000 and 2003.

Short term variability prevents to derive long-term signals for the overflow water masses from these five cruises alone, but the enhanced Atlantic influence shall be considered in the discussion of the mooring time series (section 5.3 and chapter 8).

Associated with an overall freshening of the northern North Atlantic, DICKSON ET AL. (2002) observed a long-term salinity decrease of the Denmark Strait Overflow of 0.013 per decade. In the hydrographic profiles of the SFB cruises 1999 – 2003, the bottom values of salinity lie within the expected range [34.877 34.894], but do not show any significant long term trend (Fig. 2.3, page 31). Since the CTD data are taken once per year only, they are likely to be affected by the much larger short term variability. Even in DICKSON ET AL. (2002), the long-term freshening is superimposed by large variability on timescales of a few years, thus, a time series of just four years is too short to prove interdecadal trends.

2.4. Alongstream development

The time averaged spatial distribution of potential density *along* the overflow path for three subsequent Poseidon cruises is shown in Fig. 2.5. The pathway was identified by maximum density at the bottom and agrees well with the direct current observations and the centre of gravity overflow pathway estimate of GIRTON (2001). 80 km upstream of the sill, dense water ($\sigma_\Theta > 27.8\,\mathrm{kg/m^3}$) is piled up to a height of 300 m above the sill crest. On its way to the sill, the dense water height has decreased by $\approx 100\,\mathrm{m}$.

Further south, the plume descends along the topography with a fairly constant rate of 6 m/km between 50 and 250 km downstream of the sill, which agrees with the observations of GIRTON (2001). The highest current velocities were observed between 50 and 100 km downstream (GIRTON, 2001), a fact that is reflected by the low plume thickness in this region. Further downstream, the plume thickness increases, and flow speed decreases (GIRTON, 2001). This may be attributed to the reduced density contrast to the ambient water, which reduces the buoyancy forcing of the descending plume. Turbulent mixing reduces the maximum density at the bottom by around 0.1 σ_Θ units along the overflow path.

Further discussion about direct current measurements and downstream plume dynamics can be found in GIRTON (2001). The observed features discussed in this section are compared with the energy balance in the high-resolution process model in section 6.2.1.
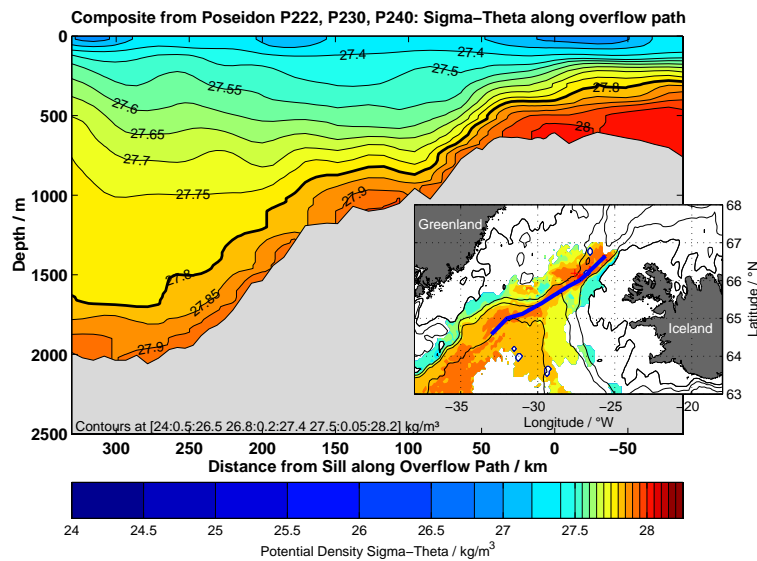
Figure 2.5.: *Hydrographic section along the overflow path. Objective analysis of three subsequent Poseidon cruises P222, P230, P244, covering different regions.* $\sigma_\Theta = 27.8 \, \mathrm{kg/m^3}$ *isopycnal marked by heavy line. Note decreasing density due to entrainment during the descent of the overflow plume. Inset map: Spatial coverage of hydrographic surveys indicated. Heavy line marks location of the section along the overflow pathway. Bottom density shaded with same colour range as in the main figure. Colour scaling similar to Fig. 2.2, page 28.*

Qualitatively, the descending isopycnals in Fig. 2.5 are suggestive for hydraulic control mechanisms. Quantitative tests in both the model and the observations (chapter 6) suggest, that the Denmark Strait Overflow is indeed hydraulically controlled.

2.5. Current structure at the sill

Despite of the large density contrast with steeply inclined pycnoclines across the sill section (Fig. 2.2, page 28), the structure of the current velocity is predominantly barotropic. This has been observed on various cruises. An extensive rapid survey with expendable probes by R/V Poseidon in 1998 confirmed, that the eddies, that dominate the variability, cover the entire water column. From vmADCP[3] sections, FRISTEDT ET AL. (1999) concluded, that the current at the sill behaves like a barotropic jet.

This structure has also been confirmed by vmADCP and LADCP[4] sections from the SFB cruises (Fig. 2.6). As expected, the northward flowing NIIC is evident on the eastern side; on the western side of the strait the EGC dominates with currents to the south-west. In addition to the highly barotropic current structure, a considerable near-bottom intensification of the outflow marks the dense overflow plume, that occupies

---

[3]vmADCP: vessel mounted ADCP, see appendix A.

[4]LADCP: Lowered ADCP, see appendix A.

the Greenland side of the section with an average thickness of $100 - 200\,\mathrm{m}$ (compare hydrographic section, Fig. 2.2, page 28).

It might be questionable, to which degree these patterns are influenced by tides, that have not been taken into account.

The observations of moored ADCPs revealed, that the barotropic M_2 tide is the dominant tide. During the time of the vmADCP sections shown in Fig. 2.6, the tidal currents at ADCP B had a typical peak-to-peak amplitude of $0.2\,\mathrm{m/s}$ (not shown). The range is consistent with an inverse model for barotropic tides (EGBERT AND EROFEEVA, 2002), which revealed, that the maximum tidal velocities at the sill reach $0.25\,\mathrm{m/s}$. Hence, the tides are much weaker than the maximum velocities in the vmADCP sections.

In contrast, the vmADCP sections (Fig. 2.6) exhibit barotropic in/outflow features with larger peak-to-peak amplitudes of $\approx 0.7\,\mathrm{m/s}$, associated with a horizontal length scale of $20 - 30\,\mathrm{km}$.

The entire section of $180\,\mathrm{km}$ took around 18 hours, and thus covered roughly 1.5 times the semidiurnal tidal cycle. Hence, the semidiurnal M_2 tides should be expected to project on a horizontal scale of $\approx 60\,\mathrm{km}$. The apparent variability on $20 - 30\,\mathrm{km}$ scales are thus likely to indicate barotropic eddy activity. They agree well with the spatial extent of eddies observed in 1998 by GIRTON (2001).

The barotropic flow structure, combined with a notable near-bottom intensification of the current, has implications for the transport mechanisms of dense overflow water across the Denmark Strait sill:

While the alongstream baroclinic pressure gradient drives a deep current, that may be assessed with the theories of hydraulic control (discussed in chapter 6), the overflow may be additionally forced by barotropic mechanisms (discussed in chapter 7). Numerical experiments suggest, that the Denmark Strait Overflow may be considered as a linear superposition of a density driven baroclinic component and a wind driven barotropic part (KÖSTERS, 2004b).
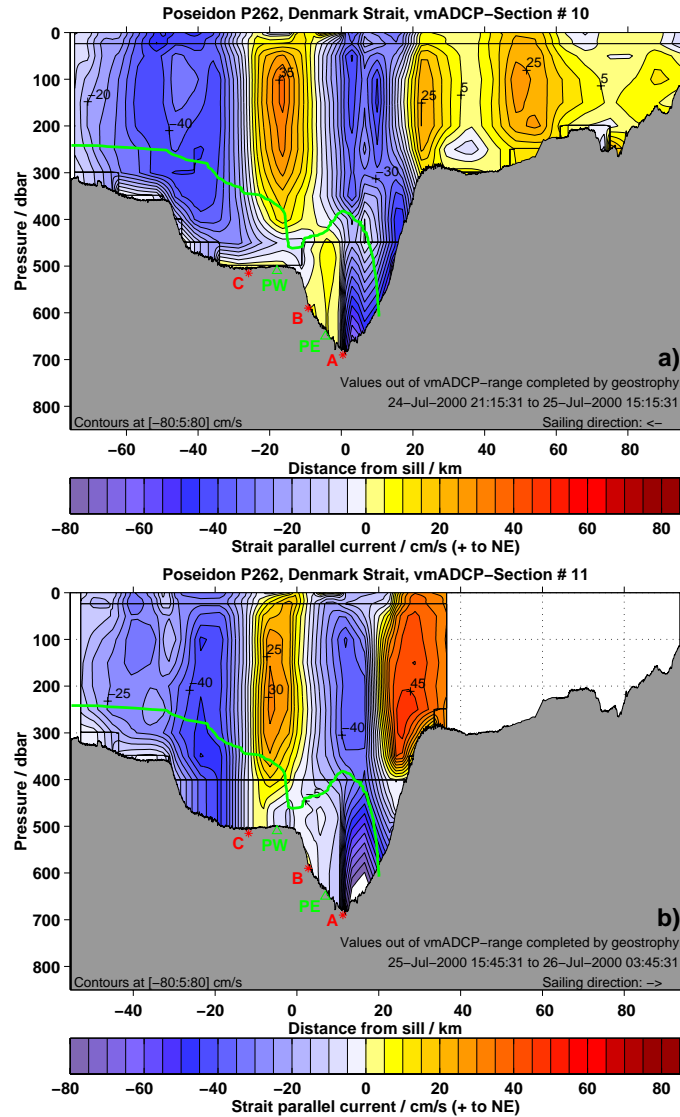
Figure 2.6.: *Examples of typical vmADCP sections across the sill, measured during R/V Poseidon P262, 2000. Blue marks outflow to the south-west, yellow and red inflow to the north-east. Current velocities out of the vmADCP range calculated with geostrophy inferred from CTD-profiles (Fig. 2.2, page 2.2). Transport estimates below the $\sigma_\Theta = 27.8\,\mathrm{kg/m^3}$ isopycnal (green line) yield values of $(2.4 \pm 0.5)\,\mathrm{Sv}$ (panel a) and $(3.3 \pm 0.5)\,\mathrm{Sv}$ (panel b), respectively.*

3. Observation methods

The main focus of the SFB project was to obtain continuous multi-year time series of the overflow by means of moored instruments. This chapter addresses the chosen observation strategy and the postprocessing methods applied to the data.

3.1. Observation strategy

The high spatial variability in Denmark Strait (shown in previous chapter) requires several moored instruments deployed at properly selected positions to obtain accurate overflow transport estimates.

Heavy fishing activities take place in parts of the Denmark Strait, which is a potential risk for loss of conventional taught wire moorings. At the sill section, this is particularly the case for the shallower part > 15 km northwest of the sill (VALDIMARS-SON, pers. comm.). Additionally, drifting sea ice of the East Greenland Current and icebergs pose danger on mooring parts close to the surface. This lead to the strategy of acoustical observation with instruments deployed at the bottom. All moorings deployed > 15 km northwest of the sill were protected against fishing by trawl-resistant shields[1].

In the Denmark Strait (maximum depth $\approx$ 600 m), bottom mounted Acoustic Doppler Current Profiler (ADCP) are capable of measuring current profiles of the entire water column.

Critical for DSOW transport observations is to obtain the thickness of the dense overflow plume. Bottom mounted instruments, though, can not measure directly the vertical Θ/S profile. The distinct stratification of light AW/PIW/PSW above the dense DSOW, however, allows for remote acoustical detection of the interface depth z_{int}:

1. Maximum of acoustic backscatter: Typically, suspended matter (e.g. plankton) accumulates in pycnoclines.

2. Maximum of current shear: Assuming geostrophic balance, an inclined pycnocline, which is normally observed in the Denmark Strait Overflow, is associated with a maximum in current shear.

---

[1] Two series of trawl-resistant shields were employed to accommodate ADCP and PIES instruments. Both types were developed at IFM-GEOMAR in Kiel.

For integrating geostrophic estimates, Pressure sensors / Inverted Echo Sounder (PIES) were deployed, which utilize the difference of sound velocity between DSOW and the warmer AW. From acoustic travel time bottom–surface–bottom, and actual bottom pressure, both interface depth and sea surface height (SSH) can be calculated with the assumption of a two layer system.

To ensure the best possible performance of the mooring array, and to obtain reliable error estimates, different configurations were simulated in a high resolution process model (KÄSE AND OSCHLIES, 2000) of the Denmark Strait, which are discussed in chapter 4.

3.2. Data processing

The postprocessing methods applied to the field data have been described in detail by MACRANDER (2001). For the integrity of this thesis, the most important steps are briefly outlined here.

3.2.1. ADCP data

Acoustic Doppler Current Profilers (ADCP) measure a vertical current profile of the water column, utilizing the Doppler frequency shift, that affects sound signals reflected by moving objects in the water (for technical details, see RD INSTRUMENTS, 1998). At the Denmark Strait sill with depths $< 650\,\mathrm{m}$, 75 kHz ADCPs are capable to scan the entire water column from bottom to surface. Depending on the reception time of the echoes, the resulting data are binned into depth cells, which, in case of the ADCPs deployed in Denmark Strait, were chosen to 16 m.

Besides the actual velocity data, ADCPs also record the acoustic backscatter amplitude for each depth bin. This allows to estimate the amount of suspended matter (e.g. plankton) in the water column.

3.2.1.1. Interface detection from maximum of current shear

Typically, the pycnoclines of the upper boundary of the overflow exhibit a large cross-stream slope, which in turn leads to maximum geostrophic current shear (for geostrophic balance of the overflow, see section 6.2.4). This is confirmed by the direct current observations (Fig. 3.1). The depth of maximum current shear has been obtained from the ADCP measurements as the maximum of the bin-to-bin difference of the strait-parallel current velocity v_p. The vertical resolution is thus given by the bin size of 16 m.

During periods with a distinct current shear (Fig. 3.1 a), the RMS error of each individual measurement equals approximately the bin size of 16 m. The uncertainties are larger (RMS error for each observation $> 100\,\mathrm{m}$) when the baroclinic component is less evident (Fig. 3.1 c).

Since the semidiurnal tides represent the fastest mode of physical variability (considering current velocity spectra, Fig. 5.2, page 64), a 5 hours low-pass filter conserves
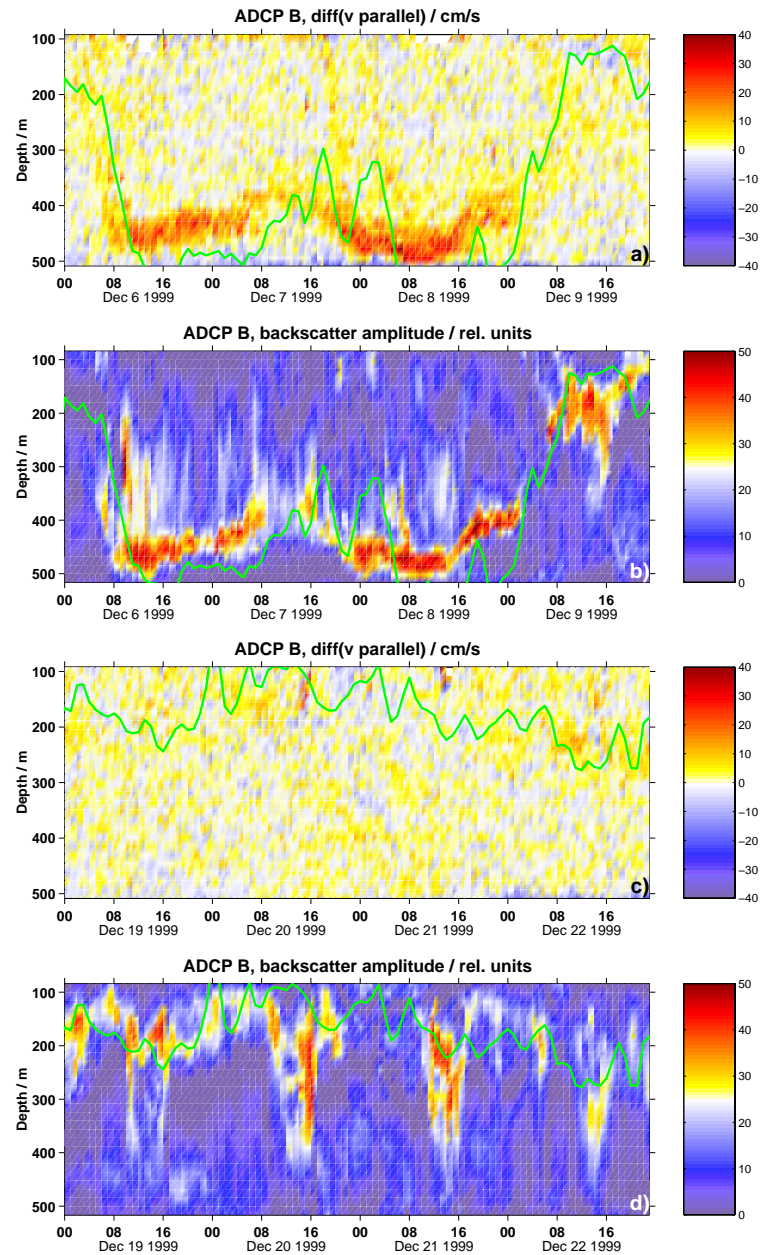
Figure 3.1.: *Example of ADCP B observations: Current shear (panels a,c) and acoustic backscatter(b,d). Green lines: DSOW/AW interface depth, obtained from PIES deployed in 500 m distance to ADCP B. Panels a,b: Typical period with large baroclinic shear. Panels c,d: Period with small baroclinic shear, and diurnal cycle of the maximum backscatter depth, likely associated with vertical excursions of plankton. Figure adopted from* MACRANDER *(2001).*

the physical variability, whereas the noise in interface depth detection is reduced due to averaging over several independent measurements. The resulting RMS error for each value is estimated to be 13 m [2]. A 40 hour low-pass filter was applied for de-tided estimates, reducing the RMS error to 2 m.

The method to determine the overflow plume thickness by current shear maximum has also been successfully applied to the Faroe Bank Channel (FBC) Overflow (HANSEN ET AL., 2001). Although the flow in the FBC is much more baroclinic than at the Denmark Strait sill, the current shear maximum is considered to be the best way to detect the upper DSOW boundary.

3.2.1.2. Interface detection from maximum of acoustic backscatter

Suspended matter, e.g. plankton, typically accumulates on pycnoclines. This leads to enhanced acoustic backscatter of the ADCP's ping. To identify these scattering layers, the background reflection of clear water has additionally to be taken into account. Since the amplitude of the backscattered signal decreases with distance, the coefficients of an exponential function $A + Be^{-Cz}$ have been empirically determined for each profile to obtain a "best fit" for the theoretical clear water backscatter profile (Examples shown in Fig. 3.2). Negative deviations from the fitted curve have been penalized by a factor of 10 to optimize its clear water characteristics. Scattering layers have then been identified by maximum positive deviations of the actual scatter amplitude from the exponential clear water fit.

During periods of large baroclinic current shear, a clear signal is typically found in the same depth range (Figs. 3.2 a, 3.1 b). During periods of weak shear, however, no clear backscatter maximum is found (Fig. 3.2 b). Occasionally, the maximum backscatter shows daily vertical excursions between the surface during the night and larger depths during daylight (Fig. 3.1 d, MACRANDER, 2001). During wintertime, the backscatter amplitudes are generally lower than in summer, which makes the determination of backscatter maxima less accurate. Both effects are likely attributed to biological activity.

In summary, acoustic backscatter is a valuable quantity to verify the results from maximum current shear or travel time measurements by PIES. For the construction of long-term DSOW transport time series, however, the depth of maximum current shear, which represents a kinematic criterion to define the overflow plume thickness, has been preferred.

3.2.2. DSOW transport calculation from ADCP data

In order to obtain the volume transport of DSOW from ADCP measurements, the strait-parallel current velocity v_p has been vertically integrated below the depth of maximum current shear z_{shearmax}. The resulting integral of transport density (units:

---

[2]RMS error estimate based on the normal distribution of the differences between consecutive values with $\sigma = 13$ m. This estimate does not account for any errors that may arise from differences between this kinematic interface definition and the depth of certain isopycnals.
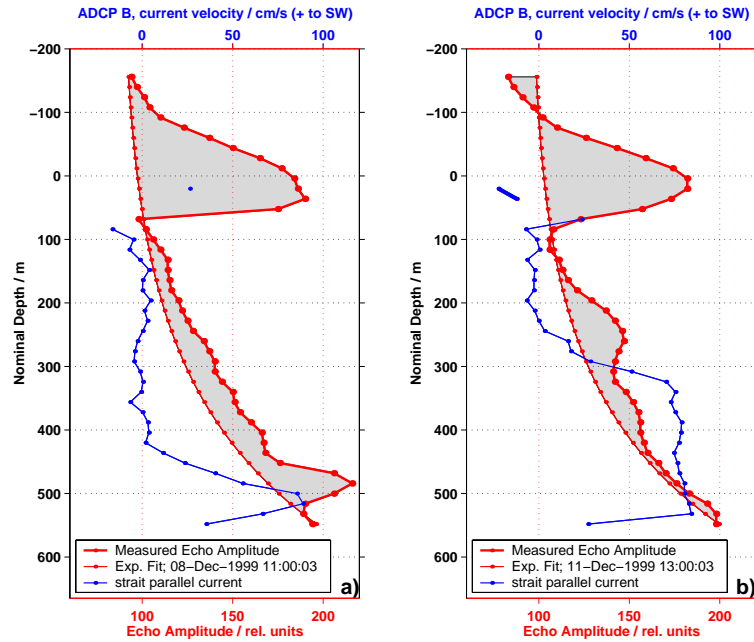
Figure 3.2.: *Two examples of vertical profiles of acoustic backscatter at ADCP B. In both panels, the heavy red line marks an individual profile of backscatter amplitude, whereas the thin red line is an empirical exponential fit for the "clear water" backscatter. The particle-associated backscatter is illustrated by grey shading. Dots denote individual bins. Positive deviations of the observed profile depict either the surface echo (*VISBECK AND FISCHER, *1995) or accumulated scattering matter. In blue, the strait parallel current profile is additionally shown. Panel a: Distinct maximum backscatter at a depth of 480 m, corresponding to a maximum current shear at the upper overflow plume boundary. Panel b: The overflow plume extends to a depth of 300 m; the backscatter maximum associated with the depth of maximum current shear is less well defined.*

m^2/s) has been multiplied with a horizontal scale width x_i for each instrument and summed over the entire array with N moorings:

$$Q_{\mathrm{ADCP}} = \sum_{i=1}^{N} x_i \int_{z_{bottom}}^{z_{\mathrm{shearmax}}} v_{p_i}(z)\, dz + Q_{\mathrm{offs}} \qquad (3.1)$$

The scale widths x_i and the correction term Q_{offs} resulted from a multilinear optimization of the array in a high resolution overflow process model (chapter 4).

Error estimates

Following, the errors in determining the DSOW transport with ADCPs shall be assessed.

Instrumental errors, associated with the uncertainties in current velocity measurements (1.9 cm/s per 10-ping ensemble), ADCP compass error ($\pm\ 5°$ at an inclina-

tion of 60°, RD INSTRUMENTS, 1998), and the uncertainties in the determination of the depth of maximum current shear (13 m for 5 hour low-passed time series), yield a total transport RMS error of 0.15 Sv for each individual value of 5 hours low-passed time series.

Array-configuration related errors: The dominant variability of the overflow on timescales of 2 – 10 days (Fig. 5.2) is associated with eddies. It depends on the mooring array configuration, how well this variability is captured. The numerical simulation yields RMS errors of 0.93 Sv for ADCPs A+B, and 1.20 Sv for B+C, respectively (see Table 4.2, page 58). For approx. 300 days of each deployment period and an integral time scale of 4 days, the time series includes 75 independent estimates (for details on error treatment, see EMERY AND THOMSON, 2001). The error of the mean transport is subsequently reduced by a factor of $\sqrt{75} \approx 8.7$ to the order 0.1 Sv.

Systematic errors: Small arrays will underestimate the true transport, since part of the flow occurs outside of the mooring array. The multilinear optimization in the process model provides an additional term Q_{offs} to correct for this systematical offset. It has been applied as an additive constant to match the temporal means of ADCP-estimated and actual transport in the numerical model, i.e. $\text{mean}(Q_{\text{DSOW(model)}}) = \text{mean}(Q_{\text{ADCP(model)}}) + Q_{\text{offs}}$. Since the actual transport in the real Denmark Strait might be larger than $\text{mean}(Q_{\text{DSOW(model)}})$, a multiplicative correction has also been tested. The differences are, however, smaller than 0.1 Sv.

Hence, the largest errors result from uncaptured spatial eddy-related DSOW transport variability. On longer timescales, the systematic error Q_{offs}, that has been derived from the numerical simulation, remains as the largest uncertainty. It depends on the assumption, that the process model realistically reproduces the spatial distribution of the overflow transport at the sill section (KÄSE ET AL., 2003).

3.2.3. Interface depth and SSH from PIES observations

As part of the SFB array, Inverted Echo Sounders (IES) with Pressure sensor (termed PIES) manufactured by the University of Rhode Island (URI) have been deployed for integrating geostrophic measurements.

PIES measure the two-way travel time t_{PIES} of an acoustic signal between bottom and surface. Additionally, the instruments are equipped with a pressure and temperature sensor, measuring bottom pressure p_{PIES} and temperature T_{PIES}. Further technical details can be found in UNIVERSITY OF RHODE ISLAND (2000).

The acoustic travel time t_{PIES} is given by:

$$t_{\text{PIES}} = 2 \int_{z_{\text{PIES}}}^{0} \frac{1}{c_s(S,T,p)} \, dz \qquad (3.2)$$

with c_s as sound velocity, which is a nonlinear function of salinity S, temperature T and pressure p (CHEN AND MILLERO, 1977).

Since sound velocity in water primarily depends on temperature, the acoustic travel time is a measure of the mean temperature of the water column. In the Denmark Strait, the cold overflow water ($T < 2\,°C$) and the warm AW ($T > 5\,°C$) are
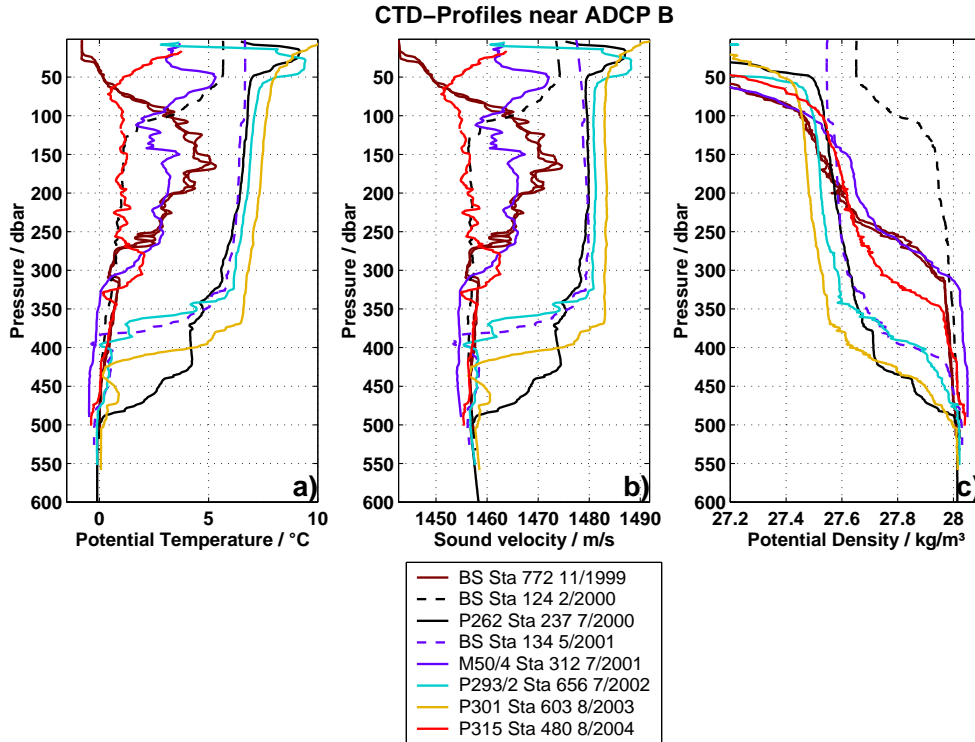
Figure 3.3.: *Hydrographic profiles close to ADCP B. Panel a: Temperature. Panel b: Sound velocity. Panel c: Potential density. Note the 2-layer sound speed characteristics for the profiles, where warm AW is situated above the DSOW. For cold EGC water conditions, the sound speed difference vanishes, although the density profile has similar 2-layer characteristics as for AW conditions.*

well approximated by a two-layer system (compare typical profiles, Fig. 3.3), with homogeneous temperatures and salinities in the upper and lower layers and a significant difference in sound velocity. When cold water of the EGC is above the overflow, the difference in sound velocity is much smaller (Fig. 3.3). During the PIES deployments 1999/2000, and 2000/2002, however, most of the time warm AW was observed above the DSOW.

Referencing equation 3.2 to pressure p instead of depth z, and introducing upper T_1, S_1 and lower T_2, S_2 layer properties, travel time is defined by

$$t_{\text{PIES}} = 2 \int_{p_{\text{PIES}}}^{p_{int}} \frac{1}{g\varrho(S_2, T_2, p)} \frac{1}{c_s(S_2, T_2, p)}\, dp + 2 \int_{p_{int}}^{0} \frac{1}{g\varrho(S_1, T_1, p)} \frac{1}{c_s(S_1, T_1, p)}\, dp \quad (3.3)$$

with pressure p_{int} at the interface depth, acceleration of gravity g and density ϱ as function of S, T and p (UNESCO International Equation of State IES80, described by FOFONOFF, 1985).

The distance between PIES and sea surface (i.e. water depth minus height of the PIES itself) D_{PIES} is then given by

$$D_{PIES} = \int_{p_{\mathrm{PIES}}}^{p_{int}} \frac{1}{g\,\varrho(S_2, T_2, p)}\, dp + \int_{p_{int}}^{0} \frac{1}{g\,\varrho(S_1, T_1, p)}\, dp \qquad (3.4)$$

With known temperatures and salinities of both layers, the system of equations 3.3 and 3.4 can be solved for the two unknowns D_{PIES} and AW/DSOW interface depth p_{int}. Since $c_s(S, T, p)$ and $\varrho(S, T, p)$ are nonlinear functions, the system has to be solved numerically, varying D_{PIES} and p_{int} to match the measured t_{PIES} and p_{PIES}.

For the lower layer, a linear T/S relation was employed to obtain S_2 in dependence of the bottom temperature T_2 that was measured by the PIES. Since the bottom mounted PIES does not measure the upper layer T/S properties, constant values of $T_1 = 6\,°\mathrm{C}$ and $S = 35.0$ derived from hydrography have been used for the AW. It might be argued that T_{PIES} underestimates the mean temperature of the lower layer. Therefore, the temperature contrast for both layers was varied systematically to obtain a realistic interface depth sensitivity for travel time and bottom pressure changes (MACRANDER, 2001). The values given above represent the best fit to minimize the differences between interface depth derived from PIES data, and the depth of maximum current shear and maximum acoustic backscatter of an ADCP, that in 1999/2000 was deployed just 500 m apart from a PIES. Fig. 3.4 (page 48) demonstrates the agreement between all three interface depth detection methods.

The absolute Sea Surface Height (SSH), which is relevant for the barotropic component of geostrophically balanced currents, can not be obtained from PIES, since the vertical position of the instrument relative to the geoid is unknown. Therefore, $D_{PIES} = \overline{D} + \zeta$ is separated into a mean depth $\overline{D}$ and fluctuating sea surface height anomalies ζ. The SSH anomalies ζ will later be used for geostrophic calculations, which, however, have to be referenced to direct current measurements (see section 6.2.4).

3.2.4. DSOW transport calculation from PIES data

At the Denmark Strait sill, the overflow is mainly in geostrophic balance. This has been verified for both the model and observations, using PIES measurements of SSH and the DSOW/AW interface depth (see Fig. 6.7, page 93).

The geostrophically balanced current velocity is given by

$$
\begin{aligned}
u &= -\frac{1}{\varrho f}\frac{\partial p}{\partial y} \\
v &= \frac{1}{\varrho f}\frac{\partial p}{\partial x}
\end{aligned}
$$

$$(3.5)$$

with pressure p, Coriolis parameter f and u, v as velocity components in x, y direction.

The horizontal pressure gradient $\nabla_h\, p = (\partial p/\partial x, \partial p/\partial y)$ includes both an external component given by the SSH slope $\varrho g\nabla_h\, \zeta$, and an internal component given by the vertically integrated density of the water column $\nabla_h \int_z^0 \varrho g\, dz$.

The assumption of a 2-layer system introduced in the previous section, allows to calculate the geostrophic current velocities of the upper (v_1) and lower (v_2) layer, using the MARGULES equation. Replacing the partial derivatives by finite differences, as obtained from instruments at two distinct positions, the following expression holds:

Upper layer:

$$v_1 = \frac{g}{f}\frac{\Delta\zeta}{\delta x} \tag{3.6}$$

Lower layer:

$$v_2 = \frac{\varrho_1}{\varrho_2}v_1 + \frac{\Delta z_{int}}{\Delta x}\frac{g}{f}\frac{\Delta\varrho}{\varrho_2} \tag{3.7}$$

with g as acceleration of gravity, Coriolis parameter f, and upper/lower layer densities ϱ_1, ϱ_2, respectively. The density difference is noted as $\Delta\varrho = \varrho_2 - \varrho_1$. SSH ζ and interface depth z_{int} is measured by e.g. moored PIES. Δx denotes the distance between the two observing instruments, and v the geostrophic velocity component perpendicular to the connecting line between both instruments.

Since the absolute height of the PIES relative to the geoid is unknown, the velocities have to be corrected by a constant offset, which may be obtained from independent current observations.

The DSOW transport is obtained by vertical integration of v_2 from bottom to interface z_{int} and horizontal integration over the distance Δx between the observation instruments.

Error estimates

Instrumental errors: The absolute accuracy of the Paroscientific pressure sensor of the PIES is ± 0.6 dbar, the resolution ± 0.002 dbar (UNIVERSITY OF RHODE ISLAND, 2000). The travel time measurement yielded an RMS error of 1.67 ms for one 12-ping ensemble mean. The resulting RMS error of the DSOW/AW interface depth is 52 m, which is primarily caused by the uncertainties of the travel time measurements. For 5-hours low-passed time series, the RMS error is reduced to 20 m, since the travel time measurements represent independent observations. The sea surface height is estimated with an RMS error of 0.039 m for each 12-ping ensemble mean, reduced to 0.013 m for 5-hours low-passed time series.

In 2001/2002, two PIES were deployed 5 and 17 km west of the sill. The uncertainties in interface and surface detection by PIES lead to errors of the 2-layer geostrophic transport estimates. A transport error of 0.12 Sv is caused by a low-pass interface depth standard deviation of 12 m for each PIES, 0.45 Sv is due to surface inclination errors of 9 mm. However, the actual mean has to be corrected by independent current observations, as PIES do not determine the absolute SSH gradient.

In addition to these instrumental errors, the natural variability of the Denmark Strait overflow is a challenge for geostrophic observations:

- The typically non-uniform slope of the DSOW/AW interface (see CTD-sections, Fig. 2.4, page 33) yields a non-uniform velocity field between the two observation positions. For standard applications with flat bottom and similar depths at

the endpoints, this is irrelevant due to the integrating character of geostrophic observations. In Denmark Strait with a complicated sloping bottom topography, this is a possible source for errors. The assessment of geostrophic estimates from hydrographic sections (section 6.2.5) reveals, that the non-uniform interface slope yields transport errors of O(0.25 Sv). Further uncertainties may result from a non-uniform external velocity component due to variable SSH.

- The (unknown) interface position outside of the array, in interaction with the irregular topography, may add an unknown additional DSOW transport volume.

As a rough estimate, integrating geostrophic transport calculations over a distance of O(50 km) to include the bulk of the overflow may yield transport errors of O(0.5 Sv) due to the effects of a non-uniform velocity field over sloping topography.

PIES deployments with a wide distance to integrate over a large part of the overflow have unfortunately not been recovered due to instrumental problems, though. Only in 2000 − 2001, two PIES could be recovered, allowing for geostrophic estimates. Here, the instruments were deployed 5 and 17 km west of the sill − thus, the transport outside of the array is likely to be the largest error source. This "small" PIES array yielded current estimates that were essentially similar to those of the local current at ADCP B, that was deployed halfway between both PIES (see section 6.2.4). Therefore, these PIES time series may be considered as "local" rather than integrating measurements, and the transport errors are similar to the error estimates of a single ADCP (see Table 4.2, page 58, for ADCP B ≈ 10 km west of the sill). For this configuration, the model simulation yields an RMS error between "observed" and actual transport of 1.22 Sv (correlation $r = 0.69$).

3.3. Validation of observation methods

In the field experiment, the accuracy of all three methods was validated in 1999/2000, when an ADCP and PIES were deployed only 500 m apart from each other. The time series allow to compare the interface depth estimates of (i) maximum current shear, (ii) maximum backscatter, and (iii) the two-layer sound propagation model for PIES observations.

The results of all three methods agree well (Fig. 3.4). The data show the large short term variability the Denmark Strait Overflow is known for (e.g. GIRTON, 2001). The interface depth exhibits typical vertical amplitudes of O(100m) and timescales of 2 − 10 days (as observed by ROSS, 1984). The mean depth of the upper overflow plume interface is (318 ± 63) m for (i) , (311 ± 67) m for (ii) and (313 ± 73) m for (iii). Moreover, the hydrographic observations (Fig. 2.4, page 33) agree well with the range established by the moored instruments. The values are highly correlated and prove the suitability of all three observation methods.

Effects of correlated variability of plume thickness and velocity
Both the plume thickness and the overflow velocity are highly variable (Fig. 3.5). On the timescales of tides (Fig. 3.5 b shows an example for ADCP B, 1999), no

Observations of ADCP and PIES at Position B: Interface Depths
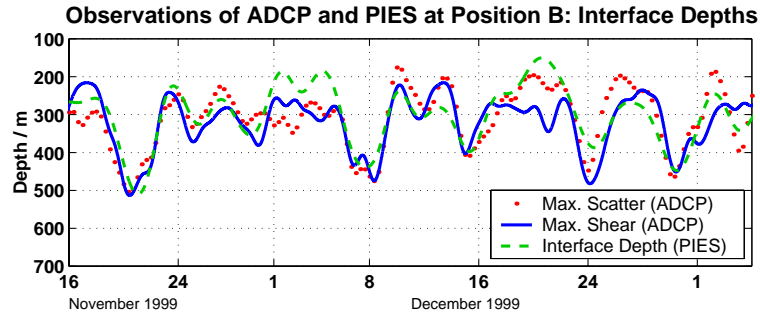
Figure 3.4.: *Test of three independent DSOW/AW interface detection methods. Both the depth of maximum current shear and maximum acoustic backscatter reveal the interface depth calculated from vertical travel time and bottom pressure data (PIES). Shown is a typical part (50 days) of the 1999/2000 time series with ADCP B and and PIES moored at the same location.*

significant correlation is evident. A quantitative analysis (not shown) revealed, that de-tiding of the interface depth and current velocity time series (with a 40 hours low-pass filter) yields DSOW transport errors $< 0.05\,\text{Sv}$.

On the timescales of the dominant eddy variability (2 – 10 days), plume thickness and current velocity at ADCP B are moderately anticorrelated (Fig. 3.5 a). Large current velocities are typically followed by minimum plume thickness a few hours later. However, the vertically integrated DSOW transport is at maximum during the times with fast current, since the thickness reduction does not outbalance the larger velocity. Separating plume thickness H_2 and strait parallel velocity v_p into mean $\overline{H_2}$, $\overline{v_p}$ and fluctuating parts H_2', v_p', transport estimates based on the mean integral $\overline{H_2} \cdot \overline{v_p}$ underestimate the actual transport by $\approx 5\,\%$ $(0.15\,\text{Sv})$, since $H_2' \cdot v_p' \neq 0$ due to the anticorrelation of both quantities.

To obtain realistic transport estimates, it is hence necessary to observe both plume thickness and current velocity.

Far downstream, e.g. in the Angmagssalik array (DICKSON ET AL., 1999), this may be different; preliminary results calculated with a fixed mean cross-section show consistent transport variability compared with transport data of the SFB array at the sill (DYE ET AL., 2004, see section 5.5).
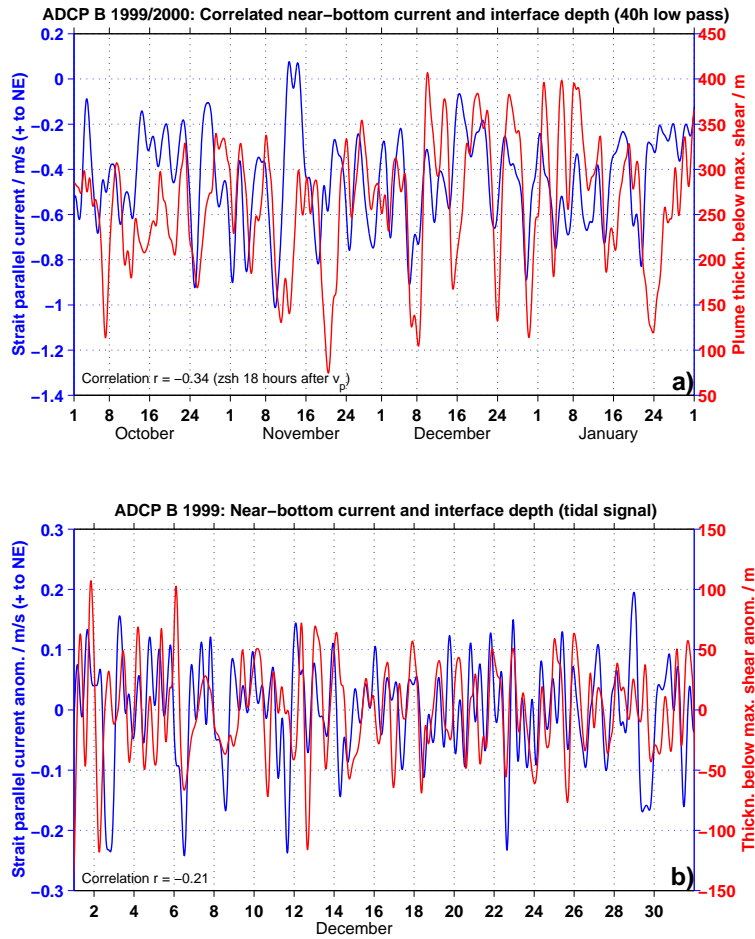
Figure 3.5.: *Correlated variability of current and interface depth at ADCP B. Panel a: 40 hours low-passed time series. Panel b: Tidal signal (5 h low-passed minus 40 h low-passed time series).*

4. Model Studies

The Denmark Strait Overflow is spatially highly variable, as shown in section 2.3. A small number of moored instruments can thus lead to large uncertainties in the determination of the actual DSOW transport volume. To find the best compromise between the number of instruments and transport estimate accuracy, a numerical process model of the Denmark Strait Overflow was used to simulate and optimize the acoustic observations.

4.1. High resolution process model

In this study, a high resolution process model of the Denmark Strait Overflow is employed. Details are discussed in KÄSE AND OSCHLIES (2000); here, a brief overview about the main features of the model is given. Table 4.1 lists the principal model parameters.

Table 4.1.: SPEM model parameters

Model parameter	Values
Horizontal grid	average 4.5 x 4.5 km resolution, curvilinear grid
Model area	$18 - 35\,°W / 62.8 - 69.5\,°N$,
	980 km along strait, 580 km cross strait
Vertical grid	31 equidistant bottom following σ levels
Boundary conditions	Closed boundaries at walls
	Free surface
	Land areas replaced by 150 m deep shelf seas
Equation of motions	Primitive Equations
Equation of state	Linear, only temperature dependent
External forcing	No surface fluxes, no meteorological forcing

The model is a version of the σ-coordinate Primitive Equation Model of Rutgers University (SPEM), documented by SONG AND HAIDVOGEL (1994). The model domain consists of a 940 km x 580 km area aligned along the axis of the strait. It has a horizontal resolution of approx. 4.5 km, with 31 bottom-following σ-levels.

The topography is a slightly smoothed version of the real topography of the strait to avoid excess errors due to numerical inaccuracies of the pressure gradient term, but the principal topographic features of the Denmark Strait are kept. The land areas
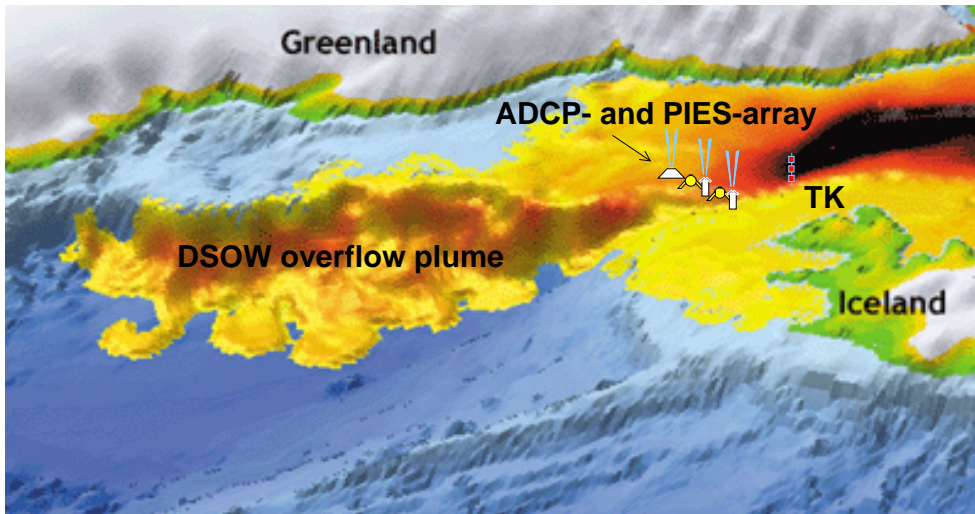
Figure 4.1.: *Denmark Strait overflow plume in the process model. Black and red denote large thickness of water colder than 2 °C, the thinner edge of the plume corresponds to yellow shading. After a "dambreak" at the sill (see text), a dense plume descends along the Greenland shelf edge. Note the formation of eddies, that agree with observations. SFB mooring array at the sill overlaid. Figure from C. Begler, IFM-GEOMAR Kiel.*

of Greenland and Iceland are replaced by shelf seas 150 m deep to avoid numerical problems with the σ coordinates at coastlines. Despite of this modification, the deep overflow is realistically reproduced.

In contrast to large-scale ocean circulation models, the KÄSE-OSCHLIES model is able to properly reproduce eddies (Fig. 4.1). This is important for realistic modelling of the overflow dynamics, since the horizontal grid resolves the Rossby-Radius of deformation, which in the Denmark Strait lies in the range of 10 km (GIRTON, 2001) to 14 km (DICKSON ET AL., 1990; WHITEHEAD, 1998). The downstream descent of the plume, and the generation of eddies compare well with observations (KÄSE ET AL., 2003).

Although the model has no meteorological forcing, the principal overflow characteristics are well represented, since windstress forcing is likely more important on interannual timescales (see chapter 7). Fig. 4.2 compares observed and modelled current profiles at the position of ADCP B at the sill. Both model and observations reveal a bottom-intensified current. Some differences are evident, e.g., the barotropic outflow is weaker in the model due to the missing barotropic forcing, and the closed model domain, that allows no barotropic net-flow over the sill. Further, the representation of the frictional near-bottom layer differs between model and observations. However, the overflow pathway, current velocities, plume thickness, spatial and temporal scales of variability and eddy scales are generally consistent with observations (GIRTON ET AL., 2001; KÄSE ET AL., 2003).

The density contrast between DSOW and AW responsible for the exchange flow
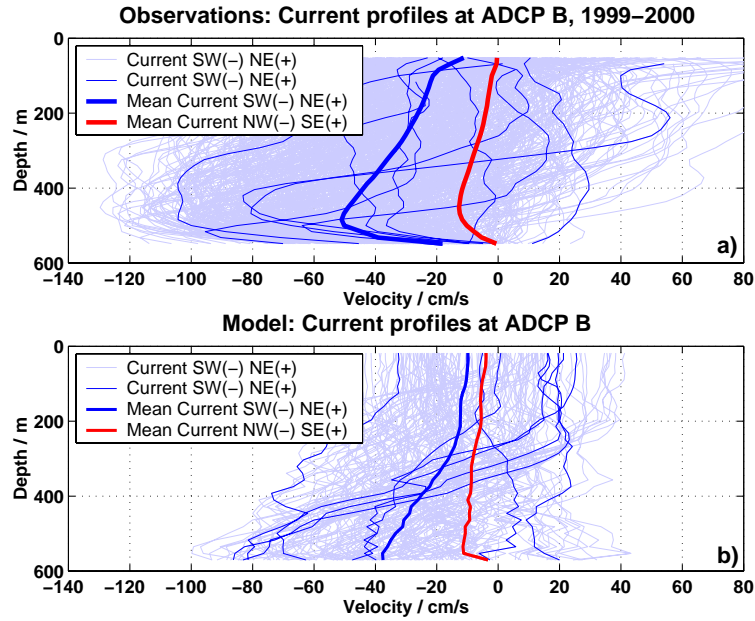
Figure 4.2.: *Vertical profiles of strait-parallel current velocity (positive: to the north-east). Panel a: Observations of ADCP B. Bold lines indicate mean profile, light blue lines mark range of variability. Narrow dark blue lines represent an arbitrary selection of individual profiles. Note, that the most distinct baroclinic shear occurs, when the surface currents are weak and the plume thickness is low (for discussion, see section 6.2.4). Panel b: As above, but for the process model. The frictional bottom layer is less well represented as in the observations. In both panels, bold red lines mark the mean cross-strait component.*

is realized by a linearized equation of state where density is entirely defined by temperature:

$$\varrho = \varrho(T) = 1027.95 \frac{\mathrm{kg}}{\mathrm{m}^3} - 0.08 \frac{\mathrm{kg}}{\mathrm{m}^{3\circ}\mathrm{C}} T_{\circ\mathrm{C}} \tag{4.1}$$

Different model runs have been studied, varying friction parameters and dense water sources. The experiments included steady sources at different upstream locations and "dambreak" experiments, where the sill is opened at $t = 0$, releasing an outflow of the dense water initially impounded in the upstream basin.

In the steady source experiments, dense water inflow was prescribed at a constant rate either at the northern boundary or at arbitrary positions in the interior of the upstream basin. The circulation in the upstream basin is influenced by the location and nature of the dense water source. In particular, the observed pathway along the Icelandic shelf edge towards the sill (JÓNSSON AND VALDIMARSSON, 2004a), i.e. the left-hand wall, is not reproduced in some of these experiments, which might be attributed to a changed potential vorticity (PV) in the upstream basin. HELFRICH AND PRATT (2003) showed, that the PV balance determines, from which side of the

basin the sill is approached (further discussion: chapter 8).

KÖSTERS (2004b) investigated the effects of different sources. Continuous flow along the left-hand wall was realized by an interior downwelling source, whereas flow along the right-hand wall (the Greenland side) was realized by a horizontal inflow at the northern boundary. A spin-down experiment with no dense water source in the upstream basin exhibited left-hand wall flow during the first 35 days, before substantial changes in the upstream flow structure occur.

The model results shown here used for the mooring array optimization result from a "dambreak" spin-down run of 32 days without a dense water source in the northern basin. It is initialized with a temperature contrast of $6\,°C$ between the warm AW ($T = 5\,°C$) and the overflow water ($T = -1\,°C$), which leads to a density contrast of $\Delta\varrho = 0.48$ kg/m^3.

Initially, dense water is located north of the sill in a depth larger than $150\,m$, and light water everywhere else. The model domain is closed, there are no sources or sinks of dense or light water. At time $t = 0$, the "dam" at the sill is removed and dense water spills over the sill into the southern basin, moving along the Greenlandic shelf edge, influenced by the effects of rotation. For at least 32 days, a realistic overflow occurs in the model; later, decreasing upstream reservoir height and fill-up of the downstream basin lead to ceasing overflow.

At least for the first 32 model days, which have been used here, plume pathway, velocities and eddy dynamics of the model are comparable to those observed in the field studies(KÄSE ET AL., 2003; GIRTON, 2001). In addition, the upstream pathway confirms recent findings of JÓNSSON AND VALDIMARSSON (2004a), who showed from observations, that a large contribution to the overflow approaches the sill in a current confined to the Icelandic shelf break (for details, see chapter 8).

The "Icelandic side pathway" is confirmed by the DSOW transport streamfunction in the model (Fig. 4.3 a). At the sill the flow is confined to a narrow band; $> 80\,\%$ of the average dense water transport occurs in a zone $< 50\,km$ wide. Due to recirculations, the DSOW transport contribution across the Greenland shelf north-west of the sill is less than $1\,Sv$ (Fig. 4.3 a).

The height h_{int} of dense water above the sill (Fig. 4.3 b) is around $500\,m$ in the interior of the upstream basin. In equivalent hydraulic transport units ($0.5\,g'h_{eff}^2/f$, KILLWORTH AND MCDONALD, 1993, see section 6.1), this would correspond to a theoretical maximum transport of $4.4\,Sv$ [1]. Along the Icelandic shelf break, where most of the transport towards the sill takes place, the dense water height decreases rapidly in cross-flow direction. Thus, upstream reservoir height measurements (e.g. by mooring "TP", Fig. 4.3) depend heavily on the actual location of the flow.

---

[1]WHITEHEAD (1998) stated a lower transport bound of $3.8\,Sv$ due to a significantly lower density contrast of $\Delta\varrho = 0.3\,kg/m^3$ (DICKSON ET AL., 1990). The assumed reservoir height was slightly larger ($580\,m$, DICKSON ET AL., 1990), though. In the model, $\Delta\varrho = 0.48\,kg/m^3$ has been used, based on hydrographic data of the SFB observations.

Model: Stream Function (Ave.); DSOW currents: actual (blue), 2–l geostr. (red)

Model: Height of interface above sill; DSOW transport vectors
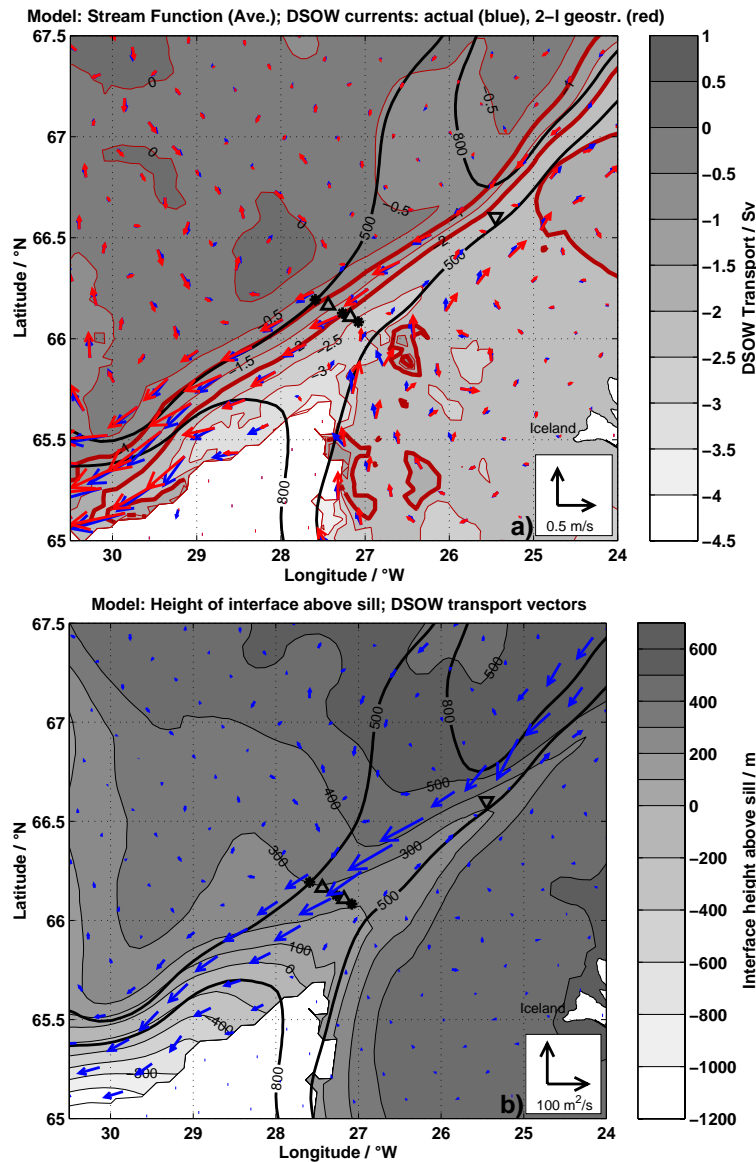
Figure 4.3.: *Panel a: Average DSOW transport streamfunction and DSOW current vectors in the model. Integrated and time-averaged DSOW transport streamfunction below the 1.88 °C isotherm (i.e. 27.8 kg/m³ isopycnal) contoured. −1 and −2 Sv contours highlighted as bold lines to denote the overflow pathway. Blue vectors indicate actual mean DSOW current, red vectors show geostrophic currents calculated from 2-layer geostrophy. Panel b: Height of the 27.8 kg/m³ isopycnal above the sill crest (depth: 600 m). Note the decreasing height in the pathway towards the sill. In the white areas, dense water is absent during the entire model run. High values on the Icelandic shelf area are an artifact of the model initialization, this water, however, does not contribute to the dense overflow (consider the streamfunction, panel a). Blue vectors represent averaged DSOW transport in m²/s. In both panels, bottom topography is indicated by heavy contours for the 500 and 800 m isobaths. Field experiment mooring positions: ● ADCPs A, B, C; △ PIES; ▽ TP.*

4.2. Simulation of acoustic observations

GIRTON (2001) and KÄSE ET AL. (2003) showed, that the model is capable to re-alistically reproduce the overflow. Therefore, it has been considered suitable for a simulation and optimization of the observation strategy for the field experiment.

For this purpose, both ADCP and PIES measurements were simulated in the model, and the resulting "measured" transport time series were compared with the known true model transport.

For direct current observations, transport estimates Q_{simADCP} can be calculated for an array with N instruments using multilinear interpolation, equivalent to

$$Q_{\text{simADCP}} = \sum_{i=1}^{N} x_i \int_{D}^{z_{\text{int}_i}} v_{i\text{p}} \, dz \qquad (4.2)$$

with water depth D, upper DSOW interface depth z_{int_i}, v_{ip} as measured current velocity parallel to the strait, x_i as a horizontal scale width and i as index for the N instruments. All x_i were determined using multilinear regression, and were optimized in a least square sense to minimize the variance σ^2 between the "measured" Q_{simADCP} and the known total DSOW transport Q_{model} in the model, defined by the transport below the $T = 1.88\,^\circ\text{C}$ isotherm (corresponding to the $\sigma_\Theta = 27.8\,\text{kg/m}^3$ isopycnal):

$$\sigma^2(Q_{model} - Q_{\text{simADCP}}) = \min \qquad (4.3)$$

Additionally, the mean difference between Q_{simADCP} and Q_{model} was determined as a systematic offset Q_{offs} due to unresolved flow outside the array:

$$Q_{\text{offs}} = \overline{Q_{model}} - \overline{Q_{\text{simADCP}}} \qquad (4.4)$$

The correlation between "measured" and actual transport is a measure for the performance of the array to capture transport fluctuations.

With simulated ADCPs and PIES at all 130 model gridpoints on a cross section at the sill, the overall RMS transport error is $< 5\,\%$ for ADCPs and interface detection by sound speed criteria (Fig. 4.4, light red line), $< 8\,\%$ for ADCPs and interface detection by maximum current shear, and $< 12\,\%$ for geostrophic estimates from simulated PIES, which demonstrates the principal suitability of the underlying concept. The temporal variability is captured with a correlation of 0.99 for ADCPs and 0.95 for geostrophic PIES measurements.

In the actual optimization procedure, the optimum positions for mooring arrays with 1 to 4 instruments were determined by multilinear regression, varying system-atically location on the cross-sill section, spacing between the moorings, and total number of instruments. As a measure of performance, for each configuration the fol-lowing quantities were determined:

- Variance σ^2 between "measured" and true transport.

- Systematic underestimate Q_{offs}, resulting from unresolved flow outside of the mooring array.
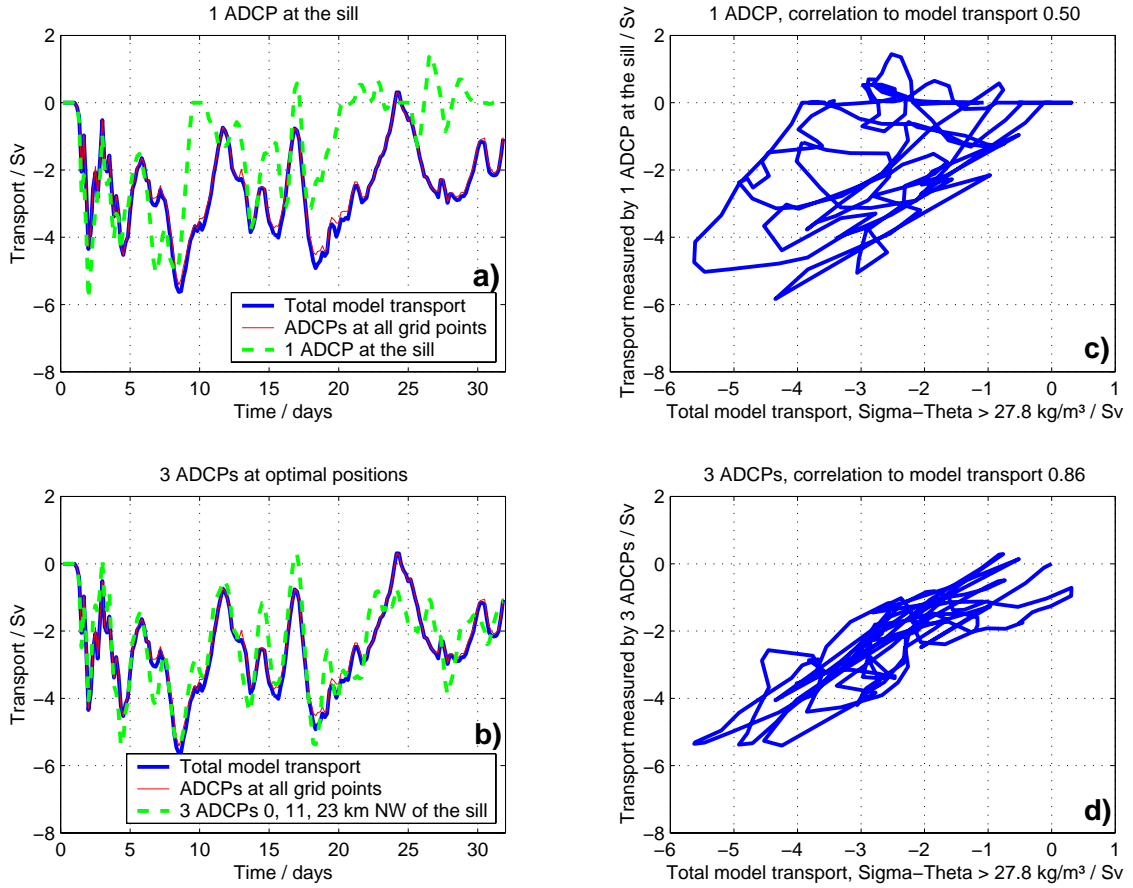
Figure 4.4.: *Model: Actual DSOW transport, compared with simulated observations of ADCPs and PIES at different locations. Panels a and b: Time series. Heavy blue line depicts actual DSOW transport, integrated across the entire sill section below the 1.88°C isotherm (corresponding to $\sigma_\Theta = 27.8\,\mathrm{kg/m^3}$). Light red line: Transport as determined by simulated ADCP and PIES at every gridpoint. Dashed green lines: Transport as determined by multilinear regression for ADCP arrays at positions given in the panel legends. Panels c and d: Scatter plot illustrating the correlation between actual and "measured" transport for a one-instrument configuration (top panels) and the optimized 3-ADCP-array. Correlation coefficients $r = 0.50$ (for one ADCP) or $r = 0.86$ (optimized 3-ADCP-array).*
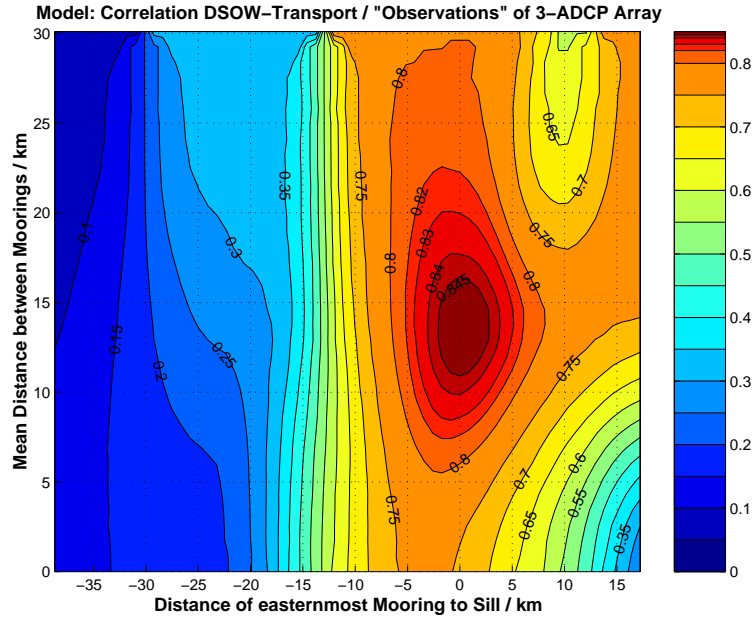
Figure 4.5.: *Model: Multilinear optimization of moored ADCP arrays. In the figure, the correlation between actual and "measured" transport is contoured for three-ADCP arrays with varying position of the easternmost mooring (x-axis) and spacing between the moorings (y-axis). The maximum at $(0, 14)$ km represents the best choice for overflow observation with three ADCPs.*

- Correlation between "measured" and true transport.

For any given number of instruments, all possible configurations were tested. Fig. 4.5 depicts the correlation for a 3 ADCP array as a function of the distance of the easternmost mooring to the sill location (x-axis) and the mean distance between the instruments (y-axis). The contours show a clear correlation maximum of 0.87 at location $(0,14)$ km. The best results are therefore obtained with the first instrument at the deepest part of the sill and the others at the Greenland slope separated by 1.5 times the Rossby-radius distance. Further investigations revealed, that the optimum 3-ADCP-configuration is achieved with instruments placed 0, 11 and 25 km northwest of the sill.

Similarly, arrays with 1, 2, or more instruments were investigated. For arrays with 1, 2, 3, and 4 ADCPs, the optimum results are listed in Table 4.2.

For one instrument, the correlation maximum between "measured" and true transport is just ≤ 0.69, unresolved spatial fluctuations yield a high variance of $Q_{model} - Q_{\text{simADCP}}$ (RMS standard deviation $\sigma = 1.22$ Sv) as best estimate for a single ADCP 10 km west of the sill. Another example, resembling the single ADCP "A" at the sill, is shown in Fig. 4.4 a, c. An additional device raises the correlation to 0.80, but still, $\sigma = 0.93$ Sv is caused by the flow across the Greenlandic shelf not covered by the array. The optimized 3-ADCP-array (correlation 0.865, $\sigma = 0.69$ Sv,

Table 4.2.: Model results of multilinear regression between simulated ADCP observations and known total model DSOW transport.

ADCP positions dist. NW of sill	deployed in field exp.	scale widths $x_i(W \leftrightarrow E)$ / km	correlation	std dev Sv	Q_{offs} Sv
[0] [A]	2003 − x	[22.6]	0.50	1.49	1.23
[10] [≈ B]		[26.1]	0.69	1.22	0.71
[11 0] [B A]	99-01 + 02-03	[21.9 12.4]	0.80	0.93	0.36
[25 11] [C B]	2001 − 2002	[10.5 24.0]	0.64	1.20	0.49
[25 11 0] [C B A]	2002 (May-Aug)	[14.0 15.5 13.9]	0.865	0.69	0.13
[45 27 13 2]		[31.7 17.8 11.7 17.2]	0.91	0.57	0.11

Fig. 4.4 b, d) was implemented in the field experiment. However, due to instrument failure only 2 ADCPs were operational most of the time (periods indicated in Table 4.2).

With more than 3 resources, the gain in correlation is smaller, since 3 ADCPs already cover more than 90 % of the total dense water transport with a resolution close to the internal Rossby radius of 10 km.

Concluding, the numerical simulation of observations proved as a useful approach to optimize the deployment configuration for the field experiment, and to evaluate the performance of the chosen 2 and 3 ADCP arrays to measure the Denmark Strait Overflow.

5. Observations in the Denmark Strait

5.1. Overview of cruises and deployments

Since 1996, numerous cruises of research vessels have been conducted in the framework of SFB TP A1 (see Table 5.1 [1]).

The first two cruises (P222, P230) investigated the downstream pathway and dynamics of the overflow plume in the Irminger Sea. On P244, rapid sections with XCTD[2] and XCP[3] were carried out close to the sill; the results are discussed in detail by GIRTON (2001).

Beginning in 1999, moorings were deployed at the Denmark Strait sill to obtain continuous time series of the overflow.

While the DS-1 ADCP "A", which forms an integral part of the SFB array, is maintained by Hafrannsóknastofnunin (Reykjavík) in the framework of the VEINS[4] and ASOF-West[5] projects, the other ADCPs, PIES and upstream temperature recording moorings deployed from 1999 to 2003 were funded by the SFB 460.

In cooperation with Hafrannsóknastofnunin, several deployments and recoveries were conducted on the regular seasonal cruises by the Icelandic research vessels Bjarni Sæmundsson and Árni Friðriksson.

Each year late summer, when meteorological and sea ice conditions in Denmark Strait are most favourable, extended surveys of R/V Poseidon and Meteor were conducted. The central section across the sill was repeatedly occupied with CTD/LADCP/vmADCP. Moreover, the annual exchange of the moored instruments was carried out.

In total, 20 moorings were deployed in the period from 1999 to 2003 (Table 5.2[1]),

---

[1] Explanations to Tables 5.1 and 5.2: *Bracketed Cruise-IDs: Arbitrary IDs for referencing in Table 5.2. For the Icelandic cruises, ports of call and cruise dates refer to the cruise legs where SFB mooring work was scheduled. Key to abbreviations: LR, NB: types of ADCPs. WD: Argos watchdog for satellite tracking of drifting equipment. ROV: Remotely Operated Vehicle. See also the glossary (appendix A).*

[2] eXpendable Conductivity-Temperature-Depth: Expendable probe to obtain a vertical profile of salinity and temperature, see appendix A.

[3] eXpendable Current Profiler: Expendable probe to obtain a vertical profile of current velocity; see appendix A.

[4] VEINS: Variability of Exchanges in the Northern Seas.

[5] ASOF: Arctic/Subarctic Ocean Fluxes.

Table 5.1.: List of all cruises in Denmark Strait contributing to SFB TP A1

Cruise-ID	Ship Name	Time	Ports of call	Instruments / Remarks
P222	Poseidon	.08.1996 .08.1996	Reykjavík Reykjavík	CTD
P230	Poseidon	14.06. − 02.07.1997	Reykjavík − Reykjavík	CTD, LADCP, vmADCP XBT
P244	Poseidon	14.09. − 04.10.1998	Reykjavík − Kiel	CTD, vmADCP XCTD, XCP
B13-1999	Bjarni Sæmundsson	20.09. − 29.09.1999	Reykjavík − Reykjavík	CTD mooring deployments
B16-1999	Bjarni Sæmundsson	10.11. − 08.12.1999	Reykjavík − Reykjavík	CTD mooring deployment
B02-2000	Bjarni Sæmundsson	16.02. − 22.02.2000	Reykjavík − Ísafjörður − Siglufjörður	CTD mooring recoveries
P262	Poseidon	19.07. − 30.07.2000	Reykjavík − Reykjavík	CTD, vmADCP, vmLRADCP mooring deployments
B10-2000	Bjarni Sæmundsson	09.08. − 05.09.2000	Reykjavík − Reykjavík	CTD mooring deployment
(HV-2001)	HDMS Hvidbjørnen	18.01. − 22.01.2001	Narssarsuaq − Reykjavík	salvage of drifting mooring
B02-2001	Bjarni Sæmundsson	13.02. − 16.02.2001	Reykjavík − Ísafjörður	CTD
B05-2001	Bjarni Sæmundsson	14.05. − 19.05.2001	Reykjavík − Reykjavík	CTD mooring recoveries
M50/4	Meteor	17.07. − 12.08.2001	Reykjavík − Rendsburg	CTD, LADCP, vmADCP mooring rec./depl.
B02-2002	Bjarni Sæmundsson	11.02. − 14.02. 16.02.2002	Reykjavík − Ísafjörður − Siglufjörður	CTD
B05-2002	Bjarni Sæmundsson	13.05. − 30.05.2002	Reykjavík − Reykjavík	CTD mooring deployment
P293	Poseidon	d 07.08. − d 17.08.2002 a 26.08.2002 d 27.08.2002 a 01.09.2002	Galway − Reykjavík − Reykjavík Reykjavík Reykjavík	CTD, vmADCP mooring recoveries CTD, vmADCP mooring deployments
(ÁF-2002)	Árni Friðriksson	08.11. − 12.11.2002	Reykjavík − Bíldudalur	CTD mooring deployment
(GF-2003)	Gunnar Friðriksson	27.05. − 28.05.2003	Ísafjörður − Ísafjörður	salvage of drifting mooring
B03-2003	Bjarni Sæmundsson	06.08. − 23.08.2003	Reykjavík − Reykjavík	CTD mooring recovery
P300/301	Poseidon	d 09.08. − d 20.08.2003 d 24.08.2003 d 06.09.2003 a 07.09.2003	Glasgow − Ísafjörður − Reykjavík − Ísafjörður − Reykjavík	CTD, LADCP, vmADCP mooring recoveries
B10-2003	Bjarni Sæmundsson	05.11. − 03.12.2003	Reykjavík − Reykjavík	CTD mooring deployment
P315	Poseidon	26.07. − 31.07.2004	Reykjavík − Reykjavík	CTD, LADCP, vmADCP; ROV (failed); mooring. rec./depl.

Table 5.2.: List of all SFB deployments in Denmark Strait

Mooring -ID	Depl. date Rec. date	Depl. position Rec. position	Depth	Depl. cruise Rec. cruise	Instruments / Remarks
V401-01	22.09.1999 18.02.2000	66°07.94' N 27°13.92' W 66°07.93' N 27°13.92' W	578 m	B13-1999 B02-2000	ADCP B LR #925
V402-01	23.09.1999 18.02.2000	66°22.51' N 26°16.71' W 66°22.50' N 26°16.70' W	640 m	B13-1999 B02-2000	ADCP NB NB # 340
V400-01	27.09.1999 18.02.2000	66°36.12' N 25°27.04' W 66°35.04' N 25°31.42' W	672 m	B13-1999 B02-2000	Thermistor chain A-TK 1133, A-TR 711
DS-1	27.09.1999 18.02.2000	66°04.73' N 27°04.97' W 66°04.70' N 27°04.98' W	648 m	B13-1999 B02-2000	ADCP A NB # 1287
V412-01	14.11.1999 18.02.2000	66°07.86' N 27°14.15' W 66°08.02' N 27°15.28' W	574 m	B16-1999 B02-2000	PIES PE P # 005
V423-01	23.07.2000 12.12.2000 20.01.2001	66°11.56' N 27°35.49' W 61°01.20' N 40°00.60' W	494 m	P262 HV-2001	ADCP C (shielded) surfaced, adrift WD recovered only
V421-01	23.07.2000 19.05.2001	66°09.92' N 27°26.28' W 66°10.12' N 27°26.55' W	493 m	P262 B05-2001	PIES PW P # 006
V422-01	23.07.2000 19.05.2001	66°06.48' N 27°10.52' W 66°06.36' N 27°11.10' W	625 m	P262 B05-2001	PIES PE P # 005
V425-01	24.07.2000 19.05.2001	66°07.60' N 27°16.10' W 66°07.60' N 27°16.10' W	582 m	P262 B05-2001	ADCP B LR # 1181
V424-01	26.07.2000	66°35.60' N 25°26.30' W	664 m	P262 P293, P302	Thermistor chain A-TK 1133, A-TRP 1356; lost
DS-1	14.08.2000 19.05.2001	66°04.96' N 27°04.79' W 66°04.96' N 27°04.79' W	650 m	B10-2000 B05-2001	ADCP A NB # 1287
V423-02	18.07.2001 18.08.2002	66°11.60' N 27°35.50' W 66°11.60' N 27°35.50' W	498 m 498 m	M50/4 P293	ADCP C (shielded) NB
V421-02	18.07.2001	66°14.00' N 27°45.00' W	487 m	M50/4	PIES PW (shielded) P # 006 (lost, AR)
V425-02	19.07.2001 18.08.2002	66°07.60' N 27°16.20' W 66°07.60' N 27°16.20' W	582 m 582 m	M50/4 P293	ADCP B LR
V422-02	19.07.2001 18.08.2002	66°06.50' N 27°10.50' W 66°06.50' N 27°10.50' W	625 m 625 m	M50/4 P293	PIES PE P # 005
DS-1	17.05.2002 28.03.2003 08.08.2003	66°04.96' N 27°04.79' W 66°04.96' N 27°04.79' W	650 m 650 m	B05-2002 B03-2003	ADCP A End of record NB # 1287 recovered
V422-03	30.08.2002 15.08.2003	66°06.45' N 27°10.55' W 66°06.24' N 27°10.60' W	623 m 618 m	P293 P301	PIES PE P # 005
V425-03	30.08.2002 15.08.2003	66°07.25' N 27°16.20' W 66°07.32' N 27°16.17' W	578 m 580 m	P293 P301	ADCP B LR
V423-03	30.08.2002	66°11.40' N 27°35.30' W	497 m	P293 P301	ADCP C (shielded) NB (release failed)
V424-02	31.08.2002 25.03.2003 28.05.2003 17.08.2003	66°40.50' N 25°26.50' W 66°32.28' N 26°06.84' W 66°40.50' N 25°26.05' W	800 m 800 m	P293 GF-2003 P301	TP WD surfaced WD salvaged mooring recovered
V421-03	10.11.2002	66°13.95' N 27°46.29' W	477 m	ÁF-2002 P301	PIES PW (shielded) P # 073 release failed
DS-1	08.11.2003 27.07.2004	66°04.96' N 27°04.79' W 66°04.96' N 27°04.79' W	650 m	B10-2003 P315	ADCP A (ASOF-W) NB # 1287 recovered
DS-1	29.07.2004	66°04.96' N 27°04.79' W	650 m	P315	ADCP A (ASOF-W) NB # 1287

which is the most extensive survey of the Denmark Strait Overflow at the sill that has been undertaken so far. Since 2003, only the ADCP A at the deepest part of the sill is continued by Hafrannsóknastofnunin; the time series of these deployments are not finally analyzed yet.

Due to technical problems, some 5 moorings were lost, however. Parts of two moorings, which surfaced unexpectedly, lead to salvage operations of the Danish Coast Guard vessel HDMS Hvidbjørnen (for V423-01, shielded ADCP C, instrument lost) and the Ísafjörður lifeboat Gunnar Friðriksson (for top float of V424-02, TP; remaining mooring recovered by P301). V421-02 (PIES) surfaced unnoticed. V424-01 (TK) has not been found and may be regarded as lost. Moreover, the release of V423-03 (shielded ADCP C) and V421-03 (shielded PIES) failed, although there are chances, that these instruments might be recovered by a ROV[6] salvage operation. The loss of 5 instruments affects the performance of the ADCP transport observations, since only three months of time series of the planned optimized 3-ADCP-array are available. Geostrophic estimates by PIES measurements now cover just one year instead of three.

However, the resulting total data set contains the records of 15 moorings, which still allows to evaluate reliable estimates of DSOW transport and temperature variability and to detect, for the first time, interannual changes.

5.2. Observed short-term variability

Earlier observations revealed, that the overflow is highly variable on timescales of a few days. The observations of the SFB array agree well with the results of AAGARD AND MALMBERG (1978); ROSS (1984); GIRTON ET AL. (2001).

Fig. 5.1 shows typical examples of the near-bottom current velocities at all three ADCPs of the SFB array. The outflow velocity is greatly modulated by eddies that pass the sill section on timescales of a few days. Superimposed on this variability, barotropic tides are evident (Fig. 5.1 b). The tidal currents of the semidiurnal M_2 tides have a mean peak-to-peak amplitude of $0.2 - 0.4$ m/s at ADCP B (Fig. 5.1) through the entire water column.

The mean near-bottom current velocity at ADCP A and B is 0.38 and 0.47 m/s, respectively, whereas further upslope on the Greenland shelf, the current is significantly weaker (ADCP C: 0.14 m/s; Fig. 5.1 a). Moreover, the ADCP measurements clearly reveal, that the large variability on timescales of several days is related with the passage of rotating eddies: In particular at the ADCPs A and B, the current direction is turning during strong outflow events, which can be attributed to propagating cyclonic eddies (in agreement with the observations of GIRTON, 2001). At ADCP C, the direction of the flow is less variable. Obviously, most eddies pass further east, and touch the ADCP C mooring site with their western edge only. Generally, the spatial mean distribution of the flow, and the larger variability in the deep part of the strait agrees with the process model (not shown).

---

[6]ROV: Remotely Operated Vehicle.
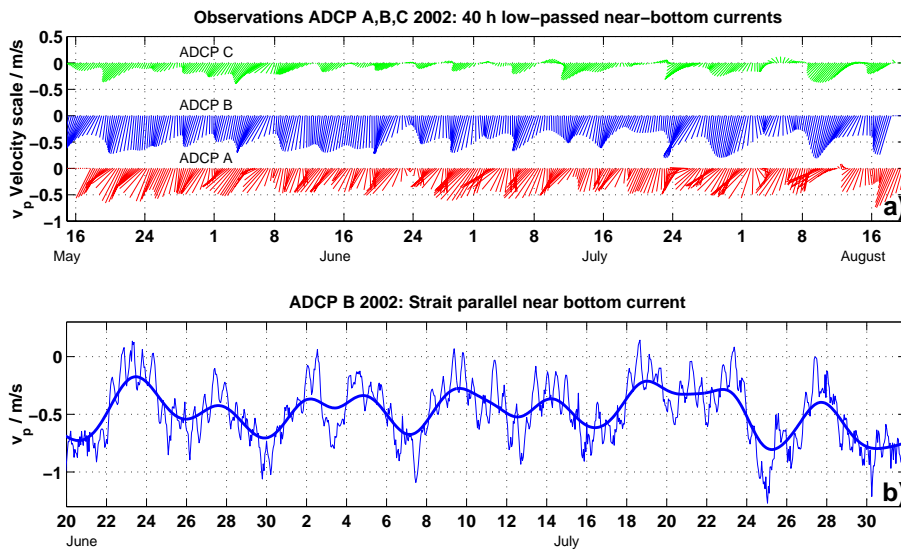
Figure 5.1.: *Evidence of tides and eddies in ADCP observations: Examples of current time series 60 – 70 m above the bottom. Panel a depicts 6 hourly values of 40 hour low-passed time series of the entire period in 2002, when all three ADCPs were operational. Rotated coordinates, outflow to SW is in downward direction. Panel b: ADCP B, unfiltered and 40 hour low-passed strait parallel current velocity. Note the semidiurnal M_2 tide and the eddy-related variability on timescales of 2 – 10 days.*

The eddy-related variability is confirmed by a power spectral density analysis (Fig. 5.2). The time series of the strait-parallel current at ADCP B (panel a) shows a distinct maximum at the semidiurnal M_2 tide, and a broad maximum for periods of a few days. Basically the same holds for the DSOW transport spectra, shown in panel b. Additionally, energy spectra have been determined by autoregressive moving-average fits (BROERSEN, 2000a,b, 2002). These smoother spectra of modelled time series with statistically similar characteristics as the original transport time series allow to more clearly determine the frequency band of eddy-related variability. While the annual mean maximum lies at periods of 4 – 5 days, the 50 % (90 %) decline spans periods from 2 – 10 (1 – 12) days, which is in agreement with previous observations (DICKSON AND BROWN, 1994; GIRTON, 2001).

5.3. Observed long-term variability

At the sill, the SFB array deployed from 1999 to 2003 corroborated the large short term variability the Denmark Strait Overflow is known for (a.o. GIRTON ET AL., 2001), but also exhibited significant interannual variability of layer thickness, volume transport and temperature properties, that have not been observed previously.

The following sections give a descriptive overview of the observed variability and serve as a basis for the evaluation of the physical mechanisms controlling the overflow.
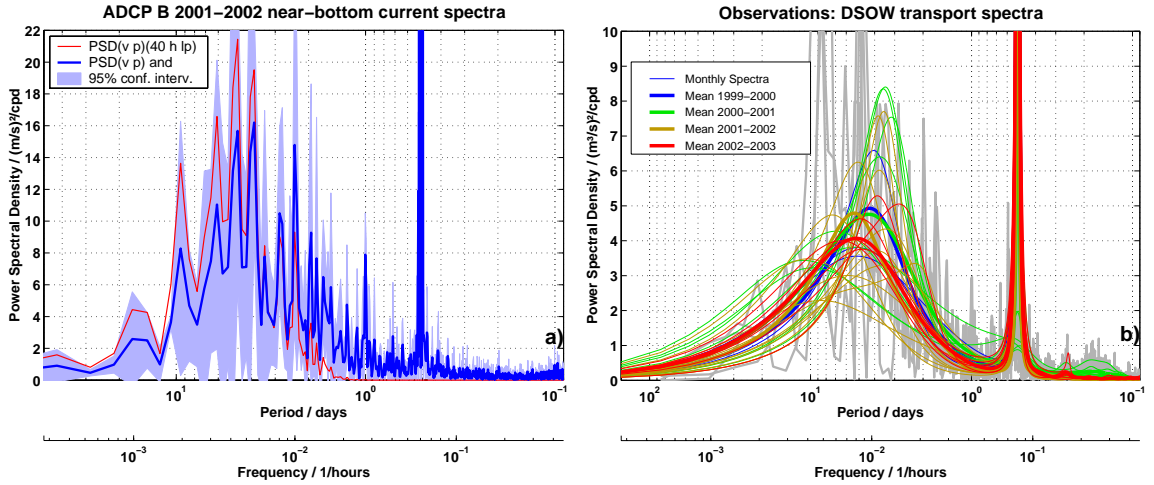
Figure 5.2.: *Power spectral density (PSD) of current and DSOW transport time series. Panel a: PSD of strait-parallel current 60 m above bottom at ADCP B, 2001 – 2002. The blue line denotes the unfiltered time series, with 95 % confidence interval shaded. Red line denotes 40 hours low-passed time series. Panel b: PSD of DSOW transport below layer of maximum current shear. Grey lines in the background denote original spectra for each deployment period, whereas coloured lines represent spectra calculated with an autoregressive-moving average model (see text). Bold lines depict mean spectra for each deployment period, thin lines monthly spectra.*

5.3.1.   DSOW transport time series

The resulting total time series of DSOW transport below the layer of maximum current shear are shown in Fig. 5.3 [7].

The average transports for the four deployment periods are 3.68 and 3.66 Sv for 1999 – 2001, 3.16 Sv in 2001/2002 and 3.07 Sv in 2002/2003. All transport numbers and error estimates are listed in Table 5.3.

Since during the 2001/2002 the less optimal mooring configuration (ADCPs B+C instead of A+B) was deployed, the time series might suffer from aliasing due to changed instrument positions. However, the time series appear consistent, and connect smoothly to the low-transport values in 2002/2003, that were obtained with the initial A+B configuration. This is confirmed during the three months period in 2002 when all three ADCPs were operational. During this time, transport estimates for different subsets (A+B, B+C, A+B+C) indicate, that the array-configuration biases of ±0.2 Sv

---

[7]Legend for Fig. 5.3 on page 65: *Total time series of the SFB array, 20 days running means. Panel a: DSOW transport below layer of maximum current shear, integrated according to multilinear regression. Colours denote certain combinations of instruments: violet: ADCPs A+B, turquoise: ADCPs B+C, black: ADCPs A+B+C (three months in 2002 only). Heavy line marks 90 days low-passed DSOW transport. Panel b: Bottom temperature, panel c: Depth of maximum current shear, panel d: Strait-parallel current 60 m above bottom. For panels b, c, d, each colour marks a particular instrument: Red: ADCP A, blue: ADCP B, green: ADCP C.*
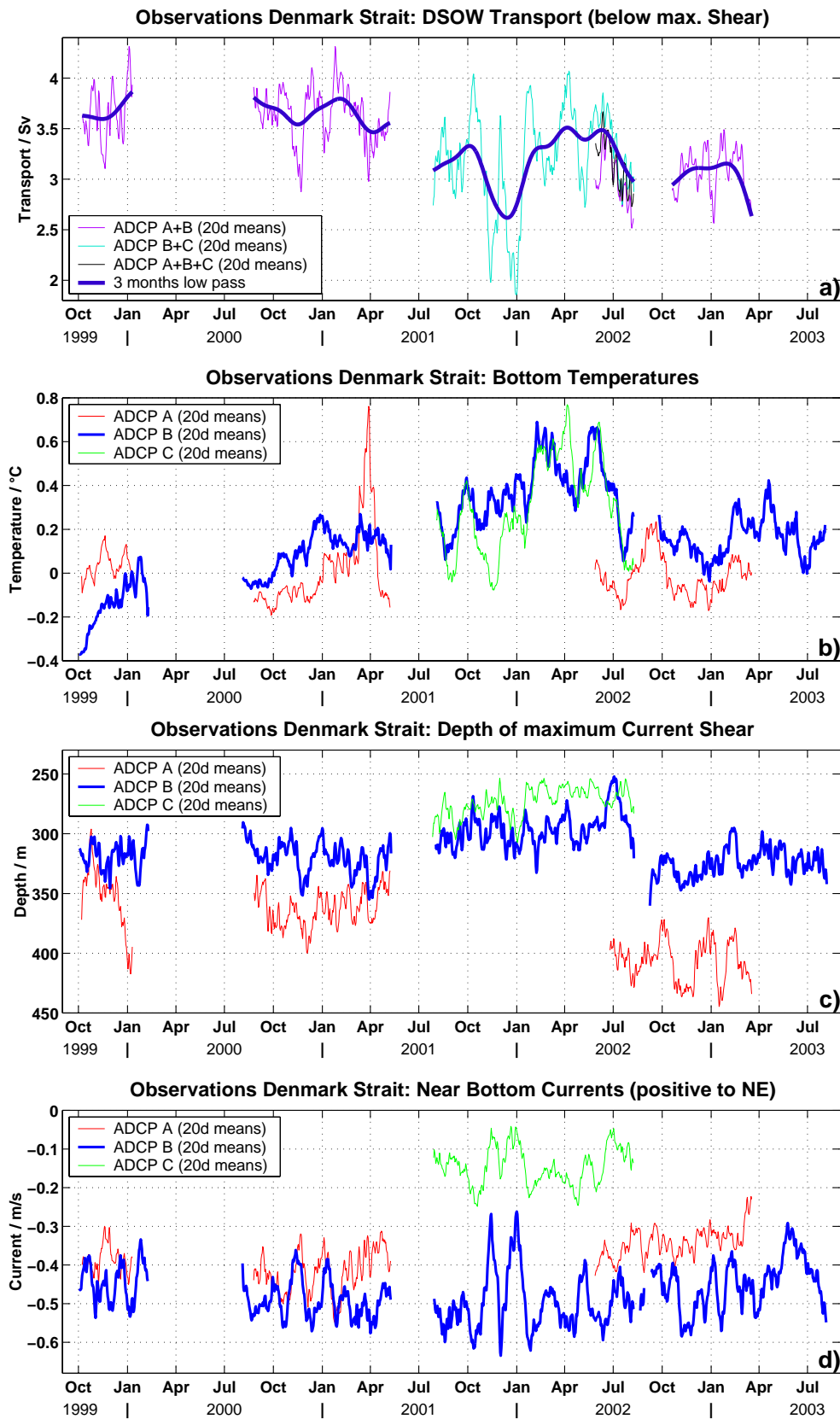
Figure 5.3.: *ADCP observations: Total DSOW transport, temperature, interface depth and strait-parallel near-bottom current time series. For a detailed figure legend, see footnote 7 on page 64.*

Table 5.3.: DSOW transports below layer of maximum current shear as determined by ADCPs at the sill, including model derived correction for systematic underestimates due to undersampling by the deployed two-ADCP-arrays.

ADCP positions	1999 − 2000 A B	2000 − 2001 A B	2001 − 2002 B C	2002 − 2003 A B
uncorr. transports	3.32±0.11 Sv	3.30±0.11 Sv	2.67±0.12 Sv	2.71±0.11 Sv
syst. underestimate	0.36 Sv	0.36 Sv	0.49 Sv	0.36 Sv
corr. transports	3.68±0.11 Sv	3.66±0.11 Sv	3.16±0.12 Sv	3.07±0.11 Sv

are smaller than the overall transport reduction of 0.6 Sv.

From earlier observations with dropped velocity probes (GIRTON, 2001) that covered part of the Greenland shelf and the model analysis it is likely that the two instrument array (ADCPs A+B) has systematically undersampled the true transport by some amount which might be as large as 0.36 Sv. For all transport numbers given above, this underestimate has already been corrected for both as an additive and as a multiplicative correction. The difference between both methods is, however, smaller than 0.1 Sv.

The standard error of each deployment period average is estimated to be 0.1 Sv, resulting from an integral timescale of four days, and hence 75 degrees of freedom for a 300 days period of observation[8].

Thus, the observed interannual transport reduction from 3.68 to 3.07 Sv is clearly larger than any errors due to measurement accuracy or changed instrument configuration.

All DSOW transport estimates are larger than previous estimates ranging from 2.5 Sv (SAUNDERS, 2001) to 2.9 Sv (ROSS, 1984; GIRTON ET AL., 2001), though on monthly timescales periods exist with values smaller than this. Including the large variability on the timescales of 2 to 10 days, transports less than 2.9 Sv occurred during 34 % of the total observation time 1999 − 2003.

Transport estimates inferred from R/V Poseidon P262 sections in August 2000 (Fig. 2.6, page 37) yielded DSOW transport values of (2.4 ± 0.5) Sv and (3.3 ± 0.2) Sv, respectively (average 2.9 Sv). These sections, calculated from integrated vmADCP current velocity below the $\sigma_\Theta = 27.8$ kg/m^3 isopycnal, overlap with the mooring time series and reveal that the ship sections were indeed measured during periods with smaller than average current.

Besides the significant interannual fluctuations, DSOW transport variability with an amplitude of > 1 Sv is evident on monthly timescales. Remarkable is the enhanced variability in 2001/2002, in particular two events of very low overflow transport in November and December 2001, where the 20-days average dropped to values of 2 Sv. One might be tempted to relate the enhanced variability to the less optimal array configuration during this period, but the continuous records of bottom temperature and

---

[8]Integral timescales obtained from the sum of the squared autocorrelation function (EMERY AND THOMSON, 2001). A time series model was used for the calculation of the autocorrelation (BROERSEN, 2000a,b, 2002).

near bottom current velocity at ADCP B (Fig. 5.3) suggest, that the large variability on monthly timescales is in fact a real signal.

5.3.2. Near bottom current velocity time series

Velocity observations at position B (Fig. 5.3 d), the only position that was occupied all the time, indicate, that near bottom currents increased slightly from 0.44 m/s in 1999 to 0.54 m/s in 2002, and returned to 0.45 m/s during the last deployment period.

The Icelandic ADCP A at the deepest point of the sill section observed smaller current velocities, averaging 0.39 m/s in 1999, and decreasing to 0.34 m/s in 2002/2003.

The ADCP C 23 km northwest of the sill measured the weakest current with a mean velocity of 0.14 m/s.

While the time series of the different ADCPs are not coherent on short timescales due to the small-scale eddy activity (see section 5.2), the larger fluctuations on monthly timescales are evident at all positions, although the amplitude of the variability is generally largest at ADCP B. Two outstanding events of low current velocity occurred in the end of 2001, where the current velocity at ADCP B and C decreased by more than 50 %, corresponding to an exceptional low transport of DSOW (Fig. 5.3 a). These fluctuations may be related to barotropic forcing, since they affect the entire water column (not shown).

5.3.3. Interface depth time series

The mean interface depth (as defined by layer of maximum current shear, Fig. 5.3 c) at ADCP B remained unchanged from 1999 to 2001 at 318 m. During the third deployment period (2001 – 2002), the average depth was 300 m (i.e., the plume thickness increased by 8 %), but then dropped to 327 m in 2003. It might be suspected, that the changes in interface depth are associated to deployment position inaccuracies, however, the consistency in current velocity, temperature and transport time series suggests, that these changes reflect physical variability of the overflow. This is supported by the interface drop beginning in July 2002, that smoothly connects the time series of the 3rd and 4th deployment period.

The interface depth at ADCP A is lower than at ADCP B, since it is located further to the east. The time series show a remarkable decrease from 359 m in 1999 to 409 m in 2003. This 50 m plume thickness reduction at the deepest part of the strait may be an indication for a general decrease of the overflow transport (Fig. 5.3 a), or a lateral shift to the Greenland side associated with enhanced inflow of Atlantic Water of the Irminger Current which is evident in hydrographic data (Fig. 2.4, page 33).

5.3.4. Temperature time series

The observed transport variability is significantly correlated with the measured bottom temperatures. Generally, reduced transport corresponds with higher temperatures, most evident in the time series of ADCP B, that was deployed during all

observation periods (Fig. 5.3 b). The time series of ADCP B (Fig. 5.3 b) show an interannual increase of the near bottom temperature from $-0.1\,°C$ to $+0.4\,°C$ from 1999 to 2002, that is coherent with the decrease in transport. In summer 2002, temperatures drop rapidly to $+0.1\,°C$, whereas the DSOW transport remains at the low level it had reached in 2002.
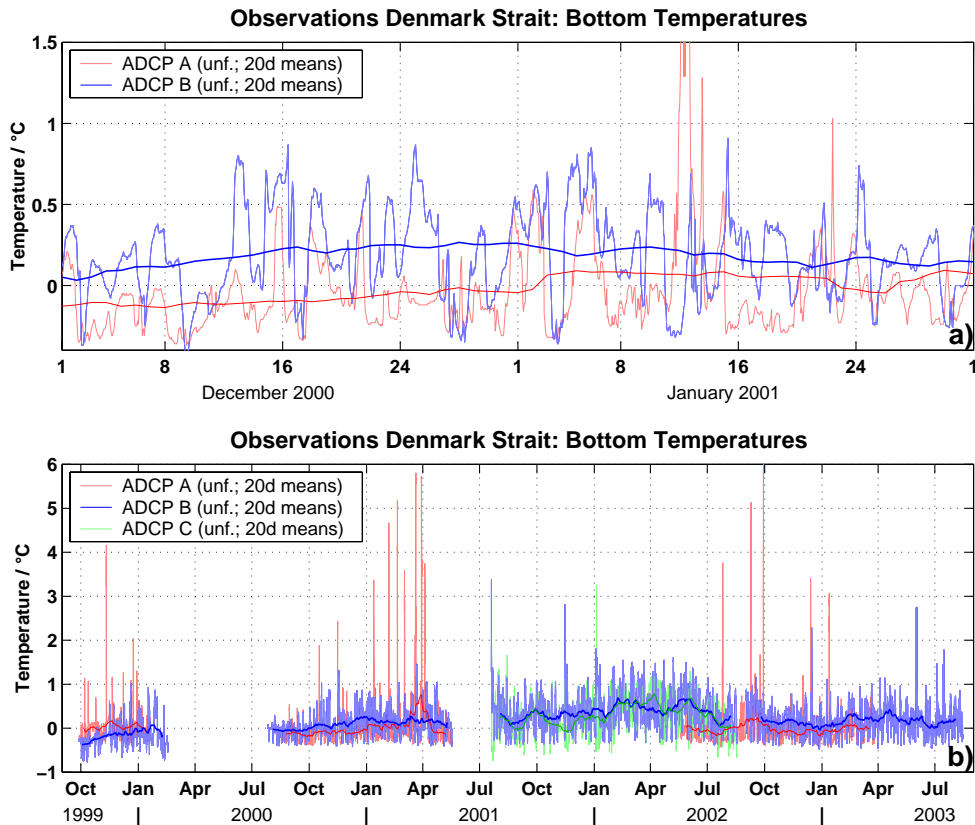
Figure 5.4.: *Unfiltered temperature time series of ADCPs A, B, C. Panel a: Typical example of short term variability. Note the abrupt shifts between "cold" ($T < 0\,°C$) and "warm" ($T \approx +0.5\,°C$) conditions, possibly indicating advection of different, not yet mixed water masses. Panel b: Entire time series. The peaks at ADCP A indicate short events, where warm Atlantic Water was present at the deepest part of the sill.*

The long term temperature variability reflects the variable composition of the dense overflow, that is evident in the unfiltered temperature records (Fig. 5.4). Generally, ADCP B is permanently located in the dense, cold overflow. The minimum temperatures on a daily timescale vary between $-0.6\,°C$ in 1999 and $-0.3\,°C$ in 2002. The maximum temperatures vary between $+0.5\,°C$ in 1999 and $+1.5\,°C$ in 2002. The enhanced variability on monthly timescales in 2001/2002 is caused by changes of the frequency of occurrence of "cold" and "warm" water.

At ADCP A, which lies at the deepest part of the sill, the DSOW minimum temperature is generally more stable at $-0.3\,°C$. Occasionally, AW with temperatures

of up to 5 °C occurs at ADCP A. These eddy-induced events typically last only a few hours, and occur at irregular intervals (Fig. 5.4). In March 2000, the "AW events" have been unusual frequent, causing the 20 day running mean temperature (Fig. 5.4) to rise by > 0.5 °C.

The very coldest, and hence densest part of the overflow has varied little in temperature, but the majority of the flow, which is further upslope to the Greenland side of the sill, has shown significant interannual variability, which might point to different entrainment rates of other water masses (further discussion in chapter 8).

The abrupt temperature changes of 1°C between the colder and warmer parts of the overflow (Fig. 5.4) suggest, that different source water masses are involved in the formation of the dense overflow, which at the sill are not yet mixed and homogenized.

5.4. Comparison with previous observations

5.4.1. Transport estimates

Before the SFB measurements, overflow transport estimates from different observations have been always around $2.5 - 2.9$ Sv (see section 1.2). Differences between the estimates are likely to be influenced by short term variability aliasing, section location and different DSOW definitions.

The choice of either of the commonly used interface definitions

i) $\Theta < 2$°C (ROSS, 1984)

ii) $\sigma_\Theta > 27.8$ kg/m^3 (DICKSON AND BROWN, 1994)

has a large effect on the DSOW transport estimates. This is illustrated by the sections obtained during the P244 cruise, where the mean transport yields 3.8 Sv for i) and 2.7 Sv for ii) (GIRTON, 2001). In general, the temperature criterion includes more of the cold, but fresher and hence less dense water masses of the East Greenland Current, that are not part of the dense overflow plume, which descends downstream of the sill to feed the NADW.

Different instrument locations, that were either near the sill (ROSS, 1984) or further downstream (AAGARD AND MALMBERG, 1978; DICKSON AND BROWN, 1994), and poor spatial coverage of the plume may also affect the transport estimates.

The OVERFLOW'73 experiment (ROSS, 1984) with good spatial coverage at the sill had a duration no longer than 5 weeks. Since the time series of the SFB array exhibit occasionally abrupt shifts in DSOW transport greater than 1 Sv on timescales of $1 - 2$ months (Fig. 5.3), the apparent long-term stability of the ROSS (1984) time series does not necessarily imply interannual stability. For the year-long mooring time series, neither AAGARD AND MALMBERG (1978) nor DICKSON AND BROWN (1994) observed any seasonal or interannual variability in volume transport, giving rise to the assumption that the Denmark Strait Overflow is stable on timescales longer than a few weeks.

Recently, there was found indirect evidence for larger interannual variability of the overflow. Based on an inverse box model, geostrophy, current measurements and mass conservation, LHERMINIER AND OVIDE-TEAM (2004) inferred from hydrographic sections between South-East Greenland and Europe in 1997 and 2002, that the total Atlantic Meridional Overturning Circulation (AMOC) had reduced by a factor of 2 from 16 Sv (1997) to (8 ± 1) Sv (2002), while the DSOW transport had decreased from 7.1 Sv to 4.8 Sv. Although the absolute DSOW transport values are considerably larger than those of the SFB array, they may be consistent due to the effects of downstream entrainment, which has been been estimated as a transport increase of 2.2 Sv between the sill and after reaching the 2000 m isobath (DICKSON AND BROWN, 1994).

However, it appears questionable to conclude on the total AMOC strength from just a single hydrographic section (KANZOW, 2004), and aliasing effects of the rapid variability of the overflow plume along the Greenland shelf break have to be taken into account for all ship-section DSOW transport estimates (e.g. WORTHINGTON, 1969; GIRTON ET AL., 2001; LHERMINIER AND OVIDE-TEAM, 2004), since they cover a period of a few days only. Moreover, the studies of DICKSON AND BROWN (1994) and LHERMINIER AND OVIDE-TEAM (2004) were conducted 500 to 1000 km downstream of the sill, where the overflow is already significantly modified by entrainment processes.

Hence, although it is likely, that the Denmark Strait Overflow experiences substantial interannual variability (numerical experiments; NILSEN ET AL., 2003; BIASTOCH ET AL., 2003; KÖSTERS, 2004b), the observational evidence in previous studies remained uncertain.

5.4.2. Water mass properties

DICKSON ET AL. (1999) discussed an anomalous warming and weakening of the overflow in 1996/97, observed by current meters of the Angmagssalik array. The authors assume, that the anomalous warming (and hence anomalous low density) caused the overflow plume to shift upslope and mostly out of the current meter array. The warming might have been advected from Fram Strait, where anomalous warming was observed three years earlier. However, the warming of the overflow DICKSON ET AL. (1999) observed in 1996/97 persisted only a few weeks. The SFB time series reveal, that variability of similar magnitude and timescales of a few weeks occurs regularly, and that this variability may at least partly reflect a changed composition of the overflow rather than property changes of an individual source water mass.

A comparison of temperature records at Kögur 5 and ADCP B (section 8.4) revealed, that the interannual warming signal might be be caused by enhanced entrainment of Atlantic Water in the region between KG5 and the sill. Thus, DSOW does not contain a fixed fraction of entrained Atlantic Water (as proposed by DICKSON ET AL., 1999). Considering interannual temperature change variations of 0.5 °C between KG5 and ADCP B, the composition of DSOW appears to be modified significantly in the region close to the sill. The varying entrainment processes make it more difficult to track short-term temperature anomalies advected from as far as Fram Strait.

However, the propagation of large-scale anomalies like the Great Salinity Anomaly (GSA) from the 1960's to the 1980's, that might also affect the overflow, has been clearly followed on its way from the Greenland Sea through Denmark Strait and further south and around the subpolar gyre (DICKSON ET AL., 1988).

Salinity was not measured by the SFB array, thus one has to rely on the hydrographic profiles taken one to two times per year only (section 2.3). The freshening of the DSOW during the past four decades observed by DICKSON ET AL. (2002) could not be verified by the SFB measurements, since the large variability on short timescales overrides the long term freshening trend of 0.013 per decade proposed by DICKSON ET AL. (2002).

5.5.   Comparison to Angmagssalik array time series

Further downstream, the Denmark Strait Overflow has been continuously observed by the "Lowestoft" (DICKSON AND BROWN, 1994) and the "Angmagssalik" arrays (unpublished, DYE ET AL., 2004). A part of these time series overlap with the SFB measurements and give the opportunity to compare the sill observations with independent estimates.

5.5.1.   Transport time series

New preliminary results from the Angmagssalik array (unpublished, DYE ET AL., 2004) approx. 600 km downstream of the sill indicate interannual transport variations of $\approx 30\%$ of the mean value. These findings corroborate the results of the SFB observations at the sill. In particular, the time series of the UK1 and UK2 moorings, that have been deployed continuously in the period from 1998 to 2004, compare well with the SFB observations (Fig. 5.5 a).

For the UK1+UK2 time series, the overflow transport increased from 2.1 Sv in early 1998 to 3.0 Sv in August 2000. From August 2000 to January 2002 (UK1+UK2) or August 2002 (UK1+UK2+G2), a decrease by 30 % (UK1+UK2 from 3.0 to 2.1 Sv) was observed, followed by a return to slightly higher values afterwards. The numbers represent preliminary calculations with horizontal and vertical integration over an assumed fixed mean-width and -height overflow cross-section derived from the plume thickness averaged over all available hydrographic cross sections (DYE, pers. comm.). Despite of the fixed-cross section assumption, the transport numbers are consistent with those obtained from the SFB array at the sill (Fig. 5.5).

It is tempting to investigate the correlation between the Angmagssalik and SFB time series. Considering the distance of 600 km, an advective timescale of O(weeks) could be expected. Short term variability is not coherently advected over this distance, though, and the 6 months running mean time series of UK1+UK2, which appear to fit nicely to the SFB time series, do not allow for a reliable correlation analysis, since the number of independent observations is too small. A further question is, why the time series that have a wider spatial coverage (UK1+UK2+G2+G1(+F1+F2)), are less coherent with the SFB time series than the UK1+UK2 subsample.
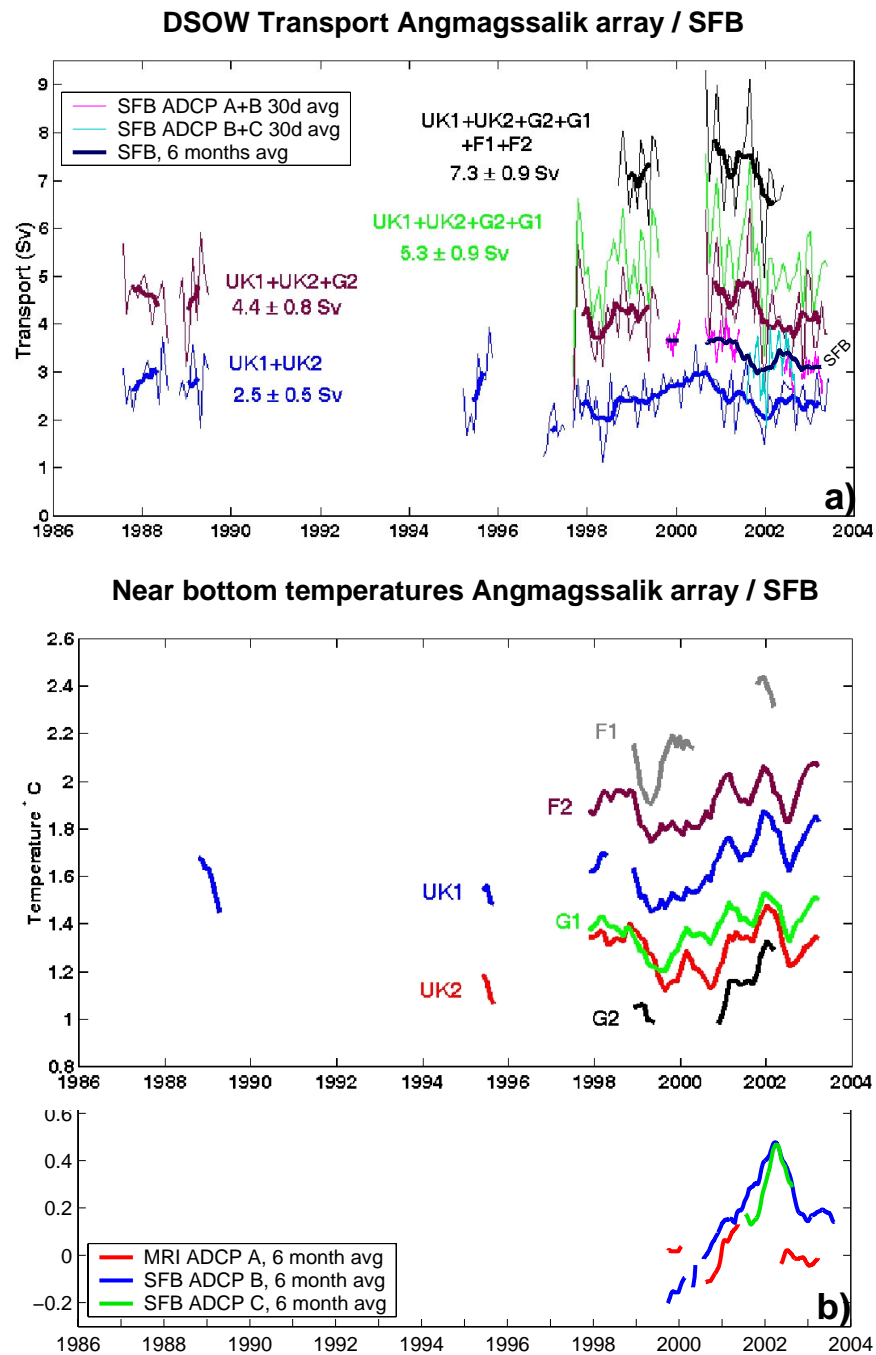
Figure 5.5.: *Time series of the Angmagssalik array (DYE ET AL., 2004) with SFB observations overlaid. For positions of all moorings, see Fig. 2.1. Panel a: Transport. Colours indicate different array configurations. For the Angmagssalik array, mooring acronyms plotted next to the lines. Time series integrated over fixed cross-sections for each mooring. For the SFB array, transports below max. current shear are shown, see legend box. Light lines: Monthly averages, heavy lines: 6 months running mean. Panel b: Near bottom temperatures. For the Angmagssalik array, values from current meters 50 m above the bottom are shown. The SFB instruments at the sill were located 5 m (ADCP A, B) or 1 m (ADCP C) above the bottom. Monthly means shown. Original figures from DYE ET AL. (2004) reproduced by courtesy of S. Dye.*

5.5.2. Temperature time series

600 km downstream of the sill, the mean near bottom temperature of the overflow has risen due to entrainment to values of +1 to +2 °C, with the lowest temperatures at the deeper mooring sites G2 and UK2 (Fig. 5.5 b).

The time series show a clear interannual warming signal of ≈ 0.4 °C from 1999 to the beginning of 2002. In 2002/2003, a temporary cooling and later warming is evident at all mooring sites.

The overlaid SFB array time series at the sill are generally > 1 °C colder, but they reflect an interannual warming of comparable magnitude (0.5 °C) from 1999 to 2002. The sill time series are much smoother than those of the Angmagssalik array, suggesting variable entrainment rates and/or entrainment of variable water masses during the descent of the overflow from the sill to the Angmagssalik array. Moreover, lateral displacements of the plume on the Greenland shelf may lead to temperature changes at certain positions, as has been suggested for an earlier warming event (DICKSON ET AL., 1999).

The maximum temperature at the Angmagssalik moorings is reached a few months earlier (!) than at the sill. This fact, however, may be attributed to downstream entrainment changes on shorter timescales.

5.5.3. Summary

Although the comparison between the transport and temperature time series of the SFB and Angmagssalik arrays is currently limited to a more qualitative analysis, the time series of the Angmagssalik array appear consistent with the SFB observations at the sill, confirming interannual transport variability of ≈ 30 % and temperature changes of 0.4 − 0.5 °C.

The Angmagssalik and SFB arrays observations offer the opportunity to study the modification of the overflow during its descent from the Denmark Strait sill to depths larger than 1500 m on interannual timescales. In particular, the evaluation of advective timescales and the downstream modification of temperature anomalies due to entrainment appears promising for future investigations.

5.6. Summary and conclusions

The SFB array delivered time series of the Denmark Strait Overflow from 1999 to 2003. For the first time, interannual changes of the overflow have been observed by continuous direct measurements at the sill. The average DSOW transport decreased from 3.68 Sv (1999) to 3.07 Sv in 2003.

The observations may be regarded as consistent with previous studies, although interannual variability might have been overlooked due to short deployment periods, poor spatial coverage, and downstream entrainment processes.

Moreover, the SFB time series are in general agreement with preliminary estimates derived further downstream in the Angmagssalik array.

An integrated view on the observations discussed in the previous sections yields the following key results, that provide the essential background for the evaluation of the relevant mechanisms that control the Denmark Strait overflow:

- With respect to the short-term variability, the SFB array time series confirmed the results of previous observations. While tides have a typical peak-to-peak amplitude of $\approx 0.2 - 0.4\,\mathrm{m/s}$, the overflow shows dominant variability on timescales of $2 - 10$ days, with near-bottom velocities varying between 0.2 and $1.4\,\mathrm{m/s}$, which is associated to strong eddy activity (studied in detail by GIRTON, 2001).

- A substantial interannual decrease of the DSOW transport from $3.68\,\mathrm{Sv}$ (1999) to $3.07\,\mathrm{Sv}$ (2003) has been observed. The transport decrease is associated with a $50\,\mathrm{m}$ reduction of the plume thickness and a $15\,\%$ velocity decrease at the deepest part of the sill, while further to the northwest, the corresponding interannual changes are significantly smaller. The changes in plume thickness might be related to a reduction of the dense water reservoir height, that drives the hydraulically controlled flow over the sill.

- Spatially coherent variability on monthly timescales has occasionally been observed. Particularly remarkable were two periods of extreme low transport ($< 2\,\mathrm{Sv}$) in November and December 2002 associated with a current velocity decrease of $50\,\%$. Since these low-current events covered the entire water column, they might be related to barotropic forcing mechanisms.

- The DSOW exhibited a temporary temperature increase of $0.5\,^\circ\mathrm{C}$ from 1999 to 2002, and a decrease of $0.4\,^\circ\mathrm{C}$ from 2002 to 2003. The temperature signal reflects variability in the composition of the overflow: While the coldest parts showed a weaker interannual variability between -0.6 and $-0.3\,^\circ\mathrm{C}$ at ADCP B, warmer water masses observed in the overflow exhibited a temperature increase from $+0.5\,^\circ\mathrm{C}$ in 1999 to $+1.5\,^\circ\mathrm{C}$ in 2002. The large temperature variability on hourly to daily timescales indicates, that the different water masses contributing to the overflow are not completely mixed and homogenized at the sill, and that changes of the mean temperature depend not only on the properties of individual source water masses, but also on their relative contribution to the overflow.

The aspects of density forcing, that may be assessed by theories of hydraulic control, of barotropic forcing likely associated with wind stress variability, and observational evidence for advection pathways that feed the overflow from different sources, shall be addressed in the following chapters.

6. Density forcing of the overflow

The Denmark Strait Overflow carries dense water from the Nordic Seas across the sill between Iceland and Greenland to the deep North Atlantic.

Generally, the flow of dense water over topographical constrictions is limited by dynamic relations termed as "hydraulic control", and the volume transport is entirely determined by the available potential energy of the upstream dense water reservoir, the strait geometry and rotation. The role of these factors and their applicability to real straits have been addressed in a number of analytical studies, laboratory experiments and numerical models (for a review, see WHITEHEAD, 1998; PRATT, 2004).

The asymmetry between the Iceland Sea, where the dense DSOW level is substantially higher than south of the Denmark Strait sill (Fig. 2.5, page 35), and the rapid downstream descent and acceleration of the overflow plume (a.o. GIRTON ET AL., 2001) suggest, that the Denmark Strait Overflow may indeed be subject to hydraulic control.

During the past decades, numerous field studies (a.o. DICKSON AND BROWN, 1994; KRAUSS AND KÄSE, 1998) and numerical experiments (KÄSE AND OSCHLIES, 2000) have been conducted to evaluate the Denmark Strait Overflow in the light of hydraulic control theories. GIRTON (2001) extensively investigated the dynamics of the descending plume based on hydrographic surveys in 1997 and 1998.

While most of the previous studies were focused on the downstream development of the overflow only, the SFB experiment obtained four years of continuous time series at the sill and further upstream, providing an excellent data set to study the governing dynamics that may actually control the dense water volume flux over the sill.

After a theoretical introduction to hydraulic control mechanisms, the SFB time series and the process model are investigated, whether a number of assumptions are met, that are critical prerequisites for the applicability of hydraulic control:

- Alongstream asymmetry: The overflow descents from an upstream dense water reservoir over the sill to larger depths further downstream. The alongstream momentum balance is examined in the process model.

- Criticality: The flow over the sill accelerates to a velocity fast enough to block information propagation from the downstream to the upstream basin.

- Potential Vorticity (PV): PV is a critical factor for the maximum volume transport over a sill.

- Geostrophy: The validity of geostrophic balance is proven in both the observations and the process model.

Then, the SFB time series are assessed in combination with hydrographic observations further upstream to evaluate the key features of the Denmark Strait overflow in the light of a density driven flow:

- Determination of the DSOW transport by the dense water reservoir height, observed by temperature recording moorings and regular hydrographic profiles upstream of the sill.

- Observational evidence, that the transport depends on the density contrast between DSOW and the overlying water masses.

Implications of hydraulic control theories for the upstream pathways to the sill, and their observational evidence are addressed in the separate chapter 8.

6.1. Theory of hydraulic control

6.1.1. Introduction to hydraulic control

The flow of dense water through Denmark Strait is likely subject to hydraulic control, considering its velocity and density characteristics (GIRTON, 2001). Hydraulic control is normally defined by the following criteria:

- The current velocity reaches or exceeds criticality (Froude-number $F \geq 1$) at the sill or during downstream descent. The "control point" ($F = 1$) separates subcritical flow in the upstream basin from supercritical downstream flow. Hence, no information can propagate by long gravity waves from the downstream region across the sill (PRATT AND LUNDBERG, 1991).

- Alongstream asymmetry, i.e. high dense water reservoir upstream, and descending isopycnals downstream of the sill (ARMI, 1986). This is the case in Denmark Strait (Fig. 2.5, page 35), although frictional processes could lead to a similar appearance (PRATT, 1986).

From this follows:

- The volume transport entirely depends on the sill geometry and the upstream conditions and is limited to a certain upper bound.

As a first theoretical approach, a simple two-layer system with a dense bottom layer (density $\varrho + \Delta\varrho$) and a lighter surface layer (density ϱ) shall be considered, following the review of WHITEHEAD (1998) (Fig. 6.1). While the upper layer is at rest (so-called "1 1/2 layer" model), the motion of the lower layer for steady state flow of inviscid, incompressible fluid is governed by inertia, pressure and rotation.
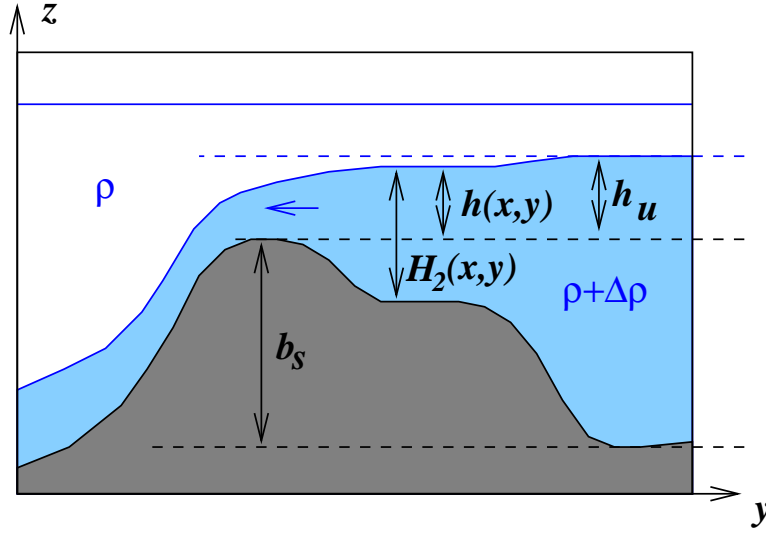
Figure 6.1.: *Sketch of the flow of dense water in a two-layer system across a sill. Section along streamlines (y-axis). Upstream reservoir height h_u, dense layer thickness $H_2(x,y)$ and density contrast $\Delta\varrho$ referenced in the text. Note the lower interface height in the sill entrance region.*

The equations of momentum are given by

$$\boldsymbol{u} \cdot \nabla\boldsymbol{u} + f\boldsymbol{k} \times \boldsymbol{u} = -\frac{1}{\varrho}\nabla p - g\boldsymbol{k} \qquad (6.1)$$

with current velocity $\boldsymbol{u}$, Coriolis parameter f, density ϱ, pressure p, acceleration of gravity g and the vertical unit vector $\boldsymbol{k}$.

The conservation of mass (volume) yields

$$\nabla \cdot \boldsymbol{u} = 0 \qquad (6.2)$$

Allowing slow variation in alongstream direction only, as is the case for Denmark Strait, the equations of motion of the lower layer reduce to

$$\boldsymbol{u} \cdot \nabla\boldsymbol{u} + f\boldsymbol{k} \times \boldsymbol{u} = -\frac{g\Delta\varrho}{\varrho}\nabla h_{int} \qquad (6.3)$$

with lower/upper layer interface height h_{int}.

With slow variations in along-strait (y-axis) direction, geostrophical balance is valid for the along-strait current velocity v, which is much larger than the cross-strait component u.

Hence, the basic dynamical relations, that hold for each fluid element, are

Bernoulli's Law

$$\frac{1}{2}v^2 + g'h = B(\Psi) \quad (6.4)$$

Inertia ──────────── **Pressure**

Conservation of
Potential Vorticity

Geostrophy

$$\frac{\frac{\partial v}{\partial x} + f}{H_2} = G(\Psi)$$

$$fv = g'\frac{\partial h_{int}}{\partial x} \quad (6.6)$$

(6.5)

Coriolis
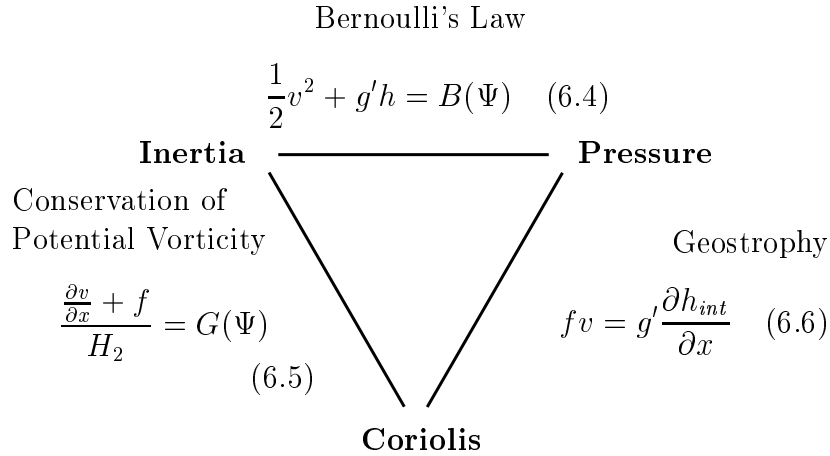
(diagram adopted from WHITEHEAD, 1998)

Basically, Eq. 6.4 is an expression for the conservation of energy ($E_{pot} + E_{kin} = const.$). Eq. 6.5 denotes the conservation of potential vorticity (angular momentum). Geostrophic balance (Eq. 6.6) is valid, since only slow changes are permitted alongstream.

The Bernoulli and potential vorticity equations are constant along each streamline, defined by the streamfunction Ψ:

$$\frac{\partial \Psi}{\partial x} = v, \qquad \frac{\partial \Psi}{\partial y} = -u \qquad (6.7)$$

These equations form the the basis for the theoretical description of the flow across topographical constrictions like e.g. the Denmark Strait sill.

The simplest model is the flow over a bump in a non-rotating system. Due to continuity, the flow has to accelerate over the bump. Eq. 6.4 then implies, that the interface between lower and upper layer is deflected downward, which further reduces the layer depth above the bump. It can be shown, that the maximum volume transport is reached when the local Froude number $F = v/\sqrt{2g'H_2}$ (with local layer depth H_2) equals unity at the sill (critical flow).

The Denmark Strait as a rotating system with complicated topography, involving frictional processes, and an additional barotropic flow component, is more difficult to assess. Of major interest for Denmark Strait are (i) the upstream circulation structure, and (ii) estimates for the maximum volume transport determined from the upstream conditions.

6.1.2. Current structure

The basic concepts of hydraulically controlled flow assume an active dense layer underneath a stagnant surface layer (Fig. 6.1, page 77), termed as 1 1/2 layer models.

WHITEHEAD ET AL. (1974) introduced a model that includes rotation. It was based on the assumption of zero PV and zero current upstream (i.e. infinite depth of the upstream basin). In a study by GILL (1977), constant potential vorticity and upstream currents are allowed. The classical GILL model was further refined and extended for nonuniform upstream conditions by PRATT AND ARMI (1987). More recently, HELFRICH AND PRATT (2003) investigated the upstream circulation for different types of dense water sources. The implications for the Denmark Strait Overflow are addressed in a separate chapter (8).

A common feature for all of these concepts is the acceleration of the flow over the sill and further downstream. Under the influence of rotation, the downstream flow is banked to the right-hand side of the strait (northern hemisphere convention). The alongstream asymmetry, with a downstream descent of the dense water, was regarded as essential for hydraulic control by ARMI (1986). However, since the plume tends to keep its height due to geostrophic balance, friction has to be considered to describe the downstream descent of the overflow.

A number of studies tried to include the more complicate effects of friction (PRATT, 1986; GARRETT, 2002), and of a non-stagnant upper layer (FARMER AND ARMI, 1986; DALZIEL, 1990). In particular, the downstream development of the overflow plume has been studied with respect to friction and turbulence (e.g. by rapid synoptic sections, GIRTON ET AL., 2001) and compared to numerical models (KÄSE ET AL., 2003; KÖSTERS, 2004a).

6.1.3.   Transport estimates: Zero PV, rectangular cross-section

Based on the models of WHITEHEAD ET AL. (1974) and GILL (1977), WHITEHEAD (1989) evaluated an upper transport bound for zero PV conditions and zero upstream current. In this case, the Bernoulli potential is $B(\Psi) = g'h_u$ (Eq. 6.4; h_u upstream dense water height above the sill). The assumption of zero PV yields $\frac{\partial v}{\partial x} = -f$ (Eq. 6.5). Hence, the cross-section of the flow is parabolic, with the maximum interface height $h_{int} = h_u$ at the right-hand wall (Fig. 6.2).

The transport can be determined by integrating $v \cdot H_2$ from the right-hand wall (here, $h_{int} = h_u$, and $v = 0$) to the intersection of the interface with the left-hand wall or the bottom.

Depending on the width L of the strait, the following transport relations hold:

$$Q_{WLK} = (\frac{2}{3})^{3/2} L \sqrt{g'} [h_u - \frac{f^2 L^2}{8g'}]^{3/2} \qquad \text{for } L < \sqrt{2g'h_u}/f \qquad (6.8)$$

$$Q_{WLK} = \frac{1}{2} \frac{g'}{f} h_u^2 \qquad \qquad \text{for } L > \sqrt{2g'h_u}/f \qquad (6.9)$$

with reduced gravity $g' = g\Delta\varrho/\varrho$ and upstream reservoir height h_u.

The length scale $\sqrt{2g'h_u}/f$ defines whether the dense water fills the entire width of the strait (Eq. 6.8) or just occupies the right-hand part (Eq. 6.9). It is proportional to the Rossby radius of deformation $R = \sqrt{g'h}/f$.
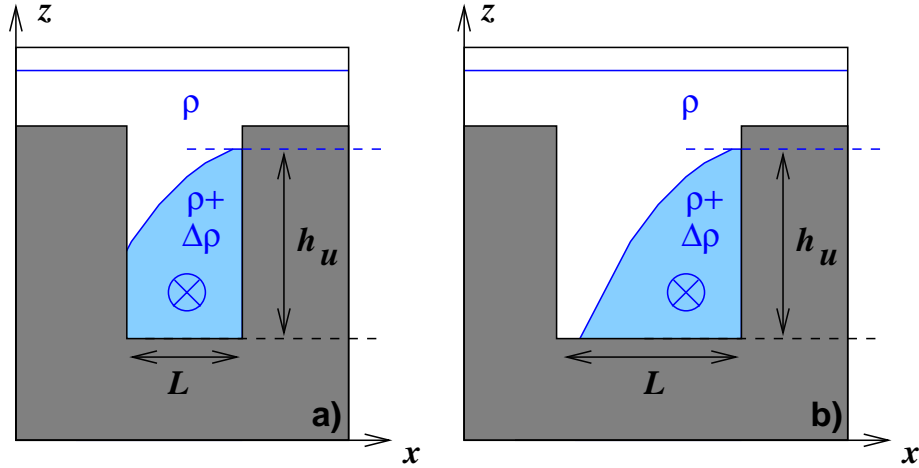
Figure 6.2.: *Cross-section of zero PV flow through a rectangular channel according to* WHITEHEAD *(1989). The view is in downstream direction. Note, that at the right-hand wall the dense water height equals the upstream value h_u, and the current velocity is zero. Panel a: "Narrow" strait equivalent to e.g. Faroe Bank Channel. Panel b: "Wide" strait equivalent to e.g. Denmark Strait.*

While Eq. 6.8 may be applied to narrow straits like the Faroe Bank Channel ($L \approx 10\,\mathrm{km} = R$), the Denmark Strait has to be regarded as "wide" strait, where the maximum transport entirely depends on the the density contrast and upstream reservoir height h_u.

According to WHITEHEAD (1998), the density contrast $\Delta\varrho$ can be obtained from the density difference between the upstream and downstream basin measured at sill depth. The reservoir height is found by identifying the "bifurcation depth". Below the bifurcation depth, the hydrographic density profiles of the downstream basin differ from those obtained upstream of the sill. For the Denmark Strait, the SFB observations yield values of $\Delta\varrho \approx 0.43\,\mathrm{kg/m^3}$ and $h_u \approx 470\,\mathrm{m}$ (compare Fig. 2.5, page 35).

The model can be extended for finite current velocities (e.g. for observations at the strait entrance, where depth is not infinitely large), using the conserved Bernoulli potential (Eq. 6.4) to obtain an "effective reservoir height" h_{eff} (KILLWORTH AND MCDONALD, 1993):

$$h_{\mathit{eff}} = h_u + \frac{1}{2g'}v^2 \tag{6.10}$$

with current velocity v.

The theoretical relation holds for straits with rectangular cross-section and assumes no friction and zero PV. KILLWORTH (1994) showed, that zero PV generally yields the maximum possible transport through a strait, which is given by Eq. 6.9.

For real straits, the actual transport is smaller. For Denmark Strait, WHITEHEAD (1998) estimated a hydraulically controlled flow of 3.8 Sv (with $h_{\mathit{eff}} = 580\,\mathrm{m}$ and

$\Delta \varrho / \varrho = 3.0 \cdot 10^{-4}$, DICKSON ET AL., 1990), while the actual flow of 2.9 Sv is smaller by a factor of 0.76. Numerical experiments of KÖSTERS (2004b) yielded a smaller scaling factor of 0.46.

Concluding, Eq. 6.9 yields an upper transport bound for dense flow through sea straits. Although Eq. 6.9 assumes highly idealized conditions, it may be regarded as a first-order approach for the Denmark Strait Overflow, since the quadratic relation between upstream reservoir height and transport, and the linear dependence between density contrast and transport has been confirmed in realistic model simulations (KÖSTERS, 2004b). Therefore, Eq. 6.9 shall also be employed in this thesis to evaluate observational evidence for hydraulic control.

6.1.4. Transport estimates: Constant PV, realistic cross-section

For all models with zero or non-zero, but constant PV (Eq. 6.5) and geostrophic balance (Eq. 6.6), a parabolic interface shape results from $\partial v / \partial x = const.$ (Figs. 6.2, 6.3). While the WHITEHEAD ET AL. (1974) zero-PV model requires, that the dense flow is banked to the right hand wall, in the more general case of finite, constant PV the parabola is not necessarily located on the right hand side of the strait (Fig. 6.3). In this case, reverse flow occurs on the right-hand side of the dense water plume.
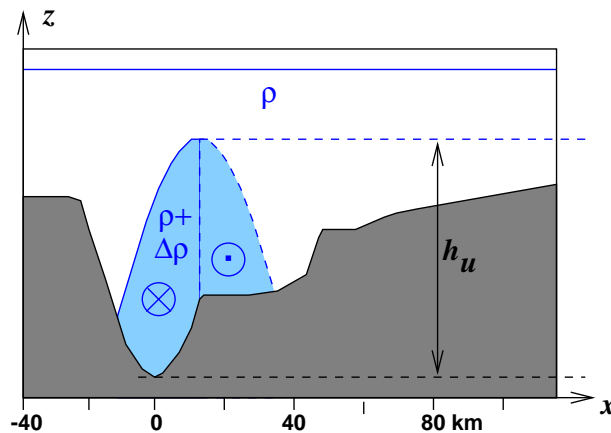
Figure 6.3.: *Cross-section of constant PV flow over realistic Denmark Strait topography (adopted from* NIKOLOPOULOS ET AL., *2003). The view is in downstream direction. The maximum height of the dense water parabola equals the upstream value h_u. The zone of reverse flow may be replaced by stagnant fluid (dashed lines* KILLWORTH, *1994). The maximum transport estimate for both cases is found by variation of the lateral location of the parabola.*

KILLWORTH (1994) suggested to replace the part of reverse flow with stagnant fluid to obtain maximum transports. Based on this theory, a method to calculate the maximum flux for realistic topographies (instead of idealized rectangular (WHITEHEAD

ET AL., 1974) or parabolic cross sections (BORENÄS AND LUNDBERG, 1986)) was developed by BORENÄS AND NIKOLOPOULOS (2000).

It was applied to hydrographic observations of the Denmark Strait by NIKOLOPOULOS ET AL. (2003). For $h_u = 520\,\text{m}$ and $370\,\text{m}$, transport estimates yielded 2.45 and 1.31 Sv with recirculation, and 4.35 and 1.79 Sv in the case without recirculation. For the Denmark Strait, the NIKOLOPOULOS ET AL. (2003) estimates may be considered as upper and lower bounds of the short-term variability, whereas the actual mean transport lies between both values (KÖSTERS, 2004b).

6.1.5. Transport estimates: Non-constant PV

Extending the GILL (1977) model for more different types of dense water sources in a finite basin, HELFRICH AND PRATT (2003) suggested a relation using the dense water height at the left-hand (h_L) and right-hand (h_R) side of the strait entrance to predict the transport:

$$Q_{HP} = \frac{g'}{2f}(h_R^2 - h_L^2) \qquad (6.11)$$

A numerical study proved, that this relation predicts values close to the actual dense water transport (KÖSTERS, 2004b).

Recently, STERN (2004) investigated upper transport limits without any vorticity restrictions for the flow over a sill with parabolic topography, which may be considered as a reasonable approximation of the deep part of Denmark Strait (NIKOLOPOULOS ET AL., 2003). With the only constraint, that the current velocity shall have a maximum at any point on a cross-sill section, STERN (2004) found, that the maximum transport is obtained for uniform geostrophic velocity, i.e. profiles with a constant interface slope across the strait (Fig. 6.4).

The transport can be derived from

$$Q = \frac{g'\mu}{f} \int_\xi^L xH_2 \, dx \qquad (6.12)$$

with reduced gravity g' and the dense water thickness $H_2 = h(x) - M(x)$ between the uniformly sloping interface $h(x)$ and the parabolic bottom height $M(x) = \mu x^2/2$ above the deepest part of the sill.

While the right-hand side intersection point of the interface with the parabolic bottom topography is kept at $x = L$, the absolute transport maximum is obtained, when the left-hand side intersection point ξ is located at $x = -L/2$. Due to the parabolic bottom topography, this implies, that the dense water height at the left-hand wall is $1/4$ of the value h_R at the right hand wall.

The integration of Eq. 6.12 yields in this particular case

$$Q_{Stern} = \frac{g'}{f}2h_R^2[\frac{3}{8} - \frac{15}{64}] \qquad (6.13)$$
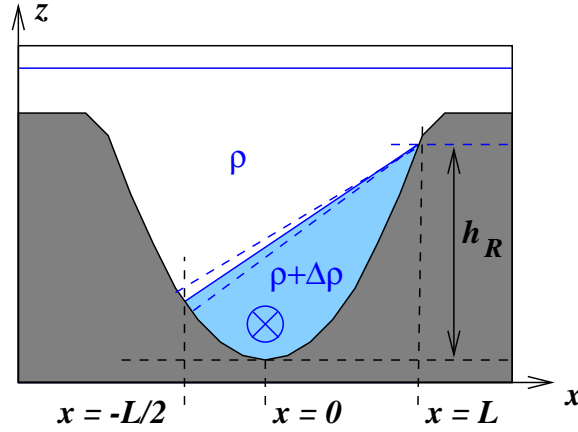
Figure 6.4.: *Cross-section of maximum flow without PV restrictions through a channel with parabolic topography (adopted from STERN, 2004). The view is in downstream direction. The transport maximum is found by varying the interface slope (dashed lines), while the dense water height on the right-hand side of the channel is kept constant at h_R. Maximum transport is achieved, when the left-hand intersection point is at $x = -L/2$, and the right-hand intersection point at $x = L$.*

where h_R is the dense water height at the right-hand wall at the sill. Hence, the transport is independent from the channel width, and depends quadratically on the right-hand wall dense water height at the sill.

If h_R equals the upstream reservoir height h_u – which is not necessarily the case – the ratio of the STERN (2004) and the zero PV WHITEHEAD (1989) estimates is

$$\frac{Q_{Stern}}{Q_{WLK}} = \frac{9}{16} \tag{6.14}$$

Basically, the STERN (2004) relation describes the maximum geostrophically balanced flow of a dense layer beneath a stagnant surface layer. It does not require any particular PV assumptions, and hence might be better suited to describe the real flow through the Denmark Strait (see section 6.2.3). Since it does not assume the conservation of the Bernoulli function, and does not depend on upstream reservoir height, it is not based on hydraulic control mechanisms, even though the transport estimates yield realistic values, whereas the Q_{WLK} bound is typically two times larger than the observed values (review of different straits: WHITEHEAD, 1998).

The introduction of friction (PRATT, 1986; GARRETT, 2002) and of a non-stagnant upper layer (FARMER AND ARMI, 1986; DALZIEL, 1990) is clearly a way to even more realistically describe the dynamics.

The more basic aim in this thesis is, however, to find indications for hydraulic control mechanisms in the observations of the moored SFB array. As a first-order approach, Eq. 6.9 and 6.14 will be used to obtain hydraulic transport estimates and to investigate the quadratic relation reservoir height – transport, the linear relation density contrast – transport, geostrophy and criticality.

6.2. Proof of preconditions for hydraulic control theories

Both the numerical process model of KÄSE AND OSCHLIES (2000) and the observations of the SFB array shall be investigated to assess the critical characteristics that define whether the theories of hydraulic control introduced in the previous section are applicable to the Denmark Strait Overflow. In the following sections, alongstream asymmetry of the overflow, criticality of the flow, potential vorticity and the validity of geostrophic balance will be discussed.

6.2.1. Alongstream momentum balance of the plume in the model

While the observed descent of the Denmark Strait Overflow (Fig. 2.5) is suggestive for a hydraulically controlled flow (ARMI, 1986), the underlying dynamic relations shall be investigated in the process model of KÄSE AND OSCHLIES (2000), that has proven to realistically reproduce the overflow (KÄSE ET AL., 2003).

The basic theories of hydraulic control essentially require the conservation of the Bernoulli potential (see section 6.1).

For real sea straits like the Denmark Strait, conservation of energy along streamlines only holds under consideration of bottom friction and interfacial stress due to current shear. In particular, the downstream descent of the plume is heavily influenced by friction, as shown by GIRTON (2001).

Here, the alongstream momentum balance of the dense water layer shall be investigated.

The equations of momentum per unit mass are given by

$$\frac{\partial \boldsymbol{u}}{\partial t} + \boldsymbol{u} \cdot \nabla \boldsymbol{u} = -\frac{1}{\varrho} \nabla p - 2\boldsymbol{\Omega} \times \boldsymbol{u} + \boldsymbol{g} + \boldsymbol{F_r} \tag{6.15}$$

with current velocity $\boldsymbol{u}$, pressure p, Earth rotation $\boldsymbol{\Omega}$, acceleration of gravity $\boldsymbol{g}$ and friction $\boldsymbol{F_r}$.

A two-layer system is considered now, with vertically averaged properties for each layer.

Hence, the friction term $\boldsymbol{F_r}$ for the lower layer contains both bottom friction and interfacial stress between the two layers. Since in the model a linear drag law was used (KÄSE AND OSCHLIES, 2000), the friction terms yield

$$\boldsymbol{F_r} = r_D \frac{\boldsymbol{u_2}}{H_2} + r_D \frac{\boldsymbol{u_1} - \boldsymbol{u_2}}{H_2} \tag{6.16}$$

as an integral effect on the entire plume with thickness H_2. $r_D = 4.15 \cdot 10^{-4}$ m/s represents the linear drag coefficient. As pointed out by KÄSE AND OSCHLIES (2000), a quadratic friction $\boldsymbol{F_r} = c_D \frac{\boldsymbol{u_2}^2}{H_2}$ would be more appropriate in some cases. KÖSTERS (2004b) applied a quadratic drag law with $c_D = 1 \cdot 10^{-3}$. The choice of either drag

law is of minor importance for the alongstream budget, however, and accounts for a 5 % change in the total alongstream budget only.

In a two layer system, the horizontal pressure gradient term for the lower layer is

$$\frac{1}{\varrho}\nabla p = g\varrho\nabla\zeta + g'\varrho\nabla h_{int} \tag{6.17}$$

with sea surface height (SSH) ζ, reduced gravity g' and interface height h_{int}.

The time-averaged energy per mass unit can be calculated by integration of Eq. 6.15 along streamlines. The first term of Eq. 6.15 vanishes since time-averaged steady state is considered.

Taking v as horizontal current component along the streamline (the normal component u vanishes), the alongstream integration of Eq. 6.15 yields

$$\underbrace{\frac{1}{2}v^2}_{A} + \underbrace{\int_{y_1}^{y_2} w\frac{\partial v}{\partial z}\,dy}_{B} = \underbrace{g\zeta}_{C} + \underbrace{g'h_{int}}_{D} + \underbrace{\int_{y_1}^{y_2} r_D\frac{v}{H_2}\,dy}_{E} + \underbrace{\int_{y_1}^{y_2} r_D\frac{v_1 - v_2}{H_2}\,dy}_{F} \tag{6.18}$$

Term "A" represents kinetic energy. Term "B" denotes entrainment stress exerted on the plume by entrainment of slower water. Term "C" is the potential energy due to changes of Sea Surface Height ζ, "D" potential energy associated with changes of the interface height h_{int}. "E" represents bottom drag, "F" interfacial stress on the plume due to velocity shear.

Due to the separation into mean and fluctuating parts ($v = \overline{v} + v'$), the non-vanishing mean $\overline{v'^2}$ term yields the eddy kinetic energy (EKE) $\overline{1/2v'^2}$, additional to the time-averaged mean kinetic energy $1/2\overline{v}^2$.

GIRTON (2001) studied the energy budget of the descending plume downstream of the sill, analyzing field observations of current velocity and density profiles. The main results of his study are, that the energy budget is dominated by potential energy loss due to the descent of the plume. The total energy appeared to increase along the descent, which might point to external forcing, e.g. due to unresolved SSH changes (GIRTON, 2001). However, there are large uncertainties due to short-term variability.

Here, the temporal mean momentum balance per mass unit along overflow streamlines shall be assessed in the process model to yield an independent estimate of the plume dynamics.

Fig. 6.5 a shows the alongstream momentum balance, integrated below the $\sigma_\Theta = 27.8\,\text{kg/m}^3$ isopycnal along the overflow path, defined by the central 1 Sv transport interval of the dense water transport streamfunction (delimited by bold transport contours in Figs. 6.6 (page 90 and 4.3 a (page 54)). All numbers are referenced to the values 250 km upstream of the sill.

In agreement with GIRTON (2001), the largest single contributor is clearly the potential energy loss of the lower layer of $-6\,\text{m}^2/\text{s}^2$ due to its descent from the sill to depths larger than 1500 m 250 km downstream of the sill. It is balanced by the other terms of Eq. 6.18, each of them being typically one order of magnitude smaller than the lower layer potential energy. Since mean and eddy kinetic energy are always

smaller than $0.5\,\mathrm{m}^2/\mathrm{s}^2$, conservation of energy along streamlines only holds under consideration of friction and entrainment.

Bottom drag and interfacial stress reduce the energy of the plume by $\approx 0.5\,\mathrm{m}^2/\mathrm{s}^2$ or $\approx 0.8\,\mathrm{m}^2/\mathrm{s}^2$, respectively. Direct observations of the descent rate of the overflow plume, however, suggest a higher drag coefficient of $c_D = 0.003$ (GIRTON AND SANFORD, 2003). Since the model reproduces the observed descent rates with $c_D = 0.001$ (GIRTON AND SANFORD, 2003) (or a linear drag coefficient $r_D = 4.15 \cdot 10^{-4}\,\mathrm{m/s}$), entrainment stress should close the alongstream momentum balance. In fact, stress due to entrainment of (slower) water lies in the order of $2.5\,\mathrm{m}^2/\mathrm{s}^2$, and is thus a more important factor than bottom and interfacial stress combined.

The alongstream momentum budget is closed (inside the error boundaries) when the potential energy associated with variable SSH is included. The apparent SSH increase along the overflow path in the model contributes $\approx 1.3\,\mathrm{m}^2/\mathrm{s}^2$. In contrast to the assumption of GIRTON (2001), the SSH effect has thus a decelerating influence on the overflow plume.

Now, the alongstream development of each term (Fig. 6.5 a) shall be considered.

Significant changes start $\approx 130\,\mathrm{km}$ upstream of the sill. From here to the sill, the energy budget is dominated by potential energy due to a downward deflection of the interface (see also Fig. 4.3 b, page 54), and an upward shift of the sea surface, which both remain remarkably constant after a steep increase over the first 30 km. Entrainment stress becomes gradually more important towards the sill. Obviously, the region between 130 km upstream and the sill may be considered as "entrance region" in the sense of HELFRICH AND PRATT (2003) (further discussion in chapter 8).

Downstream of the sill, the lower layer potential energy decreases rapidly. With increasing velocity, friction becomes significant $\approx 100\,\mathrm{km}$ downstream of the sill. This agrees well with observations, which show a maximum in current velocity (GIRTON, 2001) and a minimum in plume thickness (Fig. 2.5, page 35). SSH increases only slightly; thus, the entrainment stress becomes the most important term for the descending plume. While at the sill the current structure is predominantly barotropic, the overflow becomes more and more baroclinic during its descent (current observations by GIRTON, 2001).

6.2.2. Criticality: Froude numbers in model and observations

Introduction

An essential feature of hydraulically controlled flow is criticality.

In the case of slow, subcritical flow (e.g. over a low bump), information may propagate from the receiving basin over the sill, and influence the upstream conditions. For fast, supercritical advection to a sill, the Bernoulli potential $E_{kin} + E_{pot}$ of the fluid is so large, that the volume flux is neither controlled by the sill height, nor by changes in the receiving basin, since information can propagate in downstream direction only.

In the ocean, where kinetic energy is usually too small to achieve supercritical advection, the maximum volume flux over a sill is reached for critical flow conditions. In this "hydraulically controlled" case, the flow passes through a subcritical-

Model: Momentum Balance along DSOW Streamlines

Model: Squared Froude Numbers along DSOW Streamlines
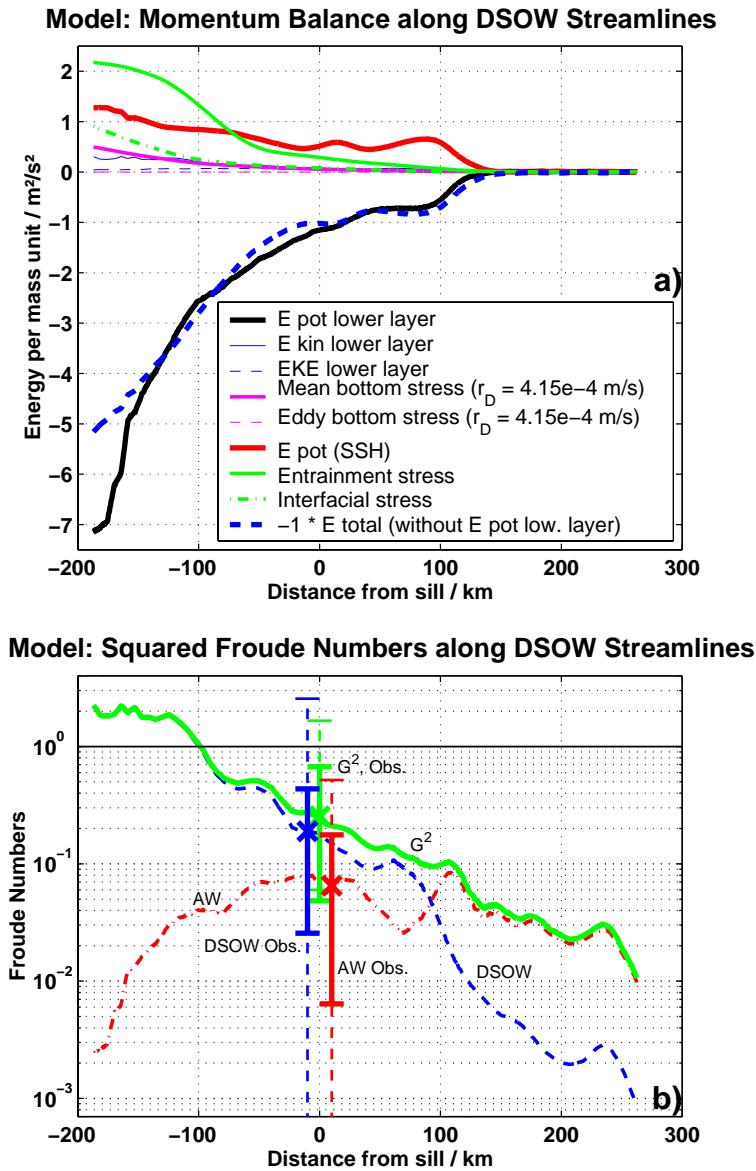
Figure 6.5.: *Denmark Strait process model: Panel a: Temporal mean of the momentum balance along DSOW streamlines. All quantities are cross-stream averages between the -2 Sv and -1 Sv contours below the $\sigma_\Theta = 27.8$ kg/m³ isopycnal of the DSOW transport streamfunction (Figs. 4.3 and 6.6), integrated along the streamlines and referenced to the northern model boundary. For explanation of terms, see text. Panel b: Squared Froude numbers for DSOW layer, upper (AW) layer and composite Froude number G^2. Spatial and temporal averaging and DSOW definition as in panel a. Crosses at the sill mark the corresponding mean values of the field observations by ADCP B at the sill, vertical bars indicate range of variability with heavy lines representing 1σ standard deviation and dashed light lines indicating 95 % range of variability. Two bars are slightly offset from the $x = 0$ position to enhance clarity.*

to-supercritical transition at a "control section" at or near the sill. The supercritical flow downstream blocks information propagation from the downstream basin, and the conditions in the upstream basin depend entirely on the sill geometry (PRATT, 2004).

In a non-rotating two layer system, the phase velocity of internal boundary long gravity waves, that alter the interface height, is

$$c = \sqrt{g'(H_2 H_1)/(H_2 + H_1)} \tag{6.19}$$

with reduced gravity $g' = g \, \Delta\varrho/\varrho$ and upper/lower layer thicknesses H_1, H_2, respectively. For a thin lower layer flowing over a sill, Eq. 6.19 is simplified to

$$c = \sqrt{g' H_2} \tag{6.20}$$

The flow is critical, when c equals the lower layer advection speed v, i.e., the squared Froude number

$$F^2 = \frac{v^2}{g' H_2} = 1 \tag{6.21}$$

For a two layer system, the Froude numbers of the upper and lower layer F_1^2 and F_2^2, respectively, can be merged to a composite Froude number G^2 (ARMI, 1986) as

$$G^2 = F_1^2 + F_2^2 - \frac{\Delta\varrho}{\varrho} F_1^2 + F_2^2 \tag{6.22}$$

Since $\Delta\varrho/\varrho = 0.48/1028 \ll 1$, Eq. 6.22 can be simplified to

$$G^2 = F_1^2 + F_2^2 \tag{6.23}$$

With $G^2 < 1$, the flow is termed subcritical, $G^2 = 1$ critical and for $G^2 > 1$ supercritical.

Criticality of the Denmark Strait Overflow

For rotating systems, other definitions of criticality have been suggested by STERN (1974), GILL (1977), PRATT ET AL. (2000) and HELFRICH AND PRATT (2003). An application of the different concepts to a Denmark Strait Overflow model showed, however, that all Froude numbers become unity at the same location (KÖSTERS, 2004b). Therefore, the definition of Eq. 6.23 will be employed in this study.

Fig. 6.5 b shows the corresponding Froude numbers along overflow streamlines in the process model. The overflow path was selected using the central 1 Sv interval of the average dense water transport streamfunction, similar to the definition in the previous section.

At the sill, the average composite Froude number $G^2 \approx 0.15$. The mean flow reaches criticality not before $\approx 100\,\mathrm{km}$ downstream of the sill, which is in agreement with model results of KÖSTERS (2004b) and observations GIRTON (2001). This can be attributed to friction (virtual control; PRATT ET AL., 2000), which tends to shift the hydraulic control point from the sill to a location further downstream.

The SFB ADCP array at the sill provides additional confirmation for the model results: The mean Froude numbers for both layers at ADCP B (marked as "×" in Fig. 6.5 b) are essentially similar to the model. During strong outflow events with current velocities exceeding $1.5\,\mathrm{m/s}$, critical flow with $G^2 = 1$ is occasionally reached even at the sill (vertical bars in Fig. 6.5 b).

6.2.3. Potential Vorticity

For most concepts of hydraulic control, the conservation of potential vorticity (PV) is a prerequisite, (e.g. WHITEHEAD ET AL., 1974; GILL, 1977; BORENÄS AND LUND-BERG, 1986; KILLWORTH AND MCDONALD, 1993; HELFRICH AND PRATT, 2003; NIKOLOPOULOS ET AL., 2003), as discussed in section 6.1.

It may be questioned, to which degree the conservation of PV holds for the Denmark Strait Overflow. In order to assess the alongstream PV development of the dense overflowing water, the numerical process model shall be investigated here.

The potential vorticity q is defined as

$$q = \frac{\xi + f}{H_2} \tag{6.24}$$

with $\xi = \partial v/\partial x - \partial u/\partial y$ as relative vorticity, Coriolis factor f and layer thickness H_2. It is conserved along streamlines in frictionless flow.

In the process model, the temporal mean of PV along streamlines

$$\overline{q} = \overline{\frac{1}{H_2} \cdot \left(\frac{\partial v}{\partial x} - \frac{\partial u}{\partial y} + f\right)} \tag{6.25}$$

is clearly not uniform (Fig. 6.6 b). The PV of the dense overflow layer increases by a factor of 5 during sill crossing and downstream descent of the overflow plume. In cross-stream direction, PV varies by a factor of 2 over the extent of the SFB mooring array at the sill (Fig. 6.6 b).

Obviously, PV is dominated by layer thickness H_2, since relative vorticity is small compared to the Coriolis factor f. Even in the region 90 km upstream of the sill (close to the TP mooring site), where the strongest current shear is found (Fig. 6.6 a), the ratio of relative vorticity to f is smaller than $(6.5 \cdot 10^{-5}\ 1/\mathrm{s})/(1.3 \cdot 10^{-4}\ 1/\mathrm{s}) = 0.5$.

The layer thickness decreases from $> 1000\,\mathrm{m}$ to a mere $< 200\,\mathrm{m}$ during the most rapid part of the downstream descent. Northeast of the sill, the reduction in layer thickness is partly compensated by a gain of anticyclonic relative vorticity at the Greenland side of the plume (Fig. 6.6 a), but further downstream relative vorticity does not compensate for the layer thinning, since frictional effects are an important factor for the downstream plume dynamics (see next section). This finding agrees with downstream current observations (GIRTON, 2001).

The SFB array proved further observational evidence, that zero or constant PV conditions are not met at the Denmark Strait sill:

For zero PV, the relative vorticity ξ needs to equal f, which yields a current velocity shear of $1.3\,\mathrm{m/s}$ over a cross-stream distance of $10\,\mathrm{km}$. This is by far larger
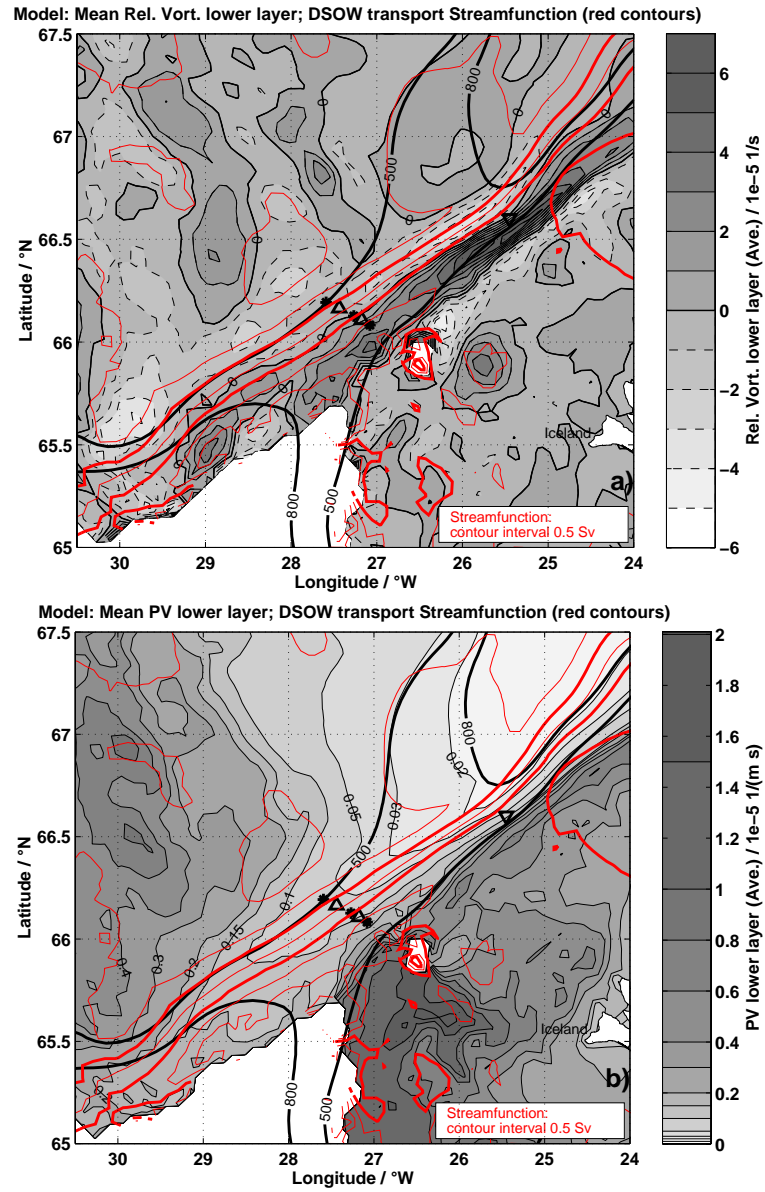
Figure 6.6.: *Denmark Strait process model: Temporal mean of DSOW vorticities. DSOW layer defined by $T < 1.88\,°C$, $\sigma_\Theta > 27.8\,kg/m^3$; shaded with grey contours. Overlaid red contour lines indicate DSOW transport streamfunction. Symbols denote SFB array mooring positions: • ADCP, △ PIES, ▽ TK/TP. Model topography indicated by 500 and 800 m isobaths (heavy black contours). Panel a: Relative vorticity. Panel b: Potential vorticity. Note the PV increase along the overflow path (indicated by the bold −1 and −2 Sv transport contours).*

than the observed average horizontal shear of $0.1\,\mathrm{ms}^{-1}/11\,\mathrm{km}$ between ADCPs A and B or $0.3\,\mathrm{ms}^{-1}/12\,\mathrm{km}$ between ADCPs B and C. For constant finite PV, no particular current shear is required, but the layer depth H_2 varies greatly between the upstream basin and different locations at the sill.

Despite of the substantial differences between the real overflow and the zero PV theories, the WHITEHEAD (1989) model shall be applied to the observation time series, since numerical experiments suggest, that the WHITEHEAD relation is a valid first-order approach to determine the maximum hydraulically controlled transport (KÖSTERS, 2004b).

6.2.4. Geostrophic balance

The theories of hydraulic control discussed in section 6.1 require, that geostrophic balance is valid. Investigations of the high resolution model showed, that $> 90\,\%$ of the Denmark Strait overflow transport at the sill is in geostrophic balance (compare geostrophic and actual current vectors in Fig. 4.3, page 54).

Provided that the real overflow is also geostrophically balanced, measurements of Sea Surface Height (SSH) and interface depth would be an option for integrating transport measurements.

6.2.4.1. Introduction to two-layer geostrophy

In the case of constant potential vorticity (PV), the DSOW/AW interface should be parabolically shaped (NIKOLOPOULOS ET AL., 2003). The overflow model reveals, however, that PV is clearly non-uniform (previous section). At the sill, the average lower layer PV varies by a factor of 2 across the SFB mooring array. Thus, the assumption of constant PV (and hence a parabolic interface shape) is not necessarily valid.

Instead, the overflow shall be treated as a two-layer system with a linearly sloping interface (as suggested by STERN, 2004) to obtain first-order estimates of geostrophic balance.

Assuming two layers of homogeneous density, which is a reasonable approximation of the actual density structure at the sill (Fig. 3.3, page 44), the geostrophic current velocities in the upper and lower layers are given by the MARGULES equation:
Upper layer:

$$v_1 = \frac{g}{f}\frac{\Delta\zeta}{\delta x} \tag{6.26}$$

Lower layer:

$$v_2 = \frac{\varrho_1}{\varrho_2}v_1 + \frac{\Delta z_{int}}{\Delta x}\frac{g}{f}\frac{\Delta\varrho}{\varrho_2} \tag{6.27}$$

v_1 and v_2 denote upper and lower layer velocity (positive = to the north), respectively, ϱ_1 and ϱ_2 upper and lower layer density, density difference $\Delta\varrho = \varrho_2 - \varrho_1$, g acceleration of gravity and Coriolis parameter f. $\Delta\zeta$ is the SSH difference (positive = higher to the east), Δz_{int} the difference of the interface depth (positive = thicker

overflow plume to the east) and Δx the distance between both instruments (13.4 km for the SFB array).

6.2.4.2. Evidence for geostrophy in model and observations

Several PIES have been deployed in the SFB array to obtain estimates of interface depth and sea surface height to test the geostrophic relation.

Due to instrumental failure, only in the period from July 2000 to May 2001 two PIES could be recovered that allow for geostrophic calculations. One constraint for the use of PIES in Denmark Strait is, that on the Greenland side, the small temperature contrast between the overflow and the East Greenland Current waters prevents any estimates of plume thickness, since the two-layer sound propagation model can not be applied. Fortunately, this was not the case for the instruments deployed 2000 – 2001. Hence, full time series of geostrophic currents for 2000 – 2001 were calculated using Eq. 6.26 and 6.27. The current shear between upper and lower layer was calculated from the absolute interface slope determined from the PIES data.

SSH anomalies are determined by each PIES with an accuracy of ± 6 mm (40 h low-passed data). However, since the absolute SSH relative to the geoid is unknown, only sea surface slope anomalies relative to an unknown constant can be derived from the PIES data. The fixed offset was determined by referencing the mean surface current to the mean surface velocity measured by ADCP "B", that was moored halfway between both PIES.

Comparing geostrophic currents with the actual current velocities at ADCP B, the 20 days running means agree well in phase and amplitude of variability. Only on shorter timescales, evidence for some ageostrophic components exists (Fig. 6.7). This indicates, that for long term overflow monitoring SSH and interface depth data (as observed by PIES) allow for realistic transport estimates, provided that there exist independent observations to convert the anomalies to absolute currents.

6.2.4.3. Interface and SSH slope correlation

The observations revealed, that SSH and interface slope anomalies are highly correlated (Fig. 6.7 a), which is corroborated by the process model (Fig. 6.7 d); on timescales longer than 20 days the correlation is even better than -0.95. A regression of this anticorrelation yields a scale factor of 1000. This means, e.g., that a positive SSH anomaly of 50 mm (e.g. by rising SSH at the eastern PIES by 50 mm) corresponds to a negative interface slope anomaly of 50 m (e.g. by thinning the overflow plume at the eastern PIES by 50 m).

As a consequence, the vertical current structure is least baroclinic during strong outflow events. These are associated with eddies, that at the sill have a large barotropic signature through the entire water column (GIRTON, 2001). When the outflow to southwest is less intense at the surface (i.e., positive SSH anomaly in Fig. 6.7), the associated negative interface slope anomaly increases baroclinicity. Since the scale factor between SSH and interface slope anomalies is not smaller than 1000, the lower layer velocity is, however, dominated by the SSH anomalies (verified below).
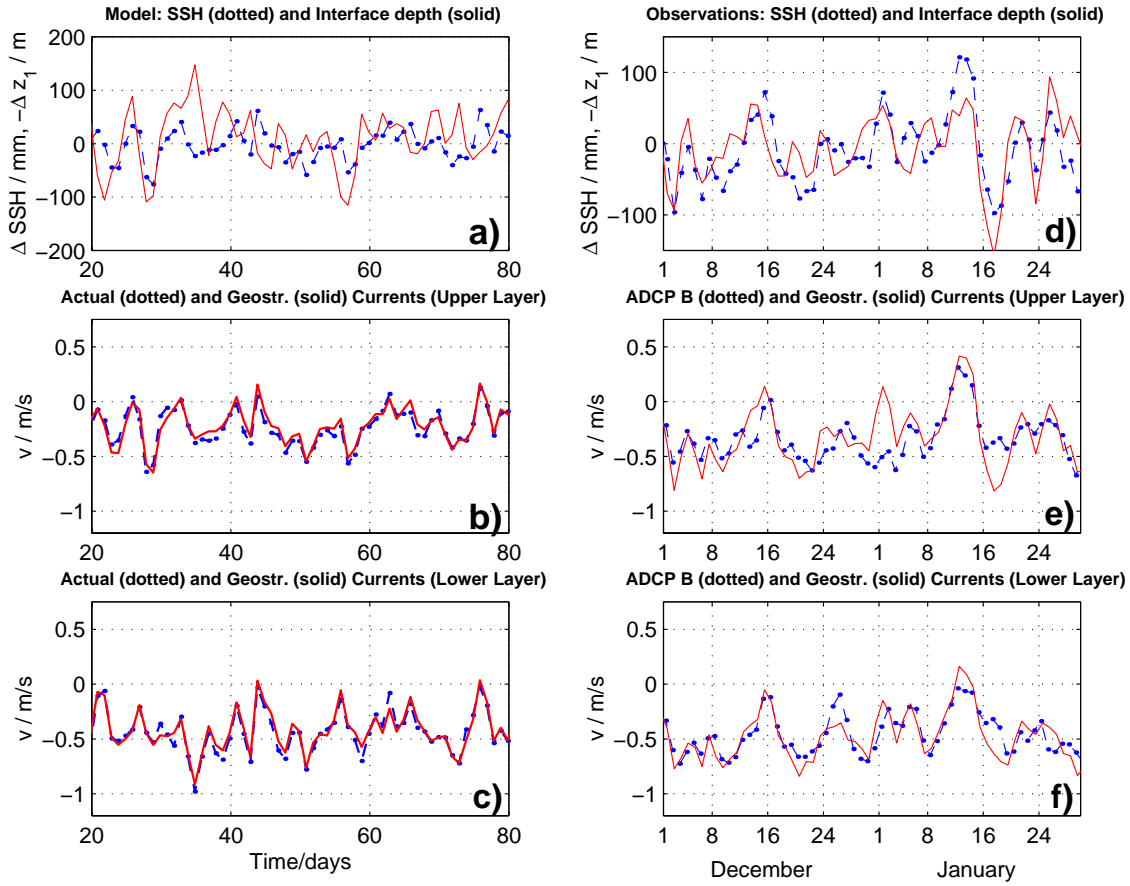
Figure 6.7.: *Comparison of geostrophic and actual currents. Panels a, b, c show results from simulated PIES and ADCP observations in the high resolution model at the same locations as the actual observations, shown on panels d, e, f.* **Top panels** *illustrate the correlation between SSH (blue dotted line) and interface slope anomalies (red line). Positive values mean "higher to the east". Note, that the interface slope is plotted with reverse sign and scaled by a factor of 1/1000.* **Centre and bottom panels** *depict geostrophic (red lines) and actual currents (blue dotted lines) for surface and overflow layer, respectively. Positive values correspond to inflow to the northeast, negative values to outflow to the southwest.*

Thus, even though baroclinicity is larger during weak currents at the surface, the absolute overflow layer current varies positively and in phase with the surface current velocity.

These conclusions agree with direct ADCP measurements, comparing profiles with weak surface currents, but strong baroclinic shear above the overflow plume, and profiles with strong barotropic outflow in the entire water column (Fig. 4.2, page 52).

The connection can be verified considering equations 3.6 and 3.7 for geostrophic currents in a two layer system. Inserting 3.6 into 3.7, and replacing Δz_{int} by the observed relation $\Delta z_{int} = -1000 \cdot \Delta \zeta$, the following relation results:

$$v_2 = \frac{g}{f} \frac{\Delta \zeta}{\Delta x} \frac{1}{\varrho_2} (\underbrace{\varrho_1}_{A} + \underbrace{(-1000) \cdot \Delta \varrho}_{B})$$

(6.28)

With $\varrho_1 = 1027.42 \, \text{kg/m}^3$ and $\Delta \varrho = 0.48 \, \text{kg/m}^3$ (GIRTON ET AL., 2001), term A, which originates from the surface current part (6.26), is larger than term B, that represents the baroclinic shear between upper and lower layer. Thus, positive SSH slope anomalies (weak outflow at the surface) imply increased baroclinicity, but positive absolute v_2 changes corresponding to weak outflow, as is evident in the observations.

Linking SSH with interface slope, this correlation opens a possible perspective for long term monitoring of the deep overflow by remote sensing (see chapter 10).

6.2.5. Comparison of observed sill sections and hydraulic estimates

To obtain realistic predictions of the hydraulically controlled part of the overflow, the skill of the theoretical relations introduced in section 6.1 has to be evaluated. Here, the observed hydrographic sections at the sill shall be investigated to compare the actual density driven, geostrophically balanced dense water transport with theoretical estimates.

In contrast to the 1 1/2 layer relations of hydraulic control, there exists a large barotropic flow component in the Denmark Strait. Numerical studies suggest, however, that the overflow may be considered as a linear superposition of a barotropic component and a density driven hydraulically controlled part (KÖSTERS, 2004b), which shall be assessed here.

As shown in the previous section, $> 90\,\%$ of the currents at the Denmark Strait sill are in geostrophic balance, and can be described with a 2-layer model. Hence, the basic assumption of geostrophy in all hydraulic theories introduced in section 6.1 is met.

Moreover, the observations revealed, that zero or constant PV is not valid for the real overflow (section 6.2.3). Therefore, the STERN (2004) relation, that requires no PV conservation, might be more appropriate than zero/constant PV hydraulic theories.

During the SFB observations 1999 – 2004, four hydrographic sections have been obtained that cover a sufficiently wide part of the overflow (P262, 2000; M50/4,

2001; P301, 2003; P315, 2004; see Fig. 2.4, page 33) to investigate different transport estimates.

These sections allow to compare

Q_{obs2l} Actual density driven flow of the DSOW layer, calculated from 2-layer geostrophy with a stagnant surface layer, and integrated between the observed depth of the $\sigma_\Theta = 27.8\,\text{kg/m}^3$ isopycnal and the real bottom topography.

Q_{Stern} STERN (2004) transport estimate, depending on the observed dense water height h_R on the right-hand side of the section.

Q_{WLK} WHITEHEAD (1989) hydraulic transport bound for zero PV / rectangular channel conditions. Here, the dense water height h_R on the right-hand side of the section is assumed to equal the upstream height h_u.

The height of the $\sigma_\Theta = 27.8\,\text{kg/m}^3$ isopycnal above the sill observed on the four selected hydrographic sections is shown on Fig. 6.8 a,b. P262 and P301 (panel a) cover the Greenland shelf to a distance of 75 km northwest of the sill; M50/4 and P315 (panel b) have a more limited range. However, they are likely to cover most of the overflow transport (considering the spatial transport distribution in the process model), and the dense water height on the Greenland side may be considered as representative for h_R, or, in the light of zero PV models, the upstream value h_u.

Based on a density contrast of $0.43\,\text{kg/m}^3$, transport integrals for Q_{obs2l}, Q_{Stern} and Q_{WLK} have been obtained (Fig. 6.8 c,d). Due to the non-linear interface slope, and the irregular topography, the spatial distribution of Q_{obs2l} (Fig. 6.8 c,d) varies considerably between the sections. Interestingly, the resulting total Q_{obs2l} transport more or less depends on the dense water height difference between the Greenland and Iceland sides only. This suggests, that the integrated influence of the non-uniform interface and bottom slope is not very large, and that integrating geostrophic end-point measurements may yield transport errors $< 0.5\,\text{Sv}$. Further, the left-hand side dense water height above the sill is approximately $1/4$ of h_R in all sections, and thus close to the relation predicted as transport extremum by STERN (2004).

The resulting transport estimates obtained with the STERN (2004) relation based on a parabolic topography and linear sloping interface (overlaid with thin lines, Fig. 6.8) are listed in Table 6.1.

Table 6.1.: Comparison of geostrophic transport estimates

Cruise/Year	P262 / 2000	M50/4 / 2001	P301 / 2003	P315 / 2004	average
Q_{obs2l}	1.50 Sv	2.58 Sv	1.27 Sv	2.43 Sv	1.95 Sv
Q_{Stern}	1.65 Sv	2.02 Sv	1.72 Sv	2.00 Sv	1.85 Sv
Q_{WLK}	2.93 Sv	3.58 Sv	3.06 Sv	3.55 Sv	3.28 Sv

On average, the actual geostrophic dense layer transport Q_{obs2l} is approximately 5 % larger than Q_{Stern}. Although it is questionable to conclude on the basis of four sections only, the STERN (2004) relation may thus be considered as a viable estimate.
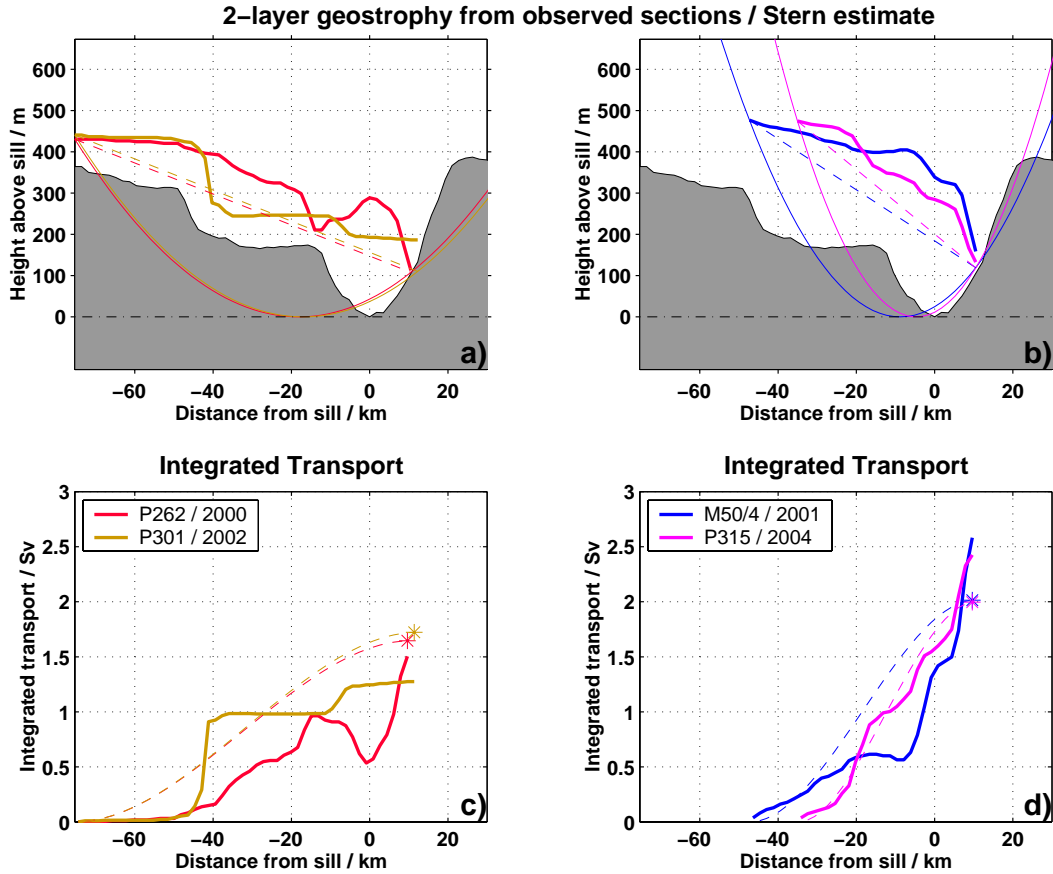
Figure 6.8.: *Observed hydrographic sections, and geostrophic transport of the dense layer below the $\sigma_\Theta = 27.8\,\mathrm{kg/m^3}$ isopycnal. To illustrate the variability range on sections with comparable east-west extension, P262(2000) and P301(2003) are shown in panel a, and M50/4 (2001) and P315 (2004) in panel b. Light lines denote corresponding parabolic bottom topography and linear interface slope according to* Stern *(2004). The bottom panels c, d show the corresponding geostrophic transport, inferred from 2-layer geostrophy with a stagnant surface layer, integrated from west to east. Dashed lines and * represent the* Stern *estimate, bold lines actual transport.*

Focusing on the hydraulic WHITEHEAD (1989) estimates, it might be argued, that Q_{WLK} requires the upstream reservoir height h_u rather than sill values.

Certainly, the dense water height at the sill is somewhat lowered due to frictional effects (see section 6.2.1 for a model analysis). In contrast, the WHITEHEAD (1989) model assumes, that h_R at the sill equals h_u.

However, the estimates in table 6.1, which are based on the right-hand wall dense water height at the sill, are likely to be representative for Q_{WLK}, since the average ratio Q_{obs2l}/Q_{WLK} is 0.59, which is a rather typical value for the comparison between zero PV / rectangular channel conditions and realistic flow:

In a numerical simulation, KÖSTERS (2004b) obtained a smaller ratio $Q_{\text{obs2l}}/Q_{WLK} = 0.46$, if the reservoir height is taken further upstream. WHITEHEAD (1998) found $Q_{\text{obs2l}}/Q_{WLK} = 0.77$ for the Denmark Strait; this estimate was based on a larger reservoir height of 580 m and a smaller density contrast (DICKSON ET AL., 1990), though. Thus, the Q_{WLK} estimates obtained here qualitatively agree with the range established by previous studies.

Concluding, the evaluation of interface depth / SSH observations (previous section) and hydrographic sections has the following implications:

- In agreement with hydraulic theories, 2-layer geostrophy is valid (section 6.2.4).

- The ratio between Q_{obs2l} and Q_{WLK} lies in the range established by WHITEHEAD (1998), whereas the STERN (2004) transport extremum yields fairly realistic estimates of Q_{obs2l}.

- The absolute values of Q_{obs2l} (average 1.95 Sv) are much smaller than the total overflow transport (3.35 Sv, ADCP observations, 1999 – 2003 mean).

Therefore, the observations suggest, that only $\approx 56\,\%$ of the Denmark Strait Overflow may be regarded as density driven flow. In contrast to previous studies, the actual upstream reservoir height might be lower than 580 m (DICKSON ET AL., 1990). This could explain, that the absolute hydraulic estimates are substantially smaller than those of WHITEHEAD (1998), NIKOLOPOULOS ET AL. (2003) and STERN (2004), even though geostrophy is valid.

6.3. Evidence for hydraulic control mechanisms in the SFB observations

The implications of hydraulic control for the Denmark Strait Overflow have been studied by various authors (WHITEHEAD, 1998; GIRTON, 2001; NIKOLOPOULOS ET AL., 2003; KÖSTERS, 2004a, a.o.). The evaluation of the process model, interface and sea surface height observations, and hydrographic sections in this study suggests, that a fraction of $\approx 56\,\%$ of the overflow might be considered as density driven, which may be assessed with hydraulic control theories.

Here, hydraulic estimates shall be applied to the observational time series of the SFB mooring array, which offer the opportunity to evaluate some new, different evidence of hydraulic control mechanisms.

The hydraulic transport estimates require knowledge about the dense water reservoir height. On the Icelandic side, reservoir height estimates are available at the "TP" mooring site 93 km upstream of the sill, and at the Kögur 5 (KG5) hydrographic station 200 km upstream of the sill (for locations, see Fig. 2.1, page 27). Considering the process model results (section 6.2.1), the "TP" position is clearly located in the entrance region of the sill, where currents are non-zero and the reservoir height lower than in the interior basin. Since the HELFRICH AND PRATT (2003) relation additionally requires the dense water height on the Greenland side, it can not be used to determine hydraulic transport estimates, though.

To evaluate the quadratic relation between reservoir height and transport, and the linear relation for the density contrast, which is valid for all hydraulic theories discussed in section 6.1, the WHITEHEAD (1989) relation shall be applied to the TP and KG5 data as a qualitative first-order estimate.

The most realistic estimates may be expected from the Icelandic Kögur 5 station. Since it lies 200 km upstream of the sill, the reservoir height at KG5 is likely less affected by "sill entrance" effects. The STERN (2004) relation (9/16 of the WHITEHEAD bound) that requires no (unrealistic) zero PV assumptions and has proven to yield realistic values, compared with actual hydrographic sections at the sill (previous section). Therefore, it shall be employed to obtain more accurate absolute transport estimates for the hydraulically controlled flow over the Denmark Strait sill. However, one has to be aware, that the STERN (2004) estimate is based on the dense water height at the right-hand side of the sill section, which has only occasionally been sampled, rather than upstream values at KG5. The observations suggest, that the minimum depth of the $\sigma_\Theta = 27.8\,\mathrm{kg/m^3}$ isopycnal at the sill section normally lies in the range of 200 to 300 m (Fig. 2.4, page 33), which is $\approx 100\,\mathrm{m}$ deeper than at the KG5 station (Fig. 6.12, page 105). Therefore, the upstream reservoir height at Kögur 5 might be considered as an upper bound for the right-hand side dense water height at the sill. Consequently, even the STERN (2004) relation applied to the KG5 reservoir height might overestimate the actual hydraulically controlled transport.

In the following sections, observational evidence for hydraulic control mechanisms shall be investigated in the time series of the SFB mooring array and Icelandic hydrographic data.

6.3.1.   TK mooring 93 km upstream of the sill 1999 − 2000

To investigate whether the overflow is hydraulically controlled, temperature recording moorings were deployed on a position 93 km upstream of the sill on the Icelandic shelf edge in 1999/2000 ("TK") and 2001/2002 ("TP"). This location is likely situated in a pathway of overflow water to the sill (see section 8.3).

Since the TK and TP moorings did not measure salinity, only warm AW could clearly be distinguished from the cold, dense overflow water.

Hydraulic transport estimates

On weekly timescales, the reservoir height (taken at the 2 °C isotherm) could be determined with reasonable accuracy, despite of instrumental problems that caused a large short term scatter of the temperature records. The scatter of individual records was as high as O(1 °C). One week low-passing (i.e. over 84 measurements) reduces this error by $1/\sqrt{84}$ to O(0.1 °C), which is sufficient to locate the thermocline between AW and DSOW.

As shown by MACRANDER (2001), the mean WHITEHEAD transport ($Q_{WLK} = 1/2 \; g'/f \; h_{eff}^2$) transport defined by the height of the 2 °C isotherm was estimated to equal $Q_{WLK} = (2.3 \pm 0.9)$ Sv (with $\Delta\varrho/\varrho = 3.9 \cdot 10^{-4}$, derived from Poseidon P 262 CTD data).

This value is significantly smaller than the actual transport of 3.68 Sv observed by ADCPs (section 5.3).

Possible reasons for the underestimate are:

- The current velocity at TK was not taken into account. Assuming a current velocity of 0.58 m/s (which is reached occasionally, Poseidon P 244 observations, GIRTON, 2001), the hydraulic estimates would reach the WHITEHEAD (1998) value of 3.8 Sv. The mean velocity, however, lies in the order of 0.1 m/s both in observations and model. Thus, the kinetic energy is of minor importance, rising the hydraulic transport bound by around 1 % only.

- At the TK mooring site, the interface depth is not necessarily representative for the entire upstream basin. Also, being located just 93 km upstream of the sill, the reservoir height is already lowered to some degree (model results: see Fig. 4.3 b, page 54), since the dynamics are influenced by the narrowing and shallowing cross section (note the onset of potential energy loss as far as 130 km upstream of the sill in Fig. 6.5 a, page 87). Moreover, the process model suggests, that the TK/TP position right at the Icelandic shelf edge is also highly sensitive to lateral shifts of the overflow pathway (note the large cross-stream gradient of the reservoir height at TP, Fig. 4.3 b, page 54).

- Recent studies (BIASTOCH ET AL., 2003; KÖSTERS, 2004b) revealed, that the Denmark Strait Overflow is only partly density driven, and is increased by barotropic forcing. This key issue shall be addressed in chapter 7.

The transport time series (Fig. 6.9 a), however, catch the short time variability fairly well, as would be expected from the model studies of KÖSTERS (2004b). The
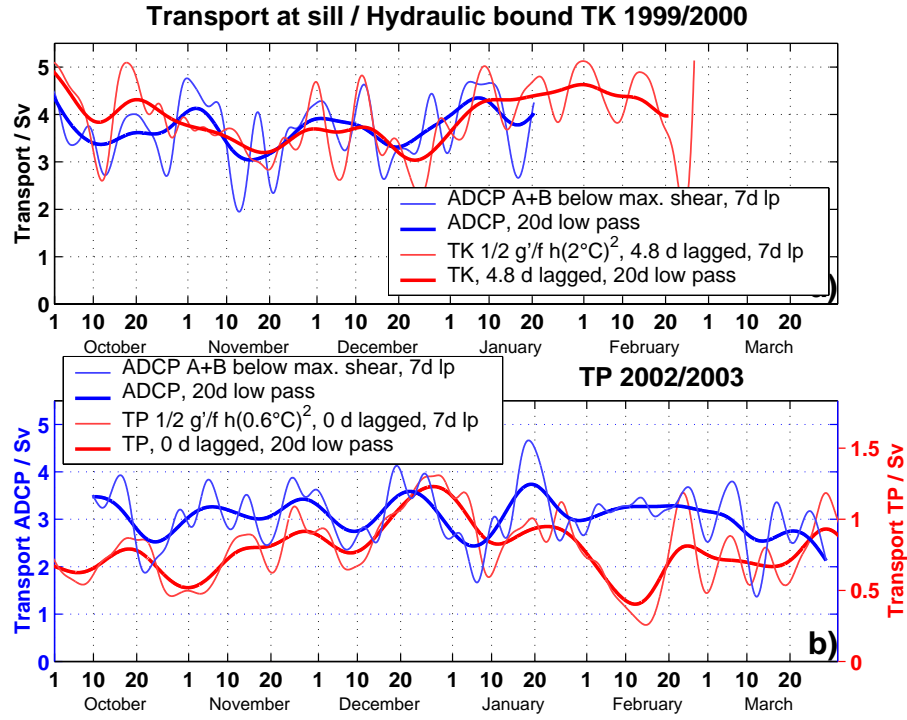
Figure 6.9.: *Hydraulic transport estimates 1/2 g'/f h_{eff}^2 at the TK/TP mooring site 93 km upstream of the sill, compared to ADCP measured transports. Reduced gravity $g' = g \cdot 0.48/1027.8$. Panel a: TK mooring 1999/2000. Reservoir height determined by depth of the 2°C isotherm. 7 and 20 day low-passed values. TK time series lagged by 4.8 days corresponding to correlation maximum. Panel b: TP mooring 2002/2003. Reservoir height determined by depth of the 0.6°C isotherm. 7 and 20 day low-passed values. Time series not lagged, since no significant correlation maximum was found. Note the different transport axis for the TP estimates.*

7 day low-passed values yields a moderate maximum correlation of $r = 0.31$ for a time lag of 4.8 days (significant at the 99 % confidence level; MACRANDER, 2001). This corresponds to a signal propagation speed of 22 cm/s, and agrees well with the observed eddy translation velocity of $12 - 28$ cm/s at the sill (GIRTON, 2001).

The advection velocity is faster than the mean current of 9.6 cm/s observed further upstream by JÓNSSON AND VALDIMARSSON (2004a), and the 10 cm/s resulting from a temperature correlation maximum found for the TP mooring in 2002/2003 (section 8.3). Considering the large cross-stream current shear at the Icelandic shelf edge (model results: Fig. 4.3, page 54), a small lateral shift of the frontal zone between overflow and the north-eastward flowing Irminger Current (NIIC) could easily affect the advection of temperature anomalies from the TK/TP site to the sill.

6.3.2.   TP mooring 93 km upstream of the sill 2002 – 2003

Hydraulic transport estimates

During the period 2002/2003, most of the time not warm AW, but colder waters of the EGC lied on top of the dense overflow water (Fig. 6.10), which makes reservoir height estimates much more difficult.
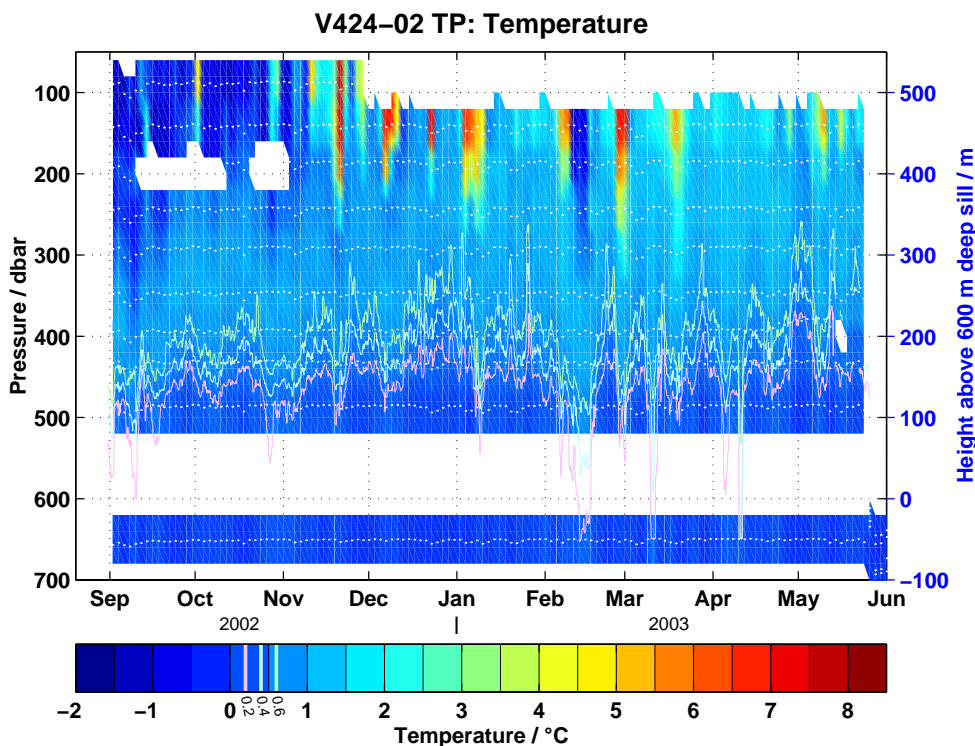
Figure 6.10.: *Temperature time series of TP mooring. Field of daily mean temperatures mapped to depth by objective analysis. White dotted lines indicate depth of Mini-TP temperature sensors. Some of them are equipped with a pressure sensor, too, allowing to estimate the vertical subduction of the mooring during strong current events. Magenta, cyan and green lines denote location of the deep 0.2, 0.4 and 0.6 °C isotherms, respectively. Above the dense overflow water, both colder water of the EGC and, occasionally, warmer AW occur.*

While at the TK mooring in 1999/2000, the 2 °C isotherm was used as an approximation of the dense water reservoir height, in 2002/2003 the $\sigma_\Theta = 27.8\,\mathrm{kg/m^3}$ isopycnal could not be tracked by a simple temperature criterion.

It is worth noting, that in 2002/2003 more warm Atlantic inflow was observed in the Denmark Strait than in 1999/2000 (discussion in section 2.3; VALDIMARSSON, pers. comm.). It is unclear, however, why in contrast to the TK mooring, the TP deployment observed AW less frequently.

The depth of certain (colder) isotherms in the 300 to 600 m depth range, is highly correlated (Fig. 6.10). In the temperature interval 0.2 °C – 0.6 °C, the isotherms are

likely to represent changes of the dense water that supplies the overflow, and are not affected by cold EGC / warm NIIC regime changes that occur at shallower depths.

Hence, the depth of the 0.6 °C isotherm, which is the warmest isotherm always observed in the 300 to 600 m depth range is taken as a measure for the reservoir height, and shall be used for a qualitative assessment of hydraulic relations.

The observed 207 m mean height of the 0.6 °C isotherm above the sill yields a maximum hydraulically controlled transport of 0.80 Sv. This figure is likely an underestimate of the actual hydraulic transport bound, since parts of the dense water are located above the deep 0.6 °C isotherm, being either colder and fresher, or warmer and more saline, and can not be resolved by temperature-only measuring instruments.

The resulting hydraulic transport time series (Fig. 6.9 b; note different scaling) are only weakly correlated with the actual DSOW transport at the sill. No significant correlation maximum exists, neither at zero time lag, nor at 4.8 days (as for the TK mooring, Fig. 6.9 a) or 11 days, as could be expected from the observed temperature correlation (see section 8.3).

In contrast to the TK mooring, which encountered warm AW most of the time, the TP mooring could not prove hydraulic constraints by using the height of certain isotherms *inside* of the dense water. This finding is confirmed considering the hydrographic time series of the Kögur 5 station 200 km upstream of the sill (Fig. 6.12): The height of deep isotherms, e.g. $\Theta = 0.5$ °C, is not generally correlated with the height of the $\sigma_\Theta = 27.8$ kg/m^3 isopycnal.

Communication by boundary layer gravity waves

Focusing on near-bottom temperatures at TP and ADCP B rather than transport estimates, a high correlation of $r = 0.8$ associated with a time lag of 11 days (see section 8.3) suggests, that the TP mooring is indeed situated in a major pathway (Jónsson and Valdimarsson, 2004a) to the sill.

On faster than advective timescales, evidence for basin-sill communication by propagation of long gravity waves has been investigated, although these signal are likely hard to detect, since strong barotropic currents of at times > 0.5 m/s and eddy activity (observations by e.g. Girton, 2001) on short timescales will override the theoretical relation.

However, the time series of near-bottom temperature at the TP mooring and ADCP B show a weakly pronounced correlation maximum of $r = 0.19$ for a time lag of 31 hours (significant to the 99 % confidence level; Fig. 6.11), which corresponds to a propagation speed of 0.83 m/s.

The phase velocity of long gravity waves at internal boundaries is given by

$$c = \sqrt{g'(H_2 H_1)/(H_2 + H_1)} \tag{6.29}$$

With parameter settings appropriate for the Denmark Strait ($g' = g \cdot (0.48 \text{ kg/m}^3/\varrho_2)$, upper and lower layer thicknesses $H_1 = 240$ m and $H_2 = 360$ m, respectively), one yields $c = 0.81$ m/s.

Thus, the observed lagged correlation is possibly a (weak) indication of communication between the upstream basin and the sill, since in a continuously stratified
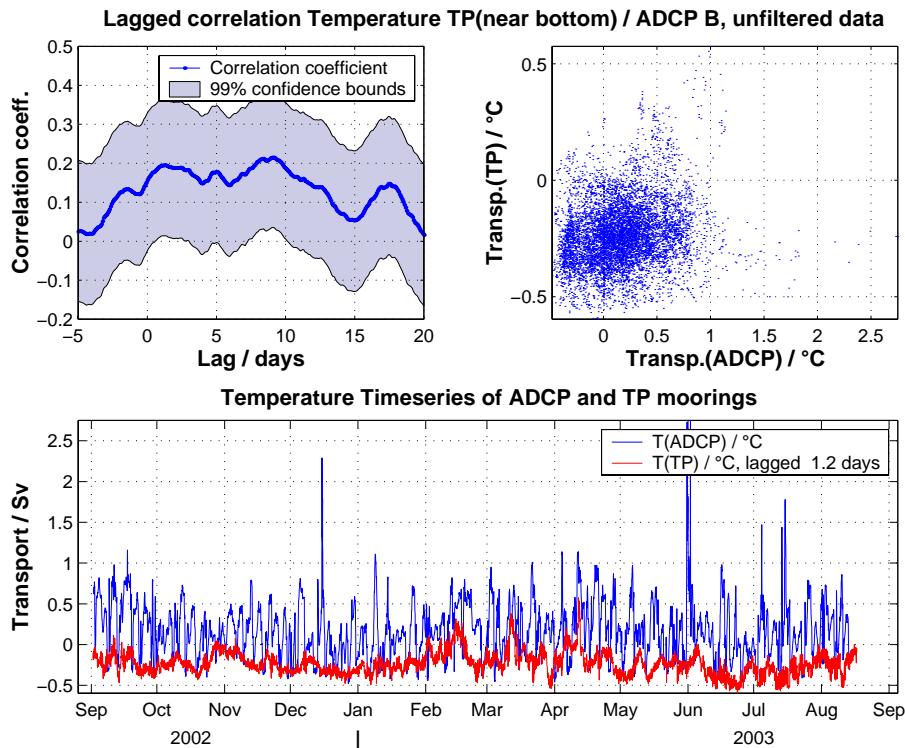
Figure 6.11.: *Lagged temperature correlation between TP mooring 93 km upstream of the sill and ADCP B, unfiltered time series. The correlation maximum at a time lag of 31 hours corresponds to the phase velocity of internal long waves (0.83 m/s).*

system, temperature changes at a given depth are associated to height changes of isotherms, and corresponding isopycnals (considering the typical Θ/S relation close to the bottom; Figs. 2.3, page 31, and 8.5, page 132).

The physically more interesting height of the upper DSOW boundary ($\sigma_\Theta = 27.8 \, \text{kg/m}^3$) could not be detected by the TP mooring, as mentioned above. Since the TK mooring in 1999/2000 does not allow any short-term analysis due to instrumental errors, the near-bottom temperature correlation maximum presented here is the only indication of communication faster than the observed advective velocities, which have been estimated with 22 cm/s for TK and 10 cm/s for the TP moorings.

6.3.3. Results from hydrographic data of the Kögur section 200 km upstream of the sill

Repeated Icelandic hydrographic stations on the Kögur section 200 km upstream of the sill (for location, see Fig. 2.1, page 27) allow the assessment of interannual variability in the upstream region.

The observations suggest, that the reservoir height experienced an interannual decrease during the SFB array deployment time 1999 – 2003, which implies a reduction

of the hydraulically controlled flow over the sill.

At the station Kögur 5 (KG5 in Fig. 2.1), which lies close to the recently documented upstream pathway to the sill (JÓNSSON AND VALDIMARSSON, 2004a), the height of the $\sigma_\Theta = 27.8\,\mathrm{kg/m^3}$ isopycnal above the 600 m deep sill varied between 500 and 400 m, with a pronounced interannual decrease from Feb. 2001 to Nov. 2002.

The resulting hydraulic transport estimates ($Q_{WLK} = 1/2\ g'/f\ h_{eff}^2$, WHITEHEAD, 1998), calculated with a density contrast of $0.48\,\mathrm{kg/m^3}$ (GIRTON ET AL., 2001) agree fairly well with the ADCP observations at the sill (Fig. 6.13 a). The individual measurements of KG5, taken about four times per year, show considerable scatter due to unresolved short term variability. The yearly averages, however, almost match the observed transports at the sill.

Typically, Q_{WLK} for zero PV and rectangular cross section overestimates the actual transport through a real strait. Applying the more realistic estimate of STERN (2004) ($Q_{Stern} = 9/16\ \cdot\ Q_{WLK}$), the KG5 results would underestimate the DSOW transport measured at the sill by about 45 %.

This significant underestimate might be attributed to the following points:

- The current velocity at KG5 (9.6 cm/s on average, JÓNSSON AND VALDIMARSSON, 2004a) has not been taken into account. However, the corresponding kinetic energy would change the effective reservoir height by 1 m, which yields a negligible transport change of O(0.02 Sv) only.

- Similar to the TP mooring, KG5 might be considered as a sill entrance location. In the process model, however, the "entrance" region, where the interface height is significantly lower than in the interior upstream basin, appears to begin $\approx$ 130 km upstream of the sill (Fig. 6.5 a, page 87). Hence, the TP site (93 km upstream) is clearly located in the "entrance" region, but not the KG5 site, which is 200 km upstream of the sill.

- The reservoir height at KG5 might be lower than further to the north-west in the interior basin, and thus be not representative for hydraulic estimates. Icelandic hydrographic surveys on the Kögur section (JÓNSSON AND VALDIMARSSON, 2004a) revealed, however, that the dense water at KG5 (which is closest to the observed current towards the sill) is higher than anywhere else on the section (Fig. 6.14).

- Parts of the Denmark Strait Overflow are likely to be driven by barotropic wind stress forcing, and not the internal pressure gradient. Model experiments of KÖSTERS (2004b) showed, that $\approx$ 34 % of the overflow are wind driven. Hence, only about 2.3 Sv need to be supplied by the hydraulically controlled flow. The hydraulic estimates from KG5, derived by Eq. 6.14 ($Q_{Stern} = Q_{WLK} \cdot$ 9/16) yield on average 1.9 Sv. With uncertainties inherent in the reservoir height evaluation from just one station, this hydraulic estimate is consistent with the results of KÖSTERS (2004b), and with the 2-layer geostrophic estimates based on hydrographic sections at the sill (section 6.2.5).
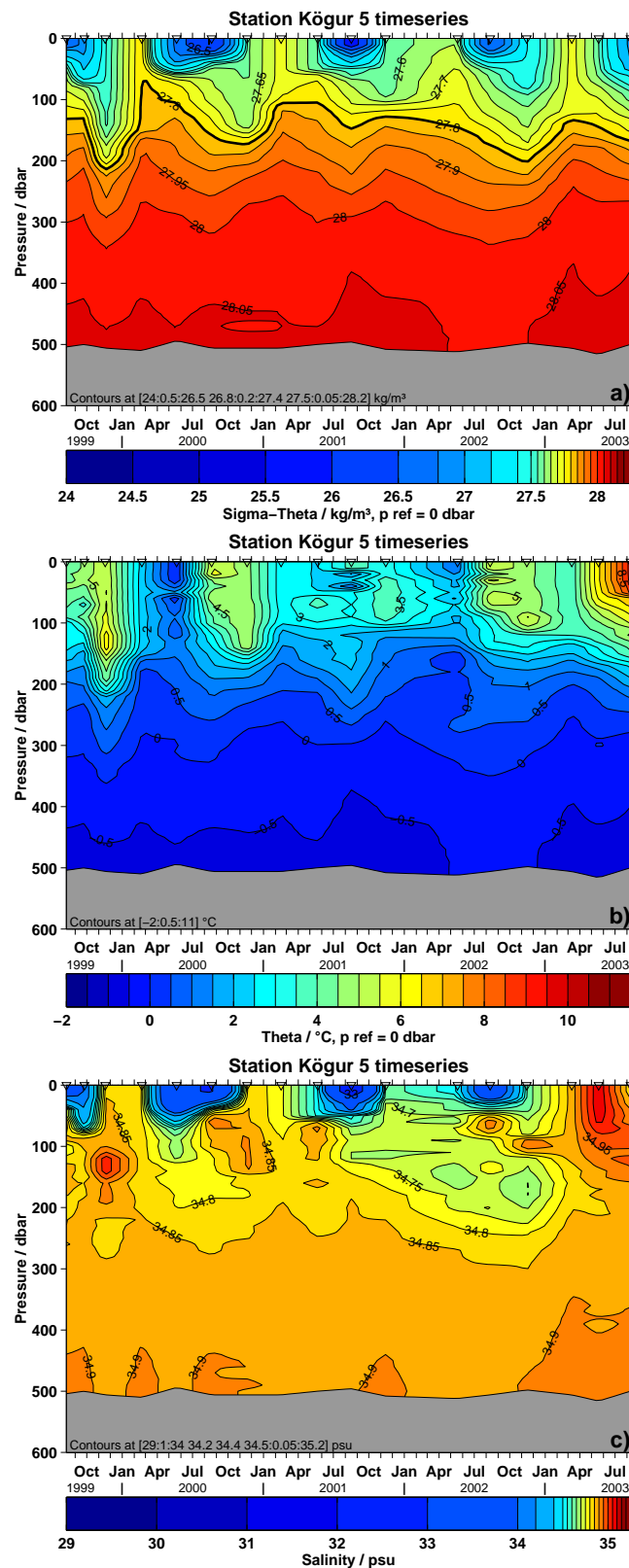
Figure 6.12.: *Potential density at Kögur 5 station. Triangles at the surface indicate, at which times the station was sampled during the seasonal Icelandic hydrographic surveys. $\sigma_\Theta = 27.8 \, \text{kg/m}^3$ isopycnal marked as heavy line. Similar colour scale as for all hydrographic section contour plots in this thesis.*

105
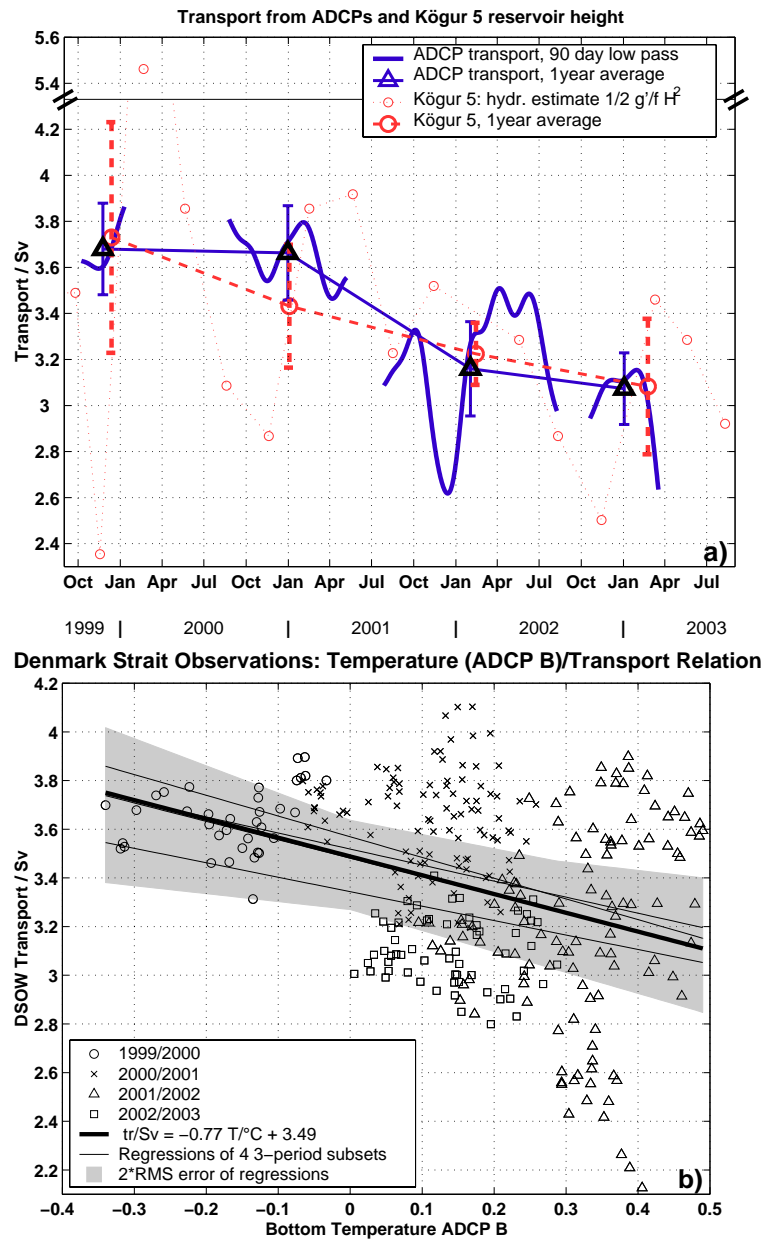
Figure 6.13.: *Tests for hydraulic control mechanisms: Panel a: Maximum hydrauli-
cally controlled transport Q_{WLK}, derived from the height of the $\sigma_\Theta =
27.8 \, kg/m^3$ isopycnal above the sill at KG5. Each red circle denotes a
single CTD observation, the heavy red line connects averages correspond-
ing to each deployment period of the ADCPs at the sill. Blue lines de-
note actual DSOW transport below layer of maximum current shear, 3
months low-pass, and deployment period averages, respectively. Vertical
bars indicate RMS variability of each period. Panel b: Local correlation of
bottom temperature (ADCP B) and DSOW transport (30 days running
means) at the sill. Different symbols mark the four deployment periods.
The total regression line (heavy line) yields a slope of $-0.77 \pm 0.13 \, Sv/°C$.
Light lines denote linear regression of four different subsets with one de-
ployment period omitted in each subset. One line is identical with the
total regression within $\pm 0.01 \, Sv$. Shading indicates area smaller than
twice the RMS error.*
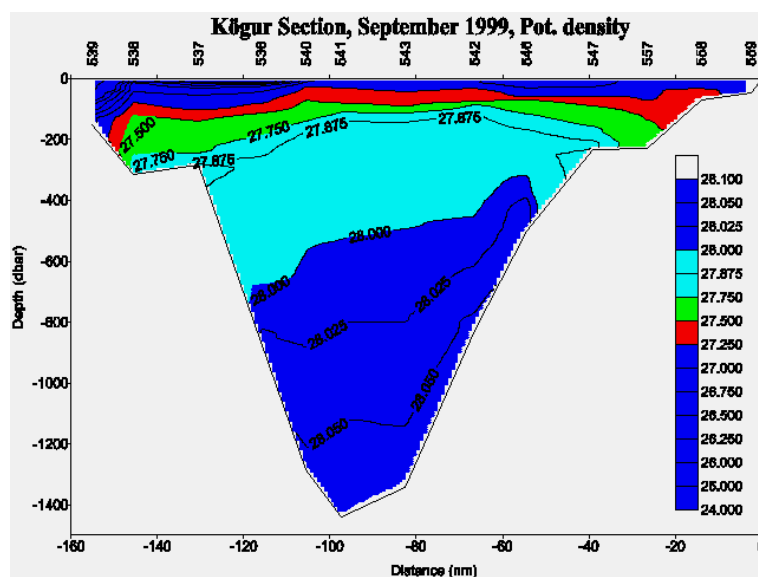
Figure 6.14.: *Potential density on the Icelandic Kögur section September 1999, cover-*
ing the entire section from Greenland (left-hand side) to Iceland (right-
hand side). Note, that the height of the $\sigma_\Theta = 27.8\,\mathrm{kg/m^3}$ isopycnal is
greatest at the Icelandic shelf edge at the KG5 station 546. This feature
is regularly observed (JÓNSSON AND VALDIMARSSON, 2004a). Section
from VEINS-cruise B19-1999, R/V Bjarni Sæmundsson; figure repro-
duced from http://www.hafro.is/Sjora/ → Hydrography.

Concluding, a decreasing trend from 1999 to 2003 is evident in both the KG5 reservoir height and the measured sill time series. If around $30 - 45\,\%$ of the overflow are regarded as wind driven, also the absolute magnitude of the hydraulic estimates is consistent with the DSOW transport observed at the sill.

The joint effects of barotropic forcing and hydraulic control are further investigated in chapter 7.

6.3.4. Local temperature / transport correlation at the sill

To test the density effect in the WHITEHEAD relation $Q_{WLK} = 1/2\,\Delta\varrho/\varrho\,g/f\,h_{eff}^2$, the local correlation between temperature and transport at the sill was examined (Fig. 6.13 b). Neglecting upstream reservoir height changes, one would expect a linear correlation due to the $\Delta\varrho/\varrho$ term in the hydraulic relation.

Deducted from the typical Θ/S relation of the bottom water at the sill (Fig. 2.3), a density-temperature relation of $0.08\,\mathrm{kg/m^3}/1\,^\circ\mathrm{C}$ (KÄSE AND OSCHLIES, 2000) was used to convert bottom water temperature anomalies to density anomalies. Taking a fixed reservoir height of $500\,\mathrm{m}$ and the upper AW density as constant (thus, the density contrast is determined by bottom water variability alone), a transport change of $-0.73\,\mathrm{Sv/^\circ C}$ would result from the hydraulic relation. The actual time series (Fig. 6.13 b) yield a regression slope of $(-0.77\pm0.13)\,\mathrm{Sv/^\circ C}$. The correlation of 0.35 is significant

at the 95 % confidence level, assuming 50 degrees of freedom for the whole time series. Although the mean regression is essentially similar within the error bounds, the low transport values in 2001/2002 (triangles at 0.4 °C/2.2 Sv) cannot be accounted for by the temperature-density relation alone and require a reduced reservoir height (Fig. 6.13 a), and/or a reduced barotropic forcing (chapter 7).

Thus, both hydraulic reservoir height changes, observed at Kögur 5 on interannual timescales, and the local density-transport correlation, which is evident at the sill on shorter timescales, are consistent with the observed transport changes.

6.4.   Summary and conclusions

The analysis of the SFB mooring array time series revealed, that the Denmark Strait overflow satisfies the criteria of a hydraulically controlled, density driven flow in agreement with the KÄSE AND OSCHLIES (2000) process model.

The mean flow exceeds criticality $\approx 80 - 100$ km downstream of the sill (observations, GIRTON (2001); model, KÖSTERS (2004b)). The downstream shift of the control point may be predominantly attributed to the effects of friction, which plays an important role for the downstream descent of the plume (GIRTON, 2001). It has been shown, that the SFB array observations at the sill agree with the model predictions, and that criticality is regularly reached at the sill during strong outflow periods.

Hence, it is likely, that the dynamics of the overflow are governed by hydraulic control mechanisms.

Both the SFB observations and the model revealed, that zero or constant PV assumptions are not valid for the Denmark Strait Overflow, since friction has an important effect on the plume dynamics. Moreover, the large barotropic current component makes it questionable, whether simple 1 1/2 layer models of frictionless flow over a sill (GILL, 1977; WHITEHEAD, 1989) are an adequate approximation of the real overflow.

Numerical experiments suggest, however, that the principal relations of zero PV theories are valid for the Denmark Strait Overflow (KÖSTERS, 2004b). These have been investigated by the combined observations of the SFB array at the sill and reservoir height estimates in the upstream region:

- SSH and interface depth measurements by PIES confirmed, that the overflow is largely geostrophically balanced at the sill, which is a prerequisite for hydraulic theories.

- Hydrographic sections at the sill revealed, that the geostrophically balanced dense water transport at the sill may be estimated to average 1.9 Sv, and that it is well approximated by the STERN (2004) transport extremum.

- Hydraulic transport estimates using the WHITEHEAD relation $Q_{WLK} = 1/2\ g'/f\ h_u^2$ at the Icelandic Kögur 5 station 200 km upstream match the actual DSOW measured by the SFB array at the sill. This suggests, that only a part

of the Denmark Strait Overflow may be considered as hydraulically controlled flow, since the zero PV / rectangular channel Q_{WLK} estimate typically overestimates the transport by a factor of 1.3 (WHITEHEAD, 1998) to 2.2 (KÖSTERS, 2004b). The STERN (2004) relation yields a possibly more realistic estimate of 1.9 Sv (average 1999 − 2003).

- At the TK site 93 km upstream of the sill, Q_{WLK} yielded substantially lower estimates than the observed DSOW transport. This might be attributed to the large cross-strait interface slope at the Icelandic side edge of the dense water, and the lowered interface in the "strait entrance" region, which in the model affects the upstream region closer than 130 km to the sill. The TP deployment in 2002/2003 failed to detect the dense water height, since most of the time, cold EGC water was located above the dense overflow, which leads to a vanishing temperature contrast.

- Hydraulic estimates (defined by the 2 °C isotherm height at TK) capture the DSOW transport variability with a time lag of 4.8 days, corresponding to an advection velocity of 22 cm/s (MACRANDER, 2001), which agrees with eddy translation velocity observations of GIRTON (2001).

- The near bottom temperature time series at the sill and at TP show a weak correlation maximum at a time lag of 31 hours, possibly suggesting communication of reservoir height changes by long gravity waves. The signal is likely overridden by strong barotropic currents and eddy activity, however.

- The observed local short term correlation between bottom temperature and transport at the sill proves the linear relation of density contrast and hydraulically controlled transport.

- The annual mean reservoir height at KG5 shows a decreasing tendency from 1999 to 2003. If a mean hydraulically controlled transport of 1.9 Sv is assumed, the 50 m reservoir height decrease yields a corresponding transport reduction of 0.3 Sv. Hence, 50 % of the observed DSOW transport decrease from 3.7 to 3.1 Sv might be attributed to a reduced density driven flow.

Concluding, the SFB mooring array yielded observational evidence, that the Denmark Strait Overflow may be governed by hydraulic control. The observed interannual transport reduction is associated with a significant upstream reservoir height decrease. Considering, that the actual hydraulically controlled flow should be substantially lower than the zero PV WHITEHEAD (1989) estimate, a value of 1.9 Sv appears as a realistic estimate. Hence, only ≈ 56 % of the total transport of 3.35 Sv (1999 − 2003 average) may be regarded as density driven flow.

7. Barotropic forcing of the overflow

It has been a common belief, that the Denmark Strait Overflow is primarily driven by the alongstream pressure gradient, since at the sill depth, much denser water is present in the Iceland Sea than in the Irminger Sea. Numerous studies investigated the overflow in the light of a density driven, hydraulically controlled flow (for a review, see WHITEHEAD, 1998). The overflow dynamics can be realistically reproduced in numerical models without any meteorological forcing (KÄSE AND OSCHLIES, 2000; KÄSE ET AL., 2003).

More recent numerical experiments suggest, however, that the Denmark Strait Overflow also includes a significant wind driven component. Likely, the effects of the pressure gradient and barotropic wind driven forcing can be superimposed linearly (KÖSTERS, 2004b), although there exists currently no theoretical approach to combine hydraulically controlled and barotropic flow.

In the previous chapter, it has been shown, that under consideration of a realistic cross-section of the Denmark Strait and the non-constant PV, the hydraulically controlled, density driven flow might only account for $50 - 60\,\%$ ($\approx 1.9\,\mathrm{Sv}$) of the observed DSOW transport of $3.35\,\mathrm{Sv}$ during the SFB array observation period 1999 – 2003. Hence, roughly $1.45\,\mathrm{Sv}$ might be attributed to barotropic forcing mechanisms, that shall be evaluated here.

7.1. Introduction to wind stress forcing and North Atlantic Oscillation

Numerical experiments suggest, that the Denmark Strait Overflow increases for stronger wind stress forcing over the North Atlantic, while the Faroe Bank Channel (FBC) Overflow is reduced (BIASTOCH ET AL., 2003). For realistic wind stress time series, the total barotropic throughflow through Denmark Strait was highly correlated with the maximum wind stress curl $\nabla_h \times \tau$ over the subpolar North Atlantic, and exhibited a strong seasonal cycle of $2\,\mathrm{Sv}$ in response to the observed $40\,\%$ seasonal $\nabla_h \times \tau$ variability.

KÖSTERS (2004b) more closely investigated the sensitivity of the dense overflows across the Greenland-Scotland Ridge (GSR), i.e. the Denmark Strait (DS), Iceland-Faroe Ridge (IFR), Faroe Bank Channel (FBC) and Wyville-Thomson Ridge (WTR)

overflows[1] on wind stress forcing. Of the DSO, $\approx 1.9\,\mathrm{Sv}$ were entirely density-driven, the remaining wind driven part of $1\,\mathrm{Sv}$ depended linearly on the difference between maximum and minimum wind stress curl over the subpolar North Atlantic. While the IFR overflow is almost zero in the model[2], the combined FBC and WTR overflows showed a weaker negative response, corroborating the results of BIASTOCH ET AL. (2003). For typical interannual wind stress curl variability, KÖSTERS (2004b) suggested a DSO variability of $20\,\%$ of the mean transport value. The total barotropic throughflow showed a similar anticorrelation, with stronger outflow through the Denmark Strait and stronger inflow into the Nordic Seas between Iceland and Scotland for enhanced wind stress forcing.
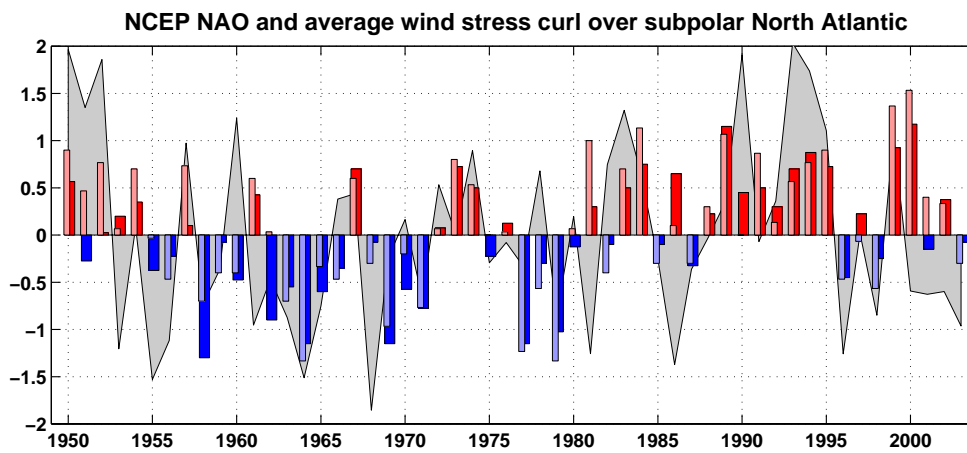
Figure 7.1.: *NCEP NAO time series 1950 − 2003. Narrow bars denote DJF, wide bars DJFM winter averages[4]. Grey shading in background denotes normalized annual mean[5] wind stress curl over the subpolar North Atlantic (62 °N − 70 °N and 35 °W − 5 °E). Note the interdecadal increase of both quantities from the 1960's until the mid-1990's, and the decrease during the SFB observations from 1999 to 2003.*

The wind stress curl over the North Atlantic is closely linked to the North Atlantic Oscillation (NAO), which is basically a measure for the pressure difference between the Iceland Low and the Azores High[3]. A positive NAO phase indicates a larger pressure gradient, and hence stronger wind stress over the North Atlantic. The most significant NAO pattern is typically observed during winter, when the larger meridional temperature and pressure gradient enhances the cyclonic activity over the northern North Atlantic. Hence, the NAO winter means[4] are suitable to character-

---

[1]For locations, see Fig. 7.2, page 113.

[2]The model of KÖSTERS (2004b) does not properly resolve the small-scale deeper gaps in the IFR.

[3]North Atlantic Oscillation: Sea Level Pressure anomaly between Iceland Low and Azores High. The station-based NAO index is typically defined by the normalized pressure difference between Stykkishólmur, Iceland, and Lisbõa or the Azores, Portugal (HURRELL, 1995; HURRELL ET AL., 2003).

[4]NAO winter mean: Both December-February (DJF) and December-March (DJFM) averages exist

ize the atmospheric circulation over the North Atlantic (for a review, see HURRELL ET AL., 2003).

Fig. 7.1 [5] shows the winter NAO from NCEP reanalysis data[6] (NCEP/NCAR REANALYSIS PROJECT, 2004). In addition to the large year-to-year variability, the NAO exhibited an interdecadal positive trend from the 1960's to the mid-1990's; during the SFB observations 1999 – 2003, the NAO decreased significantly. The mean wind stress curl over the subpolar North Atlantic as a measure for the strength of the Iceland Low is largely correlated with the NAO index (Fig. 7.1).

A positive NAO leads to enhanced northeasterly winds over the Denmark Strait, and stronger westerly winds over the Faroe-Shetland Channel, which is evident comparing the wind stress between the NAO+ winter 1999/2000 and 2002/2003 (NAO−; Fig. 7.2). Via Sverdrup dynamics, the barotropic cyclonic circulation around Iceland increases for NAO+ phases (MARSHALL ET AL., 2001), which may also affect the dense overflows. A theoretical study of EDEN AND WILLEBRAND (2001) revealed, that there exists both a fast barotropic (timescales of $\approx$ 3 days), and a delayed (6 – 8 years) baroclinic transport response.

Fig. 7.2 shows, moreover, that the average wind stress is much larger over Denmark Strait than over the FBC, while the IFR region exhibits the weakest forcing. Hence, the much larger barotropic component and the higher sensitivity of the Denmark Strait Overflow to wind stress forcing expected from numerical models (KÖSTERS, 2004b) is qualitatively supported by the comparison of NAO + /NAO− wind stress forcing.

A number of studies addressed possible observational evidence for these relations: BLINDHEIM ET AL. (2000) found, that the inflow of Atlantic Water into the Nordic Seas through the Faroe-Shetland Channel increases for positive NAO. ORVIK AND SKAGSETH (2003b) observed a strengthening of the Norwegian Atlantic Slope Current for positive NAO, which they successfully regressed to the wind stress curl over the North Atlantic(ORVIK AND SKAGSETH, 2003a). HILMER AND JUNG (2000) suggested an increased Arctic Sea ice export due to enhanced northerly winds over the East Greenland Current. Based on reservoir height and direct transport measurements, HANSEN ET AL. (2001) observed a decrease of the FBC overflow since the 1950's, that might be related to the increasing NAO trend until the mid-1990's (Fig. 7.1). In contrast, the Denmark Strait Overflow appeared to remain stable (DICKSON AND BROWN, 1994). Seasonal or interannual variability could not be verified, even though model experiments predict, that the DSO sensitivity on wind forcing changes is the largest for all deep overflows across the GSR.

Here, the SFB array time series shall be investigated with respect to NAO and wind stress forcing.

---

in the literature. In analogy to HURRELL (1995), the DJFM values are used here.

[5] Annual means were obtained from July year $x - 1$ to June year x in order not to split the winter NAO into two different averaging periods.

[6] NCEP: National Centers for Environmental Prediction, operates reanalysis models that assimilate various observation data from 1948 to present.
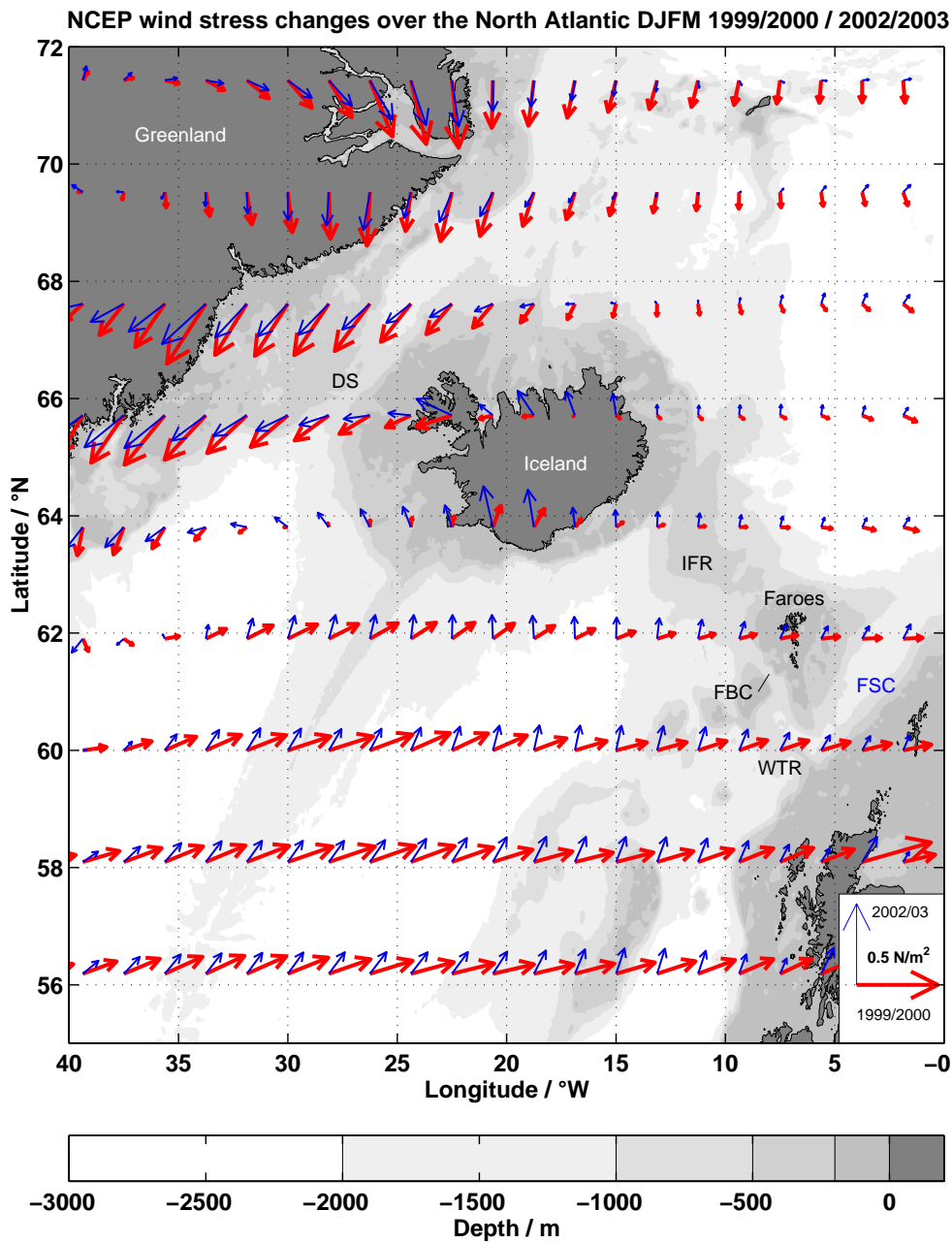
Figure 7.2.: *Map of NCEP wind stress forcing over the North Atlantic. Bold red arrows denote winter 1999/2000 DJFM mean during positive NAO. Light blue arrows depict winter 2002/03, when the NAO was in a negative phase. Topographical features: DS: Denmark Strait, IFR: Iceland-Faroe Ridge, FBC: Faroe Bank Channel, WTR: Wyville-Thomson Ridge. FSC: Faroe-Shetland Channel. Note, that the wind stress basically resembles the SLP pattern of the NAO, with enhanced northeasterlies over Denmark Strait in 1999/2000. Although the response is weaker, the westerlies over the FBC/WTR are also stronger in 1999/2000.*

7.2. Denmark Strait Overflow response to the NAO

As pointed out in the previous section, the windstress curl over the Nordic Seas is closely linked to the North Atlantic Oscillation (NAO). Hence, a positive correlation of the Denmark Strait Overflow to the NAO should be expected. While for the FBC overflow, an anticorrelation on decadal timescales has been shown by HANSEN ET AL. (2001), observational evidence for the Denmark Strait Overflow has been little so far.

NILSEN ET AL. (2003) studied simulated North Atlantic – Nordic Seas water mass exchanges in an isopycnic coordinate OGCM[7] forced by daily NCEP/NCAR data from 1948 to 1999. They found an NAO-like Sea Level Pressure (SLP) regression pattern for the total net flow of 4.3 Sv through the Denmark Strait.

Also, the numerical experiments of KÖSTERS (2004b) suggest a positive correlation of NAO and DSOW transport.
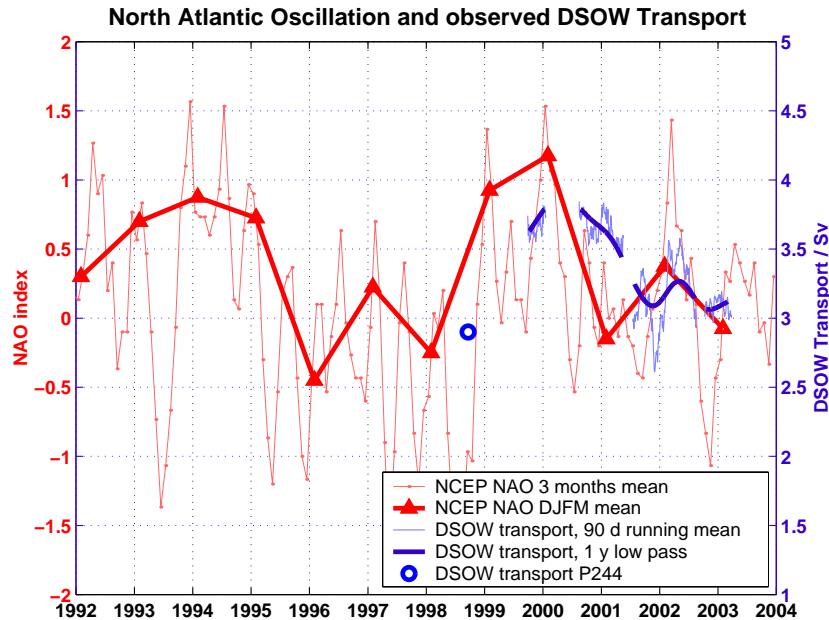
Figure 7.3.: *NCEP NAO and observed DSOW transports. The bold red line marks winter (DJFM mean) NAO values, whereas the light red line depicts 3-months running means. Blue lines indicates DSOW transports, as observed by ADCP below layer of maximum current shear.*

A time series of monthly NCEP NAO is depicted in Fig. 7.3. For interannual timescales, the winter NAO (December-January-February-March (DJFM) mean) is shown, since the most significant NAO forcing generally occurs during winter, when the meridional SLP gradient, and hence the wind stress, is much larger than in summer(HURRELL ET AL., 2003).

---

[7]OGCM: Ocean General Circulation Model.

Overlaid are the observed DSOW transport time series from 1999 to 2003. While the NAO exhibits large fluctuations on monthly and seasonal timescales, no clear connection could be found with the Denmark Strait overflow. Only the exceptional large NAO fluctuations in 2001/2002 appear to be reflected in the overflow transport; possibly with a time lag of 2.5 months. Obviously, the overflow has a weaker response on monthly and seasonal NAO forcing than expected from numerical models, and the response is overridden by other forcing mechanisms such as reservoir height changes, that affect the density driven part. This will be assessed in chapter 9.

Considering interannual timescales (Fig. 7.3), a decreasing trend both in winter NAO and DSOW transport is evident between 1999 and 2003. The higher transport values observed by the SFB array are also consistent with the estimates of GIRTON ET AL. (2001) from September 1998 (2.9 Sv), since in 1998, the NAO was substantially lower than in 1999/2000.

Although the four years of time series are too short to prove the relation, and the seasonal response expected from models could not be verified, observational evidence exists, that at least on interannual timescales the Denmark Strait Overflow may be modulated by the North Atlantic Oscillation. In the following sections, the influence of NAO related wind stress forcing are assessed in more detail.

7.3. Wind stress forcing

7.3.1. Introduction and previous studies

While the NAO is basically a station-based index of SLP anomalies only, the actual driving mechanism for the barotropic circulation is the wind stress $\boldsymbol{\tau}$ over the subpolar North Atlantic. In order to analyze the effects of wind stress on the barotropic cyclonic circulation around Iceland, the wind stress curl shall be assessed instead of the individual components of $\boldsymbol{\tau}$.

The curl of the wind stress field at the sea surface is defined as

$$\nabla_h \times \boldsymbol{\tau} = \frac{\partial \tau_y}{\partial x} - \frac{\partial \tau_x}{\partial y} \tag{7.1}$$

In an experiment with realistic forcing time series (1992 – 1997, obtained from the ECCO model, STAMMER ET AL., 2002, 2003), BIASTOCH ET AL. (2003) investigated the barotropic transport response to the maximum of $\nabla_h \times \boldsymbol{\tau}$ over the area 62°N – 70°N and 35°W – 5°E. The barotropic net transport Q_{barotr} through Denmark Strait almost exactly followed the seasonal cycle of $\max(\nabla_h \times \boldsymbol{\tau})$ with a linear response of

$$\Delta Q_{\mathrm{barotr}} = \frac{2\,\mathrm{Sv}}{2.2\,\mathrm{Nm}^{-3}} \cdot \max(\nabla_h \times \boldsymbol{\tau}) \tag{7.2}$$

The sensitivity of the DSOW transport was investigated by multiplying the mean wind stress field with factors of 0, 1, 2 and 4, which yielded a linear overflow response with transports of 1, 2.2, 3.5 and 6 Sv, respectively. Provided that $\max(\nabla_h \times \boldsymbol{\tau})$ is

an appropriate measure for the wind driven part of the DSO (in analogy to the total barotropic throughflow), the following linear relation holds:

$$Q_{\max\tau} = 1.25\,\mathrm{Sv}\ \cdot\ \frac{\max(\nabla_h \times \boldsymbol{\tau})}{\mathrm{mean}(\max(\nabla_h \times \boldsymbol{\tau}))} \tag{7.3}$$

with $= \mathrm{mean}(\max(\nabla_h \times \boldsymbol{\tau})) = 7.32 \cdot 10^{-7}\,\mathrm{N/m^3}$ as average maximum wind stress curl over the subpolar North Atlantic from 1992 to 1997. Since the Biastoch et al. (2003) model generally underestimates the Denmark Strait overflow transport by $12 - 45\,\%$ (comparing the mean dense water transport of $2.2\,\mathrm{Sv}$ of Biastoch et al. (2003) with observations ranging from $2.5\,\mathrm{Sv}$ (Saunders, 2001) to $3.35\,\mathrm{Sv}$ (this study)), the actual response to wind stress forcing might even be larger than in Eq. 7.3.

In contrast to Biastoch et al. (2003), Kösters (2004b) investigated the dense overflow response to the difference $\Delta\tau$ between maximum and minimum wind stress curl in the area of the GSR ($58\,°\mathrm{N} - 66\,°\mathrm{N}$, $45\,°\mathrm{W} - 5\,°\mathrm{E}$). While the density driven part of the overflow equalled $1.92\,\mathrm{Sv}$, a linear regression of the wind driven part $Q_{\Delta\tau}$ on $\Delta\tau$ yielded

$$Q_{\Delta\tau} = \frac{0.1292\,\mathrm{Sv}}{1 \cdot 10^{-7}\,\mathrm{N/m^3}} \cdot \Delta\tau \tag{7.4}$$

Additionally, Kösters (2004b) showed, that the deep overflow and the total barotropic throughflow both depend linearly on the wind stress forcing, which supports the findings of Biastoch et al. (2003).

Here, both model-derived relations shall be tested with the observational time series of the SFB array. The SFB array has been optimized for monitoring the dense overflow. The total barotropic throughflow, which includes the large southward transport of the EGC over the Greenland shelf, and the northward transport of the NIIC over the Iceland shelf, is poorly resolved by the SFB mooring array, since it only covers the central deep part of the Denmark Strait. Therefore, the analysis will be focused on the DSOW transport, while the barotropic flow through the array will be assessed qualitatively only.

For the analysis of the SFB array time series, gridded monthly wind stress data from the NCEP reanalysis (NCEP/NCAR Reanalysis Project, 2004) have been used. A landmask obtained from the ETOPO5 topography[8] was applied to avoid aliasing by wind stress values over land.

$\max(\nabla_h \times \boldsymbol{\tau})$ and $\Delta\tau$ have been calculated according to Biastoch et al. (2003) and Kösters (2004b). Additionally, the mean wind stress curl over the subpolar North Atlantic, and the local strait parallel wind stress, averaged over the Iceland Sea and Denmark Strait "entrance" region ($65.5\,°\mathrm{N} - 70\,°\mathrm{N}$ / $28\,°\mathrm{W} - 18\,°\mathrm{W}$) is examined.

Since the wind field primarily reflects the SLP field, the mean wind stress curl over the subpolar North Atlantic is largely correlated with the NAO (Fig. 7.4). Generally

---

[8]ETOPO5: Earth topography on 5' grid. Available from
http://www.ngdc.noaa.gov/mgg/global/relief/ETOPO5/TOPO/ETOPO5/ .

the same holds for the estimates $\max(\nabla_h \times \boldsymbol{\tau})$ (BIASTOCH ET AL., 2003) and $\Delta\tau$ (KÖSTERS, 2004b). In contrast, the local forcing over the Iceland Sea and Denmark Strait is less well correlated to the NAO, since it depends more on the pressure gradient between the Greenland High and the Iceland Low.
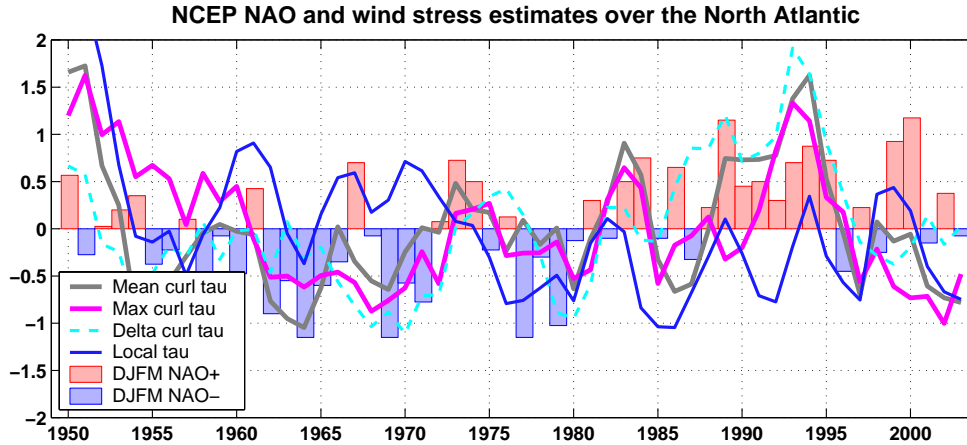
Figure 7.4.: *NCEP NAO and wind stress estimates over the North Atlantic. Shaded bars: NCEP DJFM winter NAO. Lines denote normalized 3-year running means of wind stress estimates: Grey: Mean wind stress curl over 62°N – 70°N / 35°W – 5°E. Magenta: Maximum wind stress curl over 62°N – 70°N / 35°W – 5°E. Cyan, dashed: Maximum - minimum wind stress curl over 58°N – 66°N / 45°W – 5°E. Blue: Local strait parallel forcing over Iceland Sea and Denmark Strait, 65.5°N – 70°N / 28°W – 18°W (positive to south-west).*

The wind stress estimates are now investigated in more detail to evaluate, which might be considered as the most likely candidate for the barotropic forcing of the Denmark Strait Overflow. The focus is set on monthly to interannual timescales, since on shorter timescales, the overflow fluctuations are primarily caused by internal instabilities and eddies (a.o. GIRTON ET AL., 2001), that previous studies could not link to synoptic meteorological forcing.

Time series of the wind stress forcing from 1992 to 2004 are shown in Fig. 7.5. The figure depicts the mean wind stress curl over the subpolar North Atlantic (62°N – 70°N / 35°W – 5°E; panel a), the maximum wind stress curl over the same region (panel b; BIASTOCH ET AL., 2003), maximum - minimum wind stress curl over the GSR region (58°N – 66°N / 45°W – 5°E; panel c; KÖSTERS, 2004b), and the local strait parallel wind stress over the Iceland Sea and Denmark Strait, (65.5°N – 70°N / 28°W – 18°W, positive to south-west; panel d).

In all time series, a strong seasonal signal with the largest forcing during winter is evident; typically, it is several times larger than the interannual fluctuations. In the mean$(\nabla \times \boldsymbol{\tau})$ estimate, the seasonal cycle is superseded by coherent variations on timescales of ≈ 4 months.
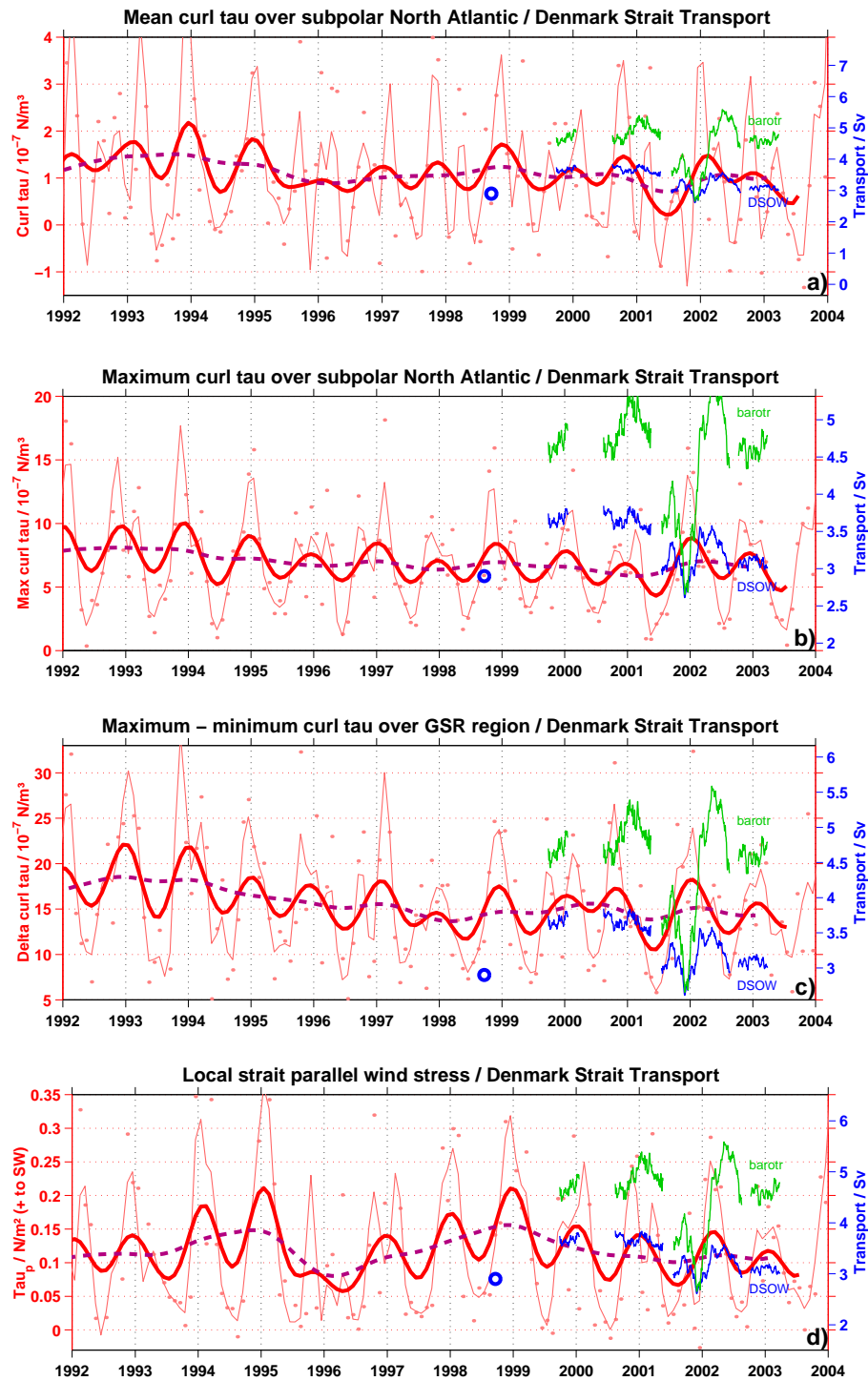
Figure 7.5.: *NCEP windstress estimates. Dots represent monthly values, and different lines 3 months, 1 and 2 years low-passed values, respectively. Blue and green lines denote 3 month running means of the observed DSOW and barotropic transport through the SFB array. Axis scaling adjusted to match a linear response of the barotropic overflow component, as predicted by numerical models. Hence, 1.9 Sv as mean hydraulically controlled transport (see section 9) corresponds to zero wind stress forcing in all panels. For details, see text.*

Additionally, the DSOW transport observed by the SFB array (this study) and the Poseidon P244 cruise in 1998 (GIRTON ET AL., 2001) is overlaid in Fig. 7.5 (blue lines / circle, respectively).

All numerical models discussed above revealed, that a certain amount of the overflow can be regarded as entirely density driven (1.0 Sv, BIASTOCH ET AL. (2003); 1.9 Sv, KÖSTERS (2004b)), while the remaining part linearly depends on the wind stress forcing. Although the absolute transport estimates differ between the models, the linearity appears to be a robust feature.

For Fig. 7.5, 1.9 Sv have been assumed as the average hydraulically controlled, density driven part of the observed overflow (chapter 6). Hence, the remaining part (1.45 Sv average 1999 – 2003) may be regarded as linearly dependent on the wind stress forcing. The scaling in Fig. 7.5 has been adjusted to the linear relations expected from the models - thus, DSOW transport and wind stress forcing lines should match perfectly, if the proposed linear response to wind stress forcing is correct[9].

It should be noted, that the time series of the barotropic flow shown in Fig. 7.5 represent the flow through the SFB array in the center of the Denmark Strait only.

Following, the different wind stress estimates shall be discussed.

7.3.2. Mean wind stress curl

While on interannual timescales the mean wind stress curl is fairly well correlated with the NAO (Fig. 7.4), the proposed fast linear response of the Denmark Strait Overflow is not evident in the observations (Fig. 7.5 a).

The mean wind stress curl exhibits large fluctuations on timescales of 4 months (verified by spectral analysis; not shown), typically varying in the range $[-0.2 + 2.3] \cdot 10^{-7} \, \mathrm{N/m^3}$ (RMS range of 3 months averages). The highest values are normally reached in early winter (November / December).

The Denmark Strait Overflow, however, is comparatively stable. If around 1.45 Sv of the overflow are regarded as wind driven, which seems to be a realistic estimate (based on the hydraulic estimate of 1.9 Sv and model results of BIASTOCH ET AL., 2003; KÖSTERS, 2004b), a linear response to the huge wind stress curl variations should yield transport variations of several Sv on timescales of 4 months. But even a weaker or lagged response is statistically not evident in the time series. The only exception might be the extraordinary rise of mean$(\nabla \times \boldsymbol{\tau})$ from Oct. to Dec. 2001, which is followed by a significant overflow and barotropic transport increase two months later. However, a delayed response of the flow through Denmark Strait to mean$(\nabla \times \boldsymbol{\tau})$ can not be proven by this single event.

On interannual timescales, the mean wind stress curl dropped from $12 \cdot 10^{-7} \, \mathrm{N/m^3}$ in winter 1998/1999 to $7 \cdot 10^{-7} \, \mathrm{N/m^3}$ in summer 2001, and recovered to $10 \cdot 10^{-7} \, \mathrm{N/m^3}$ in 2003. During the SFB observations from Oct. 1999 to summer 2003, however, no

---

[9]In Fig. 7.5, a mean density driven part of 1.9 Sv has been assumed. A transport decrease of 0.3 Sv may be attributed to a reduced reservoir height. Since this trend has not been removed from the DSOW transport time series in Fig. 7.5, the wind stress estimates may have a smaller interannual decrease to close the transport estimate.

significant interannual trend is evident. The observed steady overflow decrease can not be explained by the large scale wind stress curl, if a fast, non-delayed barotropic response (EDEN AND WILLEBRAND, 2001) is assumed.

A ≈ 1 year time lag might more appropriate to regress the observed transport reduction on the mean wind stress curl. However, four years of time series are too short to prove this relation.

7.3.3.   Maximum wind stress curl

In contrast to the mean wind stress curl, $\max(\nabla \times \boldsymbol{\tau})$ (Fig. 7.5 b) has a clearer seasonal cycle.

BIASTOCH ET AL. (2003) found a close non-lagged correlation of the barotropic net transport through Denmark Strait with $\max(\nabla \times \boldsymbol{\tau})$, and yielded a response of 2.2 Sv for the 1-year smoothed annual cycle. Although the SFB array observed the central part of the Denmark Strait only, and thus no quantitative estimates of the barotropic flow can be made, the observations might agree with the results of BIASTOCH ET AL. (2003), in particular for the winters 1999/2000 and 2000/2001. In 2001/2002 however, the time series suggest either a response delayed by several months, or the barotropic transport is controlled by other mechanisms than $\max(\nabla \times \boldsymbol{\tau})$.

The linear relation of the overflow transport to $\max(\nabla \times \boldsymbol{\tau})$ would yield a seasonal DSOW transport signal of $0.3 - 0.6$ Sv based on 1-year smoothed $\max(\nabla \times \boldsymbol{\tau})$ time series. A quantitative analysis of the dense overflow revealed no significant seasonal cycle, however. The large overflow and barotropic fluctuations in December 2001 – March 2002 are out of phase with $\max(\nabla \times \boldsymbol{\tau})$, in contrast to the fast, seasonal response suggested by BIASTOCH ET AL. (2003).

Moreover, the $\max(\nabla \times \boldsymbol{\tau})$ exhibits no significant interannual decrease from 1999 – 2003, and is therefore inappropriate to explain the observed reduction of the overflow.

7.3.4.   Maximum - minimum wind stress curl

The difference between maximum - minimum wind stress curl over the GSR region has been taken as a measure of wind stress forcing by KÖSTERS (2004b). It is dominated by the seasonal cycle (Fig. 7.5 c).

A comparison with the overflow and barotropic transport time series reveals no apparent response to $\Delta \tau$. The overflow fluctuations are much weaker than in the relation suggested by KÖSTERS (2004b), and seem to be lagged by $4 - 5$ months to $\Delta \tau$, which is in contrast to the numerical experiments.

On interannual timescales, $\Delta \tau$ may only account for a minimal overflow reduction of 0.07 Sv, which is $\approx 10\,\%$ of the observed decrease. Therefore, it appears unlikely that $\Delta \tau$ acts as an appropriate forcing parameter for the Denmark Strait Overflow during 1999 – 2003.

7.3.5. Wind stress forcing over the Iceland Sea and Denmark Strait

The local wind stress forcing over the Iceland Sea and the "entrance" region northeast of the sill is much larger than anywhere else over the subpolar North Atlantic (see map Fig. 7.2), and might play a role in modifying the flow through Denmark Strait.

The time series shown in Fig. 7.5 d might support this hypothesis: In contrast to the large scale wind stress estimates discussed in the previous sections, the exceptional large overflow transport variations in 2001/2002 are more or less in phase with the local strait parallel wind stress. The amplitude of the overflow transport variability, however, is smaller than would be expected if the wind driven overflow part showed a linear, fast response to the local wind stress forcing.

On interannual timescales, the local wind stress decreases from 1999 to 2003 by $\approx 17\,\%$, which is consistent with the interannual DSOW transport reduction. In chapter 9, it shall be further investigated, which barotropic forcing mechanism is most likely to control the wind driven component of the Denmark Strait Overflow.

7.4. Summary and conclusions

One may speculate, why the overflow does not reflect the strong seasonal changes in both the large scale and local wind stress forcing, as might be expected from numerical models.

Additionally to the fast response of the barotropic transport (BIASTOCH ET AL., 2003), EDEN AND WILLEBRAND (2001) suggested a delayed baroclinic response. It is difficult, however, to identify and separate in the four years of SFB array time series the individual influences of

- fast barotropic response to the large scale wind stress field (EDEN AND WILLE-BRAND, 2001),

- baroclinic response to large scale wind stress field, delayed on timescales of 6 to 8 years (EDEN AND WILLEBRAND, 2001),

- local wind stress forcing over Iceland Sea and Denmark Strait entrance region

- indirect influence of wind stress curl via reservoir height changes in the Iceland Sea induced by $\nabla \times \boldsymbol{\tau}$ anomalies (MALMBERG AND JÓNSSON, 1997),

- reservoir height changes due to changed dense water formation rates in the Greenland and Iceland Seas (reservoir height estimates at KG5 have a coarse resolution in time only),

- changes of the DSOW / AW/PIW density contrast (complete T, S, σ_{Θ} profiles were measured only a few times per year).

In the previous sections, two further issues have not been considered:

- BIASTOCH ET AL. (2003) emphasized, that the shallow parts of the Denmark Strait become increasingly important for increased wind stress forcing. They suggest, that some dense water might cross the sill over the Greenland shelf and joins the deep overflow $\approx 100\,\mathrm{km}$ downstream. This view is supported by observations (RUDELS ET AL., 1999). Strong seasonal fluctuations have been observed by current meters on the Greenlandic side upstream of the sill (JÓNSSON, 1999), with the current even reversing during summer. However, the seasonal variations should then be evident in the downstream records of the MONA, Lowestoft and Angmagssalik arrays, but neither AAGARD AND MALMBERG (1978) nor DICKSON AND BROWN (1994) report any seasonal signals. Obviously, the seasonally varying EGC does not contribute much to the deep overflow.

- The density driven part of the Denmark Strait Overflow depends on the reservoir height upstream of the sill, which might counteract the seasonality imposed by variable barotropic wind stress forcing. While the maximum wind stress forcing is typically in December/January, the observations suggest, that the largest reservoir height is also reached during winter. The hydrographic time series at the Icelandic station Kögur 5, 200 km upstream of the sill (Fig. 6.12 a, page 105) show a clear seasonal density signal close to the surface. Even the $\sigma_\Theta = 27.8\,\mathrm{kg/m^3}$ isopycnal, which is commonly used as upper DSOW boundary, exhibits some seasonality. Although the station is normally sampled four times per year only, it appears consistent that the 27.8 isopycnal is typically 50 m higher in winter (January to March), when dense water is formed in the Iceland Sea (MALMBERG AND JÓNSSON, 1997), and decreases until late summer. Although both mechanisms are not perfectly in phase, the seasonal cycle due to the wind stress forcing might even be amplified, and not dampened by the density driven overflow part.

Also previous studies have failed to relate the Denmark Strait Overflow transport to wind stress forcing on synoptic (i.e. a few days; WORTHINGTON, 1969; AAGARD AND MALMBERG, 1978; GIRTON, 2001) or seasonal timescales (AAGARD AND MALMBERG, 1978; DICKSON AND BROWN, 1994). Instead, the short term variability can entirely be explained by internal instability mechanisms (GIRTON, 2001), while on seasonal timescales, variable wind stress forcing apparently does not play an important role.

The SFB array observations suggest, that the **barotropic flow** through the central part of Denmark Strait shows some response to the wind stress forcing, possibly with a time lag of a few months. It is likely, that it is controlled both by the large scale wind field as well as the local strait parallel wind stress forcing. However, the SFB measurements are also influenced by lateral changes of the NIIC/EGC frontal zone, and conclusions about the total barotropic flow are beyond the scope of the SFB observations. Current measurements on the Greenland shelf (JÓNSSON AND

VALDIMARSSON, 2004a) suggest, that at least over the shallow parts of the Denmark Strait the East Greenland Current has a significant seasonal cycle.

Focusing on the **dense overflow**, it remains unclear, why it does not show the expected seasonal variability, even though models predict a close correlation between overflow and total barotropic transport. The only striking agreement to wind stress forcing was found for Dec. 2001 – March 2002, when the DSOW transport appeared to follow anomalies of the local wind stress forcing.

On interannual timescales, only 10 % of the observed DSOW transport reduction could be related to the decreasing large scale $\nabla \times \boldsymbol{\tau}$ differences ("$\Delta \tau$", KÖSTERS, 2004b). In the same period, the local wind stress decreases by 17 %; a linear coupling could account for $\approx 0.3\,\text{Sv}$ transport reduction. This suggests, that the observed total DSOW transport decrease of 0.6 Sv might by equally attributed to reduced reservoir height and wind stress forcing.

Based on theoretical considerations, the large scale wind stress field, which drives the subpolar barotropic gyre (CURRY AND MCCARTNEY, 2001), might be considered to be more appropriate than the local wind stress over the Iceland Sea. However, the observed overflow decrease is not consistent with the large scale $\nabla \times \boldsymbol{\tau}$ field from 1999 – 2003, if an instantaneous response is assumed. The assumption of a delayed response could explain the observed DSOW transport decrease, but a time lag of one year appears unlikely for barotropic response mechanisms.

Possibly, the overflow response on NAO-related large scale wind stress forcing acts on timescales longer than the four year of SFB observations, whereas the variability on monthly to yearly timescales is more affected by local wind stress forcing. Thus, the SFB time series suggest, that on interannual to decadal timescales, the Denmark Strait Overflow might show the expected linear response to wind stress forcing, whereas on monthly to annual timescales the sensitivity is clearly much smaller.

The role of large scale and local wind stress forcing, and the importance of fast barotropic and delayed baroclinic coupling mechanisms have to be further investigated to better understand the Denmark Strait Overflow response to wind stress forcing, and to resolve the discrepancy between numerical models, which generally exhibit a large, linear and instantaneous overflow response and the observed variability.

In chapter 9 it shall be attempted to find a possible synthesis of the wind stress and dense water reservoir height forcing mechanisms, based on their evidence in the observations.

8. Upstream pathways to the overflow

To assess the hydraulically controlled flow through Denmark Strait, it is critical to observe the upstream reservoir height at a point, where a continuous flow of dense water to the sill exists. Moreover, conclusions on the effects of wind stress forcing, water mass properties and mixing processes of the overflow are closely linked to the knowledge of the pathways, where the Denmark Strait Overflow Water approaches the sill.

In the past, there has been no consensus about whether the Denmark Strait Overflow is fed more by the East Greenland Current (hydrographic observations, e.g. RUDELS ET AL., 2002) or from the Iceland Sea (current observations, JÓNSSON AND VALDIMARSSON, 2004a). In this chapter, both theoretical aspects of the upstream basin circulation and observations of the SFB array are investigated to evaluate the critical regions, that determine the characteristics and volume transport of the Denmark Strait Overflow.

8.1. Theoretical studies of upstream basin circulation

In the classical GILL (1977) model of rotating hydraulics, a flow approaching the sill from the left-hand side (looking downstream towards the sill; i.e. the Iceland side in Denmark Strait) can be established by a dam-break scenario. In this case, the flow is initiated by a Kelvin wave propagating upstream along the left-hand side of the basin. The Kelvin-wave induced decrease of the dense water height feeds a geostrophically balanced current towards the sill. Due to the infinite upstream basin size, the right-hand side is not reached by the Kelvin wave, hence limiting the flow to the left-hand side.

Whereas the GILL (1977) model of rotating hydraulics was based on the assumption of an infinite upstream basin, HELFRICH AND PRATT (2003) extended this model to finite basin geometry.

The structure of the upstream basin circulation is governed by the potential vorticity (PV) budget, which is now assessed, following the theoretical studies of PRATT AND SMITH (1997) and HELFRICH AND PRATT (2003).

The shallow water momentum equation is given by

$$\frac{\partial \boldsymbol{u}}{\partial t} + \boldsymbol{u} \cdot \nabla_h \boldsymbol{u} + \boldsymbol{k} \times \boldsymbol{u} = -\nabla_h(h+b) + \boldsymbol{F_r} + \boldsymbol{M} \tag{8.1}$$

with $\boldsymbol{k}$ as vertical unit vector, h dense water layer depth and b bottom elevation above the deepest point of the basin (Fig. 8.1 a). ∇_h represents the horizontal gradient operator, $\boldsymbol{F_r}$ the bottom drag (in the numerical model, a linear drag $\boldsymbol{F_r} = r\boldsymbol{u}$ was used), and $\boldsymbol{M}$ the momentum flux due to vertical downwelling as dense water source in some of the experiments.

Integrating a steady-state of Eq. 8.1 (i.e., $\partial \boldsymbol{u}/\partial t$ vanishes) along a closed contour C along the rim of the upstream basin (see Fig. 8.1 b, c), one yields

$$\oint_C q H_2 \boldsymbol{u} \cdot \boldsymbol{n} \, ds = \oint_C (\boldsymbol{M} - r\boldsymbol{u}) \cdot \boldsymbol{t} \, ds \tag{8.2}$$

with the non-dimensional PV $q = (1+\xi)/H_2$ where $\xi = \partial v/\partial x - \partial u/\partial y$ represents the vertical relative vorticity. $\boldsymbol{n}$ and $\boldsymbol{t}$ are the local outward normal and tangential unit vectors along the integration path C.

Since the vertical velocity w and hence $\boldsymbol{M}$ equals zero at the basin boundary for steady state conditions, the net PV flux through the basin boundary (left-hand side of Eq. 8.2) must balance the net tangential friction $-\oint_C r\boldsymbol{u} \cdot \boldsymbol{t} \, ds$ along the boundary.

In the case of interior downwelling (resembling e.g. convection in the Greenland or Iceland Seas), the only contribution to the left-hand side of Eq. 8.2 is positive due to the outflow through the strait (with $q > 0$). Thus, a predominantly anticyclonic circulation along the basin boundary ($-\oint_C r\boldsymbol{u} \cdot \boldsymbol{t} \, ds > 0$) is established (Fig. 8.1 b).

For the case of horizontal inflow into the basin (resembling e.g. the EGC inflow into the Iceland Sea), $\oint_C q H_2 \boldsymbol{u} \cdot \boldsymbol{n} \, ds = 0$ if the potential vorticity q is the same for inflow and outflow. The right-hand side then implies, that the current towards the sill along the boundary has to split in order to satisfy Eq. 8.2. If the inflow is located opposite to the outflow, both branches are symmetrical (Fig. 8.1 c). If the inflow is situated asymmetrical to the outflow, the shorter branch has to be stronger to meet Eq. 8.2.

A numerical model used by HELFRICH AND PRATT (2003) confirmed these theoretical findings (Fig. 8.2). It also revealed, that at the sill and further downstream, the flow structure is governed by the strait geometry, and only weakly depends on the upstream basin current structure and the type of the dense water source (interior downwelling or horizontal boundary inflow; Fig. 8.2).

KÖSTERS (2004b) investigated the influence of different dense water sources on the upstream circulation in a model with realistic topography of the Denmark Strait. An interior downwelling source indeed yielded an anticyclonic circulation, with the overflow fed by a left-hand side boundary current along the Icelandic shelf edge. For a boundary inflow located at the northern edge of the model domain close to the East Greenland shelf, a cyclonic circulation sets up, with the East Greenland Current feeding the overflow. Moving the boundary inflow gradually further to the east into the Iceland Sea, the resulting circulation pattern becomes more anticyclonic. The numerical experiments (KÖSTERS, 2004b) hence agree with the predictions of HELFRICH AND PRATT (2003).
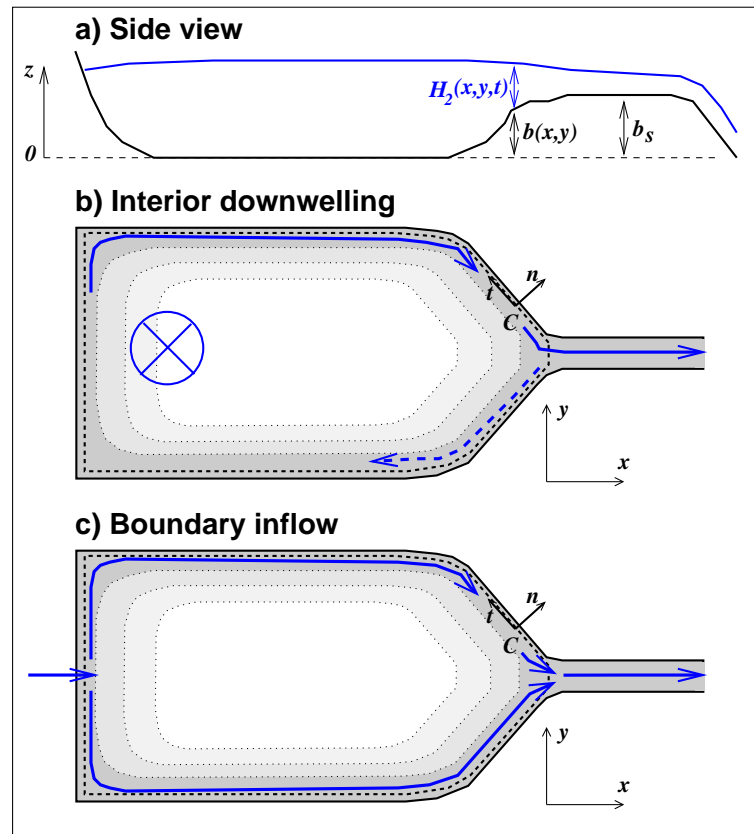
Figure 8.1.: *Principal sketch of a finite upstream basin, adopted from* HELFRICH AND PRATT *(2003). Panel a: Side view of the basin geometry with bottom elevation above deepest point of the basin $b(x, y)$, sill height b_s, and dense water layer thickness $H_2(x, y, t)$. Panels b and c: Plan views of the basin. Shading indicates topography. $\boldsymbol{n}$ and $\boldsymbol{t}$ represent outward normal and tangential unit vectors along the integration path C along the basin boundary (dashed line). Panel b: Dense water source by downwelling in the interior basin. Anticyclonic circulation balances PV loss by the outflow over the sill. Panel c: Dense water source by boundary inflow. The current splits into two branches both flowing towards the sill to close the PV balance.*
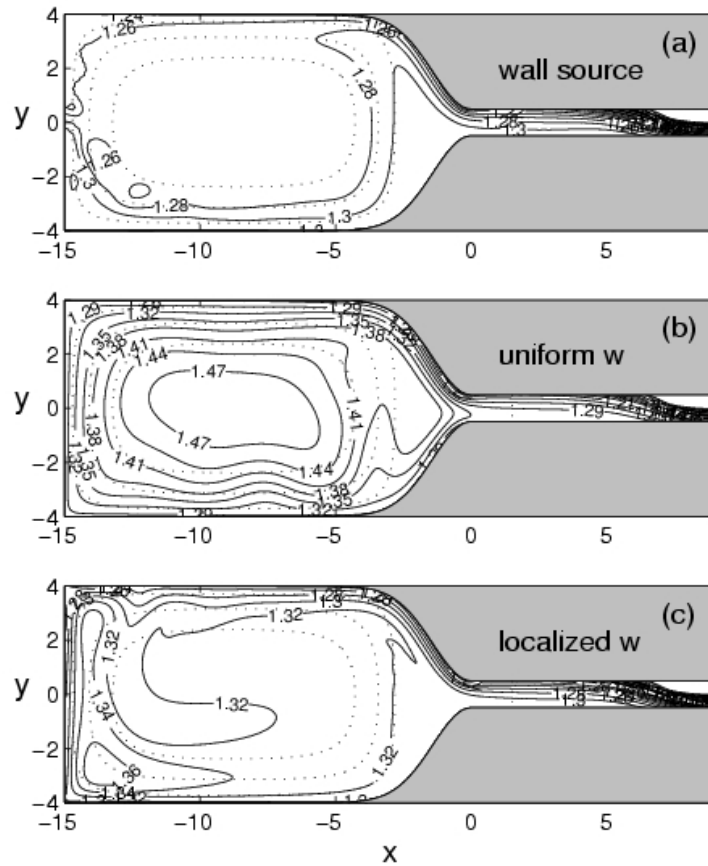
Figure 8.2.: *Upstream basin circulation, from* HELFRICH AND PRATT *(2003). Shown are contours of free surface height $h + b$ as indication of geostrophically balanced steady state flow. Dotted lines indicate basin topography. Panel a: Boundary inflow at $x = -15, y = 0$. Surface depression at left-hand wall ($y = 4$) and elevation at right-hand wall ($y = -4$) indicates flow towards the sill (Fig. 8.1 c). Panel b: Uniform dense water downwelling in the entire basin. Surface depression along the left-hand wall indicates flow towards the sill. A smaller depression at the right-hand wall indicates a weak anticyclonic recirculation (Fig. 8.1 b). Panel c: Experiment with localized downwelling close to $x = -15$. Basically similar to previous panel, although the anticyclonic recirculation pattern is less evident. Note, that the structure at and downstream of the sill is similar for all three experiments.*

8.2.   Previous observations of the upstream pathways

The importance of long-distance advection of DSOW source water masses, and local formation processes in the Iceland Sea has been discussed in sections 2.1 and 2.2. The implications for the circulation in the upstream basin and entrance region of the Denmark Strait are to a certain degree controversial.

The theoretical studies of HELFRICH AND PRATT (2003) and KÖSTERS (2004b) allow both advection on the left-hand and the right-hand side of the upstream basin, depending on the type of the dense water source. Hence, it remains to observations to resolve, which pathway is the most important source for the Denmark Strait Overflow.

From water mass analysis SWIFT ET AL. (1980) concluded that the overflow was mainly supplied by Upper Arctic Intermediate Water (UAIW), formed in the Iceland Sea during winter. It was assumed that the UAIW was advected by the East Greenland Current (EGC) to the sill, since closed dynamic height contours appeared to not allow a direct flow from the Iceland Sea to the Denmark Strait.

Based on hydrographic surveys from Fram Strait via Denmark Strait to the Irminger Sea, RUDELS ET AL. (1999, 2002) state that most of the overflow components originate from the Greenland Sea (STRASS ET AL., 1993; RUDELS ET AL., 2002), advected by the East Greenland Current, since water of similar properties could be followed all along the EGC. The less saline upper part of the overflow was identified as Polar Intermediate Water already present in the thermocline of the EGC in Fram Strait. RUDELS ET AL. (2002) did not observe a major contribution from the Iceland Sea, but stated, that the temperature reduction in the core of the overflow could partly have been caused by mixing with the colder Iceland Sea Arctic Intermediate Water. They discuss briefly possible alternative circulation schemes including two different sources for the Iceland Sea Arctic Intermediate Water (IAIW) in the Iceland Sea. If IAIW is formed due to cooling of Returned Atlantic Water (RAW), it possibly would supply both Denmark Strait and Faroe Bank Channel overflows. The authors question, what in this case would happen to the bulk of the EGC. Alternatively, RUDELS ET AL. (2002) suggested, that a branch of the EGC enters the Iceland Sea, becomes transformed into IAIW, and continues from there to the Denmark Strait. This option is considered as unlikely, however, since the short residence time of less than a year in the Iceland Sea should lead to a higher IAIW variability than observed (RUDELS ET AL., 2002).

In contrast to these findings, that are based on single research cruises, JÓNSSON (1999) continuously observed the currents on a section 200 km upstream of the sill three years from 1988 to 1991. Since the overflow does not show significant seasonal transport signals (AAGARD AND MALMBERG (1978); DICKSON AND BROWN (1994); this study), the same should hold for the upstream pathways. On the Greenland side, JÓNSSON (1999) found strong seasonal and interannual current variability. JÓNSSON AND VALDIMARSSON (2004a) thus ruled out that the direct EGC path is a major source for the overflow.

On the Icelandic shelf edge at the mooring position IS7 [1], however, JÓNSSON

(1999) observed a steady current of water with DSOW properties with a mean velocity of 9.6 cm/s towards the sill. This current was confirmed by several vmADCP sections further to the east at Hornbanki section[1] (Jónsson and Valdimarsson, 2004a).

A recent analysis of hydrographic T/S data at the Siglunes 8 station[1] showed that this current can even be tracked back to the Kolbeinsey Ridge[1] region north of Iceland (Jónsson and Valdimarsson, 2004b).

Whether it is fed from further east or from a branch of the East Greenland Current – which would account for the observed T/S continuity along the path of the EGC (Rudels et al., 2002) – has to be resolved in future investigations.

Since the overflow temperature at the sill is somewhat higher than at IS7 ($\Delta T \leq 0.3\,°C$), Jónsson and Valdimarsson (2004a) argue, that on the way to the sill some other water masses have to be entrained. Upstream of the sill, the dense water observed in the jet towards the sill was surrounded by the northeastward moving AW to the east (warm, saline), and Atlantic Intermediate Water (AIW; slightly warmer, less saline) to the west. The observed warming may thus be attributed to entrainment processes of the adjacent water masses (Jónsson and Valdimarsson, 2004a).

The SFB array supported further evidence for the "Iceland side pathway", which will be addressed in the next sections.

8.3. Advection of temperature anomalies

Primarily to observe the upstream reservoir height, temperature recording moorings were deployed from 1999-2000 ("TK") and 2002-2003 ("TP") at the Icelandic shelf edge at 670 m depth 93 km northeast of the sill[1]. Based on the results of the process model (chapter 4), this position was expected to lie in the main pathway towards the Denmark Strait sill. The 1999/2000 mooring (TK) data are less suitable to track overflow temperature anomalies, which have a typical amplitude of $\leq 0.5\,°C$, since instrumental problems greatly reduced the absolute accuracy of the individual temperature records.

The 2002/2003 deployment (TP), however, allowed for a more detailed data analysis. Close to the surface, occasionally warm Atlantic Water (AW) was observed, more often, however, cold water of the East Greenland Current was present (Fig. 6.10, page 101). Due to the lacking temperature contrast to the dense overflow water, the TP data could not verify hydraulic control (section 6.3.2), but the near-bottom temperature time series suggest, that in fact the water passing the TP mooring site contributes to the overflow at the sill.

To prove the upstream pathway, temperature time series of the deepest sensor at TP and of ADCP B at the sill were compared. The short time variability is not significantly correlated, since the sill time series frequently exhibit abrupt changes of more than $0.5\,°C$ (Fig. 8.4), likely due to entrainment of different water masses into the plume.

---

[1]For geographical locations, see Fig. 2.1, page 27.
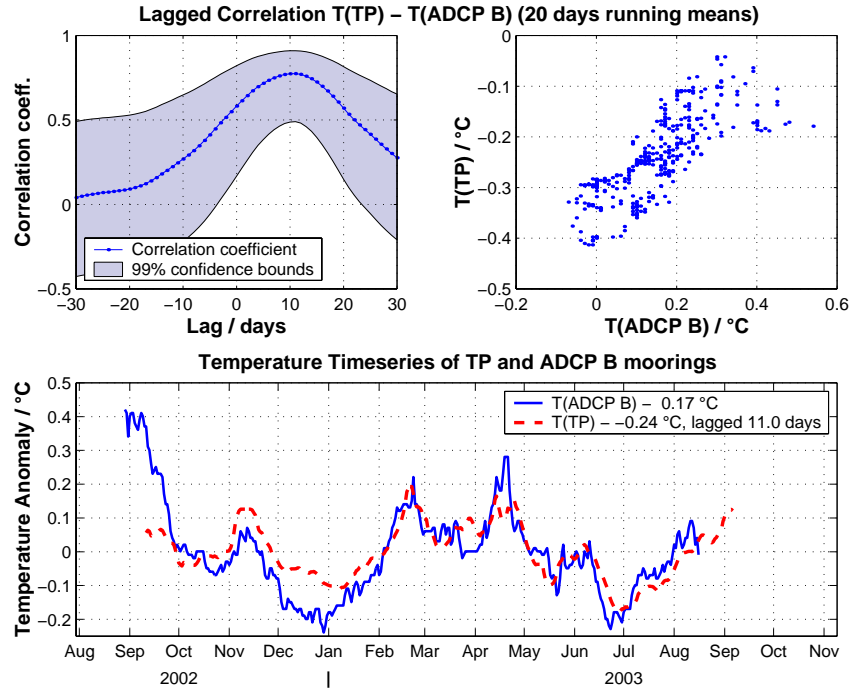
Figure 8.3.: *Lagged long-term temperature correlation between TP mooring 93 km upstream of the sill on the Icelandic slope, and ADCP B at the sill. 20 days running mean time series.*

On longer timescales, the 20 days running mean time series reveal a significant correlation maximum of $r = 0.78$ for a time lag of 11 days between TP mooring and ADCP B (Fig. 8.3). This corresponds to a mean advection velocity of 10 cm/s for temperature anomalies from the TP site 93 km northeast of the sill, and is essentially similar to the mean velocity of 9.6 cm/s, observed by JÓNSSON (1999) and JÓNSSON AND VALDIMARSSON (2004a) at the IS7 mooring site on the Icelandic shelf edge 200 km upstream of the sill[1]. The continuation of this flow towards the sill is additionally supported by expendable current profiler measurements (GIRTON, 2001).

8.4. Θ/S properties and upstream entrainment

JÓNSSON AND VALDIMARSSON (2004a) observed a warming of up to 0.3 °C between the Kögur 5 (KG5) station 200 km upstream and the overflow at the sill varying between different years of observation, which they attributed to entrainment of warmer AW or AIW adjacent to the dense current to the sill. JÓNSSON AND VALDIMARSSON (2004a) found, that the highest warming occurred, when the weakest current was observed.

The continuous time series of the SFB array allow for a more detailed investigation. In fact, the temperature difference between the TP mooring 93 km upstream and the ADCP B at the sill varies between 0 °C during strong currents (measured by ADCP

B) and approx. 0.7°C during weak outflow periods (Fig. 8.4). The differences in warming correspond to the higher short term temperature variability at ADCP B, that is correlated with the current velocity (Fig. 8.4; for ADCP A, a similar correlation of temperature and current velocity was found on monthly timescales by JÓNSSON, 1999).

The minimum temperatures during weak outflow at the sill are well correlated with the near-bottom temperatures at TP (as reflected in Fig. 8.3), suggesting, that during these times water has been advected almost unchanged from TP to the sill.

The warmer and more variable temperatures during strong outflow periods associated with the passage of eddies might be attributed to enhanced entrainment (as suggested by JÓNSSON AND VALDIMARSSON, 2004a), or the passage of other water masses that might have been advected by the East Greenland Current (according to the advection scheme of MAURITZEN, 1996a).

Example of temperature / current velocity timeseries, 2002
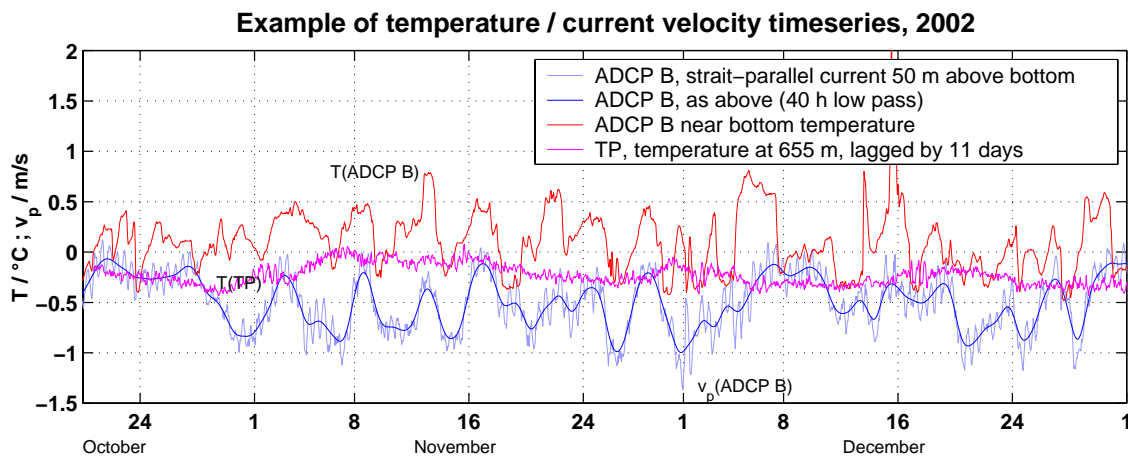
Figure 8.4.: *Example of temperature time series at TP 93 km upstream and ADCP B at the sill. Overlaid, the strait parallel current at ADCP B indicates, that the highest temperatures at ADCP B occur during weak outflow. All time series unfiltered to resolve the typical short term variability. TP time series lagged by 11 days to account for the advective timescale.*

These issues shall be investigated considering the Θ/S profiles at KG5 from 1999 to 2003 (Fig. 8.5). The range of variability in the dense overflow water at KG5 is much smaller than at the sill (compare KG5 data to sill profiles (grey background dots in Fig. 8.5)). Obviously, at the sill, a greater variety of different water are advected and mixed than at KG5. Nevertheless, the Θ/S properties observed at KG5 are also represented at the sill, which supports the assumption of a direct flow from KG5 to the sill (JÓNSSON AND VALDIMARSSON, 2004a).

At the bottom, the sill profiles are around 0.1°C warmer than at KG5, with little change in salinity. JÓNSSON AND VALDIMARSSON (2004a) attribute this to entrainment of warmer and saltier AW and slightly warmer, but fresher AIW into the overflow water.
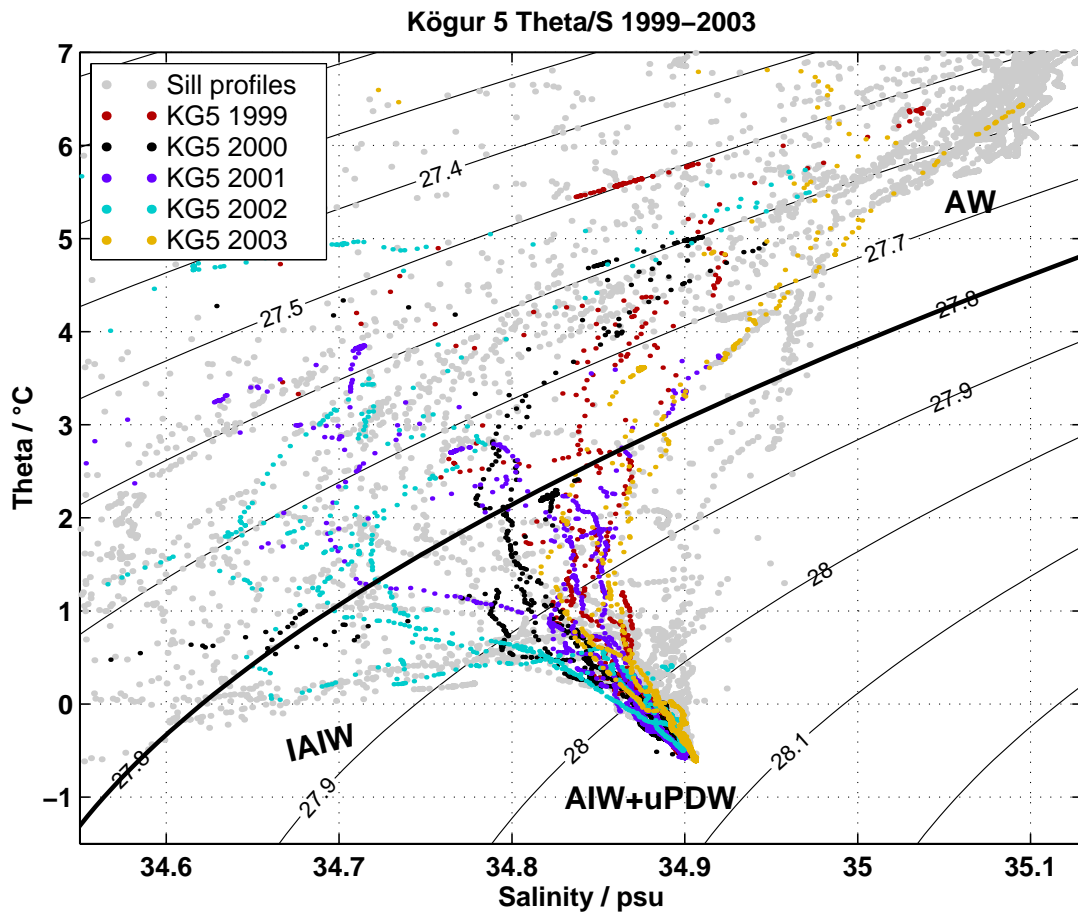
Figure 8.5.: Θ/S diagram of Kögur 5 station 1999 – 2003. Colours denote year of observation; they are similar to Fig. 2.3 for the sill sections. Grey dots denote all sill profiles from 2000 – 2004. In the density range $\sigma_\Theta > 27.9\,\mathrm{kg/m^3}$, the Kögur 5 profiles lie within the range of the sill profiles, but occupy the cold/low-saline edge only of the sill profile range.

In the density range $\sigma_\Theta > 27.95\,\mathrm{kg/m^3}$ (used as overflow definition by STRASS ET AL., 1993), the KG5 profiles occupy the cold/fresh edge of the variability range at the sill. Water with $\Theta \approx +1\,°C$ / $S \approx 34.9$, which was attributed as LAIW[1] in the sill profiles (Fig. 2.3, page 31) is not present at KG5.

The presence of this warmer and saltier water at the sill might point towards some direct advection of LAIW (also named RAW, MAURITZEN, 1996a) by the East Greenland Current, not passing KG5. Moreover, entrainment of warmer and saltier AW is possible, although this is less evident for the bottom end of the profiles (where the ADCPs have sampled the temperature) than in the lighter part of the overflow ($27.8\,\mathrm{kg/m^3} < \sigma_\Theta < 27.95\,\mathrm{kg/m^3}$). Here, the sill profiles clearly show products of diapycnal mixing of IAIW with PIW, modified PIW (RUDELS ET AL., 2002) and, in particular, AW (further discussion in section 2.2).

---

[1]Lower Arctic Intermediate Water, see section 2.2.

The **interannual variability at KG5** from 1999 to 2003 is much smaller than at the sill. For the near-bottom density range $\sigma_\Theta > 27.95\,\mathrm{kg/m^3}$, some of the 2002 profiles, and all of the 2003 profiles are generally $\approx 0.2\,°\mathrm{C}$ warmer and ≈ 0.01 psu saltier than those from 2000/2001 (Fig. 8.5). Although one has to take into account short-term variability aliasing of the KG5 time series (which was sampled 4 times per year only), the magnitude of interannual warming is clearly smaller than the 0.5 °C warming from 1999 to 2002 observed at the sill.

The following mechanisms are possible reasons for the larger temperature variability at the sill:

- Enhanced entrainment of Atlantic Water between KG5 and the sill.

- Constant entrainment rates of Atlantic Water, that has become warmer and saltier in 2002/2003.

- Variable advection of LAIW or PIW/AW mixing products by the EGC.

Enhanced entrainment points towards an enhanced Atlantic Inflow of the North Iceland Irminger Current (NIIC; HANSEN AND ØSTERHUS, 2000). This is, although not evident in the absolute near-surface or near-bottom current velocities measured by ADCP (not shown), reflected in the ADCP interface depth time series (Fig. 5.3 c, page 65): While the mean plume thickness at ADCP B 11 km northwest of the sill has only slightly changed, the dense water thickness at the easternmost ADCP A has decreased by 56 m from 1999 to 2003. This might be an indication of a northwestward shift of the DSOW/AW frontal zone due to enhanced AW inflow. With a larger fraction of the dense overflow overlaid by warm AW instead of the EGC, it is likely that more warm water is entrained into the overflow.

Considering the hydrographic sections at the sill from 2000 to 2004 (Fig. 2.4, page 33), the AW inflow has warmed significantly during this period. The core of the NIIC was more than 1 °C warmer in 2003 than in 1999, while the salinity increased by around 0.1 psu. At constant entrainment ratios, this signal would cause a warming of the overflow.

On the other hand, the advection of LAIW by the EGC, as suggested by MAURITZEN (1996a), is another plausible explanation. In particular, the sudden temperature shifts at ADCP B between "cold phases" during weak outflow and "warm phases" during the passage of eddies and the virtual absence of intermediate temperatures (Fig. 8.4) suggest, that ADCP B sampled different water bodies, which have been advected from different origins and which have not much mixed and homogenized with each other before reaching the sill.

Clearly, continuous time series of temperature *and* salinity would help to answer this question.

Since the hydrographic sections also include unresolved short term variability, it can not be decided to what extent entrainment changes, Atlantic Water warming, or LAIW advection by the EGC contribute to the observed interannual overflow warming from 1999 to 2002.

In any way, the Θ/S properties of the overflow at the sill and further downstream do not only reflect long term changes in the source regions in the Nordic Seas, but are also heavily influenced by entrainment processes and mixing ratios of different water masses in the upstream entrance region of the sill.

8.5.   Circulation pattern in NCEP forced model

Recent numerical models with realistic forcing may help to resolve the upstream pathways of the Denmark Strait Overflow. Here, first results of the high resolution MITgcmUV[2] model of the subpolar North Atlantic currently run by R. H. Käse at IfM Hamburg shall be investigated. The model domain extends from 51 °N to 78.2 °N and 46 °W to 16.9 °E with $1/10° \cos(\varphi)$ horizontal resolution, forced by daily NCEP data.

In the model, there is evidence for a confined current towards the sill on the Icelandic shelf edge (Fig. 8.6; KÄSE, pers. comm.). Between Kolbeinsey ridge and the Denmark Strait sill, the current is well defined by topography. At Kolbeinsey Ridge, it appears to be fed by both a deep north-east Iceland coastal current and a part of the East Greenland Current, recirculating in an anticyclonic gyre in the Iceland Sea off western North Iceland.

To prove the results of the MITgcmUV model, it is intended to study the influence of basin geometry, location of source regions, and different meteorological forcing on the Iceland Sea and Denmark Strait region. This issue will be discussed in a paper by KÄSE (in preparation).

The model agrees with the observations at the IS7 current meter site, and the observed current at the Kögur and Hornbanki sections (JÓNSSON AND VALDIMARS-SON, 2004a). There exists observational evidence, based on hydrographic profiles at the Siglunes 8 station (Fig. 8.6), that the current can be tracked back to the Kolbeinsey Ridge (JÓNSSON AND VALDIMARSSON, 2004b). Its continuation further to the north and east as suggested by the model, has not yet been resolved by observations, and remains for future investigations.

8.6.   Summary and conclusions

The origin and upstream dense water pathway towards the Denmark Strait sill has been subject to controversial discussion. SWIFT ET AL. (1980) assumed, that the overflow is fed from the Iceland Sea via the East Greenland Current. STRASS ET AL. (1993); MAURITZEN (1996a) and RUDELS ET AL. (2002) proposed the direct advection of water with DSOW properties by the EGC. JÓNSSON AND VALDIMARSSON (2004a) did not observe a steady flow of the EGC towards the sill, but instead found a current with DSOW properties at the Iceland shelf edge, which could be tracked back further to the east by hydrographic data (JÓNSSON AND VALDIMARSSON, 2004b).

---

[2]MITgcmUV: Massachusetts Institute of Technology general circulation model Ultrahigh Versatility

temp at 27.95 25July−1992 MITgcmuv 1/10 deg resolution
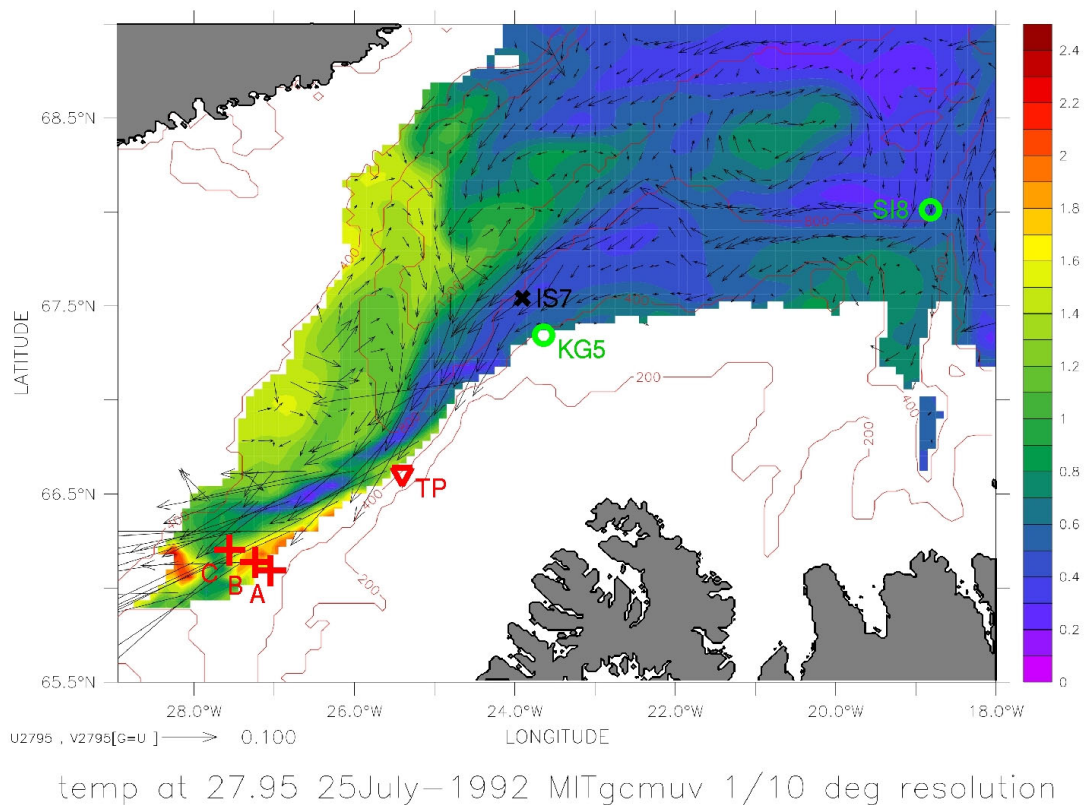
Figure 8.6.: *MITgcmUV model: Temperature and currents at $\sigma_\Theta = 27.95\,\mathrm{kg/m^3}$. Arbitrary snapshot from 25.07.1992, that reflects the typical current structure in the model. Note the coherent current along the Icelandic shelf edge from Kolbeinsey ridge to the Denmark Strait sill. Additionally, there exists a minor direct contribution to the overflow from the East Greenland Current. Positions of ADCPs A/B/C, TP mooring and IS7 current meter mooring overlaid. KG5 and SI8 mark Icelandic hydrographic stations.*

The SFB array corroborated the evidence for the "Iceland side pathway": For the TP and ADCP B moorings, a high temperature correlation was found (Fig. 8.3). The time-lag of 11 days corresponds to the advection velocity measured by JÓNSSON AND VALDIMARSSON (2004a). The Θ/S profiles at the sill contain similar water masses than those at KG5.

The high resolution process model (chapter 4) is capable to reproduce the observed features, as does the MITgcmUV model with full meteorological forcing (KÄSE, pers. comm.).

However, the EGC might also contribute to the overflow to some degree: At the sill, substantial amounts of LAIW were regularly observed, which are not present at the KG5 station. Since the SFB array did not cover the northwestern part of the upstream region, no estimates on advection velocities or pathways can be made for this side.

Theoretical studies of the upstream basin circulation (Helfrich and Pratt, 2003) do not exclude either of the two advection pathways. Due to the conditions in the Iceland Sea, it is likely that both "boundary inflow" and "interior downwelling" conditions (Helfrich and Pratt, 2003) can be applied:

The EGC enters the Iceland Sea at its northern edge (at $\approx 65°30\,$'N / $19°$W). Its continuation along the East Greenland shelf is well established (Swift et al., 1980; Strass et al., 1993; Rudels et al., 2002). However, Rudels et al. (2002) observed a separation of a warmer part of the EGC from the Greenland shelf close to $65°30\,$'N / $19°$W. They state, that EGC water might enter the Iceland Sea right here, where the Greenland shelf turns westward, if the EGC does not directly feed the overflow. This theory would resemble the "boundary inflow" case of Helfrich and Pratt (2003), with currents flowing along the East Greenland shelf edge and the Kolbeinsey Ridge / Icelandic shelf edge towards the sill.

In the Iceland Sea, at least some dense water is formed during winter cooling (Swift et al., 1980; Malmberg and Jónsson, 1997; Rudels et al., 2002). Although it is under debate, to what extent this water contributes to the Denmark Strait Overflow, dense water formation due to cooling / convection could be associated with the "interior downwelling" case of Helfrich and Pratt (2003), which would lead to a current approaching the sill on the Icelandic side.

Since the Helfrich and Pratt (2003) model is governed by a linear equation of the potential vorticity budget in the upstream basin, both processes might add up linearly.

Concluding, the key results of the SFB observations are:

- A major part of the overflow is fed by a current approaching the sill from the Iceland side of the Denmark Strait. In particular, it has been shown, that the coldest and densest parts of the DSOW are advected from the Iceland Sea. The observations agree with Jónsson and Valdimarsson (2004a) and the NCEP-forced MITgcmUV model (Käse, pers. comm.).

- At the sill, warmer water masses, that show considerably larger variability, have been observed. These may be attributed to entrainment of warmer AW or AIW into the overflow in the sill entrance region, or the advection of LAIW by the East Greenland Current. However, it can not be decided from the SFB array observations, which of both mechanisms is more important.

- The Iceland Sea may be considered as a critical region for the overflow, since local modification of water masses advected through the Iceland Sea determine the density and T/S properties of a large part of the Denmark Strait Overflow. Moreover, the hydraulically controlled overflow component is governed by the upstream dense water reservoir height (discussed in chapter 6).

9. Synthesis of hydraulic and wind stress forcing and large scale coupling mechanisms

Numerical experiments (Biastoch et al., 2003; Kösters, 2004b) suggest, that the Denmark Strait Overflow may be understood as a combination of hydraulically controlled flow, which is driven by the baroclinic along strait pressure gradient, and wind driven barotropic flow.

In the previous chapters, observational evidence in the SFB time series for both mechanisms, and the upstream pathways to the sill have been investigated.

Here, a synthesis of both forcing mechanisms will be attempted to merge the observed characteristics of the overflow into a consistent theory of the processes, that control the dense overflow over the Denmark Strait sill. As a validation, the observed DSOW transport shall be reconstructed from estimates of density and wind stress forcing.

Further, large scale coupling mechanisms with the Faroe Bank Channel overflow, which is the second large dense overflow across the Greenland-Scotland Ridge, shall be investigated to yield an integrated view on the processes that control the dense overflows from the Nordic Seas into the Atlantic ocean.

9.1. Reconstruction of the DSOW transport from density and wind stress forcing

The SFB observations suggest, that the Denmark Strait Overflow comprises both a density driven, hydraulically controlled and a barotropic component.

For the reconstruction of DSOW transport time series, the overflow shall be treated as a linear combination of both parts, as suggested from evidence in numerical models (Kösters, 2004b).

9.1.1. Hydraulically controlled flow

A number of studies has addressed the hydraulically controlled flow through the Denmark Strait for frictionless 1 1/2 layer flow with zero or constant potential vorticity (PV; a.o. Whitehead, 1998; Helfrich and Pratt, 2003; Nikolopoulos

ET AL., 2003). Although these approaches require highly idealized conditions, they proved fairly well in predicting the actual transport over the sill.

In the light of more recent model results (BIASTOCH ET AL., 2003; KÖSTERS, 2004b), which attribute a large fraction of the overflow to barotropic rather than hydraulically controlled flow, the zero-PV theories may yield too high estimates. Moreover, the SFB mooring array observations and process model analysis (see section 6.2.3) revealed, that constant PV does not hold for the real overflow.

In section 6.2.5, it has been shown, that the STERN (2004) estimate appears as a more appropriate approach. While retaining the quadratic relation between reservoir height and transport, it does not require constant PV conditions, and hence yields quite realistic transport values.

Hence, the hydraulically controlled flow is assessed by

$$Q_{KG5} = Q_{WLK} \cdot \frac{9}{16} = \frac{1}{2}\frac{g'}{f}h_u^2 \cdot \frac{9}{16} \tag{9.1}$$

with $g' = 0.43/1027.8 \cdot g$ as reduced gravity (GIRTON, 2001) and f as Coriolis factor. h_u represents the upstream dense water reservoir height, which is taken as the height of the $\sigma_\Theta = 27.8\,\mathrm{kg/m^3}$ isopycnal at the Kögur 5 station 200 km upstream of the sill (see section 6.3.3).

Kögur 5 may be regarded as a feasible location for realistic upstream reservoir height estimates, since it is close to an observed pathway to the sill (JÓNSSON AND VALDIMARSSON, 2004a). Moreover, the level of dense water at KG5 is higher than anywhere else on the Kögur section (see Fig. 6.14, page 107, and JÓNSSON AND VALDIMARSSON, 2004a). The analysis of the process model revealed, that KG5 lies outside of the "entrance region" (HELFRICH AND PRATT, 2003), where h_u is significantly reduced (see Fig. 6.5). It appears hence unlikely, that KG5 underestimates the actual reservoir height.

The resulting time series is shown in Fig. 9.1 (green lines); the mean hydraulically controlled flow of 1.9 Sv agrees well with the estimate of KÖSTERS (2004b). A decrease from 2.0 Sv (1999) to 1.7 Sv (2003) is caused by an interannual reservoir height reduction of 50 m at the Kögur 5 station (see also Fig. 6.12, page 105).

Hence, $\approx 57\,\%$ of the observed 3.35 Sv DSOW transport (mean value 1999 – 2003) may be attributed to hydraulically controlled flow. The reservoir height decrease accounts for 50 % (0.3 Sv) of the measured 0.6 Sv transport reduction from 1999 to 2003.

9.1.2. Wind-driven barotropic flow

If 1.9 Sv of the Denmark Strait Overflow are regarded as density driven, the remaining 43 % (1.45 Sv; mean value 1999 – 2003) may be attributed to barotropic flow.

Numerical models suggest, that the barotropic part of the overflow is closely linked to the wind driven barotropic circulation (BIASTOCH ET AL., 2003; NILSEN ET AL., 2003; KÖSTERS, 2004b), and is positively correlated to the large scale NAO-related wind stress field. BIASTOCH ET AL. (2003) found a significant seasonal cycle of the

net transport through Denmark Strait, implying a fast barotropic response (EDEN AND WILLEBRAND, 2001). In experiments with different wind stress forcing, both BIASTOCH ET AL. (2003) and KÖSTERS (2004b) found a clear linear relation between wind forcing, barotropic net transport and the barotropic overflow component.

The analysis of the observed transports and wind stress forcing (section 7.3) yielded a more complicated picture, however. While the barotropic transport – although not properly sampled by the SFB array – might be consistent with a wind stress imposed seasonal cycle, hardly any seasonality could be detected in the overflow (corroborating observations of AAGARD AND MALMBERG (1978) and DICKSON AND BROWN (1994)).

9.1.2.1. Interannual variability

Focusing on interannual timescales, the barotropic part of the overflow (mean value 1999 – 2003: 1.45 Sv) should decrease by 20 % (0.3 Sv) to explain the observed DSOW transport reduction at the sill.

Since the linearity between wind stress forcing and barotropic transport is a robust feature in numerical models (BIASTOCH ET AL., 2003; KÖSTERS, 2004b), the relevant barotropic forcing should also exhibit an interannual decrease of $\approx 20\,\%$ between 1999 and 2003. Section 7.3 revealed, that the large-scale wind field showed a much weaker decrease during this period; only a delayed response might be consistent with the observed DSOW transport decrease. The four years of SFB observations are too short to prove any delayed or interannual to decadal timescale relation between NAO-related large scale wind stress forcing and the Denmark Strait overflow, even though a causal link appears likely.

For the period from 1999 – 2003, the local wind stress forcing over the Iceland Sea and Denmark Strait decreased by $\approx 17\,\%$ from 1999 to 2003. This makes the local forcing a likely candidate for the control of the barotropic flow through Denmark Strait, at least on timescales of months to years.

Therefore, the barotropic part of the overflow shall be assessed with the linear relation

$$Q_{\tau_{\mathrm{p}}} = \frac{1.45\,\mathrm{Sv}}{0.11\,\mathrm{Nm}^{-2}} \cdot \tau_p \tag{9.2}$$

The empirical relation is adjusted to match the average transport and wind stress values with 1.45 Sv as mean wind driven overflow transport between 1999 and 2003, and $0.11\,\mathrm{N/m^2}$ as mean strait parallel wind stress τ_p during the same period.

The wind driven overflow component calculated with Eq. 9.2 decreases by 0.3 Sv from 1999 to 2003 (Fig. 9.1, red lines) and hence meets the proposed reduction.

9.1.2.2. Monthly variability

The importance of the Iceland Sea wind stress forcing is supported from the observational evidence, that local wind stress anomalies are often reflected by the overflow (Fig. 7.5 d, page 118). In particular, the exceptional large DSOW transport variations

in end-2001 are correlated with wind stress anomalies, that occurred over the Iceland Sea, but are not evident in the large scale wind field.

Although there is some evidence, that the Denmark Strait Overflow has a response lagged by a few days to weeks to the monthly Iceland Sea wind stress forcing variability, a correlation analysis did not yield significant results (not shown). One reason might be, that changes of the density driven overflow part have not been resolved on monthly timescales, since the reservoir height at KG5 has been measured four times per year only.

Supposed, that the linear response expressed by Eq. 9.2 is also valid on shorter timescales, the overflow should exhibit a seasonal cycle of $O(1\,\mathrm{Sv})$ and monthly variability of $O(3\,\mathrm{Sv})$. This has not been observed by the SFB array, though (compare wind stress and DSOW transport time series in Fig. 7.5 d, page 118). Obviously, the overflow response to monthly wind stress variability is about 10 times smaller than would be expected from Eq. 9.2. Further investigations are needed to resolve the overflow response amplitudes and timescales on short term wind stress variability.

9.1.3. Reconstructed DSOW transport time series

In the previous sections, estimates of the hydraulically controlled, density driven overflow component (Eq. 9.1) and the barotropic part have been evaluated. For the latter, an empirical linear relation to the strait-parallel wind stress over the Iceland Sea and Denmark Strait region (Eq. 9.2) was used.

The resulting total DSOW transport $Q_{KG5} + Q_{\tau_\mathrm{p}}$ almost perfectly matches the observed interannual transport decrease from 1999 to 2003 (Fig. 9.1). The 2-year low-passed values have an RMS deviation to the observed DSOW transport of $0.25\,\mathrm{Sv}$, while the interannual decrease from 1999 to 2003 is reproduced with a difference of $< 0.1\,\mathrm{Sv}$.

In parts of the time series, the agreement becomes even better, if the annual cycle of the reservoir height and wind stress are included. However, the monthly variability can not be realistically reproduced with this model, since it greatly overestimates the short-term sensitivity of the overflow.

9.1.4. Discussion

The agreement between the observed and the reconstructed DSOW transport time series shown in Fig. 9.1 is remarkable.

One has to bear in mind, though, that a number of simplifications have been made for the transport re-calculation:

- A linear superposition of hydraulically controlled and barotropic transport has been assumed.

- The hydraulic transport is based on the non-constant PV relation of STERN (2004). The upstream reservoir height has been derived from single point measurements at Kögur 5, which is sampled four times per year only.
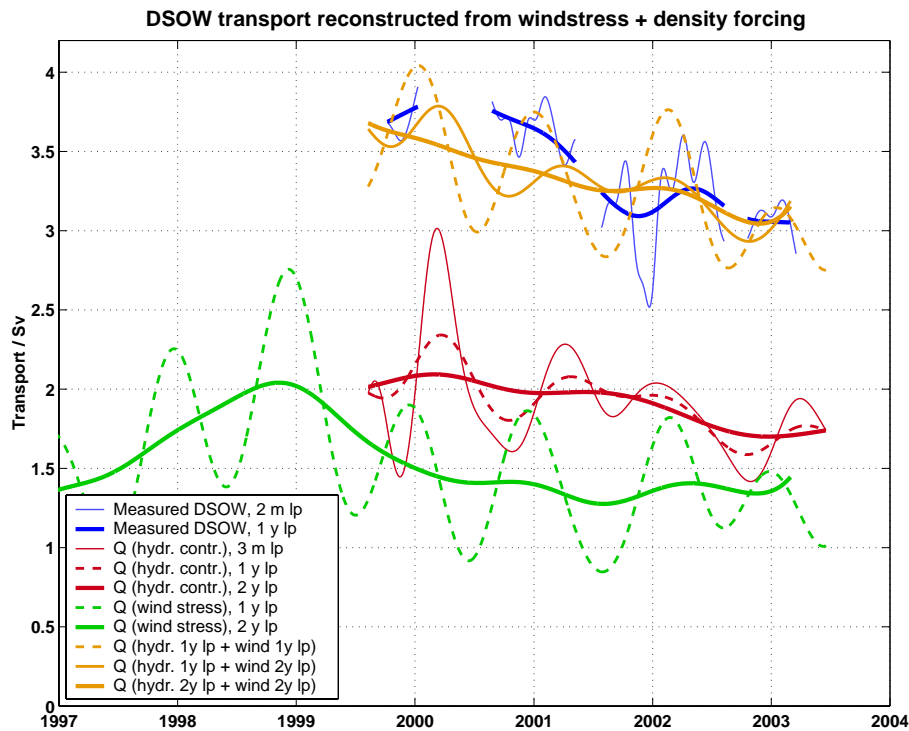
Figure 9.1.: *DSOW transport reconstruction from density and wind stress forcing. Red lines show hydraulically controlled flow derived from the $\sigma_\Theta = 27.8\,\mathrm{kg/m^3}$ isopycnal height at station Kögur 5. Green lines represent the wind driven, barotropic overflow transport, based on an empirical linear relation to the strait-parallel NCEP-windstress over the Iceland Sea and upstream region in Denmark Strait. Yellow lines depict the sum of both components. The actual transport observed by the SFB mooring array is marked with blue lines. 2 and 3 months and 1 and 2 years low-pass, respectively, are differentiated by the linestyle (see legend box).*

- The barotropic transport has been calculated with a simple linear relation, adjusted to match the mean values. Instead of the large scale wind field, the local wind stress forcing over the Iceland Sea and Denmark Strait has been selected, since it better fits to the observed overflow decrease, and also shows a higher correlation on monthly timescales. The linear equation, however, greatly overestimates the overflow response to short-term variability.

- Possible changes of the density contrast have not been taken into account.

The main results of the time series reconstruction may be summarized as following:

- Of the observed DSOW transport of $3.35\,\mathrm{Sv}$ (1999 – 2003 average), $1.9\,\mathrm{Sv}$ (57 %) may be regarded as density driven, hydraulically controlled flow. From 1999 – 2003, the hydraulically controlled part decreased by $0.3\,\mathrm{Sv}$ (16 %) related to an interannual reservoir height decrease of $50\,\mathrm{m}$ at Kögur 5.

- The remaining 1.45 Sv (1999 – 2003 average) may be considered as barotropic, wind driven flow. To match the observed total DSOW transport decrease from 3.7 Sv (1999) to 3.1 Sv (2003), an interannual reduction of 0.3 Sv (20 %) is required for the barotropic component.

- The local wind stress over the Iceland Sea and Denmark Strait decreased by 17 % from 1999 to 2003 (in contrast, the large scale wind field exhibited a much weaker reduction). A linear relation between wind stress forcing over the Iceland Sea and the barotropic overflow component is capable to explain the interannual decrease within ±0.1 Sv.

- The combined density and wind stress forcing explain the observed interannual overflow decrease within ±0.1 Sv.

The proposed influence of the NAO-related large scale wind stress field over the North Atlantic on the barotropic circulation around Iceland and the overflows across the GSR (model experiments, BIASTOCH ET AL., 2003; KÖSTERS, 2004b) may be important on longer timescales. This is consistent with long-term observations of the FBC overflow (HANSEN ET AL., 2001). The SFB time series are too short to prove yet, to what extent the Denmark Strait Overflow is influenced by the large scale wind field. For the Denmark Strait Overflow variability between 1999 and 2003, the local wind stress forcing over the Iceland Sea appears to be particularly important.

Further investigations, including wind stress time series with higher temporal resolution, and hydrographic observation data of the Iceland Sea, are necessary to evaluate the critical role of the Iceland Sea region for the Denmark Strait Overflow.

9.2.   Correlation with Faroe Bank Channel Overflow

The total dense water export across the GSR depends on the mean density gradient between the Nordic Seas and the North Atlantic (BIASTOCH ET AL., 2003). The spatial distribution between the Denmark Strait (DS), Iceland-Faroe Ridge (IFR), and Faroe Bank Channel (FBC)/ Wyville-Thomson Ridge (WTR)[1], however, is influenced by the wind driven barotropic circulation around Iceland.

At the Faroe Bank Channel (FBC), enhanced westerlies during positive NAO phases enhance the AW inflow (BLINDHEIM ET AL., 2000) and reduce the dense outflow of Iceland Scotland Overflow Water (ISOW; HANSEN ET AL., 2001).

Based on model experiments, NILSEN ET AL. (2003) proposed an anticorrelation between Denmark Strait and FBC net transports, with enhanced AW inflow across FBC and enhanced Denmark Strait outflow during high NAO phases. For the dense overflows, a similar response should be expected.

Also KÖSTERS (2004b) investigated the NAO influence on the overflows. As discussed in section 7.3.1, he attributed 35 % of the Denmark Strait Overflow to be

---

[1]For locations, see Fig. 7.2, page 113.

wind-driven. While the DSO was positively correlated to the wind stress curl forcing, the combined FBC/WTR overflows showed a negative response. The amplitude of the FBC/WTR overflows response was about one third of the DSO.

Here, time series of the Denmark Strait and the FBC overflows shall be investigated to evaluate observational evidence for the proposed anticorrelation of both overflows.

9.2.1. Observational evidence for a DSO/FBC overflow anticorrelation

Observations of the FBC overflow appear to confirm these model results: Based on hydrographic profiles upstream of the FBC, HANSEN ET AL. (2001, 2004b) observed an interdecadal decrease of the FBC overflow from the 1950's to the mid 1990's by 20 %, that might be associated with a long term freshening of the Nordic Seas (BLINDHEIM ET AL., 2000; DICKSON ET AL., 2002). Moreover, the FBC overflow transport reduction is consistent with the long term increasing trend of the NAO until the mid-1990's (HURRELL, 1995).

Since 1995, the FBC overflow has been continuously monitored by a bottom mounted ADCP. Since the FBC is fairly narrow (10 km, i.e. not wider than one Rossby-radius), the current structure is spatially coherent, and allows a good extrapolation from one ADCP (HANSEN ET AL., 2004a). The ISOW/AW interface depth has been defined kinematically by the depth where the along-channel velocity is reduced to 50 % of the overflow core velocity. Due to the distinct baroclinic structure of the FBC overflow, this definition agrees closely with the depth of certain isopycnals.
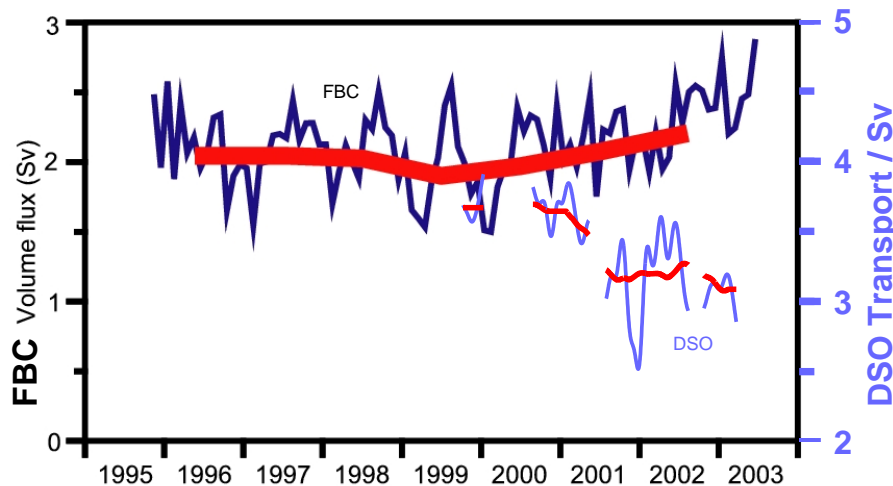

Figure 9.2.: *Transport time series of the Faroe Bank Channel overflow from 1992 to 2003. Overlaid are the SFB array time series of the Denmark Strait Overflow. Note the different scaling. Thin lines represent running monthly averages, bold red lines denote annual means. Original figure of the FBC overflow reproduced by courtesy of B. Hansen (HANSEN ET AL., 2004a).*
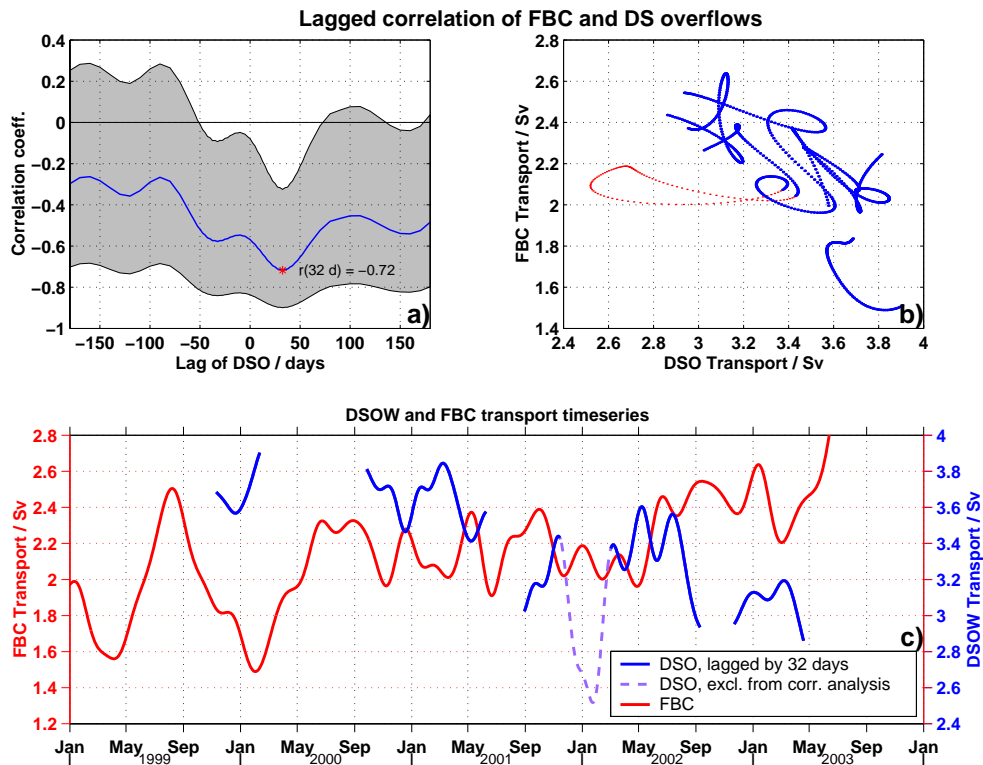
143

Figure 9.3.: *FBC and DSO correlation analysis. Time series of monthly means, smoothed with a 2 months low-pass filter have been used. Note, that the exceptional low DSO event (14.10.2001 – 28.01.2002) has been excluded from the correlation analysis.*

The time series (HANSEN ET AL. (2004a), unpublished, pers. comm., Fig. 9.2) show from 1995 to 1999 a slightly decreasing trend, and a significant seasonal signal, with transport values of $\approx 1.5\,\mathrm{Sv}$ in winter and $2.5\,\mathrm{Sv}$ in summer. This agrees with the anticorrelation to the wind stress or NAO forcing, which is strongest during winter (see chapter 7).

From 2000 to 2003, the seasonal signal is less evident, but there exists an interannual increase from $2.0\,\mathrm{Sv}$ to $\approx 2.4\,\mathrm{Sv}$. This increase corresponds to the recent decrease of the NAO (section 7.2). Moreover, it agrees well with the observed $0.6\,\mathrm{Sv}$ reduction of the Denmark Strait Overflow (overlaid in Fig. 9.2). Also on monthly timescales, the time series of the DS and FBC overflows appear to be anticorrelated: Most of the monthly fluctuations of the FBC overflow, which during 1999 – 2003 have a peak-to-peak amplitude of typically $0.6\,\mathrm{Sv}$, are reflected in the DSO with reverse sign.

A lagged correlation analysis confirmed the apparent anticorrelation (Fig. 9.3): For a delay of 32 days, the FBC and DSO transport time series yielded a maximum negative correlation. Both in the scatter plot (Fig. 9.3 b), and in the actual time series (Fig. 9.3 c), a single very large deviation is caused by the exceptionally low DSOW transport between Oct. 2001 and Jan. 2002. This extreme low-transport event may
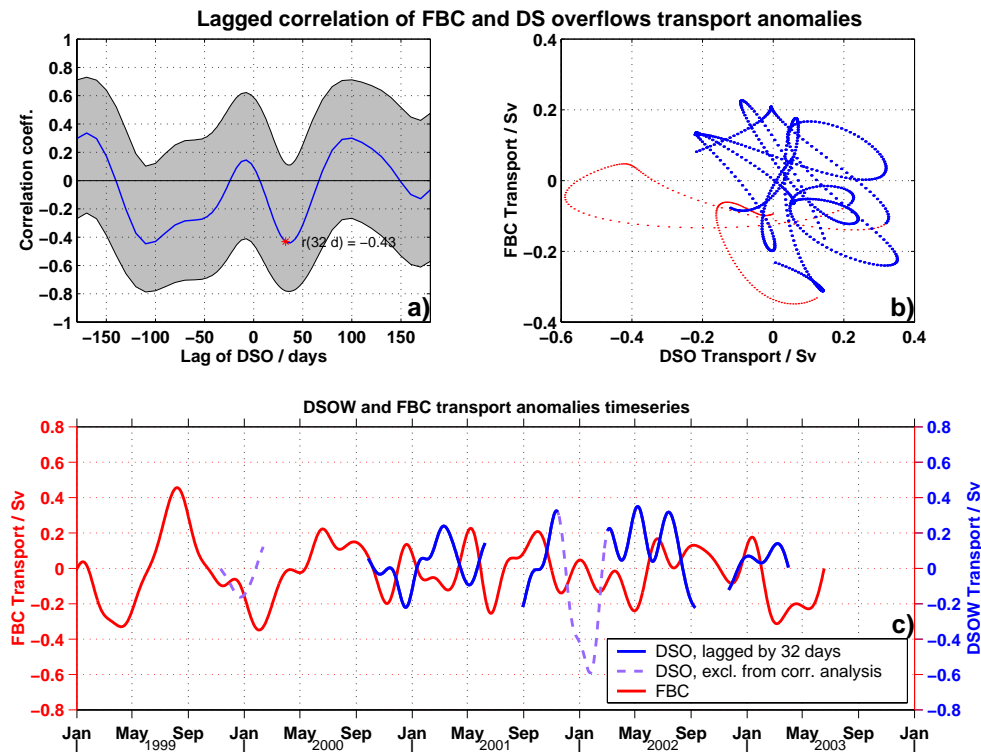
Figure 9.4.: *FBC and DSO correlation analysis, interannual signal removed. Time series of monthly means, smoothed with a 2 months low-pass filter have been used. The 1 year low-passed interannual signal has been removed. Note, that the exceptional low DSO event (14.10.2001 – 28.01.2002) has been excluded from the correlation analysis. The time lag of 32 days has been selected to match the most significant correlation in the previous figure.*

be attributed to an anomalous low wind stress forcing over the Denmark Strait (see section 7.3.5).

Excluding this part of the DSO time series (14.10.2001 – 28.01.2002), raised the correlation maximum from $r = -0.48$ to a value of $r = -0.72$. Its significance is well above the 99 % confidence level[2]. The time lag of 32 days applies both to the complete records and the time series where the low-DSO transport event 2001/02 has been removed.

The results imply, that the fluctuations of the FBC overflow are anticorrelated to DSO variations that occurred 1 month earlier.

While the correlation shown in Fig. 9.3 c is apparently dominated by the interannual reduction of the DSO and the increase of the FBC overflow, an analysis of the transport with the interannual signal removed corroborated the anticorrelation max-

---

[2]Confidence levels have been calculated based on an autocorrelation analysis, which yielded 20 degrees of freedom for the smoothed DSO time series. For details, see EMERY AND THOMSON (2001).

imum for a time lag 32 days (Fig. 9.4 a), although on a weaker level ($r = -0.27$). A linear regression yields a FBC/DSO response ratio of O(1). The impression is complicated by several positive and negative correlation maxima at other time lags. Further investigations are necessary to resolve, whether these represent any physical relations, or are caused by coincidence of the comparatively short time series.

9.2.2. Potential large scale coupling mechanisms of FBC and DS overflows

An integrated analysis of the SFB time series of the Denmark Strait Overflow, its coupling with the Faroe Bank Channel overflow, and of barotropic forcing mechanisms may improve the understanding of the processes, that control the transport of dense water across the Greenland-Scotland Ridge.

On interannual timescales, the recent increase of the FBC overflow, the reduction of the Denmark Strait Overflow, and the reduction of the NAO-related wind stress forcing appear consistent with the predictions of numerical models. However, four years of SFB time series of the DSO are too short to verify a causal relationship, and to exclude pure coincidence or other forcing mechanisms.

An empiric linear transport regression of the lagged time series (Fig. 9.3) yields

$$Q_{\mathrm{DSOW}} = (5.75 \pm 0.2)\,\mathrm{Sv} - (1.05 \pm 0.34) \cdot Q_{\mathrm{FBC}} \qquad (9.3)$$

From 1999 to 2003, the combined DS and FBC overflows yield an almost constant transport of 5.6 Sv (standard deviation $\sigma = 0.19$ Sv). The compensation of DS and FBC overflows is consistent with the numerical experiments of BIASTOCH ET AL. (2003), which revealed, that changes of the wind stress forcing has little influence on the total dense overflows across the GSR, but is relevant for its spatial distribution between the DS and FBC.

Eq. 9.3 does not account for the additional overflows over the IFR and WTR, that have not been measured in 1999 – 2003. The contribution of these overflows is likely of minor importance, though, since observations yielded a mean transport of 1 Sv for the IFR overflows (HANSEN AND ØSTERHUS, 2000). NILSEN ET AL. (2003) showed in a model study, that the flow over the IFR has no clear relation to the wind stress field, and more depends on the actual location of the Northern Center of Action (NCA) of the NAO (HILMER AND JUNG, 2000). In the experiments of KÖSTERS (2004b), the IFR overflows were basically absent, independent from the applied wind stress forcing.

The WTR overflow exhibits a clear negative correlation to the wind stress forcing (model results, KÖSTERS, 2004b). From observations, HANSEN AND ØSTERHUS (2000) estimated a mean WTR overflow transport of 0.2 Sv. This amount is easily accommodated in the error bounds of Eq. 9.3.

Thus, it may be concluded from the observations of a reduced DSO and an increased FBC overflow, that the total dense overflow transport across the GSR may have not significantly changed from 1999 to 2003.

Focusing on shorter timescales (O(months)), the most striking result of the DSO/FBC overflow time series is the correlation maximum of $r = -0.72$ for a time lag of 32 days [3], i.e., the FBC overflow "reacts" to Denmark Strait Overflow variations with a delay of 1 month and in opposite sign.

The question is, whether this time lag represents a physical coupling mechanism of both overflows.

In the following paragraphs, a potential integrated hypothesis for the coupling of FBC and DS overflows shall be evaluated. This hypothesis may be regarded as highly speculative, however, it may provide guidelines for future research to better understand the key processes that steer the dense overflows across the GSR.

According to the circulation scheme suggested by HANSEN AND ØSTERHUS (2000), the FBC overflow is at least partly fed by currents from the Iceland Sea. Hence, changes in the Iceland Sea region might have an impact on the FBC overflow. Preliminary results suggest, that the Faroe Bank Channel overflow is significantly correlated to wind stress anomalies over the Iceland Sea. During the entire period from 1995 – 2003, a maximum correlation of -0.6 is found, which is primarily related to the large seasonal signal in both time series until 2000. In 1999 – 2003, the correlation is reduced to -0.44 for a time lag of 27 days, but the correlation is still much larger than between FBC overflow and large scale wind stress field (not shown). This evidence further suggests, that the Iceland Sea might indeed be a critical region for both dense overflows.

To cover the distance of roughly 1000 km between the Iceland Sea and the FBC in one month, a propagation velocity of 0.36 m/s is required. While this velocity appears too fast for purely advective processes, it roughly corresponds to the phase velocity of internal Kelvin waves, that might travel along the northeastern flank of the IFR.

Moreover, the scales agree with the translation speed of density anomalies on a sloping bottom. According to NOF (1983), isolated cold eddies propagate with

$$c_{\mathrm{Nof}} = \frac{g'\alpha}{f} \tag{9.4}$$

where $g' = g\,\Delta\varrho/\varrho$ represents the reduced gravity, α the bottom slope, and f the Coriolis parameter. With a typical value for $\alpha = 1500\,\mathrm{m}/100\,\mathrm{km}$ (compare IFR topography on Fig. 7.2, page 113) and a density contrast of $0.3\,\mathrm{kg/m^3}$ (obtained as a first-order estimate from CTD-sections off northeast Iceland[4]), one yields $c_{\mathrm{Nof}} = 0.33\,\mathrm{m/s}$.

Both mechanisms might communicate reservoir height changes from the Iceland Sea along the GSR to the FBC. Hence, the Iceland Sea might thus have a key role in controlling the FBC overflow on monthly timescales.

---

[3] As shown above, the "32 days" time lag represents the absolute correlation maximum of $r = -0.72$ for the non-detrended time series. With the interannual signal signal removed, r is reduced to -0.27, but it still represents a local extremum of the correlation.

[4] The Icelandic CTD-sections Langanes NE and E extend northeast or eastward, respectively, from the Langanes peninsula in NE Iceland, covering the proposed pathway from the Iceland Sea along the IFR to the FBC. Sections available at http://www.hafro.is/Sjora → Hydrography.

But how can the *negative* correlation between Denmark Strait and FBC overflows be explained with the proposed FBC control via reservoir height changes?

The Denmark Strait lies adjacent to the Iceland Sea; a direct path of overflow water from the Iceland Sea to the Denmark Strait sill has been observed by Jónsson and Valdimarsson (2004a). Since a substantial part of the Denmark Strait Overflow has to be regarded as barotropic, wind driven flow (Biastoch et al., 2003; Kösters, 2004b), more dense water leaves the Iceland Sea over the Denmark Strait sill than would be the equivalent hydraulically controlled density driven flow alone. A temporary decrease of the Iceland Sea wind stress forcing reduces the barotropic component of the Denmark Strait Overflow, and might thus lead to an accumulation of dense water in the Iceland Sea. Transferred via internal Kelvin or slope waves (Nof, 1983), this reservoir height increase may cause a delayed increase of the FBC overflow, which is much more baroclinic (Hansen, pers. comm.) and hence is likely to be controlled to a higher degree by reservoir height changes than the Denmark Strait overflow.

In the opposite case with strong Iceland Sea wind stress forcing, the increased barotropic flow drains much more dense water from the Iceland Sea through Denmark Strait leading to a lower reservoir.

It remains for future investigations to validate the large scale coupling mechanisms, that control both deep overflows across the Greenland-Scotland Ridge.

9.3.   Summary and conclusions

The integrated analysis of density and wind stress forcing revealed, that the observed interannual reduction of the Denmark Strait Overflow transport from 1999 – 2003 is likely related to an upstream reservoir height decrease and a reduced wind stress forcing.

No clear evidence has been found for a non-delayed overflow response to the NAO-related large wind stress curl, though, but an interannual decrease of the local wind stress over the Iceland Sea and Denmark Strait region is consistent with the observed interannual overflow transport reduction. An empirical linear combination of hydraulically controlled and wind driven flow proved to predict the observed DSOW transport decrease within $\pm 0.1\,\text{Sv}$.

On monthly and seasonal timescales, the overflow response is apparently about 10 times weaker than expected for an instantaneous, linear coupling. In particular, no significant seasonal cycle has been found. Interestingly, seasonal variability has been measured in the FBC overflow from 1995 – 1999/2000, but not during the SFB observation period 1999 – 2003. The reason for the temporary occurrence of a seasonal signal is not yet clear, and the Denmark Strait Overflow time series only cover the later four years.

However, there is some evidence, that the Denmark Strait Overflow and the barotropic currents in Denmark Strait react more sensitive to the wind stress forcing over the Iceland Sea, than to the mean large scale wind stress field over the subpolar North Atlantic.

To obtain an integrated view of both dense overflows across the GSR, the large-scale coupling of the Denmark Strait and FBC overflows has been investigated.

Although these recent results have not yet been finally analyzed, they suggest, that Denmark Strait Overflow and FBC overflow are indeed anticorrelated. During the SFB observation period 1999 – 2003, the interannual reduction of the Denmark Strait Overflow is largely balanced by a corresponding increase of the FBC overflow, which agrees with predictions of numerical models (BIASTOCH ET AL., 2003; KÖSTERS, 2004b). Moreover, the observational evidence points to a coupling of both overflows on monthly timescales. The FBC overflow appears to react with opposite sign on DSO variations with a delay of 1 month. A yet unproven potential explanation for the observed coupling has been proposed.

It remains an issue for future investigations to resolve

- whether the Iceland Sea is in fact a key region that controls both the DS and FBC overflows

- the relative importance of large scale vs. local wind stress forcing over the Iceland Sea for the barotropic transport through Denmark Strait, and in turn for the FBC overflow

It appears promising to further analyze the time series to evaluate the critical processes steering both dense overflows from the Nordic Seas to the North Atlantic that feed the North Atlantic Deep Water.

10. Perspectives

In this study, observations at the Denmark Strait sill and further upstream have been investigated to better understand the mechanisms controlling the variability of the dense overflow. With respect to climate change, long-term monitoring of the overflows from the Nordic Seas to the Atlantic ocean is important to detect changes of the deep branch of the Thermohaline Circulation (THC). In this chapter, future perspectives of overflow observations shall be outlined.

10.1. Remote Sensing

Since the ocean is largely geostrophically balanced, surface currents have a signature in Sea Surface Height (SSH). Radar altimetry by satellites has therefore proven as a useful tool to observe the global ocean surface (as a primer, see CHELTON, 1988).

It is known, that the Denmark Strait Overflow has a clear surface signature due to barotropic eddies (KRAUSS AND KÄSE, 1998; GIRTON, 2001). Moreover, a high correlation between SSH slope anomalies and interface slope has been found by PIES observations (section 6.2.4).

In the subtropical Atlantic, SCHMIDT (2004) compared PIES and altimeter observations of SSH anomalies. On monthly timescales, both in-situ and satellite observations proved to be well correlated. For the Bering Strait, time series of barotropic transport have been successfully derived from altimetry (CHERNIAWSKY ET AL., 2004).

It is tempting to employ remote sensing methods also for the observation of the deep overflows across the Greenland-Scotland Ridge.

Past studies evaluated statistical properties (e.g. eddy kinetic energy) in the pathways of the Denmark Strait and Faroe Bank Channel overflows (HØYER AND QUADFASEL, 2001; GIRTON, 2001). Surface circulation patterns of the Denmark Strait region were investigated by MORTENSEN (1997). Transport time series of the deep overflows, however, have not yet been obtained. Here, the perspectives for Denmark Strait Overflow monitoring by altimetry are examined.

10.1.1. Satellite coverage of the Denmark Strait region

Currently, two different pairs of satellites (ERS1/2 and Topex/Poseidon / Jason-1) are in operation, that measure Sea Level Anomalies (SLA) relative to a reference geoid by radar altimetry.

The Topex/Poseidon(T/P) and Jason-1 (Js-1) satellite tracks cover the global ocean between 66.2°N and 66.2°S with a repeat period of 9.92 days. T/P provides time series of SLA since 1992. In August 2002, T/P has been moved to a different orbit, but its follower Js-1 continues on the original T/P tracks since January 2002. Hence, a consistent data set of SLA exists for the last 12 years.

The Denmark Strait is situated close to the turning latitude of T/P / Js-1. Therefore, the satellite groundtracks are closely spaced, and three satellite tracks (# 219/220, 144 and 41) lie in almost exact east-west direction across the sill area (Fig. 10.1).

In contrast, the ERS1/2 orbits cover higher latitudes to 81.5°N/S, but their tracks cross the Denmark Strait with a wider spacing (not shown). Moreover, the repetition period of 35 days is more than three times longer than for T/P / Js-1.

Thus, T/P / Js-1 are in several respect the most favourable satellites to observe the Denmark Strait:

- Along-track altimetry allows for more accurate, synoptic SLA measurements.

- Three tracks increase the repetition period from 1 to 3 passes in 10 days.

Gridded T/P / Js-1 data sets allow only the assessment of statistical properties of the Denmark Strait Overflow region (e.g. Høyer and Quadfasel, 2001), since the high temporal variability on timescales of a few days (Girton, 2001) leads to aliasing effects between different satellite passes.

To obtain actual current estimates, along-track altimetry is much more accurate: Geoid uncertainties have a spatial scale of O(10000 km), and thus are negligible for distances of O(100 km) as relevant for Denmark Strait. Since T/P / Js-1 pass the deep part of the strait (100 km) in less than 20 s, a synoptic cross section of SLA is obtained every three days.

A major limitation for the use of altimetry is sea ice, since no accurate SLA estimates are obtained in or near to ice-covered areas. The Greenland side of the Denmark Strait is occupied by drifting sea ice, which occasionally also covers the deep part were the dense overflow crosses the sill. The mean temporal coverage of altimeter data therefore decreases from 94 % 60 km east of the sill over 86 % close to ADCP A to 77 % 50 km further west on the Greenland side of the sill, with the largest sea ice extent typically observed in spring (not shown). Hence, at most times the deep part of the Denmark Strait can be assessed by altimetry.

For this study, the 1-second data product of SLA from T/P / Js-1-1 (Benada, 1997; Berwin, 2003b,a) is used[1]. The alongtrack spatial resolution is approx. 6 km, which resolves the Rossby radius (10 − 14 km, Girton, 2001; Dickson et al., 1990).

The RMS noise of each altimeter observation is 1.7 cm (T/P) or 1.6 cm (Js-1). All other errors resulting from geoid uncertainties and atmospheric effects, have much larger scales (O(1000 − 10000 km)), and are irrelevant for along-track altimetry on scales of O(100 km).

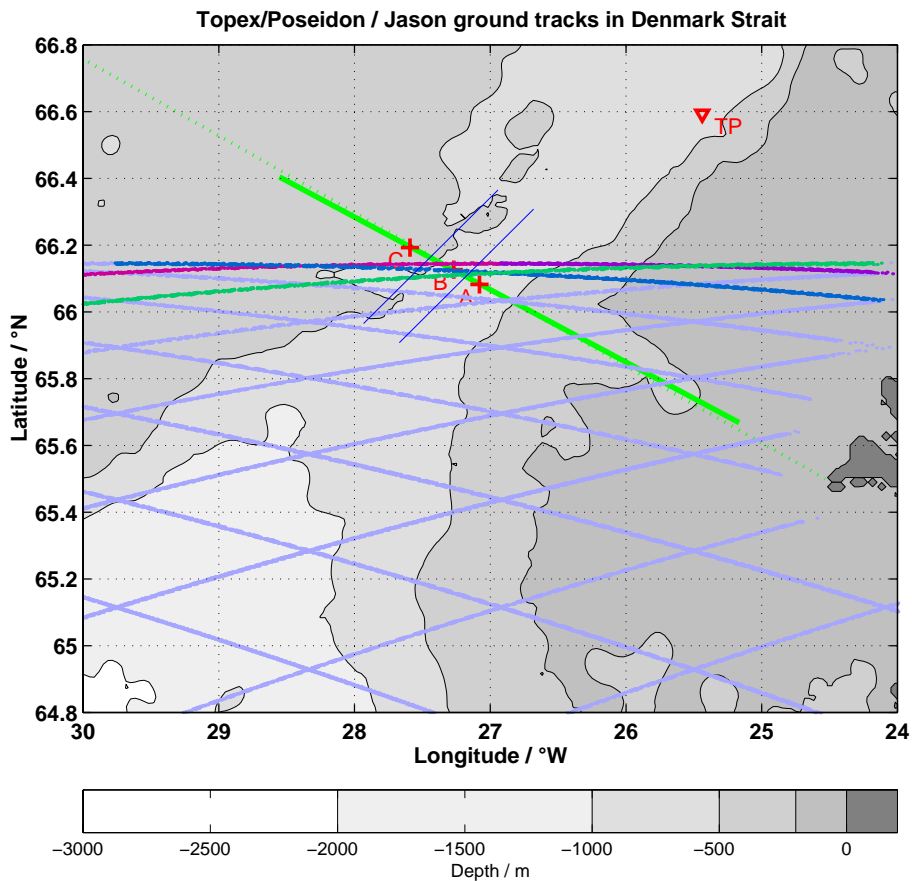[1]Available from http://podaac.jpl.nasa.gov/ .

Figure 10.1.: *Map of Topex/Poseidon / Jason-1 ground tracks in Denmark Strait. Tracks marked in light blue. Red/violet marks track # 219/220, green # 144 and dark blue # 41. Close to coastlines, no altimeter SLA data are available. Additionally, the positions of the ADCP moorings is marked. The two thin blue lines in NE-SW direction sketch the alongstream projection of the altimeter data to the positions of the PIES, which are located at the intersection of these lines with the central CTD section (bold green line).*
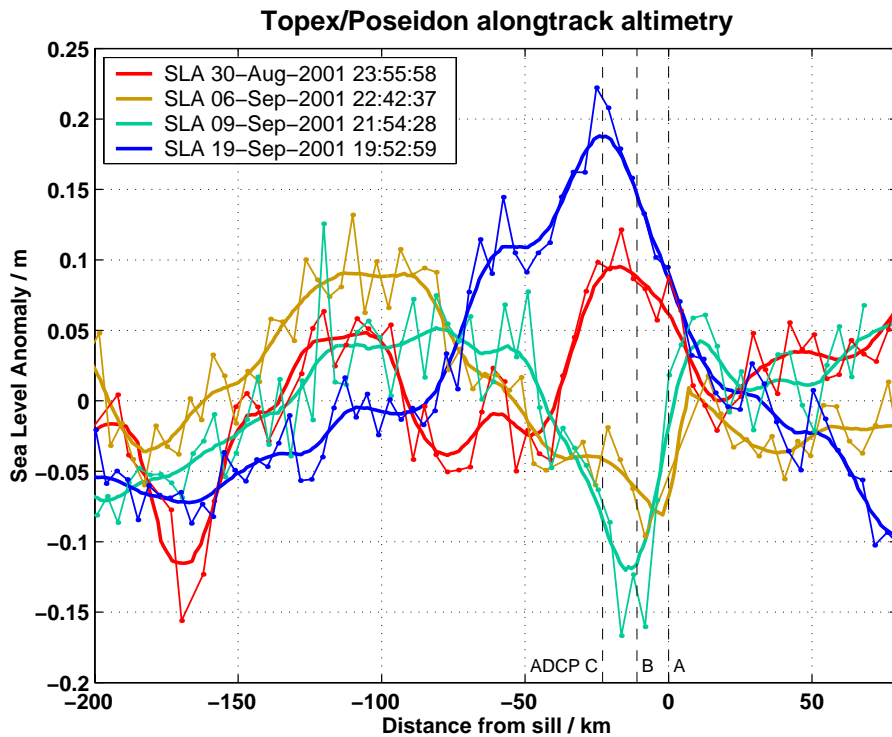
Figure 10.2.: *Alongtrack SSH anomalies, observed by Topex/Poseidon. The figure shows four arbitrarily selected profiles. Each dot on the light lines corresponds to an individual altimeter observation. Bold lines denote profiles smoothed by a 10 km Gaussian filter. The x-axis denotes a projection of the satellite tracks on the standard CTD section across Denmark Strait (see previous figure). Approximate locations of the SFB mooring array marked by dashed lines.*

In the Denmark Strait, SSH anomalies of up to 10 cm / 10 km (Fig. 6.7, page 93) have been observed by PIES. Therefore, it may be expected, that altimetry clearly resolves the physical variability. This is confirmed by Fig. 10.2, that depicts typical alongtrack profiles of SSH anomalies. Typically, SSH anomalies of O(0.2 m) are observed on horizontal scales of 50 − 100 km, while the maximum slope agrees well with the PIES measurements. The largest variability is found between 70 km west and 10 km east of the sill, were most of the dense overflow passes the sill. Based on the alongtrack SSH anomalies, current and transport estimates shall be assessed in the next sections.

Along-track satellite altimetry has been successfully applied to determine the barotropic transport during the ice-free period through Bering Strait (CHERNIAWSKY ET AL., 2004), which is like Denmark Strait located close to the turning latitude of T/P / Js-1.

10.1.2.   Surface currents determined by altimetry

To calculate geostrophic surface currents from SSH anomalies, the alongtrack SSH anomalies of the tracks #219/220, 144 and 41 have been projected onto a common cross-sill axis parallel to the central CTD- and mooring section (Fig. 10.1). A 10 km Gaussian filter was applied to reduce the scatter from individual measurements.

The selected tracks #219/220, 144 and 41 cross the location of ADCP B in a distance of < 5 km (smaller than the Rossby radius of deformation), hence, the altimeter observations may be directly compared with direct ADCP current measurements. The comparison of PIES and ADCP B observations revealed, that the surface currents at ADCP B may be assessed by SSH anomalies obtained at the PIES positions 5 and 17 km northwest of the sill (Fig. 6.7, page 93).

Therefore, the alongtrack SLA data have been subsampled at the PIES positions. The resulting geostrophic surface currents agree reasonably well with the direct observations of ADCP B (Fig. 10.3).

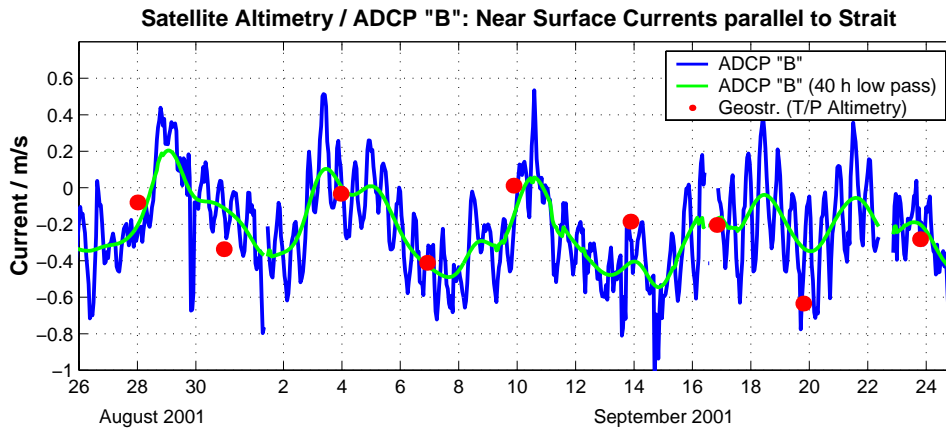**Satellite Altimetry / ADCP "B": Near Surface Currents parallel to Strait**

Figure 10.3.: *Near surface currents at ADCP B: Direct observations and satellite altimetry. The blue and green lines show unfiltered and 40 hours low-passed near-surface current observed by ADCP B. The unfiltered data clearly exhibit semidiurnal tides and the dominating 2 – 10 days eddy timescale variability. Red dots indicate currents geostrophically inferred from T/P alongtrack altimetry. Absolute values were derived by a least-square fit of the current anomalies to the absolute ADCP measured currents.*

The unfiltered time series are significantly correlated ($r = 0.49$, exceeding the 99 % confidence level). A constant velocity correction of 0.28 m/s had to be applied to the altimeter-derived currents, since the altimeter obtains SSH anomalies relative to a (possibly sloping) mean sea surface[2].

On longer timescales, aliasing effects lead to a weaker correlation, since the altimeter data obviously include much of the short-term variability (Fig. 10.3). Averages over

---

[2]The correction was obtained by a least-square fit of the satellite estimates to the direct observations of ADCP B.

several satellite passes (three passes in 9.92 days, 2.966, 2.966 and 3.985 days apart) are thus likely to be aliased by by e.g. tides. The semidiurnal M_2 tide that is clearly evident in the ADCP records (Fig. 10.3) has a period of 12 h 50 min. This is close to the inertial period $T = 2\pi/f = 13\,\mathrm{h}\,6\,\mathrm{min}$ at 66 °N. Consequently, geostrophic adjustment might be important even on tidal timescales.

On monthly timescales, tidal aliasing is less significant, and the 90 day low-passed surface current time series are largely consistent with direct ADCP observations (Fig. 10.4 a).

10.1.3. DSOW transport determined by altimetry

The high correlation of SSH slope and interface slope anomalies found in the PIES observations (section 6.2.4) suggests a close relation between SSH slope detected by satellite altimetry and actual DSOW transport.

However, due to aliasing of short-term variability, the correlation between satellite derived SSH anomalies and DSOW transport observed by ADCPs is not larger than 0.35 for 40 hour low-passed data. Hence, the primarily eddy-related anticorrelation of SSH slope and interface depth (section 6.2.4) is not well captured by altimetry. Therefore, monthly to annual timescales shall be investigated here.

It may be expected, that the satellite "sees" the barotropic component of the overflow, which is associated with a cross-strait SSH slope. The SFB observations suggest, that $\approx 1.45\,\mathrm{Sv}$ (1999 – 2003 average) may be regarded as barotropic, wind driven part of the overflow. To assess the barotropic part by altimetry, the SSH slope obtained over the spatial extent of the SFB array has been converted by an empiric linear relation to transport fluctuations.

The resulting time series are shown in Fig. 10.4 b. The altimetry-inferred transport estimates agree moderately well with the direct ADCP observations. However, it has to be taken into account, that the dense overflow is additionally affected by reservoir height changes. On interannual timescales, the altimetry-inferred transports decrease significantly from 1999 to 2003, which agrees with reduced wind stress forcing (chapter 7). A clear seasonal signal is not evident, but the large "peaks" in end-1999 and begin of 2002 suggest a close correlation with the NAO index (Fig. 7.3, 114).

The addition of the altimetry-inferred transports and the hydraulic estimates calculated from reservoir height at Kögur 5 (Fig, 10.4, green line) agrees within ± 0.5 Sv with the observed DSOW transport. Hence, the combination of alongtrack altimetry and upstream hydrographic data might be employed to obtain long-term Denmark Strait Overflow transport time series.

Concluding, in-situ hydrographic measurements are certainly necessary to assess the upstream reservoir height and the water mass properties of the dense overflow, whereas the barotropic component may possibly be assessed by remote sensing methods. It remains to future research to prove the performance of altimetry-based overflow transport monitoring.
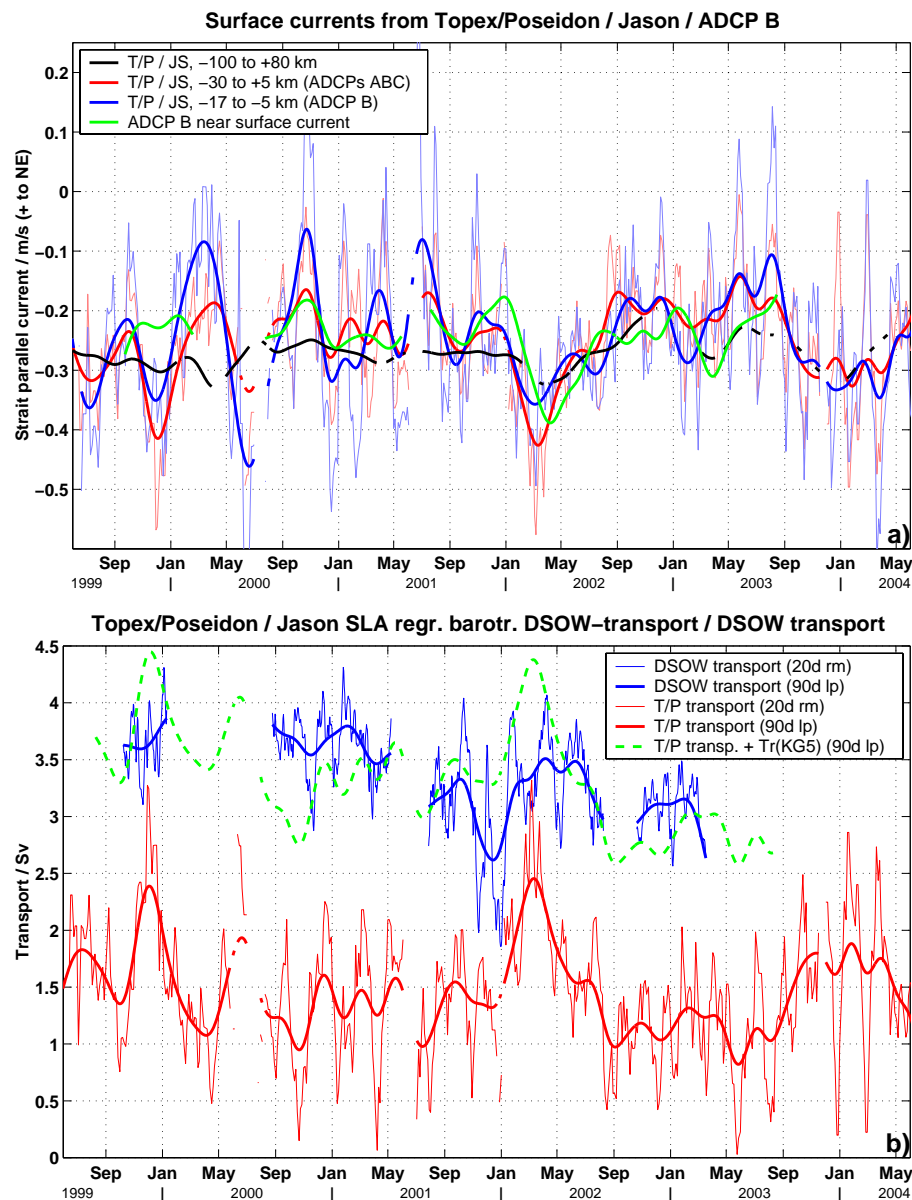
Figure 10.4.: *Surface currents and DSOW transport inferred from altimetry. Panel a: Geostrophic surface currents, inferred from alongtrack altimetry. The black line corresponds to the mean velocity from 100 km west of the sill to 80 km east of the sill. The red line marks mean current over the entire ADCP-array. The blue line denotes the estimate for the ADCP B location, and may be compared with the direct observations of ADCP B (green line). Thin lines denote 20 days running means, heavy lines represent 90 days low-passed time series. Panel b: Blue lines mark 20 days running averages and 90 days low-pass of actual DSOW transport, respectively. In red, an empirical regression of the altimeter derived SSH anomalies on the barotropic part of the overflow transport is shown. The dashed green line depicts the sum of barotropic transport (red line) and the hydraulically controlled flow, inferred from reservoir height at Kögur 5 (chapter 9).*

10.2. Outlook

The Meridional Overturning Circulation (MOC) has a fundamental role for ocean heat transport and climate (BROECKER, 1997; IPCC, 2001). There is growing evidence, that the MOC, and in particular the formation of dense water in the North Atlantic, may substantially decrease under global warming conditions (IPCC, 2001). However, the sensitivity of the MOC to greenhouse gas forcing differs greatly between different numerical models (IPCC, 2001).

The dense overflows from the Nordic Seas to the Atlantic are a major contribution to the deep branch of the AMOC. A reduction of the dense water formation in the Nordic Seas will therefore have immediate effects on the dense overflows. The sills of the Greenland-Scotland Ridge, where the exchanges between Nordic Seas and Atlantic Ocean are focused by topography, are hence the most appropriate locations to monitor the Thermohaline Circulation in the Nordic Seas / northern North Atlantic with respect to climate change.

In contrast to previous studies, which regarded the Denmark Strait Overflow as stable on longer timescales (DICKSON AND BROWN, 1994), the continuous SFB observations from 1999 – 2003 revealed significant interannual variability. Although the time series are too short to resolve decadal timescales and climate change processes, the results of this study suggest, that the overflow in fact is sensitive to forcing changes.

Following, the main implications of this study, and future perspectives for long-term monitoring shall be outlined.

Mechanisms controlling the dense overflows across the GSR
The integrated investigation of the SFB Denmark Strait Overflow time series, in combination with Faroe Bank Channel (FBC) overflow and wind stress observations yielded new insight into the governing processes that control both dense overflows.

It remains to future research to further evaluate

- whether the Iceland Sea is indeed a key region controlling both Denmark Strait and FBC overflows.

- the upstream pathways of both overflows. The Denmark Strait Overflow has been tracked back to the Kolbeinsey Ridge (JÓNSSON AND VALDIMARSSON, 2004b); analysis of hydrographic data may help to determine, whether it is fed by a branch of the East Greenland Current or from further east.

- numerical models with realistic forcing and high resolution, e.g. the MITgc-mUV model at IfM Hamburg, and the 1/12° FLAME model at IFM-GEOMAR Kiel, to improve the understanding of upstream circulation and the overflow sensitivity to forcing changes.

- the importance of local vs. large scale wind stress forcing and the North Atlantic Oscillation for both the FBC and Denmark Strait Overflows.

- the relative contributions of the Iceland Sea, the East Greenland Current and upstream entrainment of warm Atlantic Water into the Denmark Strait Overflow.

- Influence of T/S changes and dense water formation rates in different regions, e.g. Fram Strait, Greenland Sea and Iceland Sea, on the Denmark Strait Overflow, and hence the densest component of the NADW.

- the relevant coupling mechanisms, that determine the apparent anticorrelation of the Denmark Strait and FBC on monthly and interannual timescales.

- whether the combination of satellite altimetry, wind stress estimates and upstream reservoir height observations can be employed to obtain long term time series of the Denmark Strait Overflow.

Operational perspectives

As a first step to longer continuous time series at the sills, the Faroe Bank Channel Overflow will be observed continuously by an ADCP maintained by Fiskiranns oknarstovan, Tórshavn. Since the FBC is not wider than one Rossby radius, one ADCP has proven as sufficient for realistic transport estimates.

In the Denmark Strait, two moorings of the SFB array, that have not been recovered due to instrumental failure, are still located on the bottom. There are some chances, however, that the shielded ADCP C, and a shielded PIES, both deployed in 2002, can be salvaged in 2005 by a ROV[3] mission. This would be a major improvement for the SFB data set. If the salvage operation is successful, one complete year of the originally planned optimized 3-ADCP-array would be available, allowing DSOW transport estimates with a significantly improved accuracy. Further, the recovery of the shielded PIES would allow the assessment of integrating geostrophic estimates, that cover most of the dense overflow.

During the next couple of years, at least one ADCP will be deployed in the framework of the ASOF-West project. The large spatial variability of the Denmark Strait Overflow implies, that one instrument is not sufficient to capture the DSOW transport. However, this study suggests, that a single ADCP may be used as a reference for barotropic velocities obtained from wind stress estimates or satellite altimetry.

The SFB array has observed large short-term temperature variability. Since salinity was not measured by the deployed instruments, it is difficult to resolve, to which degree the warmer parts of the overflow can be attributed to water masses advected by the East Greenland Current or to entrainment of Atlantic Water. To better understand the highly variable composition of the dense overflow, it is suggested, to deploy temperature *and* conductivity sensors at the sill.

The density driven part may be assessed by upstream reservoir height estimates. Repeat stations, including the Kögur, Siglunes and other upstream sections, are part of the regular hydrographic surveys of Hafrannsóknastofnunin Reykjavík.

---

[3]ROV: Remotely Operated Vehicle.

Global warming has likely a substantial impact on the Meridional Overturning Circulation. There is evidence, that the inflow of warm, saline water of the North Atlantic Current into the Nordic Seas, the outflow of cold, fresh waters of Arctic origin, and the dense overflows are sensitive to climate change processes.

An integrated system to observe both surface currents and deep overflows across the Greenland-Scotland Ridge will help to better understand the climate system, and improve predictions of future climate change.

11. Conclusions

The importance of the deep overflows across the Greenland-Scotland Ridge for the formation of North Atlantic Deep Water and hence the Thermohaline Circulation has made the Denmark Strait Overflow to a subject of major research efforts.

The descent of the plume downstream of the sill and the strong near-bottom current velocities may be understood in the light of a hydraulically controlled, density driven flow. The large short-term variability, eddy activity and entrainment processes have been investigated by numerous hydrographic surveys and mooring deployments, whereas the critical dynamics at the sill and further upstream have been less well known.

Based on four years of continuous overflow time series in combination with hydrographic observations at the sill and further upstream, the processes, that actually determine the volume transport of the Denmark Strait Overflow, have been investigated in this study. The consistent data set from 1999 – 2003 allowed for the first time to evaluate the control mechanisms of the Denmark Strait Overflow on interannual timescales.

Previously, the overflow has been regarded as a primarily density driven flow, which is stable on timescales longer than a few weeks. This view is modified by the present study:

- For the first time, interannual variability of the Denmark Strait overflow has been observed. The transport of DSOW decreased from $(3.68 \pm 0.1)\,\mathrm{Sv}$ in 1999 to $(3.07 \pm 0.1)\,\mathrm{Sv}$ in 2003.

- The observations suggest, that the overflow comprises both a hydraulically controlled and a wind driven component. This agrees with recent modelling results of BIASTOCH ET AL. (2003) and KÖSTERS (2004b).

- About $50\,\%$ of the interannual transport reduction may be related to an upstream reservoir height decrease of $50\,\mathrm{m}$. The remaining $0.3\,\mathrm{Sv}$ transport decrease is consistent with a reduced NAO-related wind stress forcing over the North Atlantic. The fast, non-delayed response to wind stress changes on monthly to seasonal timescales is weaker than expected, although there is evidence, that the Iceland Sea region plays an important role for short-term variability.

- The direct path from the Iceland Sea to the Denmark Strait suggested by JÓNS-SON AND VALDIMARSSON (2004a) has been confirmed by the SFB observations.

The larger temperature variability at the sill suggests, however, that either entrainment processes in the sill entrance region, or advection of LAIW by the East Greenland Current also play role in determining the water mass properties of the overflow.

- A significant anticorrelation has been found between Denmark Strait and Faroe Bank Channel overflow. A time lag of one month suggests, that on monthly timescales the FBC overflow reacts on reservoir height changes in the Iceland Sea. There is evidence, that the Iceland Sea region may be considered as a key region controlling both dense overflows from the Nordic Seas to the Atlantic ocean.

A. Abbreviations

AAW Arctic Atlantic Water. Cf. page 30.

ADCP Acoustic Doppler Current Profiler: Instrument for acoustical measurement of current velocities; utilizes Doppler frequency shift of a sound pulse reflected from suspended matter in the water. Cf. page 39.

ADCP A Arbitrary abbreviation for the Icelandic Narrowband-ADCP at the mooring location DS-1 at the deepest part of the sill.

ADCP B Arbitrary abbreviation for the IFM-GEOMAR Longranger-ADCP at the mooring location V401 and V425 11 km north-west of the deepest part of the sill.

ADCP C Arbitrary abbreviation for the IFM-GEOMAR Longranger-ADCP mounted in a trawl resistant shield at the mooring location V423 23 km north-west of the deepest part of the sill.

AIW Arctic Intermediate Water. Cf. page 29.

AMOC Atlantic Meridional Overturning Circulation. Cf. page 17.

AR Autorelease: URI-PIES include a timed release after completion of their measurement schedule.

ASOF Arctic/Subarctic Ocean Fluxes project.

AW Atlantic Water. Cf. page 30.

CEFAS Centre for Environment Fisheries and Aquaculture Science, Lowestoft, UK.

CTD Probe lowered from a vessel to measure a vertical profile of **C**onductivity–**T**emperature–**D**epth (actually pressure, not depth). Salinity, density and sound velocity can be calculated of these quantities.

DS Denmark Strait.

DSO Denmark Strait Overflow. Cf. page 26.

DSOW Denmark Strait Overflow Water. Cf. page 29.

EGC East Greenland Current. Cf. page 26.

EKE Eddy kinetic energy. Cf. page 85.

ERS European Remote-Sensing Satellites that provide altimetry data. ERS-1 and ERS-2 have more polar orbits than → T/P.

ETOPO 5 Earth TOPOgraphy – 5 Minute: Worldwide topography data set with 5' grid spacing. Available from
http://www.ngdc.noaa.gov/mgg/global/relief/ETOPO5/TOPO/ETOPO5/ .

FBC Faroe Bank Channel. Cf. page 142.

FLAME Family of Linked Atlantic Model Experiments, comprises several models of the Atlantic with different resolution at IFM-GEOMAR, Kiel.

GEBCO '97 GEneral Bathymetric Chart of the Ocean (1997): Topography of the ocean floor with isobaths.

GSA Great Salinity Anomaly. Cf. page 71.

GSR Greenland-Scotland Ridge.

IAIW Iceland Sea Arctic Intermediate Water. Cf. page 30.

IC Irminger Current. Cf. page 26.

IES Inverted Echo Sounder. Measures acoustical travel time of a sound pulse from instrument to sea surface and back. Cf. page 43.

IfM Institut für Meereskunde an der Universität Hamburg.

IfM Institut für Meereskunde an der Universität Kiel.

IFM-GEOMAR Leibniz-Institut für Meereswissenschaften an der Universität Kiel.

IFR Iceland-Faroe Ridge.

IPCC Intergovernmental Panel on Climate Change.

IS7 Icelandic mooring site located on the Icelandic shelf edge approx. 200 km upstream of the sill. Cf. page 27.

ISOW Iceland Scotland Overflow Water. Cf. page 20.

Js-1 Jason-1; Satellite with RADAR altimetry for SLA observation. Cf. page 151.

KG5 Icelandic hydrographic station Kögur 5, located on the Icelandic shelf edge approx. 200 km upstream of the sill. Cf. page 27.

LADCP Lowered Acoustic Doppler Current Profiler. Attached to a rosette / CTD, it measures a current profile of the whole water column. Ship drift and lateral movements of the CTD probe have to be corrected for by optimum fitting of the ship's navigation data, subsequent current profiles, and bottom track data of the LADCP to obtain actual current velocities.

LAIW Lower Arctic Intermediate Water. Cf. page 29.

LR-ADCP Longranger-ADCP. Due to the low frequency of 75 kHz, its range exceeds 600 m.

MITgcmUV Massachusetts Institute of Technology general circulation model Ultrahigh Versatility. Cf. page 134.

MONA **M**onitoring the **O**verflow to the **N**orth **A**tlantic. Project established in 1975 to observe all dense overflows across the → GSR. Current meter moorings MONA5 and 6 were deployed for one year 200 km downstream of the Denmark Strait sill. The location was chosen to avoid trawling hazards. See Fig. 2.1, page 27.

MRI Marine Research Institute, i.e. Hafrannsóknastofnunin Reykjavík, Iceland.

NADW North Atlantic Deep Water. Cf. page 26.

NAO North Atlantic Oscillation: Normalized Sea Level Pressure anomaly between Iceland Low and Azores High. Time series typically defined by pressure difference between Stykkishólmur, Iceland, and Lisbõa or Azores, Portugal. Cf. page 111.

NB NB-ADCP: Narrowband-ADCP. 150 kHz-ADCP with a range of max. 500 m.

NCA Northern Center of Action of the NAO. See Hilmer and Jung (2000).

NCEP/NCAR National Centers of Environment Prediction / National Center for Atmospheric Research. Runs reanalysis models that assimilate all available observation data to provide gridded data sets of wind stress etc. from 1948 to present.

NIIC North Iceland Irminger Current. Cf. page 26.

OGCM Ocean General Circulation Model.

PIES Pressure sensor / Inverted Echo Sounder. Measures bottom pressure and acoustical travel time of a sound pulse from instrument to sea surface and back. By assumption of a two-layer model, sea surface and interface height can be calculated. Cf. page 43.

PIW Polar Intermediate Water. Cf. page 29.

PSD Power Spectral Density. Cf. page 64.

psu practical salinity unit, defined by conductivity, temperature and pressure (Fofonoff and Millard, 1983).

PSW   Polar Surface Water. Cf. page 30.

PV   Potential Vorticity. Without friction, this property is conserved along streamlines: $q = (\partial v/\partial x + f)/H_2 = const$. Cf. page 89.

R   Internal Rossby radius $R = \sqrt{g'H_2}/f$. Measure for the length scales influenced by Earth's rotation.

RAW   Returned Atlantic Water. Cf. page 29.

RMS   Root Mean Square. RMS error corresponds to standard deviation.

ROV   Remotely Operated Vehicle. Underwater robot, connected by power and control cable with the vessel. In this project, ROV "Cherokee" of the University of Bremen is scheduled for salvage operations of the shielded ADCP C V423-03 and the shielded PIES V421-03 in 2004 and 2005.

R/V   Research Vessel.

SFB 460   Sonderforschungsbereich 460 "Dynamik Thermohaliner Zirkulationsschwankungen" at IFM-GEOMAR Kiel.

SI8   Icelandic hydrographic station Siglunes 8, located on the western edge of Kolbeinsey Ridge. Cf. page 27.

SLA   Sea Level Anomaly.

SLP   Sea Level Pressure.

SPEM   Sigma-Coordinate Primitive Equation Model: Primitive-Equation model with topography-following grid. Cf. page 50.

SSH   Sea Surface Height.

SST   Sea Surface Temperature.

Sv   Sverdrup: $1\,\mathrm{Sv} = 10^6\,\mathrm{m}^3/\mathrm{s}$.

THC   Thermohaline Circulation. Cf. page 17.

TK   Thermistorkette: Cable, several hundreds meters in length, equipped with temperature sensors at regular intervals and a single data recorder. Cf. page 99.

TP   Mooring equipped with MiniTPs. Instruments developed at IfM Kiel to measure temperature and (optionally) pressure. Cf. page 101.

T/P   Topex/Poseidon: Satellite with RADAR altimetry for SLA observation. Cf. page 151.

TP A1   Teilprojekt A1 "Overflow und Vermischungsprozesse in der Irmingersee" at SFB 460.

UAIW   Upper Arctic Intermediate Water. Cf. page 29.

uPDW   upper Polar Deep Water. Cf. page 31.

URI   University of Rhode Island. Manufacturer of the PIES deployed in this project.

VEINS   Variability of Exchanges in the Northern Seas.

vmADCP   Vessel Mounted ADCP: Downward looking ADCP, mounted at the bottom of a vessel. Allows current profile measurement of the upper approx. 400 m from the moving vessel.

vmLRADCP   Vessel Mounted Longranger ADCP: 75 kHz ADCP tested on Poseidon P262 as vmADCP to obtain profiles to > 600 m depth.

WD   Watchdog: Argos transmitter attached to floatation of a moored instrument. If the mooring surfaces, it can be tracked via the Argos satellite system.

XCTD   eXpendable Conductivity-Temperature-Depth: Expendable probe that provides a vertical profile of temperature and electrical conductivity. It can be operated from a moving vessel. Depth (i.e. pressure) is not actually measured, but computed from the known falling rate of the probe.

XCP   eXpendable Current Profiler: eXpendable probe that provides a vertical profile of current velocity relative to an unknown constant. It uses the principles of geomagnetic induction (SANFORD ET AL., 1978, 1993). Can be operated from a moving vessel.

Bibliography

AAGARD, K. and S.-A. MALMBERG, 1978: Low frequency characteristics of the Denmark Strait Overflow. *ICES*, **CM 1978/C:47**.

ARMI, L., 1986: The hydraulics of two flowing layers with different densities. *J. Fluid. Mech.*, **163**, 27–58.

BACON, S., 1998: Decadal variability in the outflow from the Nordic Seas to the deep Atlantic Ocean. *Nature*, **394**, 871–874.

BENADA, J. R., 1997: *PO.DAAC Merged GDR (TOPEX/POSEIDON) Generation B User's Handbook*. Version 2.0.

BERWIN, R., 2003a: *Jason-1 Sea Surface Height Anomaly Product User's Reference Manual*. Version 2.

BERWIN, R., 2003b: *TOPEX/POSEIDON Sea Surface Height Anomaly Product, User's Reference Manual*. Version 2.

BIASTOCH, A., R. H. KÄSE and D. B. STAMMER, 2003: The Sensitivity of the Greenland-Scotland Overflow to Forcing Changes. *J. Phys. Oceanogr.*, **33**, 2307–2319.

BJERKNES, V., 1964: Atlantic Air-Sea Interactions. *Adv. In Geophys.*, **10**, 1–82.

BLINDHEIM, J., V. BOROKOV, B. HANSEN, S.-A. MALMBERG, W. R. TURRELL and S. ØSTERHUS, 2000: Upper layer cooling and freshening in the Norwegian Sea in relation to atmospheric forcing. *Deep-Sea Research Part I*, **47**, 655–680.

BÖNING, C. W., F. O. BRYAN, W. R. HOLLAND and R. DÖSCHER, 1996: Deep-water formation and meridional overturning in a high-resolution model of the North Atlantic. *J. Phys. Oceanogr.*, **26**, 1142–1164.

BORENÄS, K. and P. LUNDBERG, 1986: Rotating hydraulics of flow in a parabolic channel. *J. Fluid Mech.*, **167**, 309–326.

BORENÄS, K. M. and A. NIKOLOPOULOS, 2000: Theoretical calculations based on real topography o the maximum deep-water low through the Jungfern Passage. *J. Marine Res.*, **58**, 709–719.

BROECKER, W. S., 1997: Thermohaline circulation, the Achilles heel of our climate system: will man-made CO_2 upset the current balance? *Science*, **278**, 1582–1588.

BROECKER, W. S., D. M. PETEET and D. RIND, 1985: Does the ocean-atmosphere system have more than one stable mode of operation? *Nature*, **315**, 21–26.

BROERSEN, P. M. T., 2000a: Autoregressive Model Orders for Durbin's MA and ARMA estimators. *IEEE Transactions on Signal Processing*, **48** (8), 2454–2457.

BROERSEN, P. M. T., 2000b: Finite Sample Criteria for Autoregressive Order Selection. *IEEE Trans. on Signal Processing*, **48** (12), 3550–3558.

BROERSEN, P. M. T., 2002: Automatic Spectral Analysis with Time Series Models. *IEEE Transactions on Instrumentation and Measurement*, **51** (2), 211–216.

BRONSTEIN, I., K. SEMENDJAJEW, G.MUSIOL and H. MÜHLIG, 1995: *Taschenbuch der Mathematik*. Verlag Harri Deutsch, Thun, Frankfurt am Main, 2nd Edition.

BRYDEN, H. L. and S. IMAWAKI, 2001: *Ocean Circulation and Climate*, Academic Press, San Diego, Volume 77 of *International Geophysics Series*, Chapter Ocean heat transport. Ed. by G. Siedler, J. Church and J. Gould.

CHELTON, D. B., 1988: WOCE/NASA Altimeter Algorithm Workshop. U.S. WOCE Technical Report No. 2, U.S. Planning Office for WOCE, College Station, TX, 70 pp.

CHEN, C. T. and F. J. MILLERO, 1977: Speed of sound in seawater at high pressures. *J. Acoust. Soc. Am.*, **62** (5), 1129–1135.

CHERNIAWSKY, J., W. CRAWFORD, E. CARMACK and O. NIKITIN, 2004: Complex relationship between winds and Bering Strait transports derived from satellite altimetry. In: *Geophysical Research Abstracts*, European Geosciences Union 1st General Assembly, Nice, 2004, Volume 6, 04555, 2004 SRef-ID: 1607-7962/gra/EGU04-A-04555.

COOPER, L. H. N., 1955: Deep water movements in the North Atlantic as a link between climatic changes around Iceland and biological productivity of the English Channel and Celtic Sea. *J. Mar. Res.*, **14** (4), 347–362.

CURRY, R., R. R. DICKSON and I. YASHAYAEV, 2003: A Change in the Freshwater Balance of the Atlantic Ocean over the past four Decades. *Nature*, **426**, 826–829.

CURRY, R. and M. S. MCCARTNEY, 2001: Ocean gyre circulation changes associated with the North Atlantic Oscillation. *J. Phys. Oceanogr.*, **31**, 3374–3400.

DALZIEL, S. B., 1990: *The physical oceanography of sea straits*, Kluwer Academic Publishers, Chapter Rotating two-layer sill flows, 309–326. Ed. by L. J. Pratt.

DEFANT, A., 1931: Berichte über die ozeanographischen Untersuchungen des Vermessungsschiffes "Meteor" in der Dänemarkstraße und in der Irmingersee. *Sitz.-Ber. Preuß. Akad. Wiss.*, **Phys.-Math. Kl. 16,19**.

DICKSON, B., J. MEINCKE, I. VASSIE, J. JUNGCLAUS and S. ØSTERHUS, 1999: Possible predictability in overflow from the Denmark Strait. *Nature*, **397**, 243–246.

DICKSON, B., I. YASHAYAEV, J. MEINCKE, B. TURRELL, S. DYE and J. HOLFORT, 2002: Rapid freshening of the deep North Atlantic Ocean over the past four decades. *Nature*, **416**, 832–837.

DICKSON, R. R. and J. BROWN, 1994: The production of North Atlantic Deep Water: Sources, rates and pathways. *J. Geophys. Res.*, **99**, 12,319–12,341.

DICKSON, R. R., E. M. GMITROWICZ and A. J. WATSON, 1990: Deep water renewal in the northern Atlantic. *Nature*, **344**, 848–850.

DICKSON, R. R., J. LAZIER, J. MEINCKE, P. RHINES and J. SWIFT, 1996: Long-term convective coordinated changes in the convective activity of the North Atlantic. *Progr. Oceanogr.*, **38**, 241–295.

DICKSON, R. R., J. MEINCKE and A. J. LEE, 1988: The "Great Salinity Anomaly" in the northern North Atlantic 1968 – 1982. *Progr. Oceanogr.*, **20**, 103–151.

DÖSCHER, R. and R. REDLER, 1997: The Relative Importance of Northern Overflow and Subpolar Deep Convection for the North Atlantic Thermohaline Circulation. *J. Phys. Oceanogr.*, **27** (9), 1894–1902.

DYE, S. R., R. R. DICKSON, J. MEINCKE, B. RUDELS and P. MAELKKI, 2004: Complete flow statistics from the Denmark Strait Overflow array. Geophysical Research Abstracts, Vol. 6, 07371, 2004, SRef-ID: 1607-7962/gra/EGU04-A-07371, Oral presentation at European Geosciences Union 1st General Assembly, Nice, 2004.

EDEN, C. and J. WILLEBRAND, 2001: Mechanism of interannual to decadal variability of the North Atlantic circulation. *J. Climate*, **14** (10), 2266–2280.

EGBERT, G. D. and S. Y. EROFEEVA, 2002: Efficient inverse modeling of barotropic ocean tides. *J. Atmos. Ocean. Tech.*, **19** (2), 183–204.

EMERY, W. J. and R. E. THOMSON, 2001: *Data Analysis Methods in Physical Oceanography.* Elsevier Science Pub Co, Amsterdam, 2nd Edition, 658 pp.

FARMER, D. M. and L. ARMI, 1986: Maximal two-layer exchange over a sill and through the combination of a sill and contraction with barotropic flow. *J. Fluid Mech.*, **164**, 53–76.

FOFONOFF, N. P., 1985: Physical properties of seawater. *J. Geophys. Res.*, **90**, 3332–3342.

FOFONOFF, N. P. and R. C. MILLARD, 1983: *Algorithms for computation of fundamental properties of seawater.* UNESCO Technical papers in marine science, No. **44**, 1–53.

FRISTEDT, T., R. HIETALA and P. LUNDBERG, 1999: Stability properties of a barotropic surface-water jet observed in the Denmark Strait. *Tellus*, **51A**, 979–989.

GANACHAUD, A. and C. WUNSCH, 2000: Improved estimates of global ocean circulation, heat transport and mixing from hydrographic data. *Nature*, **408**, 453–456.

GARRETT, C., 2002: Frictional processes in straits. In: *The 2nd Meeting on the physical Oceanography of Sea Straits, Villefranche, 15th – 19th April 2002*, D. Smeed and L. Pratt, Eds., Southampton Oceanography Centre, 17–24.

GERDES, R. and C. KÖBERLE, 1995: On the influence of DSOW in a numerical model of the North Atlantic general circulation. *J. Phys. Oceanogr.*, **25**, 2624–2642.

GILL, A. E., 1977: The hydraulics of rotating-channel flow. *J. Fluid Mech.*, **80**, 641–671.

GIRTON, J. B., 2001: Dynamics of Transport and Variability in the Denmark Strait Overflow. PhD Thesis, University of Washington, Seattle, WA.

GIRTON, J. B. and T. B. SANFORD, 1999: Velocity profile measurements of the Denmark Strait Overflow. *Int. WOCE Newslett.*, **37**, 28–30.

GIRTON, J. B. and T. B. SANFORD, 2003: Descent and modification of the overflow plume in the Denmark Strait. *J. Phys. Oceanogr.*, **33** (7), 1351–1364.

GIRTON, J. B., T. B. SANFORD and R. H. KÄSE, 2001: Synoptic sections of the Denmark Strait Overflow. *Geophys. Res. Lett.*, **28** (8), 1619–1622.

HANSEN, B. and S. ØSTERHUS, 2000: North Atlantic-Nordic Seas exchanges. *Progr. Oceanogr.*, **45**, 109–208.

HANSEN, B., S. ØSTERHUS and D. QUADFASEL, 2004a: Changes in the Faroe Bank Channel Overflow. In: *Berknes Centenary 2004 Climate Change in High Latitudes*, Bergen, Poster Presentation S1-21.

HANSEN, B., S. ØSTERHUS, D. QUADFASEL and W. TURRELL, 2004b: Already the Day after Tomorrow? *Science*, **305**, 953–954, DOI: 10.1126/science.1100085.

HANSEN, B., W. R. TURRELL and S. ØSTERHUS, 2001: Decreasing overflow from the Nordic seas into the Atlantic Ocean through the Faroe Bank channel since 1950. *Nature*, **411**, 927–930, doi:10.1038/35082034.

HARVEY, J. G. and A. N. SHOR, 1961: Overflow of cold deep water across the Iceland-Greenland Ridge. *Nature*, **189**, 911–913.

HELFRICH, K. R. and L. J. PRATT, 2003: Rotating hydraulics and upstream basin circulation. *J. Phys. Oceanogr.*, **33**, 1651–1663.

HELLAND-HANSEN, B. and F. NANSEN, 1909: The Norwegian Sea, its physical oceanography based upon the Norwegian researches 1900 – 1904. *Fiskeridir. Skr. Ser. Havunders.*, **3** (p. 1, no. 2), 390 pp.

HILMER, M. and T. JUNG, 2000: Evidence for a recent change in the link between the North Atlantic Oscillation and Arctic sea ice. *Geophys. Res. Lett.*, **27** (7), 989–992.

HØYER, J. L. and D. QUADFASEL, 2001: Detection of deep overflows with satellite altimetry. *Geophys. Res. Lett.*, **28** (8), 1611–1615.

HURRELL, J. W., 1995: Decadal Trends in the North Atlantic Oscillation: Regional Temperatures and Precipitation. *Science*, **269**, 676–679.

HURRELL, J. W., Y. KUSHNIR, G. OTTERSEN and M. VISBECK, Eds., 2003: *The North Atlantic Oscillation Climate Significance and Environmental Impacts*, Volume 134. Geophysical Monograph Series.

IPCC, 2001: *Climate Change 2001: The Scientific Basis.* IPCC, Cambridge, Contribution of Working Group I to the Third Assessment Report of the Intergovernmental Panel on Climate Change, ed. by J. T. Houghton, Y. Ding, D. J. Griggs, M. Noguer, P. J. van der Linden, X. Dai, K. Maskell and C. A. Johnson.

JÓNSSON, S., 1999: The circulation in the northern part of the Denmark Strait and its variability. *ICES CM*, **L:06**, 9 pp.

JÓNSSON, S. and H. VALDIMARSSON, 2004a: A new path for the Denmark Strait overflow water from the Iceland Sea to Denmark Strait. *Geophys. Res. Lett.*, **31** (L03305), doi:10.1029/2003GL019214.

JÓNSSON, S. and H. VALDIMARSSON, 2004b: An ocean current over the continental slope northwest of Iceland carrying Denmark Strait overflow water from the Iceland Sea to the Denmark Strait. *ICES CM*, **N:04**, 11 pp.

KANZOW, T., 2004: Monitoring the Integrated Deep Meridional Flow in the Tropical North Atlantic. PhD Thesis, Mathematisch-Naturwissenschaftliche Fakultät der Christian-Albrechts-Universität zu Kiel.

KARSTENSEN, J., P. SCHLOSSER, D. WALLACE, J. BULLISTER and J. BLINDHEIM, 2004: Variability of water mass formation in the Greenland Sea during the 1990's. *J. Geophys. Res.*, submitted.

KÄSE, R. H., J. B. GIRTON and T. B. SANFORD, 2003: Structure and variability of the Denmark Strait Overflow: Model and Observations. *J. Geophys. Res.*, **108** (C6).

KÄSE, R. H. and A. OSCHLIES, 2000: Flow through Denmark Strait. *J. Geophys. Res.*, **105**, 28,527–28,546.

KILLWORTH, P. D., 1994: On Reduced-Gravity Flow Through Sills. *Geophys. Astrophys. Fluid Dyn.*, **75**, 91–106.

KILLWORTH, P. D. and N. R. McDONALD, 1993: Maximal reduced-gravity flux in rotating hydraulics. *Deep-Sea Research*, **I** (42), 859–871.

KNUDSEN, M., 1899: The Danish Ingolf-Expedition. *Hydrography*, **I** (2), 23–161, Copenhagen.

KÖSTERS, F., 2004a: Denmark Strait Overflow: Comparing Model Results and Hydraulic Transport Estimates. *J. Geophys. Res.*, accepted.

KÖSTERS, F., 2004b: Modelling the Denmark Strait Overflow During the Last Interglacial Cycle - From Regional Dynamics to Basin Wide Impacts. PhD Thesis, Mathematisch-Naturwissenschaftliche Fakultät der Christian-Albrechts-Universität zu Kiel.

KÖSTERS, F., R. H. KÄSE, K. FLEMING and D. WOLF, 2004: Denmark Strait overflow for Last Glacial Maximum to Holocene conditions. *Paleoceanography*, **19** (PA2019), doi:10.1029/2003PA000972.

KRAUSS, W. and R. H. KÄSE, 1998: Eddy formation in the Denmark Strait Overflow. *J. Geophys. Res.*, **103**, 15,525–15,538.

LATIF, M., E. ROECKNER, U. MIKOLAJEWICZ and R. VOSS, 2000: Tropical stabilisation of the thermohaline circulation in a greenhouse warming simulation. *J. Climate*, **13**, 1809–1813.

LAVÍN, A., H. L. BRYDEN and G. PARRILLA, 1998: Meridional transport and heat flux variations in the subtropical North Atlantic. *The Global Atmosphere and Ocean System*, **6**, 269–293.

LHERMINIER, P. and OVIDE-TEAM, 2004: Variability of the North Atlantic Meridional Overturning Cell between 1997 and 2002. In: *Geophysical Research Abstracts*, European Geosciences Union 1st General Assembly, Nice, 2004, Volume 6, 01742, 2004, SRef-ID: 1607-7962/gra/EGU04-A-01742.

LOHMANN, G. and R. GERDES, 1998: Sea ice effects on the sensitivity of the Thermohaline Circulation in simplified atmosphere-ocean-sea ice models. *J. Climate*, **11**, 2789–2803.

MACRANDER, A., 2001: Wassermassentransport in der Dänemarkstraße. Diplomarbeit, Mathematisch-Naturwissenschaftliche Fakultät der Christian-Albrechts-Universität zu Kiel.

MACRANDER, A., U. SEND, H. VALDIMARSSON, S. JÓNSSON and R. H. KÄSE, 2004: Interannual changes in the overflow from the Nordic Seas into the Atlantic Ocean through Denmark Strait. *Geophys. Res. Lett.*, submitted.

MALMBERG, S. A. and S. JÓNSSON, 1997: Timing of deep convection in the Greenland and Iceland Seas. *ICES Journal of Marine Science*, **54**, 300–309.

MANN, C. R., 1969: Temperature and salinity characteristics of the Denmark Strait Overflow. *Deep-Sea Res. (Suppl.)*, 125–138.

MARSHALL, J., Y. KUSHNIR, D. BATTISTI, P. CHANG, A. CZAJA, R. DICKSON, M. MCCARTNEY, R. SARAVANAN and M. VISBECK, 2001: North Atlantic Climate Variability: Phenomena, impacts and mechanisms. *Inter. J. Climatology*, **21** (15), 1863–1898.

MARSHALL, J. and F. SCHOTT, 1999: Open-ocean convection: Observations, theory and models. *Rev. Geophys.*, **37** (1), 1–64.

MAURITZEN, C., 1996a: Production of dense overflow waters feeding the North Atlantic across the Greenland-Scotland Ridge: Part 1. Evidence for a revised circulation scheme. *Deep-Sea Research*, **43**, 769–806.

MAURITZEN, C., 1996b: Production of dense overflow waters feeding the North Atlantic across the Greenland-Scotland Ridge. Part 2: An inverse model. *Deep-Sea Research I*, **43**, 807–835.

MCCARTNEY, M., K. DONOHUE, R. CURRY, C. MAURITZEN and S. BACON, 1998: Did the overflow from the Nordic Seas intensify in 1996-1997? *Int. WOCE Newsletter*, **31**, 3–7.

MORTENSEN, J., 1997: Satellite Altimetry and Circulation in the Denmark Strait and adjacent Seas. PhD Thesis, Department of Geophysics, Niels Bohr Institute, University of Copenhagen.

NCEP/NCAR REANALYSIS PROJECT, 2004: Monthly averages of u momentum and v momentum. http://www.cdc.noaa.gov/cgi-bin/db_ search/ DB-Search.pl?Variable=Momentum+Fluxanalogous for V.

NIKOLOPOULOS, A., K. BORENÄS, R. HIETALA and P. LUNDBERG, 2003: Hydraulic estimates of Denmark Strait overflow. *J. Geophys. Res.*, **108** (C3), 3095, doi:10.1029/2001JC001283.

NILSEN, J. E. Ø., Y. GAO, H. DRANGE, T. FUREVIK and M. BENTSEN, 2003: Simulated North Atlantic-Nordic Seas water mass exchanges in an isopycnic coordinate OGCM. *Geophys. Res. Lett.*, **30(10)** (1536), doi:10.1029/2002GL016597.

NOF, D., 1983: The translation of isolated cold eddies on a sloping bottom. *Deep-Sea Res.*, **30**, 171–182.

ORVIK, K. A. and Ø.. SKAGSETH, 2003a: The impact of the wind stress curl in the North Atlantic on the Atlantic inflow to the Norwegian Sea toward the Arctic. *Geophys. Res. Lett.*, **30** (17), 1884, doi: 10.1029/2003GL017932.

ORVIK, K. A. and Ø.. SKAGSETH, 2003b: Monitoring the Atlantic Inflow to the Norwegian sea by using one moored current meter and one profiling CTD. *Continental Shelf Research*, **23**, 159–176.

OTTERÅ, O. H., H. DRANGE, M. BENTSEN, N. G. KVAMSTØ and D. JIANG, 2003: The sensitivity of the present-day Atlantic meridional overturning circulation to freshwater forcing. *Geophys. Res. Lett.*, **30**, doi:10.1029/2003GL017578.

PEDLOSKY, J., 1987: *Geophysical Fluid Dynamics*. Springer, New York, NY, 2nd Edition.

PRATT, L. J., 1986: Hydraulic control of sill flow with bottom friction. *J. Phys. Oceanogr.*, **27**, 1970–1980.

PRATT, L. J., 2004: Recent progress on understanding the effects of rotation in models of sea straits. *Deep-Sea Res.*, **51**, 351–369.

PRATT, L. J. and L. ARMI, 1987: Hydraulic control of flows with nonuniform potential vorticity. *J. Phys. Oceanogr.*, **17**, 2016–2029.

PRATT, L. J., K. R. HELFRICH and E. P. CHASSIGNET, 2000: Hydraulic adjustment to an obstacle in a rotating fluid. *J. Fluid Mech.*, **404**, 117–149.

PRATT, L. J. and P. A. LUNDBERG, 1991: Hydraulics of Rotating Strait and Sill Flow. *Annu. Rev. Fluid Mech.*, **23**, 81–106.

PRATT, L. J. and S. G. L. SMITH, 1997: Hydraulically drained flows in rotating basins. Part I: Method. *J. Phys. Oceanogr.*, **27**, 2509–2521.

RAHMSTORF, S., 1995: Bifurcations of the Atlantic thermohaline circulation in response to changes in the hydrological cycle. *Nature*, **378**, 145–149.

RAHMSTORF, S., 1996: On the freshwater forcing and transport of the Atlantic thermohaline circulation. *Clim. Dyn.*, **12**, 799–811.

RAHMSTORF, S., 2002: Ocean circulation and climate during the past 120,000 years. *Nature*, **419**, 207 – 214.

RAHMSTORF, S., 2003: The current climate. *Nature*, **421**, 699.

RD Instruments, 1998: *Workhorse Long Ranger Acoustic Doppler Current Profiler Technical Manual*. RD Instruments, San Diego, CA.

ROSS, C. K., 1984: Temperature-salinity characteristics of the "overflow" water in Denmark Strait during "OVERFLOW '73". *Rapp. P.-v. Réun. Cons. int. Explor. Mer.*, **185**, 111–119.

RUDELS, B., P. ERIKSSON, H. GRÖNVALL, R. HIETALA and J. LAUNIAINEN, 1999: Hydrographic observations in Denmark Strait in fall 1997, and their implications for the entrainment into the overflow plume. *Geophys. Res. Lett.*, **26** (9), 1325–1328, doi:10.1029/1999GL900212.

RUDELS, B., E. FAHRBACH, J. MEINCKE, G. BUDÉUS and P. ERIKSSON, 2002: The East Greenland Current and its contribution to the Denmark Strait overflow. *ICES Journal of Marine Science*, **59**, 1133–1154.

SANFORD, T. B., E. A. D'ASARO, E. L. KUNZE, J. H. DUNLAP, R. G. DREVER, M. A.KENNELLY, M. D. PRATER and M. S. HORGAN, 1993: An XCP user's guide and reference manual. Tech. rep. apl/uw 9309, Applied Physics Laboratory, University of Washington, Seattle, WA.

SANFORD, T. B., R. G. DREVER and J. H. DUNLAP, 1978: A velocity profiler based on the principles of geomagnetic induction. *Deep-Sea Res.*, **25**, 183–210.

SARNTHEIM ET AL., 2001: *The Northern North Atlantic: A changing environment*, Springer Verlag, Berlin, Chapter Fundamental modes and abrupt changes in North Atlantic circulation and climate over the last 60 ky – Concepts, reconstructions and numerical modelling, 365–410. Ed. by P. Schäfer, W. Ritzrau, M. Schlüter and J. Tiede.

SAUNDERS, P. M., 2001: *Ocean circulation and climate*, Academic Press, San Diego, Volume 77 of *International Geophysics Series*, Chapter The dense northern overflows, 401–418. Ed. by G. Siedler, J. Church and J. Gould.

SCHMIDT, H., 2004: Anwendung von Satellitenaltimetrie zur Verbesserung von integralen in situ Transportmessungen. Diplomarbeit, Mathematisch-Naturwissenschaftliche Fakultät der Christian-Albrechts-Universität zu Kiel.

SCHMIDT, S., 2003: Süßwassereinflüsse auf die Konvektionsaktivität in der Labradorsee. Diplomarbeit, Mathematisch-Naturwissenschaftliche Fakultät der Christian-Albrechts-Universität zu Kiel.

SCHMITZ, W., 1995: On the interbasin-scale thermohaline circulation. *Rev. of Geophys.*, **33**, 151–173.

SCHWECKENDIEK, U. and J. WILLEBRAND, 2004: Mechanisms for the Overturning Response in Global Warming Simulations. *J. Climate*, submitted.

SMITH, P. C., 1976: Baroclinic Instability in the Denmark Strait Overflow. *J. Phys. Oceanogr.*, **6**, 355–371.

SMITH, W. H. F. and D. T. SANDWELL, 1997: Global sea floor topography from satellite altimetry and ship depth soundings. *Science*, **277**, 1956–1962.

SONG, Y. T. and D. HAIDVOGEL, 1994: A semi-implicit primitive equation ocean circulation model using a generalized topography-following coordinate system. *J. Comput. Phys.*, **115**, 228–244.

STAMMER, D., C. WUNSCH, R. GIERING, C. ECKERT, P. HEIMBACH, J. MAROTZKE, A. ADCROFT, C. N. HILL, and J. MARSHALL, 2003: Volume, heat, and freshwater transports of the global ocean circulation 1993 – 2000, estimated from a general circulation model constrained by World Ocean Circulation Experiment (WOCE) data. *J. Geophys. Res. C*, **108** (C1), 3007, doi:10.1029/2001JC001115.

STAMMER, D., C. WUNSCH, R. GIERING, C. ECKERT, P. HEIMBACH, J. MAROTZKE, A. ADCROFT, C. N. HILL and J. MARSHALL, 2002: The Global ocean circulation during 1992 -1997, estimated from ocean observations and a general circulation model. *J. Geophys. Res. C*, **107** (C9), 3118, doi:10.1029/2001JC000888.

STEIN, M., 1972: Observation of the Denmark Strait Overflow in August 1971. *ICES CM 1972/C:5*.

STERN, M. E., 1974: Comment on rotating hydraulics. *Geophys. Fluid Dyn.*, **6**, 127–130.

STERN, M. E., 2004: Transport extremum through Denmark Strait. *Geophys. Res. Lett.*, **31**, L12303, doi:10.1029/2004GL020184.

STÖCKER, H., 1998: *Taschenbuch der Physik*. Verlag Harri Deutsch, Thun, Frankfurt am Main, 3rd Edition.

STOMMEL, H., 1961: Thermohaline convection with two stable regimes of flow. *Tellus*, **13**, 224–230.

STRASS, V. H., E. FAHRBACH, U. SCHAUER and L. SELLMANN, 1993: Formation of Denmark Strait Overflow Water by mixing in the East Greenland Current. *J. Geophys. Res.*, **98**, 6907–6919.

SWIFT, J. H., 1980: Seasonal processes in the Iceland Sea with especial reference to their relationship to the Denmark Strait overflow. PhD Thesis, University of Washington, Seattle, WA.

SWIFT, J. H., K. AAGARD and S.-A. MALMBERG, 1980: The contribution of the Denmark Strait overflow to the deep North Atlantic. *Deep-Sea Research*, **27A**, 29–42.

University of Rhode Island, 2000: *Inverted Echo Sounder User's Manual*. University of Rhode Island, Narragansett, RI.

VELLINGA, M. and R. A. WOOD, 2002: Global climatic impacts of a collapse of the Atlantic thermohaline circulation. *Clim Change*, **54**, 251–267.

VISBECK, M., E. CHASSIGNET, R. CURRY, T. DELTWORTH, B. DICKSON and G. KRAHMANN, 2003: *The North Atlantic Oscillation*, AGU monograph, Washington, Chapter The Ocean's Response to North Atlantic Oscillation Variability, 113–146. Ed. by J. Hurrell, Y. Kushnir, G. Ottersen and M. Visbeck.

VISBECK, M. and J. FISCHER, 1995: Sea Surface Conditions Remotely Sensed by Upward-Looking ADCPs. *Journal of Atmospheric and Oceanic Technology*, **12**, 1,141–1,149.

WHITEHEAD, J. A., 1989: Internal hydraulic control in rotating fluids – applications to oceans. *Geophys. Astrophys. Fluid Dyn.*, **48**, 169–192.

WHITEHEAD, J. A., 1998: Topographic Control of Oceanic Flows in Deep Passages and Straits. *Reviews of Geophysics*, **36** (3), 423–440.

WHITEHEAD, J. A., A. LEETMAA and R. A. KNOX, 1974: Rotating hydraulics of straits and sill flows. *Geophys. Fluid Dyn.*, **6**, 101–125.

WORTHINGTON, L. V., 1969: An attempt to measure the volume transport of Norwegian Sea overflow water through the Denmark Strait. *Deep-Sea Research*, **16**, 421–432.

WUNSCH, C., 2002: What is the thermohaline circulation? *Science*, **298**, 1179–1181.

Erklärung

Hiermit erkläre ich, daß diese Arbeit meine eigene Arbeit ist, die ich, abgesehen von den Beiträgen meiner akademischen Lehrer, selbständig und nur unter Verwendung der angegebenen Hilfsmittel verfaßt habe. Sie hat weder ganz noch in Teilen einer Prüfungskommission vorgelegen.

Kiel, den 03. November 2004.

_____

Andreas Macrander

Lebenslauf

Persönliche Daten

Andreas Macrander
Hanssenstraße 1a
24106 Kiel

Tel.: 0431 / 667 29 48
E-Mail: amacrander@gmx.de

Geb. am 22.02.1975 in Otterndorf
deutsche Staatsangehörigkeit

Schulbildung

1981 – 1994	Grundschule, Orientierungsstufe und Gymnasium Otterndorf
1994	Abitur

Zivildienst

1994 – 1995	Zivildienst im Bereich des Umweltschutzes bei der Samtgemeinde Hemmoor

Studium

1995 – 2001	Studium der Ozeanographie an der Christian-Albrechts-Universität zu Kiel
2000 – 2001	Diplomarbeit zum Thema „Wassermassentransport in der Dänemarkstraße"
2001	Abschluß mit Diplom in Physikalischer Ozeanographie
ab 2001	Promotion in Ozeanographie an der Christian-Albrechts-Universität zu Kiel zum Thema „Variabilität und Prozesse des Dänemarkstraßen-Overflows"

Kiel, den 03.November 2004.